USGS
science for a changing world

Summary of Creepmeter Data from 1980 to 2020—Measurements Spanning the Hayward, Calaveras, and San Andreas Faults in Northern and Central California

Open-File Report 2024–1011

U.S. Department of the Interior
U.S. Geological Survey

Cover. Photographs showing offset pavement on California Route 25, just north of the Melendy Ranch creepmeter. Periodically, California's Department of Transportation will repave this road, smoothing out the effects of steady slip (16.8 millimeters per year) on the San Andreas Fault. Photographs by Roger Bilham, University of Colorado Boulder.

Summary of Creepmeter Data from 1980 to 2020—Measurements Spanning the Hayward, Calaveras, and San Andreas Faults in Northern and Central California

By John Langbein, Roger G. Bilham, Hollice A. Snyder, and Todd Ericksen

Open-File Report 2024–1011

U.S. Department of the Interior
U.S. Geological Survey

U.S. Geological Survey, Reston, Virginia: 2024

Suggested citation:
Langbein, J., Bilham, R.G., Snyder, H.A., and Ericksen, T., 2024, Summary of Creepmeter Data from 1980 to 2020—Measurements Spanning the Hayward, Calaveras, and San Andreas Faults in Northern and Central California: U.S. Geological Survey Report 2024–1011, 110 p., https://doi.org/10.3133/ofr20241011.

ISSN 2331-1258 (online)

Acknowledgments

Funding is provided primarily by the U.S. Geological Survey National Earthquake Hazards Reduction Program. The first author gives a big thank you to his immediate predecessors, Kate Breckenridge and Rich Liechti, for their contributions to the creepmeter project and the documentation and training they provided.

Contents

Figures

Tables

Conversion Factors

U.S. customary units to International System of Units

Multiply	By	To obtain
	Length	
inch (in.)	2.54	centimeter (cm)
inch (in.)	25.4	millimeter (mm)
foot (ft)	0.3048	meter (m)
mile (mi)	1.609	kilometer (km)
	Area	
square inch (in^2)	645.2	square millimeter (mm^2)
square foot (ft^2)	0.09290	square meter (m^2)
	Mass	
ounce, avoirdupois (oz)	28.35	gram (g)
	Density	
pound per cubic foot (lb/ft^3)	0.01602	gram per cubic centimeter (g/cm^3)
	Force	
pound-force (lbf)	4.4482	Newton (N) ($kg\ m/s^2$)

International System of Units to U.S. customary units

Multiply	By	To obtain
	Length	
centimeter (cm)	0.3937	inch (in.)
millimeter (mm)	0.03937	inch (in.)
meter (m)	3.281	foot (ft)
kilometer (km)	0.6214	mile (mi)
	Area	
square millimeter (mm^2)	0.00155	square inch (in^2)
square meter (m^2)	10.76	square foot (ft^2)
	Mass	
gram (g)	0.03527	ounce, avoirdupois (oz)
	Density	
gram per cubic centimeter (g/cm^3)	62.4220	pound per cubic foot (lb/ft^3)
	Force	
Newton (N) ($kg\ m/s^2$)	0.2248	pound-force (lbf)

Temperature in degrees Celsius (°C) may be converted to degrees Fahrenheit (°F) as follows: $°F = (1.8 \times °C) + 32$.

Temperature in degrees Fahrenheit (°F) may be converted to degrees Celsius (°C) as follows: $°C = (°F - 32) / 1.8$.

Datum

Coordinate information is referenced to the World Geodetic System 1984 (WGS 84).

Abbreviations

EDM	electronic distance measuring
GOES	Geostationary Operational Environmental Satellite
GPS	global positioning system
InSAR	interferometric synthetic aperture radar (InSAR)
lidar	light detection and ranging
LVDT	linear voltage displacement transformers/transducers
µm	micrometer
ppm	parts per million
SAF	San Andreas Fault
USGS	U.S. Geological Survey

Summary of Creepmeter Data from 1980 to 2020—Measurements Spanning the Hayward, Calaveras, and San Andreas Faults in Northern and Central California

By John Langbein,[1] Roger G. Bilham,[2] Hollice A. Snyder,[1] and Todd Ericksen[1]

Abstract

This report is an update to the presentation by Schulz (1989) introducing potential users to the creepmeter data collected between the publication of Schulz's report and mid-2020. The creepmeter network monitors aseismic, surface slip at various locations on the Hayward, Calaveras, and San Andreas Faults in northern and central California. There are different designs of creepmeters and these are briefly described. For a majority of the creepmeters, these data are automatically sent to the U.S. Geological Survey (USGS) offices where they are stored and processed. In addition, for most of the creepmeters, occasional manual measurements are made and these are compared with digitally recorded data. For some sites, the comparisons indicated degradation of the electronic sensor and consequently corrections are made to the digital data. The largest transient deformation is that which followed the 2004, *M*6, Parkfield earthquake. Various functions found in the literature that have been used to model postseismic slip were tested with the observed postseismic behavior seen on the creepmeters in the vicinity of Parkfield, California. No single function adequately fit all the data from these Parkfield instruments. This report is a discussion and analysis of data from creepmeters deployed by the USGS. The discussion primarily focuses on instruments that are currently operating in 2020 or have operated quite recently but are no longer in service.

Introduction

It has been more than 30 years since the last catalog of creepmeter measurements was published by Schulz (1989). Here, the U.S. Geological Survey (USGS) updated these data with measurements extending through mid-2020. These data have been brought online in digital format and are available for download from USGS Creepmeter data (2022). Over the past 30 years, several creepmeters were removed due to various reasons, new creepmeters have been installed, newer methods have been established to characterize these data. Significantly, the long anticipated, Parkfield, California, earthquake occurred in 2004, yielding a near complete record of one "seismic cycle" of moderate sized earthquakes on this segment of the San Andreas Fault (SAF).

Since the discovery of aseismic slip in 1955 (Steinbrugge and Zacher, 1960; Tocher, 1960) on the SAF, various institutions have fabricated and installed instruments that are capable of measuring slip at Earth's surface with sub-millimeter resolution, and typically with a 10-minute sampling interval. Various sensors have been employed but the basic scheme measures the displacement between two monuments or piers separated by 10 to 30 meters (m) with the active, creeping fault located halfway between these monuments. The monuments are configured such that the baseline between the monuments is 30° from the strike of the fault. Hence, the change in distance between the monuments due to slip is proportional to 1/cos(30°). What follows is a discussion and analysis of data from creepmeters deployed by the USGS on the San Andreas Fault system in central California, including the Hayward and Calaveras Faults in central and northern California, whose locations are shown in figure 1. The discussion primarily focuses on instruments that are currently operating in 2020 or have operated until quite recently but are no longer in service.

Appendix 1 contains the primary product of this review, where the data are presented and summarized for each creepmeter. The appendix includes the metadata that provide the location, the azimuth of the instrument, the baseline length, the type of instrument, and any salient notes that might affect the interpretation of these data.

The main part of the report describes the types of creepmeters now in use, field maintenance, and methods used to compare onsite, manual measurements with the data recorded electronically in the "Instrumentation, Methods, and Data" section. Following that is the "Data Summary" section, a summary of the creepmeter data grouped into different segments of the fault. That includes the creep rates and a budget of creep that distinguishes between steady state and episodic events that occur over the period of a day or so. Lastly, the report provides an update to postseismic slip, in the "Parkfield Postseismic Creep" section, as measured by the creepmeters from the 2004, *M*6, Parkfield earthquake (Langbein and others, 2006).

[1]U.S. Geological Survey.

[2]University of Colorado Boulder, Colorado.

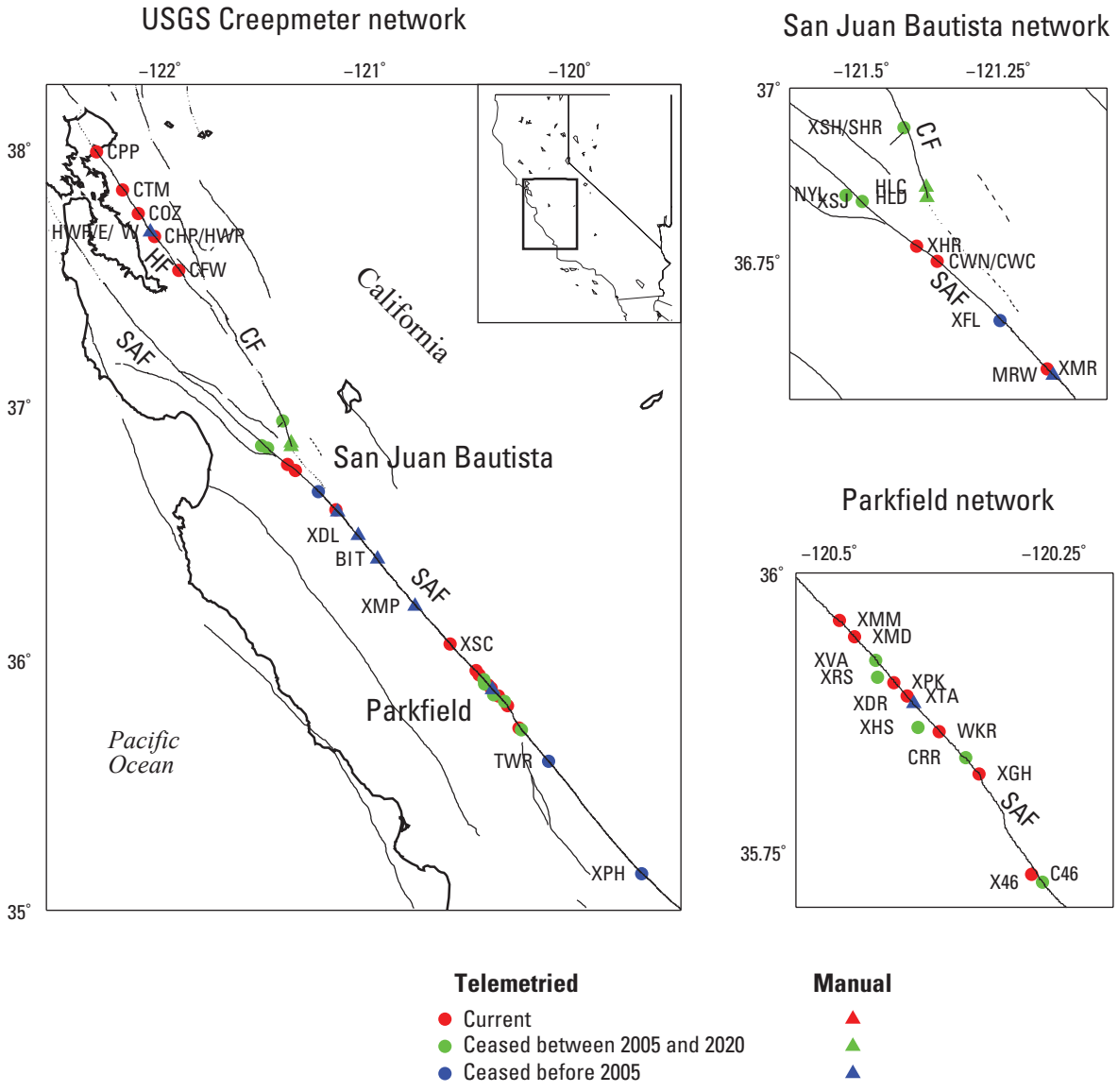

Figure 1. Maps showing the distribution of creepmeters in central California along with the major Quaternary faults. The creepmeters measure aseismic slip on the Hayward (HF), Calaveras (CF), and San Andreas (SAF) Faults. The creepmeters are represented by two symbols, circles for those with telemetry, and triangles for those with occasional manual measurements. The colors represent the status of each creepmeter. In the lefthand map, an inset shows that outline of the State of California and the rectangle outlines the region where the creepmeters are located. For the San Juan Bautista and Parkfield areas, the creepmeters are shown on an expanded scale. Note that in 2021, the creepmeters labeled NYL and XSH in the Hollister area have been rebuilt. Appendix 1 contains the creepmeter site abbreviations and summaries used in this report.

Instrumentation, Methods, and Data

The following section updates the creepmeter catalog of Schulz (1989). Below, the different types of instruments and their sensors, the method used to convert the recorded digital counts to dextral slip, and a summary for each creepmeter are discussed. Most of the creepmeters discussed here use telemetry, but there are several that have no telemetry, are visited occasionally and measurements are made manually.

Instrumentation

Several types of sensors are used to measure creep. The most common design, designated here as the USGS standard instrument, was deployed starting in the 1970s and is still in use. More recently, one of this report's co-authors, Roger Bilham, introduced newer designs and these have been installed at sites starting in the 1990s. In addition, there are a few older instruments that were inherited by the USGS. Requirements common to all designs are (1) low sensitivity to changes in temperature, (2) monuments that are "stable" including effects from rainfall, and (3) a sensor that has at least a 0.1-millimeter (mm) sensitivity. Consequently, the length standard that bridges the distance between the monuments uses low coefficient of expansion materials such as Invar, glass fiber, or more recently, carbon fiber. Monuments tend to extend to at least 2-m depth, and the sensors are usually linear voltage displacement transformers/transducers (LVDT).

At most sites digital telemetry has been used to retrieve data. Prior to the mid-1980s, that telemetry used telephone circuits to route the data to USGS offices in Menlo Park, Calif., for archiving. Subsequently, the telemetry now uses the Geostationary Operational Environmental Satellite (GOES) system (operated by the National Weather Service) to retrieve data. This is the same method used by the Water Resources Division of USGS to retrieve streamgage data. The earlier equipment used 12-bit data loggers, but with the newer equipment the resolution has increased to 16 bits. For a 12-bit logger with 5-volt (V) range and with a sensor having 5 mm/V sensitivity, the nominal resolution is 0.006 mm. With the limited bandwidth of both the telephone and GOES system, the collection and transmission rate has been every 10 minutes. More recently, at some sites the collection rate was increased to 1-minute intervals but the transmission rate remains at 10-minute intervals.

USGS Standard

Most of the creepmeters operated by the USGS were designed and built by the USGS in the 1970s. A sketch of this type of meter is presented in figure 1 of Schulz (1989). Schulz and Burford (1978) provide a thorough description of one such meter and its installation at Panorama Hills, site XPH. Essentially, the instrument consists of a 0.75-mm diameter Invar wire stretched between the two monuments that is anchored at one end. Between the two monuments, the wire hangs freely in the form of a catenary and is enclosed in a 20-centimeter (cm) diameter polyethylene conduit. The wire at the sensor end is draped over a rocker arm where the wire makes a 90° bend to which the core of an LVDT is fastened. Tension is maintained by a weight hanging off the end of the Invar wire below the LVDT. In addition, a micrometer is added to the sensor end to facilitate manual measurements of displacement for comparison with the telemetered values of displacement. Since the range of the LVDT is 25 mm, the creepmeter needs to be reset periodically depending upon the rate of slip. This entails adding an additional length of wire between the two monuments by loosening the clamp that pins the wire to the anchor at the distant end and feeding sufficient extra wire, stored at the anchor, to null the LVDT.

After many years of operation, the conduit containing the Invar may collapse or separate due to extension resulting from fault slip. This may deflect the wire or adversely introduce friction into the measurement, and possibly change its sensitivity to creep. Occasionally too, the Invar wires corrode and break. In locations where the surface fault zone is narrow compared to the length of the creepmeter, the conduit is slowly deformed into an s-shaped configuration (an arc-tan function) requiring the conduit to be realigned to permit the wire to hang freely. If the deformation is excessive the wire within the conduit where it crosses the creeping fault may be deflected sufficiently to reduce its obliquity, thereby increasing its sensitivity to dextral slip (for example, $1/\cos(30°-\Delta°)$, where Δ is the change in obliquity). Even where the shear zone above the subsurface fault is wider than the aperture spanned by the creepmeter, cumulative slip on the fault slowly reduces its obliquity. Note that the configuration of the monuments is such that, with dextral slip, the distance between the monuments becomes longer.

Figure 1 of Schulz (1989) shows that both ends of the instrument are installed in vaults at depths between 0.5 and 2 m below grade. An additional 20-cm diameter hole was augured to about 2-m depth below the floor of the vaults into which a 7.5-cm diameter steel pipe was inserted vertically into the borehole. The lower part of the hole was filled with cement, and the instrument hardware was attached to the upper end of the pipe.

Caltech Design

Three sites near the town of Parkfield, Carr Ranch (CRR), Work Ranch (WKR), and Twisselman Ranch (TWR) which the USGS inherited from the California Institute of Technology (appendix 1), use a different instrument design. Schulz and others (1982) provides a brief description. These instruments consist of a 1.6-mm diameter Invar wire pinned at one end and held under tension at the sensor end by a beam-balance. The electronic measuring unit is a linear potentiometer that measures rotation of the beam balance with a 2:1 gain. The potentiometer acts as a voltage divider, which requires a regulated source of DC. A thin Kevlar thread loops

around the shaft of the potentiometer, whose diameter dictates the sensitivity. One wrap of the potentiometer is equivalent to about 10-mm displacement, corresponding to 5 mm displacement between the end anchors due to the mechanical gain of the beam-balance. The potentiometer has a short dead zone as it transitions from 360° to 0°, where the resistance hovers between zero and full-scale, requiring some editing of the data to remove that portion of the data. In addition, a mechanical dial gauge is provided to facilitate periodic manual measurements. Both the potentiometer and the mechanical dial gauge are associated with friction which occasionally can result in stick-slip "steps" in the recorded data.

Bilham #1 Design

At five sites on the Hayward Fault in the San Francisco Bay Area (CPP, Pinole Point; CFW, Fremont; CTM, Temescal; COZ, Oakland Zoo; CHP, City of Hayward—Palisade St.) the suspended tensioned wires used elsewhere on the San Andreas system were abandoned in favor of stiff rods that slide within narrow PVC tubes. The rationale for this decision was that rates on the Hayward fault are low (4–9 millimeters per year [mm/yr]) relative to the central creeping zone of the San Andreas Fault and most of the anticipated measurement sites on the fault are subject to annual flooding, a condition that would change the catenary sag, and hence measurement datum of a tensioned wire. Unlike the freely suspended wire arrangement, the sliding rod is associated with friction. However, it was reasoned that if the forces involved with fault-zone slip could be exploited with rigid attachment anchors and comparably stiff measurement rods, stick-slip motion of the free end of the sliding rods could be reduced to the sub-micrometer (μm) level. Invar or glass fiber rods were initially used (3/8 to 5/16-inch diameter) but the favored material adopted in all recent systems is pultruded carbon fiber. The latter material has a density of approximately equal to (≈) 1.5 grams per cubic centimeter (g/cm^3) and is formed by pulling more than fifty thousand 8-μm diameter high-strength carbon fibers through a steel die immersed in water-proof epoxy (pull-extrusion hence "pultrusion"). The carbon density exceeds 60 percent and since all the fibers in the composite are pre-tensioned the resulting rod optimizes the strength of the single fibers. The outer finish is glassy in appearance and slides with low friction within a PVC tube.

In the perceived view that monument wobble or instability (Langbein and others, 1990, 1995; table 2, and figs. 3 and 4) contributes to spurious changes in creep rate, the monuments for these sites consisted of three 5-cm-square steel helical-piles screwed by a powerful rotary drive to 8- to 10-m-depth and welded at a common point at ≈1 m depth. One of the piles is vertical and the other two piles are used as "tie-backs" inclined at 45° respectively in-line with, and orthogonal to, the creepmeter path as shown in figure 2.

The sensors adopted are the LVDT used in the USGS standard creepmeters which have been proven to be immune to occasional submersion. The LVDTs for the Hayward Fault sites have a range of twice those used with the standard USGS instruments. In addition, the electronics are completely self-contained within the sensor and, unlike the USGS instruments, do not require an external, precision voltage reference supply. The thermal coefficient of LVDT sensors is typically less than 0.05 percent per °Celsius (°C) of full scale (for example, 25 μm/°C for a 50 mm range sensor) with linearities of 0.25 percent of full-scale (for example, 125 μm for a range of 50 mm).

Bilham #2 Sensor

This alternate design evolved from a series of large range "rupture-meters" that were installed at all five of the Hayward Fault creepmeters. While the initial design used a potentiometer configured as a voltage divider similar to that used in the Caltech design above, subsequent sensors used a Hall-effect rotary sensor with an output of 0.2–4.8 V and with 12-bit resolution of 2.5 μm when used in a 10 mm full-scale configuration. The sensors have a thermal sensitivity of 20 parts per million (ppm) per °C (0.2 μm/°C for 10 mm range) and although they are linear to less than (<) 0.3 percent (30 μm/10 mm range) and have a small 0–360° transition angle (<1°), as with the Caltech rotary potentiometers, the transition duration during which the signal is ambiguous depends on the fault-slip rate. If prolonged more than a few minutes manual editing is needed to suppress spurious data. Like the potentiometer sensor, the Hall-effect sensor does require an external, precision voltage source.

In this design, a 0.3-mm-diameter Teflon-coated, 19-strand stainless-steel cable is attached to the rod (6 Newtons [N] breaking force). This wire is held in tension by a constant-tension spring motor on which is spooled approximately 1.7–3 m of wire which sets the range limit before mechanical adjustment is needed. Between the motor and the carbon-fiber rod, the cable is wrapped once around the shaft or wheel of a Hall-effect sensor. The diameter of the shaft and the sensitivity of the Hall-effect device provide the scale factor needed to convert the voltage output to displacement. Initially the calibration (the transition from 0° to 360°) is determined in the lab, but instrument sensitivity is subsequently confirmed and monitored by transitions in the recorded data whose frequency depends on the fault slip rate, but typically occurs every year or two. If slip were to exceed 10 mm between samples, then there would exist potential ambiguity in the number of rotations during that interval. To overcome this at some sites, a second rotary sensor with larger diameter wheel provides the creepmeter with two ranges both to resolve ambiguity and to capture large slip as may occur in an earthquake. The second wheel is arranged with a circumference greater than or equal to (≥) 100 mm, or alternatively with a ten-turn 360° Hall sensor that measures rotation of the spool motor directly (an effective wrap of 1.3 m). To prevent the inbound and outbound wire from touching where they enter and leave the rotary sensor shaft, a pair of 5-mm-diameter nylon rollers are arranged to guide the wire to and from the sensor. These cause the measurement wire to spiral around the shaft, reducing the calibration by approximately 1 percent, a value that is determined prior to deployment. Although the rollers ensure smooth operation, they introduce slight hysteresis should the fault-slip reverse in direction.

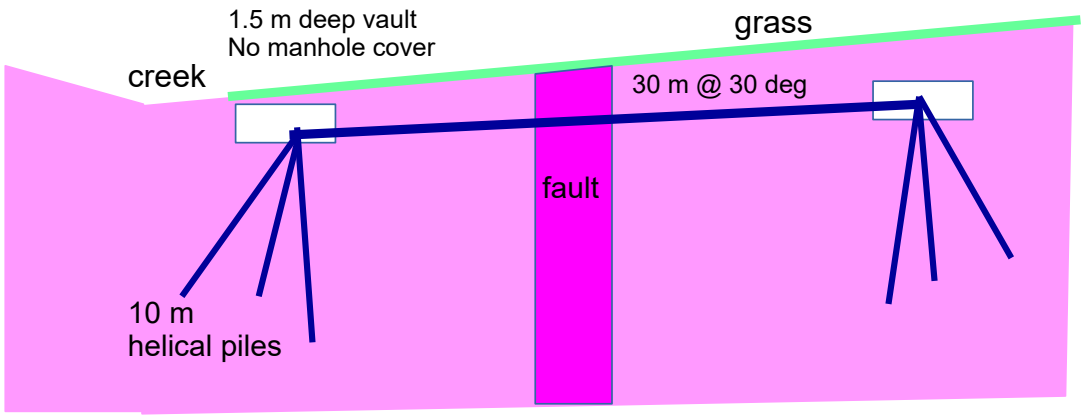

Figure 2. Cross section of a Bilham #1 type creepmeter installation at the Oakland Zoo (COZ), California. The cross section shows schematically the orientations and depths of the helical piles and the distance between the two ends of the creepmeter. m, meter; @, at; W, west, E, east.

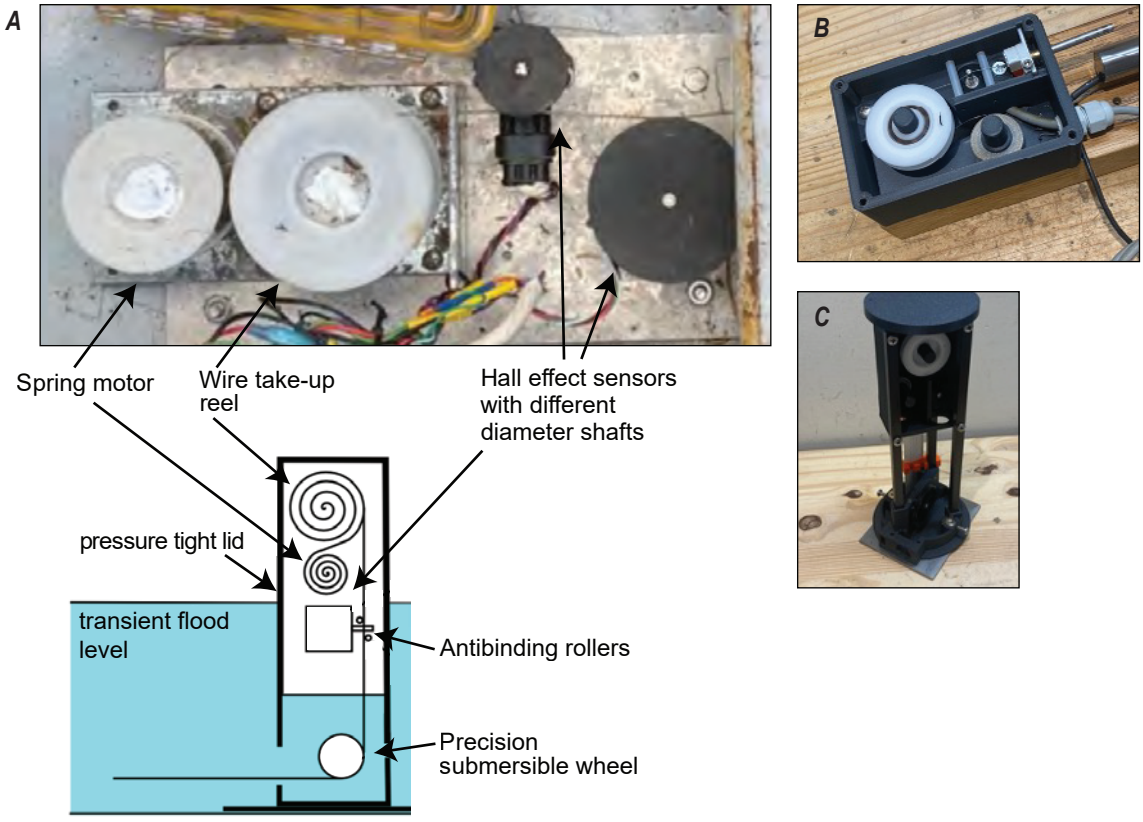

Figure 3. Three pictures and one schematic showing the sensing unit of the second generation, Bilham #2 rupture/creepmeter. *A*, steel wire extends from the take-up reel to a rod (Invar, glass fiber, or carbon fiber) and is looped around the shafts of the Hall-effect sensor. Earlier models used potentiometers. *B*, the wire exits to the right to attach to the rod. The vertical sensing unit is enclosed in a PVC pipe configured as a diving bell to keep water from the actual sensor. For *C*, the vertical unit, the wire exits to the left to attach to the rod. The bottom two pictures are a refined version of the above.

A 10-mm-range rotary sensor and a 10-mm-range LVDT have similar linearity in scale (0.3 percent full-scale), but the Hall sensor has an order of magnitude lower thermal coefficient and admits two orders of magnitude greater range before mechanical adjustment is required. The advantage of the LVDT is its simplicity and its immunity to prolonged flooding. At rotary-sensor sites where annual flooding is anticipated, an additional wheel directs the measurement path vertically and the Hall sensors are mounted within a down facing sealed cylinder (a diving bell) that prevents rising waters from immersing the sensor mechanism.

Maintenance

Periodic maintenance has been undertaken on the creepmeters during the past several decades to maintain the creepmeters to be on scale and to ensure optimum performance. For both the USGS and Caltech instruments, micrometer measurements of slip are manually read and recorded during visits, as are voltages, especially from the voltage regulator. For all creepmeters, the battery is evaluated and replaced as needed. Prior to about 2007, when the second generation GOES data collection platform was installed, the telemetry units needed to have their time reset to correspond to Coordinated Universal Time (UTC) time, to prevent data transmissions interfering with the scheduled transmission from another site. In general, maintenance visits are scheduled at 6-month intervals for creepmeters on the San Andreas Fault where creep rates are measured as high as approximately (~) 15 mm/yr. With a 25 mm range of the LVDT, the creepmeters at sites with fast creep rates would need to be reset once every two years; but to be conservative, these sites were often reset more frequently on the chance that the rate became faster, or the maintenance was delayed. During the recent COVID-19 pandemic from 2020 to 2021, delayed maintenance has been the rule for all the Parkfield sites as they required a lengthy trip from the USGS office in Menlo Park.

Data Processing

Since the measurements are recorded and sent via the GOES system once every 10 minutes, these data are stored on a computer. These data, in digital counts, are scaled to a voltage and multiplied by a scale factor for the LVDT to convert to displacement, then divided by the cosine of the obliquity to obtain a value of right-lateral slip (appendix 2). Periodically, either from resets or site visits, the data from the telemetry shows a step. That step is removed either using a graphical data editor, or using the offset feature of the program, cleanstrain (Langbein, 2010). In addition, spikes due to spurious glitches from the telemetry are removed either using a graphical editor or using cleanstrain. Prior to about the 2008 to 2012 interval, all edits and offset adjustments were made with the graphical editor; the more recent data use cleanstrain. With the graphical editor, the mode of operation was to clean up data over 6-month to 1-year intervals in one session. With cleanstrain, the clean-up operation occurs daily to weekly, so these data are immediately available online.

Note: A key assumption carried throughout this report is that any change in distance between the monuments is due only to dextral (or sinistral) slip on the fault.

If the anchors move perpendicular to the fault, either due to dilation of the fault zone during slip, desiccation of the fault gouge during drought, or monument tilt, these orthogonal movements may be incorrectly interpreted as slip on the fault. A discussion on the effect of both the change in obliquity and fault-normal displacement is found in appendix 2.

In addition, initial measurements assumed that the obliquity of the baseline for the creepmeter remains constant. As mentioned above, the fault-crossing obliquity of a creepmeter decreases with time. For example, after 60 years monitoring a 20 mm/yr slip rate, a creepmeter with a 10-m baseline that initially crossed the fault at 30° would now be at 28.5°, thereby reducing the scale-factor relating change in distance to fault slip by 1.5 percent. Without this correction the 20 mm/yr fault slip rate would appear to have accelerated (non-linearly with time) to 20.3 mm/yr. For short time spans and obliquities less than or equal to (≤) 30° this correction can be ignored.

The processing uses the 10-minute sampled data (and more recently, 1-minute sampled data). Edited, 10-minute data typically extend back to about 1990. Prior to 1990, the 10-minute data were edited, but decimated to 1-day samples, and the 10-minute edited data were deleted to save disk space on the computer. However, the raw, unedited data have been saved. In principle, it is possible to re-edit those older data, but that has not been undertaken. Consequently, the online creepmeter archive (USGS Creepmeter data (2022) includes a mix of 1-minute, 10-minute, and daily sampled data.

The archived micrometer data provide an independent measure of creep either in the form of creep rate between measurement intervals, or as cumulative slip since start time. As with measurements made manually, these calculations may result in entry blunders, which when calculating cumulative slip, can introduce artificial offsets in the cumulative data. For the USGS creepmeters, the processed creep derived from the telemetry data are compared directly with the micrometer measurements. On occasion the comparisons lead to apparent discrepancies between the two time-series.

An example of the reconciliation of one such discrepancy is shown in figure 4. The upper plot in figure 4*A* shows telemetered Gold Hill (XGH1) site data sampled at 1-day intervals overlayed with cumulative creep derived from the micrometer data. Both time series have had a trend removed based on the telemetered data from 2006 to 2020. The occurrence of the 2004 Parkfield earthquake corresponds to an abrupt increase in fault slip rate. The lower left plot shows the differences between the two sets of observations. Prior to 2003, the difference curve remains approximately constant, but during and following the Parkfield earthquake significant scatter is evident. This is in part due to the rapid deformation that is aliased when down sampling from

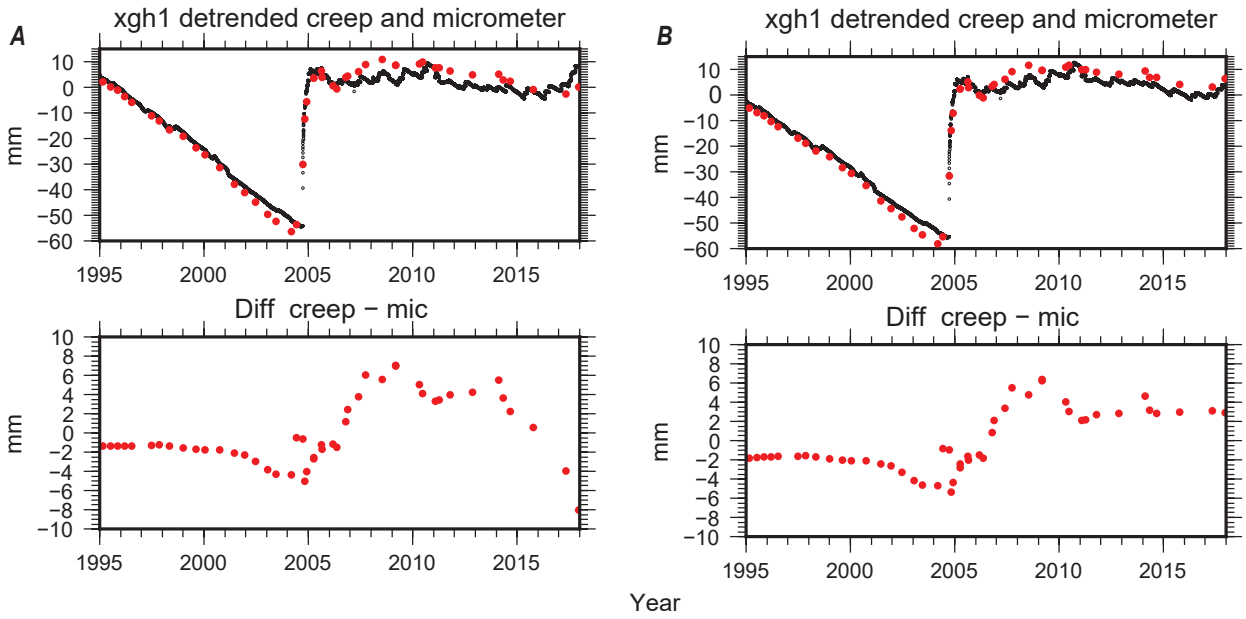

Figure 4. Plots of two decades of telemetered data and micrometer creepmeter data from the Gold Hill site (XGH1) on the San Andreas Fault southeast of Parkfield, California (fig. 1). The periodically measured micrometer data (red dots) are shown in the top two graphs, with the raw telemetered data in *A* and with the rescaled telemetered data in *B* (black). The data have been detrended using the creep rate from 2006 through 2020 accentuating the low 1995–2004 creep rate and its resumption to pre-1995 levels following the 2004 Parkfield *M*6 earthquake (see fig. 10). The set of lefthand plots show the comparison using a constant in time scale factor for the telemetered data. The righthand set of plots show the comparison after rescaling the telemetered data due to possible drift in the creepmeter's LVDT. The lower plots show the differences between the micrometer record and the raw and adjusted telemetered data. mm, millimeter.

10-minute intervals to 1-day intervals. However, scatter after 2005.0 cannot be explained by aliasing. One possibility is that after 2005 the scale factor of the LVDT and (or) its associated electronics no longer remained constant. This hypothesis is tested in figure 4*B* where we have rescaled the telemetered data for discrete time intervals, by comparing the raw micrometer measurements with the output voltages of the LVDT, and the amplifier between the LVDT and the telemetry data logger. In this example the tabulation of the raw micrometer measurements provides an in situ sequential suite of calibration data.

Appendix 3 goes into more detail about resolving and calculating the changes in the scale factor used to convert the output of the LVDT into values of slip. For XGH1, it became apparent that the scale factor changed at least twice and two new estimates of sensitivity of the LVDT are used to adjust the XGH1 telemetry-derived creep. The revised scale factor spanning the 2006 to 2014 interval has no visual effect on the differences between the micrometer and the creep data. However, the later adjustment, representing a nearly 50 percent change, has a noticeable effect by removing the apparent drift between the two sets after 2014.

Several of the USGS creepmeters needed adjustment of their scale factors, but none as large as seen for XGH1 (see appendix 3). The scale factors will be noted in the site summaries provided in the site descriptions in appendix 1 and have been applied to the online data archive (USGS Creepmeter data (2022). Some calibration factors have remained remarkably stable—a laboratory re-calibration of the CPP site LVDT after two decades showed the calibration was within 1 percent of its original value.

Data Summary

The data for the past 30-plus years are summarized in ten figures (figs. 5–14) and one table (table 1) that provide time series of creep and creep rates grouped by networks. The most notable events over the past 30 years are (1) the occurrence of the Parkfield, *M*6.0, earthquake in 2004 and its postseismic transient, (2) the installation of five creepmeters on the Hayward Fault in the San Francisco Bay Area, and (3) the gradual reduction in the numbers of creepmeters south of Hollister, CA. Creep rates and a breakdown of the creep budget, between episodic-events versus steady-state creep, are presented in table 1. The rates estimated for each creepmeter have had the change in obliquity factored into the calculation which is discussed in appendix 2. For each creepmeter site, two plots are shown: one showing the creep data (with all artifacts removed) and a second that shows the residuals after

removing both a constant slip-rate and two sinusoids that represent seasonal periodicities. The vertical scaling for these residual plots is roughly the same throughout this section. Although most of the creep data consist of 10-minute samples, these plots use data decimated to intervals between 1 and 4 days. Monthly rainfall data are provided based upon National Weather Service rain gauges and those data are obtained from the California Data Exchange Center (2021, https://cdec.water.ca.gov). The records of rainfall are not necessarily complete. Additional discussion of the seasonal transients is found in appendix 4.

Creep rates are estimated using least squares regression, with the key assumption that the data are temporally correlated, and those correlations can be modeled in the form of a power-law that is related to the frequency content of those data (Langbein, 2004, 2017). Temporal correlations, which are seen on other geophysical data sets (Agnew, 1992), are believed to be produced by a combination of random motions of the monuments and time-varying creep. The model used to characterize temporal correlation has a significant effect on the calculated uncertainties for rate, and less so on the calculated rate. Using site CPP as an example, if it is assumed that these data have no temporal correlations, then the calculated rate is 5.115±0.001 mm/yr. At the other extreme, if it is assumed that these data are temporally correlated over its entire frequency range, then the calculated rate becomes 5.05±1.02 mm/yr with a factor 1,000 difference in the uncertainty. However, additional analysis (Langbein, 2004) of these data suggests that, for periods longer than 5 years, the data become uncorrelated and the calculated rate is 5.12±0.04 mm/yr (table 1).

The breakdown of the slip budget is presented in table 1 under the heading of "Creep Events." Examination of the time series of slip shows that slip occurs over many timescales, from long-term, steady rate of slip, to slip events that can occur in less than one day. To distinguish the events from steady-state slip, a creep event is defined as slip that occurs over one day and that exceeds the long-term slip rate by a factor of 10. For instance, CPP has a slip rate of 6 mm/yr, or 0.016 mm/day. A creep event is identified when the increment of slip over 1 day exceeds 0.15 mm (or about 10× the background rate). The sum of all those events is compared with the total slip accumulated over the entire time series, and the ratio of the two is presented as a percentage in table 1. Note that the data have had the seasonal periodicity removed by fitting one-year and half-year sinusoids. The presence of seasonal trends can artificially increase or decrease the apparent slip rate for any specific time interval. The total accumulated slip is computed in two ways: (1) An arithmetic sum of all successive one-day measures of slip, and (2) An arithmetic sum excluding those days for which slip is negative. For some sites, transient left lateral slip is recorded (typically following heavy rain), which reduces the cumulative offset. This affects the denominator when the percentages in table 1 are computed. Sites such as Shore Road (XSH) are affected where significant episodes of apparent sinistral fault-displacement are recorded, as listed in table 1, where

Table 1. Creep rates and a breakdown of the creep budget for Hayward, Calaveras, and San Andreas Faults, including the area around Parkfield, northern and central California. Creep rates and a breakdown of the creep budget, between episodic-events versus steady-state creep, are presented here. The rates estimated for each creepmeter have had the change in obliquity factored into the calculation which is discussed in appendix 2. Creep events, a breakdown of the slip budget, is defined as slip that occurs over one day and that exceeds the long-term slip rate by about a factor of 10. Total creep, the ratio of the sum of all the creep events is compared with the total slip accumulated over the entire time series. The Parkfield earthquake occurred Sept. 28, 2004 (Langbein and others, 2005). SW, southwest; mm/yr, millimeters per year; eq, earthquake; Site locations and summaries are given in appendix 1.

Site	Rate (mm/yr)	Interval (year)		Creep events			Notes
				Min. event size (mm)	Total creep (%)	Dextral creep (%)	
Hayward Fault							
CPP	5.12±0.04	1995.6	2020.7	0.15	5.9	4.9	
CTM	4.07±0.12	1997.2	2020.7	0.15	2.7	2.4	
COZ	3.53±0.19	1996.8	2020.7	0.15	18.2	11.3	
HWR1	3.98±0.64	1969.4	1988.7	—	—	—	
HWR2	4.10±0.45	1969.4	1995.4	—	—	—	
HWE1	0.91±0.45	1969.4	1995.3	—	—	—	To obtain full rate across double trace here, sum HWE & HWW
HWW1	3.27±0.46	1969.4	1994.8	—	—	—	
HWP1	3.26±0.51	1970.4	1994.0	—	—	—	CHP replaced HWP1 after 1994
CHP	4.22±0.07	1994.2	2020.7	0.15	8.5	4.7	
CHP/HWP1	3.84±0.04	1970.4	2020.7	—	—	—	HWP1 CHP concatenated reveals influence of 1989 Loma Prieta earthquake on Hayward creep
CFW	6.64±0.04	1994.0	2020.7	0.15	41.7	34.2	
Calaveras Fault							
XSH1	9.46±0.41	1971.5	2016.8	0.25	163.9	59.7	Inflated percentage due to sinistral motion
HLC1	5.21±0.28	1970.3	2009.6	—	—	—	

Table 1.—Continued

Site	Rate (mm/yr)	Interval (year)		Creep events			Notes
				Min. event size (mm)	Total creep (%)	Dextral creep (%)	
HLD1	1.53±0.29	1970.3	2008.4	—	—	—	
San Andreas Fault							
NYL	8.87±0.17	2004.2	2012.2	0.25	14.9	7.6	
XSJ	9.02±0.41	1969.4	2016.9	0.25	64.0	45.8	
XHR	11.35±0.49	1970.7	2020.8	0.35	72.0	63.6	
XHR	12.83±0.53	1985.3	2020.7				
CWN1	13.25±0.39	1972.5	2019.5	0.35	68.5	54.5	
CWC3	10.99±0.33	1968.9	1999.0	0.35	78.4	54.2	
XFL1	7.21±0.10	1973.3	1995.2	0.20	36.5	24.5	Incompletely spans the surface fault?
XMR	16.85±0.33	1969.4	2020.7	0.50	50.2	42.6	
MRW1	17.19±0.35	1972.8	2004.8	—	—	—	
XDL2	0.73±0.51	1978.3	2002.1	—	—	—	Missed the fault!
BIT1	16.48.44	1969.5	1995.9	—	—	—	
XMP	14.66.42	1969.4	1997.5	—	—	—	
San Andreas Fault, Parkfield							
XSC	21.30±0.24	1969.4	2020.5	0.50	3.2	2.9	
XSC	19.75±0.57	1980.0	2004.7				Pre-Parkfield eq
XSC	21.21±0.87	2009.0	2020.5	—	—	—	Post-Parkfield eq
XMM	14.98±0.56	1980.0	2004.7	0.40	56.9	45.5	Pre-Parkfield eq
XMM	17.90±0.95	2009.0	2019.4				Post-Parkfield eq
XMD	11.87±1.42	1986.7	2004.7	0.35	73.1	38.1	Pre-Parkfield eq; Inflated percentage due to sinistral motion
XMD	9.60±2.22	2009.0	2020.7				Post-Parkfield eq
XVA	9.18±1.20	1987.4	2004.7	0.25	86.3	45.0	Pre-Parkfield eq; inflated percentage due to sinistral motion
XVA	6.45±1.66	2009.0	2017.8				Post-Parkfield eq
XPK	8.60±0.60	1980.0	2004.7	0.25	62.3	34.9	Pre-Parkfield eq
XPK	9.49±1.46	2009.0	2020.0				Post-Parkfield eq
XTA	9.26±0.49	1986.0	2004.7	0.25	3.0	2.3	Pre-Parkfield eq
XTA	10.19±0.90	2009.0	2020.2				Post-Parkfield eq
WKR	8.05±1.18	1980.2	2004.7	0.20	14.2	8.4	Pre-Parkfield eq
WKR	7.00±1.71	2009.0	2020.7				Post-Parkfield eq
CRR	4.83±0.81	1980.0	2004.7	0.15	92.5	39.7	Pre-Parkfield eq
CRR	2.15±1.93	2009.0	2017.2				Post-Parkfield eq
XGH	2.11±0.47	1980.0	2004.7	—	—	—	Pre-Parkfield eq; inflated percentage due to sinistral motion
XGH	4.96±0.69	2009.0	2020.7	0.15	106.9	43.6	Post-Parkfield eq
C46	3.84±0.10	2004.8	2020.7	0.15	51.0	36.5	Initial data includes minor postseismic afterslip—nominal replacement for X46
X46	0.70±0.34	1986.8	2016.9	0.15	—	37.2	
X46	−0.03±0.65	1986.8	2004.7	—	—	—	Pre-Parkfield eq
X46	0.02±1.60	2009.0	2017.0	—	—	—	Post-Parkfield eq
XRSW	0.04±0.05	1987.4	2005.7	—	—	—	SW trace offset from the San Andreas Fault near Parkfield
XHSW	−0.460.12	1987.5	2010.4	—	—	—	SW trace offset from the San Andreas Fault near Parkfield
San Andreas Fault south of Parkfield							
TWR1	−0.69±0.08	1979.9	2007.5	—	—	—	
XPH1	−0.11±0.01	1977.7	2007.8	—	—	—	

the cumulative slip from creep events may exceed the observed cumulative slip. However, the difference in accounting for cumulative slip becomes less important for most of the Hayward sites where sinistral motion is minor. Consequently, these percentages should be considered upper and lower bounds for the effect of creep events on the total slip budget. When values are provided in appendix 1, we have chosen values that are roughly mid-way between the bounds.

Note that there are other methods to identify the times of creep events. For example, Gittins and Hawthorne (2022) use a template matching scheme to identify creep events, which also allowed them to identify the onset and duration of these events.

Currently unknown is the cause of the apparent, left-lateral slip. Only the length change of a single baseline is measured and any motion that is orthogonal to the fault can manifest itself as a change in the length of the baseline, too. Also, not detectable is whether the change in baseline length is due to fault-slip or due to tilting of the creepmeter monuments from seasonal wetting and drying of the surrounding soils. Langbein and others (1990) noted that some monuments in the Parkfield two-color electronic distance measuring (EDM) network exhibit seasonal tilt. Those monuments were constructed using similar methods to those used by many of the early creepmeters, but importantly, the EDM monuments were exposed at the surface, while the top end of the creepmeter monuments is located below the ground surface and is probably less sensitive to soil expansion.

Hayward Fault

Due to the likelihood of a moderate sized and potentially hazardous earthquake on the Hayward Fault (fig. 1), (Field, 2015), five creepmeters were installed starting in 1993. These instruments are spaced at 15–30 kilometers (km) distances along the fault from Pinole Point in the north to Fremont in the south. It was known from several sets of observations, including cracked sidewalks and streets, alinement array measurements, and older creepmeters, that the Hayward Fault had ongoing surface slip rates averaging between 3 and 6 mm/yr. Despite observed surface creep, both historical seismicity and regional geodetic measurements indicated that the geological slip-rate exceeds the surface fault creep rate. The observed slip since the installation of these instruments is shown in figures 5 and 6. All sites from which these data are derived use the Bilham #1 design. This includes helical piles, usually installed to 8-to 10-m depth, and a 100-mm range LVDT. Initially these used Invar or glass-fiber rods, but the three northern sites have now been provided with carbon-fiber rods. In addition, both CPP and CFW sites include boreholes that have an inclinometer inserted to measure possible deformation at the ends of the creepmeter. Measurements at CFW reveal that the Hayward Fault dips at 70° to the west as the borehole intersects the fault at 21-m depth (Bilham and Whitehead, 1997). These have been remeasured as recently as 2021 and show slip at depth is similar to surface creep with minor surface deformation above the fault at depth. As of 2000, the 6-m boreholes at CPP did not reveal any detectable tilt but have not been measured since then.

Although observed rates of creep vary by a factor of two over the past three decades, the secular creep rate at each site has remained constant to within ±1 mm/year (fig. 6). The highest rate of creep is observed at the fault's southern end, CFW (6.5 mm/yr), with the lowest rate at the central creepmeter, COZ (3.2 mm/yr), located in west Oakland. Seasonal variations are present with an amplitude of approximately 1 mm/yr. Figure 6 shows the residuals (difference between observed and predicted) after removing both the secular rate and two sinusoidal terms representing annual and semi-annual variations. At all sites, the residual departure from a linear slip rate at 1-to-10-year periods (≈5 mm) exceeds these seasonal terms.

Of special interest in these residuals is the observation of distinct increases in rate between 2005 and 2008 at CTM and COZ south of Berkeley (concave-up residuals in figure 6), and a distinct decrease in rate at about the same time at CHP, Hayward (concave down residual).

At CFW, periods of episodic slip occur, where, over the period of a day or two, the creep rate is substantially greater than the background rate. Accelerations in creep rate at COZ, and less so at CTM, follow local moderate earthquakes (moment magnitude [M_w] ≤4). These can be distinguished from creep events by their longer duration with characteristic decay time constants of several weeks. We provide additional observations centered at COZ in appendix 5. A nearby borehole tensor-strainmeter shows the same transient behavior as the creepmeter. As listed in table 1, episodic creep accounts for 40 percent of the total slip measured at CFW, which is at least twice the amount seen at the other four sites along the Hayward Fault.

The CHP creepmeter is a replacement for the older HWP creepmeter at the same location. CHP uses helical piles as monuments replacing the original monuments for HWP but due to constraints at the site it retained the same 45° obliquity to the fault. Interestingly, the combined time series for that site extends back to 1970 (see CHP in appendix 1) and clearly shows the response of the Hayward Fault to the Loma Prieta earthquake in 1989. Following the earthquake, the rate of creep decreased until 1997 when the rate surged for about 10 years, after which it resumed its approximate pre-1989 rate (Lienkaemper and others, 1997). Because CHP was only installed in 1995, the time series shown in figure 6 does not show strong evidence of the decrease in slip after the Loma Prieta earthquake.

Table 2 provides a comparison between the creep rates measured by the creepmeters since the mid-1990s (except for the CHP/HWP combination) and the alinement arrays located closest to each creepmeter. Note that there are two listings for each alinement array creep rate, one listed by McFarland and others (2016), and a second estimate using the data through 2018 which also incorporates temporal correlations (Langbein, 2004) in each time series of slip measurements. Factoring in correlated noise tends to increase the uncertainty in rates by a factor of 3 over the McFarland and others (2016) calculations. Comparisons between the revised estimate of rate from the alinement arrays and the

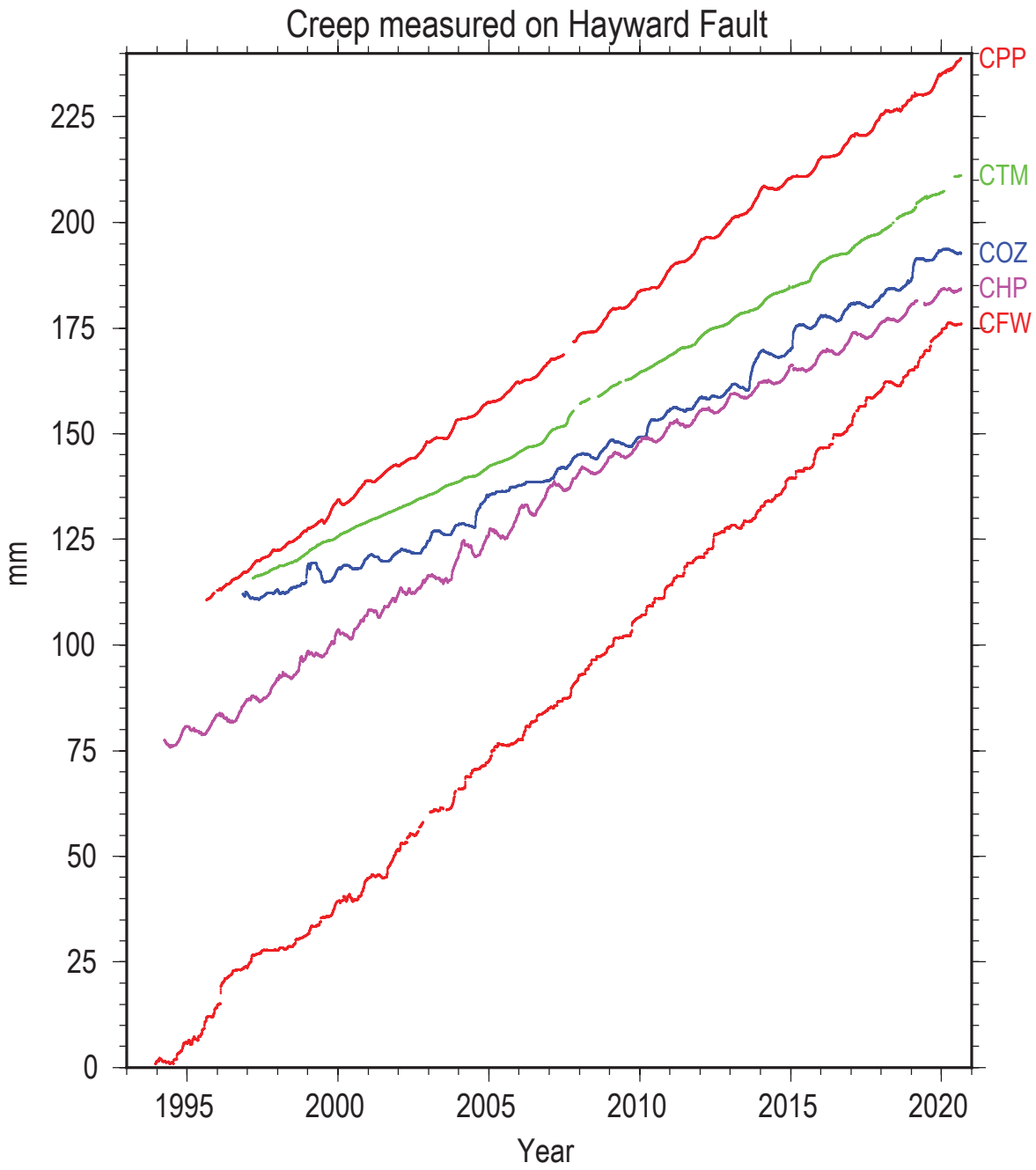

Figure 5. Plots of the cumulative creep measured at five sites on the Hayward Fault in the San Francisco Bay Area, California. From the top to the bottom of the plots, the data are shown from north (CPP, Pinole Point) to the south (CFW, Fremont). CTM, Temescal; COZ, Oakland Zoo; CHP, City of Hayward, Palisade St. See appendix 1 for locations and summaries of sites. mm, millimeter.

creepmeters does not show any significant difference except in the case of CHP and the HPAL alinement array. Those measurements indicate that the CHP rate is too low by 1 mm/yr (~25 percent), presumably because its fault-normal aperture is insufficient to span a strand of the fault located about 30 m west of the creepmeter. The motion of the secondary strand is captured by the alinement array.

One interesting observation is the presence of the diurnal and semi-diurnal load tides recorded by the northernmost creepmeter, CPP, acting as a strainmeter. This is discussed in appendix 6. Of all the creepmeters discussed in this report, CPP is the closest (within 0.5 km) to the shoreline of San Francisco Bay.

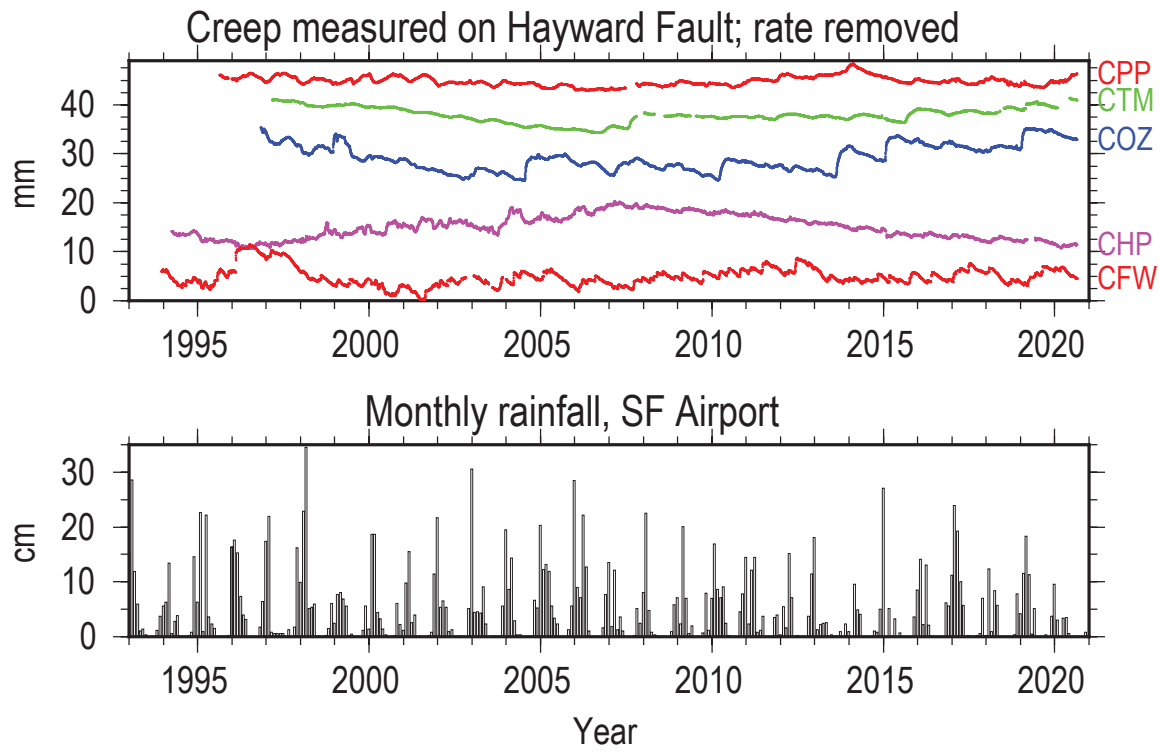

Figure 6. The plots show the residual variations after a linear trend or rate, and seasonal sinusoids have been removed Hayward Fault, California. The rainfall record from the San Francisco Airport is provided. CPP, Pinole Point; CTM, Temescal; COZ, Oakland Zoo; CHP, City of Hayward, Palisade St.; CFW, Fremont; mm, millimeter; cm, centimeter. Monthly rainfall from California Data Exchange Center, (2021). See appendix 1 for locations and summaries of sites.

Table 2. Comparison of creepmeter and neighboring alignment array rates for the Hayward Fault, northern and central California. The CHP creepmeter is a replacement for the older HWP creepmeter at the same location. Note that there are two listings for each alignment array creep rate, one listed by McFarland and others (2016), and a second estimate using the data through 2018 which also incorporates temporal correlations (Langbein, 2004) in each time series of slip measurements. CPP, Pinole Point; CTM, Temescal; COZ, Oakland Zoo; CHP, City of Hayward, Palisade St.; CFW, Fremont. Creepmeter and their nearby alignment array locations and site summary in appendix 1. mm/yr, millimeters per year; km, kilometers; m, meter.

Creepmeter	Rate, (mm/yr)	Alignment array	Distance from creepmeter (km)	Length of array, (m)	Years of observation	Rate[1] (mm/yr)	Rate[2]; correlated noise, (mm/yr)
CPP	5.12±0.04	HCCC	2.6	142	35.1	5.2±0.1	5.0±0.3
CTM	4.07±0.12	HTEM	0.6	154	41.5	4.3±0.1	4.3±0.3
COZ	3.53±0.19	HENC	0.15	124	26.1	2.5±0.1	3.2±0.3
CHP	4.22±0.07	HPAL	0.0	132	38.7	4.9±0.2	4.7±0.5
CHP/HWP1	3.84±0.04						
CFW	6.64±0.04	HRKT	1.3	103	36.0	5.4±0.1	5.6±0.3
		HHAN	0.9	89	33.7	6.4±0.2	6.1±0.4
		HUNI	0.5	168	22.7	6.5±0.1	6.6±0.1
		HPIN	1.7	98	26.5	7.6±0.3	7.6±0.8

[1]McFarland and others, 2016.

[2]Langbein, 2004.

Calaveras Fault—Hollister

Three creepmeters measure surface slip on the southern Calaveras Fault in the Hollister area (figs. 7 and 8). Although initial observations were frequent, manual measurements were reduced after the mid 1990s to about once per year. Except for the Shore Road creepmeter (XSH), which was revived in 2020, sites within the city of Hollister no longer operate. The long-term rates for these three sites averaged 9.5 mm/yr for XSH, 5.2 mm/yr for Hollister Central (HLC), and 1.5 mm/yr for Hollister D Street (HLD). Both the plots in figures 7 and 8 indicate that all three of these creepmeters were affected by the 1989 Loma Prieta earthquake, as the rates decreased immediately following that earthquake. Although XSH appears to have resumed its long-term average slip rate by the mid-1990s, the other two meters continued to exhibit slip rates substantially less than their pre-Loma Prieta rates. Table 1 lists episodic creep at XSH as contributing more than 100 percent to the total slip. This "anomaly" is caused by including transient sinistral slip in the cumulative slip. If sinistral slip is suppressed in the cumulative record, the contribution of episodic creep falls to 60 percent. A possible interpretation of the Shore Road creepmeter (XSH) behavior is that *all* the observed fault slip occurs during episodic events, between which the surface fault is locked, and the creepmeter measures soil expansion and contraction associated with flooding and desiccation of a stream ≈7 m north of the eastern anchor. Schulz (1989) provided more information on these sites. On p.107 of that report a typo states incorrectly that the XSH creepmeter operates in contraction across the fault (it acts in extension).

San Andreas Fault—San Juan Bautista

Over the past 30 years, 11 creepmeters have been operating on the central San Andreas Fault from San Juan Bautista to just north of Parkfield, Calif. (fig. 1). (The Parkfield network is discussed below.) Of those instruments, only three have remained in operation with continuous telemetry. A fourth site, San Juan Bautista (XSJ), remained operational until 2017 when the site was destroyed by farming operations. A fifth site, San Juan—Nyland (SJN), has had intermittent operation. Table 1 lists the average creep rates for all 11 instruments from the north to the south.

At the north end for SJN and XSJ creep averages about 9 mm/yr, then increases southward to 12 to 13 mm/yr at Harris Ranch (XHR) and Cienega Winery North (CWN). Suspiciously, it decreases to 7 mm/yr at Frank Lewis Long (XFL), suggesting that this instrument may incompletely span the fault. Consequently, this site was abandoned. A few km to the south, Melendy Ranch (XMR) and Melendy Windmill (MRW) record 17 mm/yr slip, followed by a very suspicious 0.5 mm/yr of slip at Dry Lake Long (XDL) (Schulz, 1989); XDL has also been abandoned. The next two sites, Bitterwater (BIT) and Monarch Peak (XMP), both record slip averaging around 15 mm/yr. The pattern of the above rates is shown in

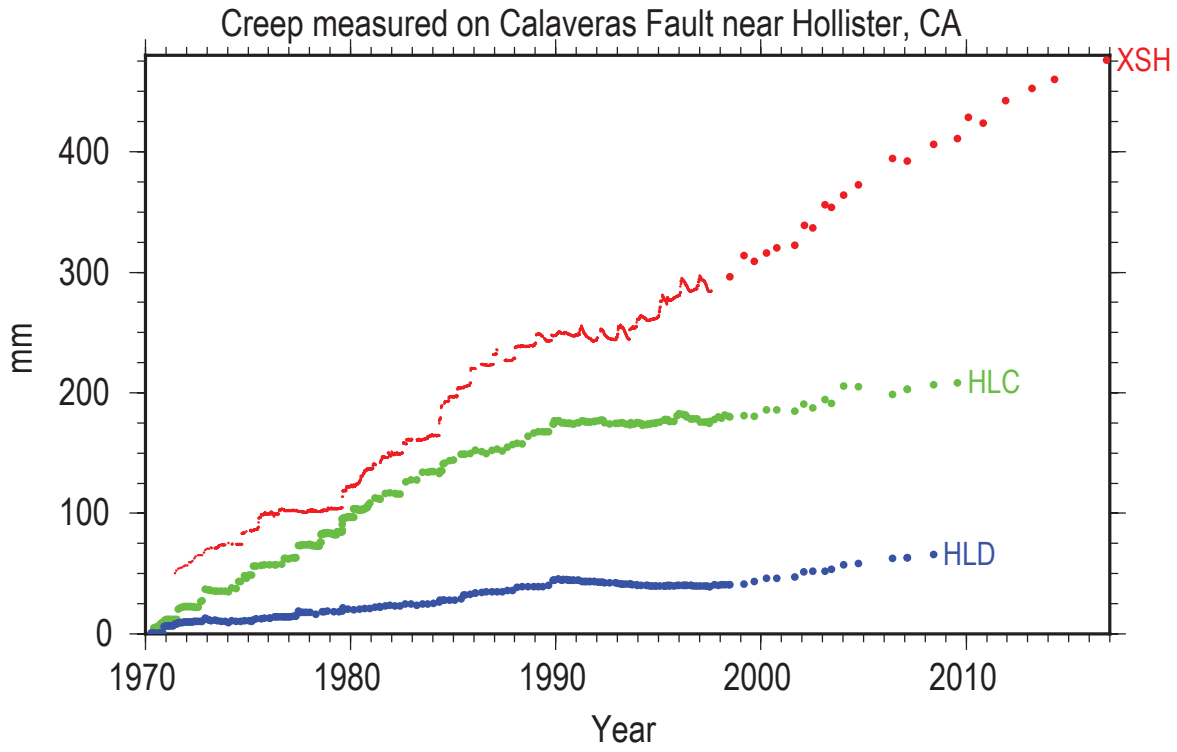

Figure 7. Plot showing the record of surface slip on the Calaveras Fault near Hollister, California. Except for the Shore Road creepmeter (XSH) which was revived in 2020, sites within the city of Hollister no longer operate. Manual measurements were reduced after the mid-1990s to about once per year. HLC/HLD, Hollister—Central and D Street; mm, millimeter. See appendix 1 for locations and summaries of sites.

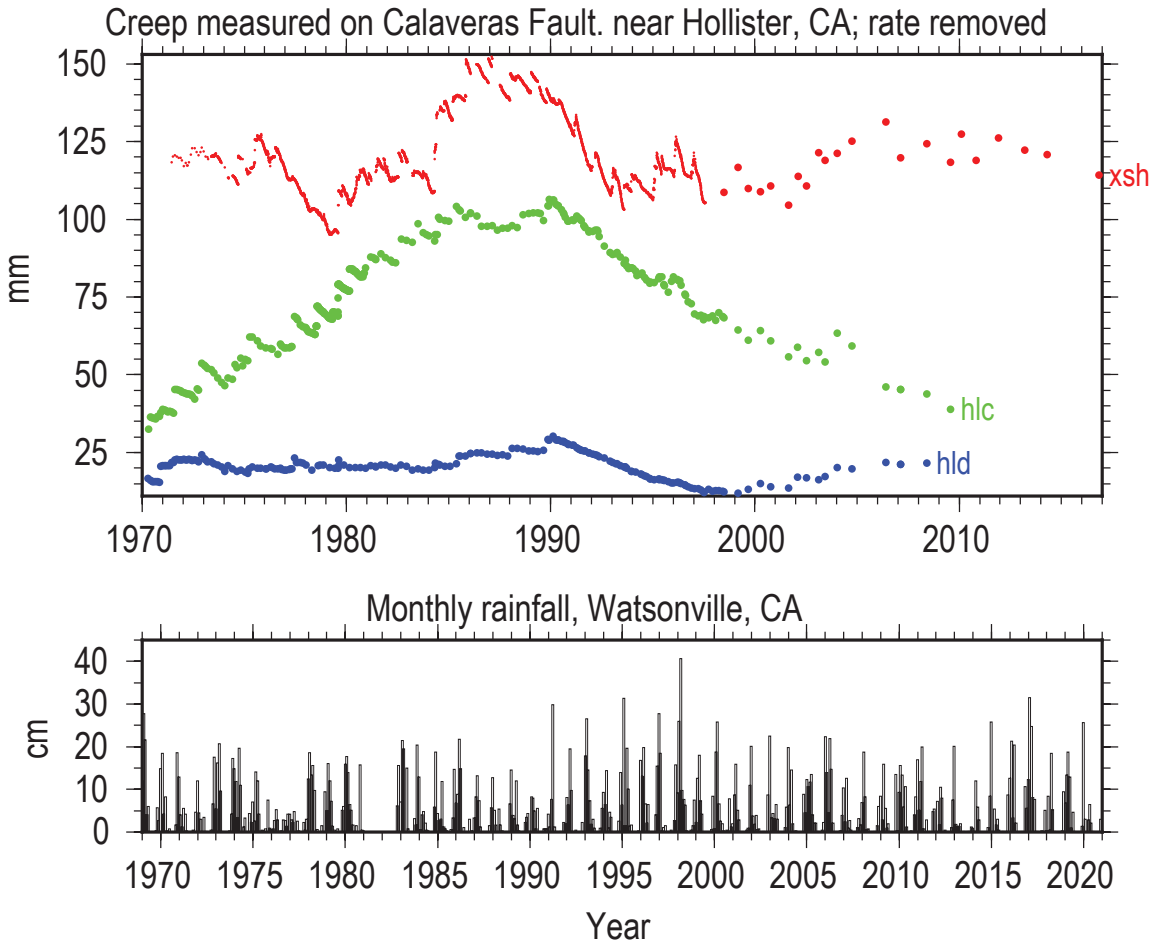

Figure 8. Plots showing the variations in slip after removing a linear trend and seasonal periodicities from the data shown in figure 7 for the Calaveras Fault near Hollister, California. The rainfall record (California Data Exchange Center, 2021) is from Watsonville, California, located 40 kilometers (km) west of Hollister. Manual measurements were reduced after the mid-1990s to about once per year. The Hollister creepmeters no longer operate. Monthly rainfall from California Data Exchange Center (2021. XSH, Shore Road; HLC/HLD, Hollister—Central and D Street; cm, centimeter; mm, millimeter. See appendix 1 for locations and summaries of sites.

the creepmeter data plotted in figure 9. The five northernmost sites (SJN, XSJ, XHR, CWN, and XMR) have been monitored using telemetry with 10-minute observations, while the remaining six sites have only had manual observations which ceased in the mid-1990s. A brief analysis of propagation directions and velocities between creepmeters XMR, CWN, XHR, and XSJ between 1996 and 2006 are available in appendix 7. Figure 10 shows the creep data with the long-term trend and seasonal periodicities removed. With the higher magnification from the detrended time series with frequent observations, the short periods of accelerated creep spanning about one day are seen as a rapid, sawtooth pattern. Except for SJN and XFL, it is apparent that episodic creep is significant, >50 percent of the total slip measured by the creepmeters for this segment. In addition, there are longer term variations with amplitudes of up to 25 mm, which contrasts with the 5 mm amplitude variations seen on the Hayward creepmeters.

The detrended time series for XSJ, XHR, and CWN show some long period transients correlated from nearby earthquakes. These earthquakes, two located near San Juan Bautista and occurring in 1972 and 1995, and the 1989 Loma Prieta earthquake all affected the creep measurements causing an increase in slip rate (fig. 10). In addition, the creep rates at these three sites prior to the 1989 Loma Prieta earthquake are low relative to the current rates.

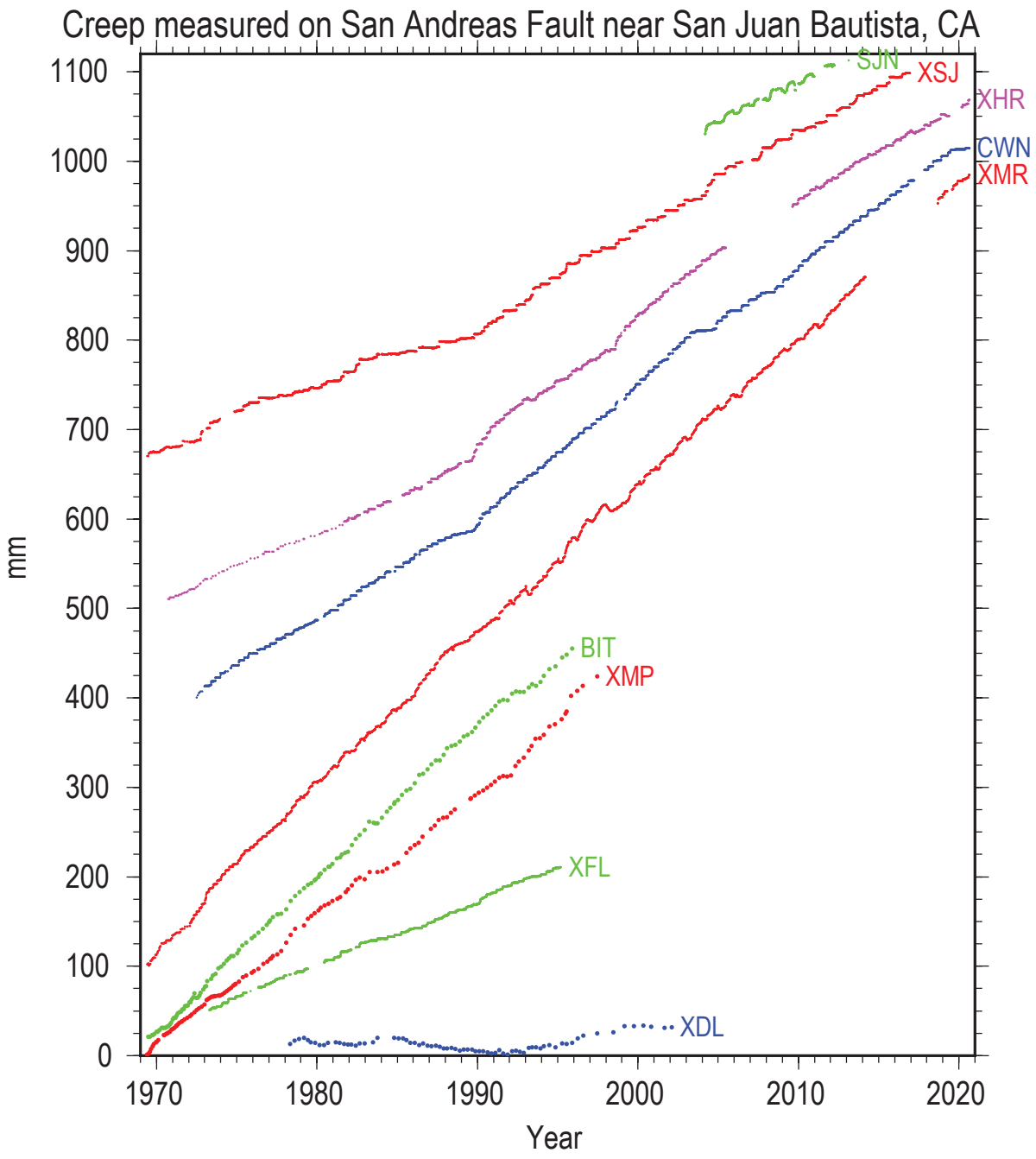

Figure 9. Plot showing the record of surface slip on the central San Andreas Fault from San Juan Bautista to north of Parkfield, California. SJN, Nyland Ranch; XSJ, San Juan Bautista; XHR, Harris Ranch; CWN, Cienega Winery North; XMR, Melendy Ranch, BIT, Bitterwater; XMP, Monarch Peak; XFL, Frank Lewis Long; XDL, Dry Lake Long. See appendix 1 for locations and summaries of sites.

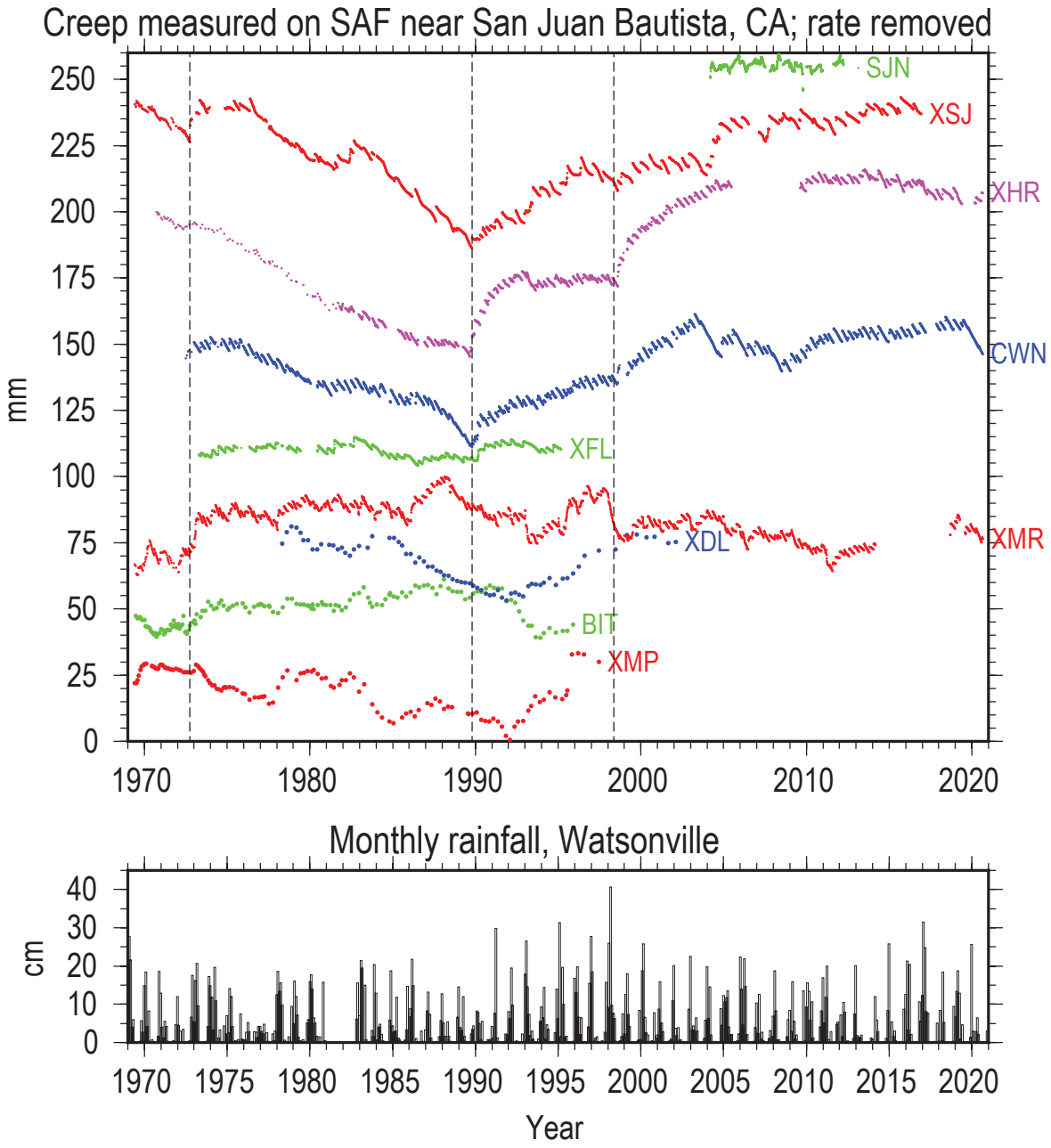

Figure 10. Plots showing the variations in slip after removing a linear trend and seasonal periodicities from the data shown in figure 9, on the central San Andreas Fault (SAF) from San Juan Bautista to north of Parkfield, California. The rainfall record is from Watsonville, CA, located 40 kilometers (km) west of Hollister. Notable changes in creep rate correspond to times of local earthquakes; 1989 M6.9 Loma Prieta, 1972 *M*4.9, and 1998 *M*5.1 San Juan Bautista earthquakes. The times of these events are shown with thin, dashed lines. SJN, Nyland Ranch; XSJ, San Juan Bautista; XHR, Harris Ranch; CWN, Cienega Winery North; XFL, Frank Lewis Long; XMR, Melendy Ranch; XDL, Dry Lake Long; BIT, Bitterwater; XMP, Monarch Peak. Monthly rainfall from California Data Exchange Center (2021). cm, centimeter; mm, millimeter. See appendix 1 for locations and summaries of sites.

San Andreas Fault—Parkfield

In the mid-1980s, the USGS increased the number of creepmeters to twelve on the Parkfield section of the San Andreas Fault in anticipation of a repeat of the 1966 *M*6 earthquake (Bakun and McEvilly, 1984). In 2004, a *M*6 earthquake did occur on this section of the San Andreas and most of the creepmeters showed significant amounts of slip, both during and after the earthquake. Those observations and resulting models have been discussed by Langbein and others (2006). In summary, coseismic offsets were recorded at nearly all the creepmeters, and within hours of the main shock the postseismic slip exceeded the range of these instruments.

Consequently, the data from those sites are missing, and manual measurements have been used to estimate the amount of slip during the interval when the instruments were off scale. At one site, Parkfield (XPK), the Invar wire broke causing an unrecoverable offset in the time series. Plots of the data spanning the interval between 1985 and 2020 are shown in figures 11 to 14. The plots illustrate the data in three forms: (1) observed fault slip (figs. 11 and 14), (2) fault slip detrended by a 1985–2004 linear slip rate (fig. 12), and (3) finally fault slip with a synthetic afterslip decay curve removed (fig. 13). The afterslip decay curve starts at the time of the 2004 earthquake and is defined by Omori's Law or $A\log(1+t/\tau)$ where τ=1-day (for example, Langbein and others, 2006). To facilitate plotting, including figure 11, a coseismic offset has been removed. For the eight central creepmeters (Middle Mountain [XMM] to Gold Hill [XGH]) the large (~10-cm) postseismic transient prominent in figures 11 and 12 is suppressed in figure 13.

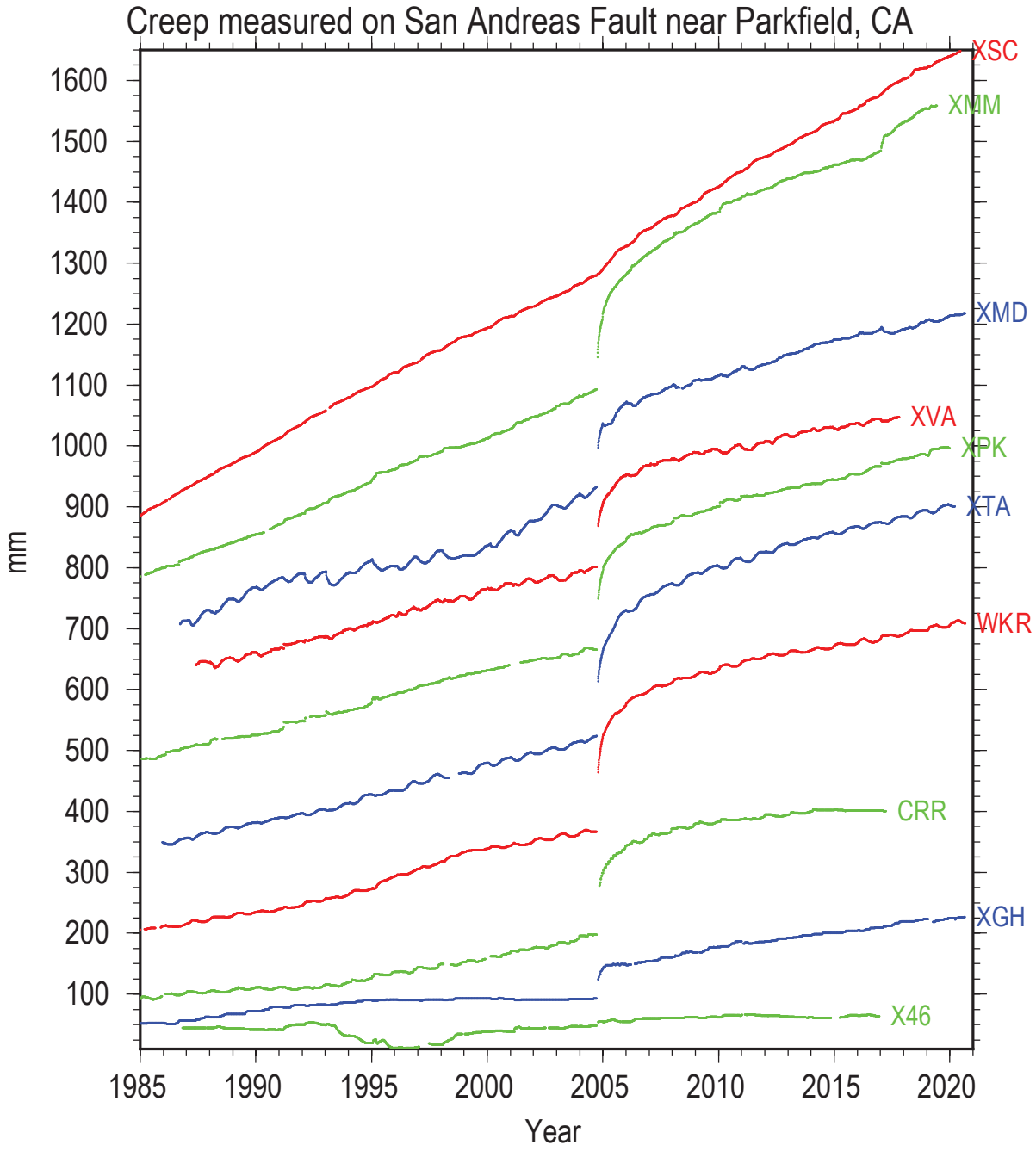

Figure 11. Plot of thirty-six years of creepmeter data for the Parkfield segment of the San Andreas Fault, California. This plot illustrates the observed fault slip. The Parkfield M6 Earthquake occurred September 28, 2004 (Langbein and others, 2005; U.S. Geological Survey, 2017). Coseismic offsets from that earthquake have been removed from this plot. XSC, Slacks Canyon; XMM, Middle Mountain; XMD, Middle Ridge; XVA, Varian; XPK, Parkfield; XTA, Taylor Ranch; WKR, Work Ranch; CRR, Carr Ranch; XGH, Gold Hill; X46, Highway 46; mm, millimeter. See appendix 1 for locations and summaries of sites.

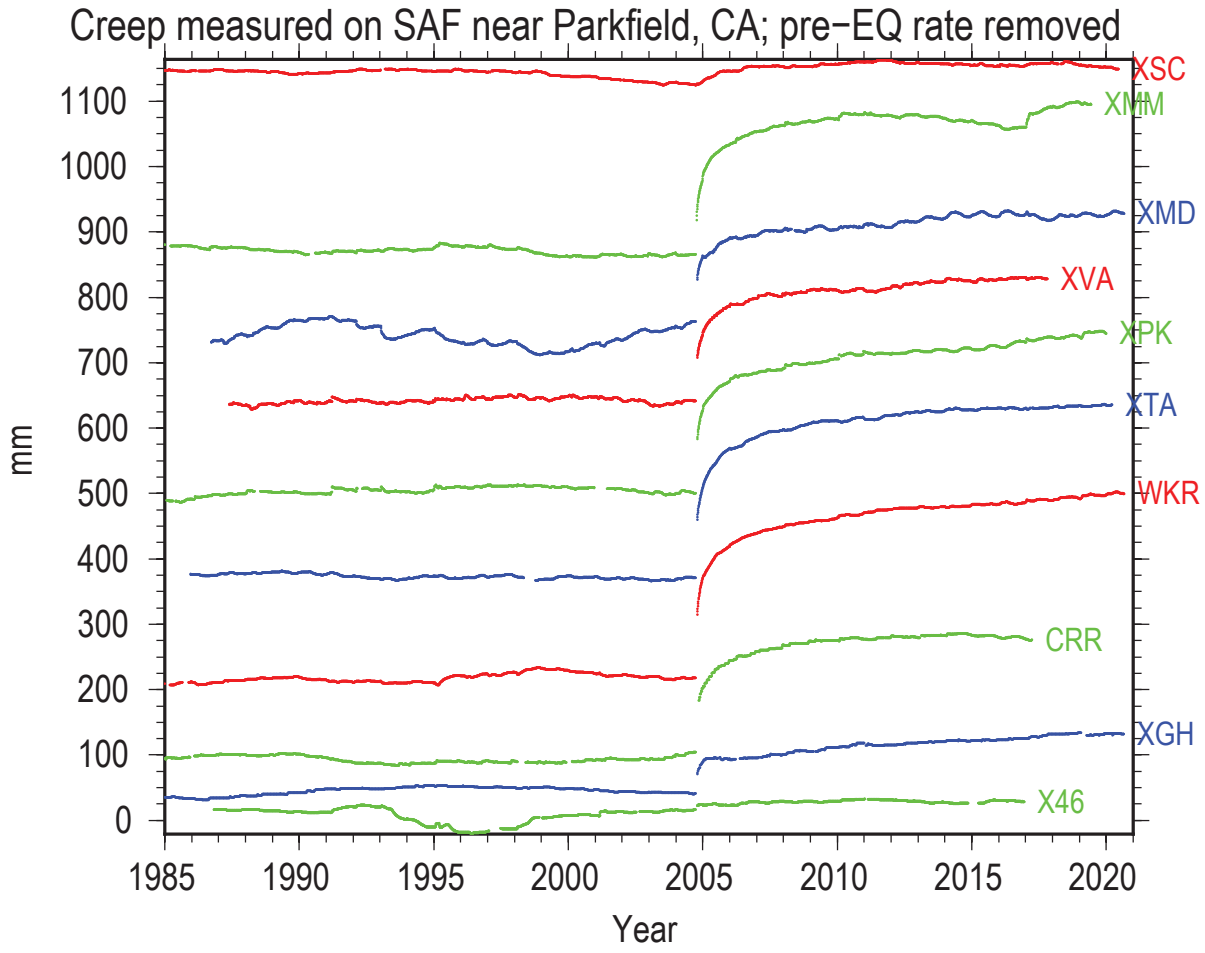

Figure 12. Graph of thirty-six years of creepmeter data for the Parkfield segment of the San Andreas Fault (SAF), California. The Parkfield M6 Earthquake occurred September 28, 2004. Data as in figure 11, but the secular trend 1985 to 2004 has been removed from the observed data. XSC, Slacks Canyon; XMM, Middle Mountain; XMD, Middle Ridge; XVA, Varian; XPK, Parkfield; XTA, Taylor Ranch; WKR, Work Ranch; CRR, Carr Ranch; XGH, Gold Hill; X46, Highway 46; mm, millimeter. See appendix 1 for locations and summaries of sites.

Of the nine creepmeters near Parkfield (Slacks Canyon [XSC] to Gold Hill [XGH]), six exhibit a significant portion of their slip budget, >50 percent, as episodic creep events (table 1). The exceptions are XSC, Taylor Ranch (XTA), and Work Ranch (WKR), where creep events only contribute less than 15 percent to the total creep.

Located near many of the creepmeters in Parkfield are borehole strainmeters. At times, the creep events are detected on both creepmeters and strainmeters. An example of one such event is discussed in appendix 5.

Figure 14 shows the creep data for five sites either located near Parkfield; Highway 46 (C46), Hearst SW Trace (XHSW) and Roberson SW Trace (XRSW); or south of Parkfield on the San Andreas' Carrizo Plain segment, TWR and XPH. The site C46 is located just north of Highway 46 (X46) (figs. 11–13) but was installed immediately following the 2004 Parkfield earthquake. In late 2010, C46 was upgraded as discussed in the site description for this site in appendix 1. Both XRSW and XHSW are on the southwest trace of the San Andreas Fault in Parkfield; this trace is offset by 1 km to the west of the main trace of the fault. During the 2004 earthquake, XRSW measured a coseismic offset but no postseismic deformation. A nearby creepmeter coWT, located ~10 km southeast of XHSW, recorded 10 mm of afterslip on this trace in the month following the earthquake (Bilham, 2005). XRSW later caved-in and was abandoned. XHSW was abandoned due to lack of any obvious motion on the SW trace.

Both TWR and Panorama Hills (XPH) are located between 45 and 110 km southeast of Parkfield and measure any surface deformation at the fault and can capture any creep on the San Andreas Fault that may occur, though so far, they exhibit none.

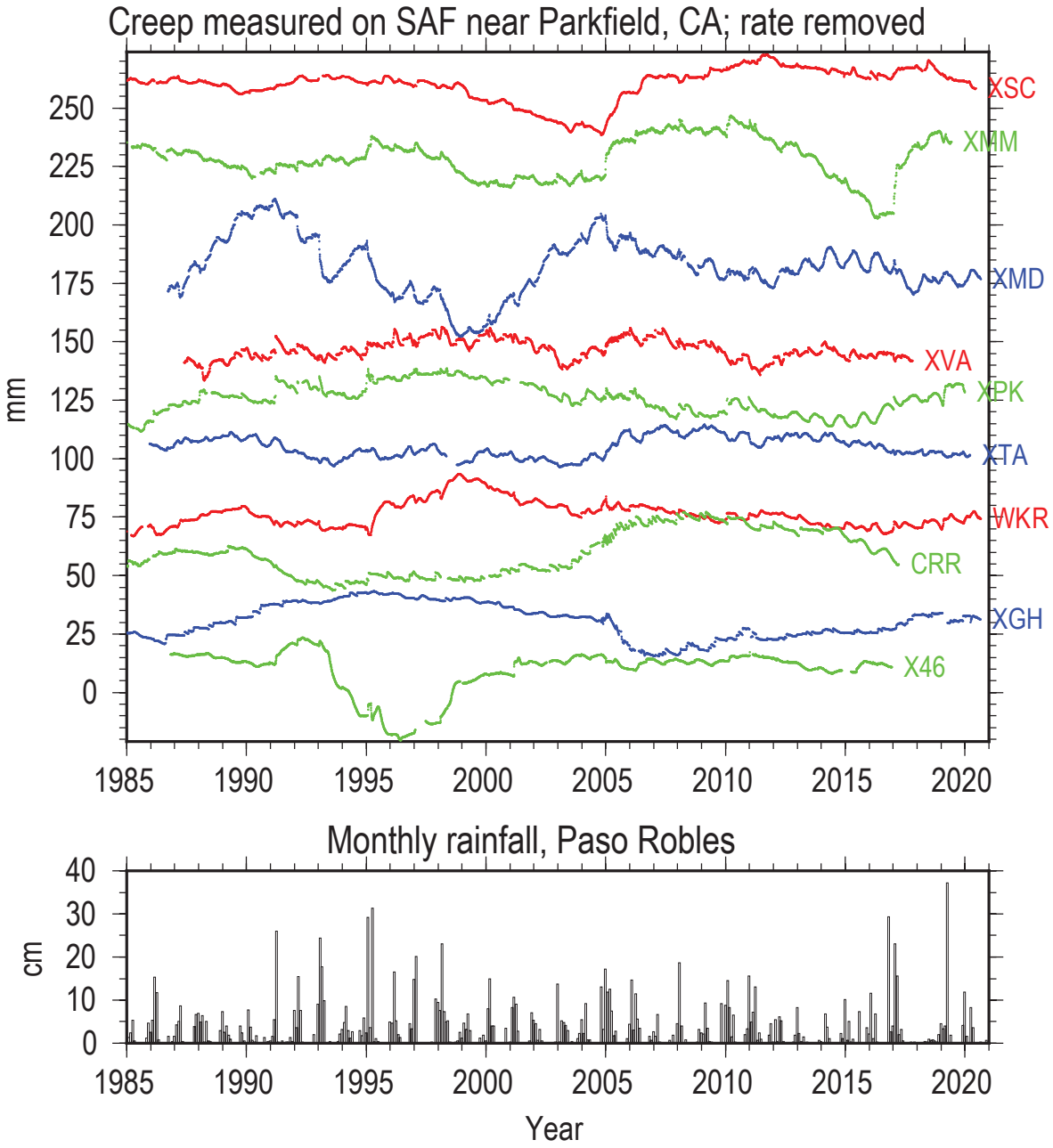

Figure 13. Graphs of thirty-six years of creepmeter data and rainfall for the Parkfield segment of the San Andreas Fault, California. The Parkfield M6 Earthquake occurred September 28, 2004. Same data as in figures 11 and 12 but now with synthetic afterslip suppressed computed for the Parkfield earthquake from Omori's Law (Langbein and others, 2006). Rainfall data recorded at Paso Robles, 40 kilometers (km) west of Parkfield are shown in the lower plot (California Data Exchange Center, 2021). XSC, Slacks Canyon; XMM, Middle Mountain; XMD, Middle Ridge; XVA, Varian; XPK, Parkfield; XTA, Taylor Ranch; WKR, Work Ranch; CRR, Carr Ranch; XGH, Gold Hill; X46, Highway 46. See appendix 1 for locations and summaries of sites. cm, centimeter; mm, millimeter.

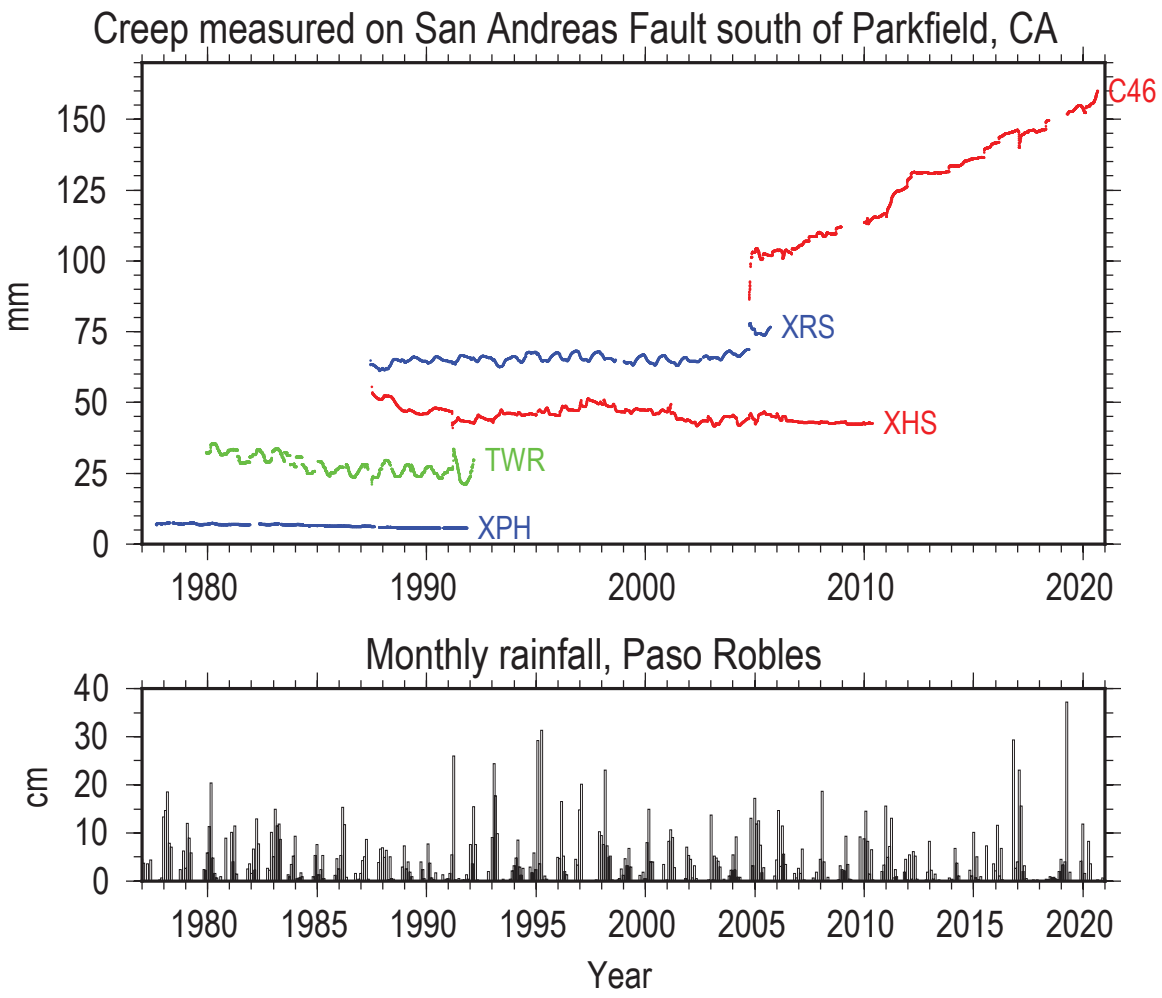

Figure 14. Graphs of creep data and rainfall for sites near and south of Parkfield, California. This plot illustrates the observed fault slip. This figure shows the creep data for five sites either located near Parkfield; C46, XHS(W) and XRS(W), or south of Parkfield on the San Andreas' Carrizo Plain segment; TWR and XPH. C46, Highway 46; XRSW, Roberson SW Trace; XHSW, Hearst SW Trace; TWR, Twisselman Ranch; XPH, Panorama Hills. See appendix 1 for locations and summaries of sites. Monthly rainfall from California Data Exchange Center (2021). cm, centimeter; mm, millimeter.

Parkfield Postseismic Creep

As shown in figures 11 and 12, the most significant perturbation to long-term slip rates within the Parkfield network was associated with the 2004 *M*6.0 Parkfield earthquake. Postseismic deformation data for creep, borehole strain, and global positioning system (GPS) are discussed by Langbein and others (2006), which included data only through mid-2005, or 0.6 years following the Parkfield earthquake. With an additional 15 years of observations, we provide some reanalysis of the creepmeter data.

Afterslip represents the response of the fault zone to the stress changes accompanying rupture, either on the mainshock rupture plane, or possibly on the contiguous regions of the fault along-strike or up-dip. Once started, the slip process decays rapidly with time and a rule-of-thumb observation is that the process obeys a logarithmic decay in amplitude. Thus, as much surface afterslip occurs in the first hour as in the next 10 hours, as in the next 4 days, and so on as illustrated in figure 15. Most of the creepmeters went off-scale in the first hour and were not set on scale again until after 2 days, thereby losing a part of the afterslip curve where typically low environmental noise prevails. Three creepmeter records, however, continued operation through this gap (low resolution rupture meters).

If we consider the time intervals depicted in figure 15 as seven observational "octaves" suited to constraining theoretical afterslip curves, then, for three sites we have all seven octaves of data (or seven orders of magnitude). We note that the eighth "octave" would include a recurrence of the earthquake, so that in practice we have reached a natural limit in our ability to characterize afterslip. In the analysis below we note also a further practical limitation associated with the increase in random and seasonal noise much beyond octave five. Our analyses also provide insights as to how afterslip might be better constrained following a future Parkfield earthquake. The next earthquake is anticipated to occur 2026–2032 (Guo, 2021).

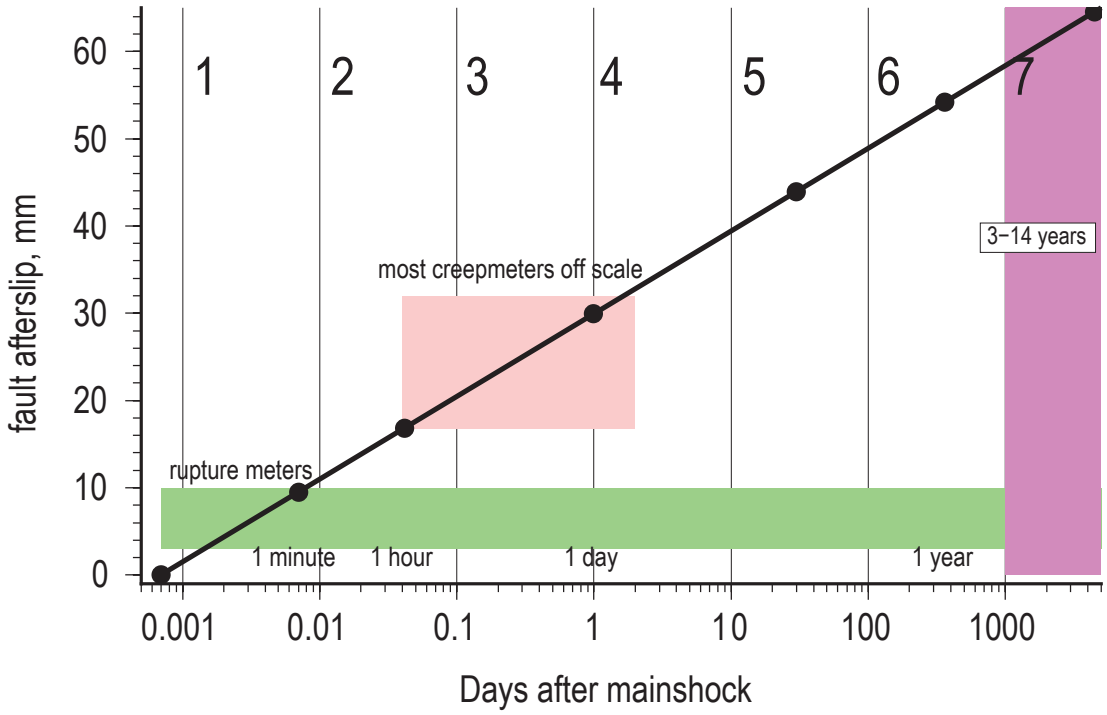

Figure 15. Plot of synthetic log-linear curve illustrating the decay in surface afterslip with time, Parkfield area, California. The Parkfield *M*6 Earthquake occurred September 28, 2004. Three rupture meters captured coseismic slip and afterslip with low resolution (green shading), but most creepmeters went off-scale soon after the mainshock until they were mechanically reset after a few days (red shading). The numbered time intervals (1–7) represent approximately equal increments in surface slip. Thus, the first 3 "octaves" in slip were recorded with low resolution, and previous analyses were largely based on afterslip recorded in intervals 4–6. The analysis presented here extends the previous analysis into the violet zone 7, a substantial fraction of the Parkfield earthquake cycle.

Although few physically based models for afterslip have been formulated (Marone and others, 1991), several empirical functions suited to modeling surface afterslip have been proposed. The primary empirical function is related to Omori's Law, in which the rate of deformation decays as $1/t$ (Utsu and others, 1995). This is typically modified to $1/t^{p}$ by introducing an index, ρ. To prevent the function from becoming indefinite at t=0, a 1 is inserted into the denominator which suggests that τ becomes the delay time following the initiation of afterslip. Integrating to provide deformation as a function of time (t) yields what is termed the modified Omori's Law:

$$\frac{A}{1-p}\left[(1+(t-T_{eq})/\tau)^{1-p}-1\right] \qquad (1)$$

where

$\frac{A}{1-p}$ is the final amplitude of slip, and

T_{eq} is the time of the earthquake.

Although the modified Omori's Law has numerous empirical applications, notably, earthquake aftershock sequences, Montési (2004) has provided a physical justification based upon a one-dimensional, spring and slider block-model using a ductile creep-law for materials.

Another empirical function has been developed to characterize alignment array measurements of fault slip following earthquakes (Boatwright and others, 1989). This function, termed "*After*" describes slip at time, t, after the mainshock in the form:

$$A\left[\frac{(t-T_{eq})/\tau}{(t-T_{eq})/\tau+1}\right]^{p} \qquad (2)$$

where

A represents the asymptotic final value for slip.

Lienkaemper and others (2006) have used this relationship to characterize their alignment array measurements following the 2004 Parkfield earthquake. The significance of the exponent, p, and the time constant, τ, differ between the modified Omori function and *After*. For the exponent, the values differ by 1. For the time constant, the modified Omori function describes the delay between the time of the earthquake and the beginning of rapid postseismic deformation. On the other hand, the value of τ in *After* is the characteristic time when postseismic deformation

ceases. In part, the development of *After* was driven by the lack of measurements of slip immediately following an earthquake since alignment array observations require field visits and, unlike creepmeter data, don't use telemetry to obtain rapid autonomous measurements.

Another function that has been used to describe a relaxation process is an exponential decay. That has been generalized to be a stretched exponential, discussed by Mignan (2015) and references within. This function has the form

$$A(1-e^{-(t-T_{eq})^p/\tau}) \quad (3)$$

When p=1, this becomes a standard exponential decay with a time constant of τ.

To better characterize both the delay for the onset of postseismic slip used in the modified Omori function, and the cessation of slip provided by *After*, a hybrid function can be introduced, termed the double Omori function

$$(1+(t-T_{eq})/\tau_1)^{1-p}-1-\left(\frac{\tau_2}{\tau_1}\right)^{1-p}\left((1+(t-T_{eq})/\tau_2)^{1-p}-1\right) \quad (4)$$

The first half of the double Omori function is a repeat of the modified Omori law with a delay time of τ_1 (equation 1). The second half introduces a second time constant, τ_2, which could be termed a relaxation time when postseismic deformation ceases.

The four functions described above are fit to creepmeter data for the sites XMM1, XMD1, XVA1, XPK1, XTA1, WKR1, CRR1, and XGH1, which all show significant postseismic slip. The results of these fits are plotted in appendix 1 in the site description for each creepmeter. Three plots of the data are shown: a plot showing the entire record length of the creepmeter, and two other plots focusing on the different intervals spanning the earthquake; the first being a 57-day interval after the earthquake, and a second being a 7-day interval after the earthquake.

In detail, we use only the data spanning the 1985.0 to 2020.5 interval to fit these functions, neglecting prior data. A rate is estimated for the pre-earthquake interval, which is removed from the observations. Ideally, all 10-minute samples would be used in the regression, but that would encompass more than 10^6 observations, which, when using a data covariance that incorporates temporal correlations, would be infeasible to invert. Instead, the time series is divided into three segments: a short time series using the 10-minute samples spanning a 10-day interval between day of year, 270 and 280 (Sept. 26, 2004, and Oct. 6, 2004, or 2.7 days before and 7.3 days after the mainshock). A second time series was created by decimating the data from 10-minute to 1-hour samples for two intervals, one from day 260 to 270 of year 2004, and another from 280 to 330. The last time series, using typically 3-day sampling, was created which spanned the 1985 to 2020 interval, with the 60-day interval spanning the earthquake removed. In addition to fitting each of the four functions, the coseismic offset and two sinusoids of 365.25- and 182.625-day periods are simultaneously fit to the data. The sinusoids represent seasonal modulation of the creepmeter data. Note, as stated above, the rate defined by the pre-earthquake interval had been removed prior to the curve-fitting.

For all creepmeters, except for XGH1, the combination of the coseismic offset and initial postseismic slip caused these meters to exceed the range of the LVDT. Consequently, the initial 1.5 to 2 days of measurements following the earthquake were lost, apart from data recorded at a few locations in the hours immediately following the mainshock. The poor sampling of measurements in the first day after the earthquake impairs our ability to estimate the delay time, τ, or τ_1, in either the modified Omori or double Omori functions. However, at two sites, XMM1 and XTA1, additional low-resolution sensors recorded slip in parallel with the LVDT and those data have been inserted to recover the missing observations. In addition, a prototype rupture meter (Bilham, 2005), was operated adjacent to WKR1, called coWKR and that instrument stayed on scale during the mainshock and initial surface afterslip. Twelve days of data from coWKR (day 268 to 280) were used to fill the missing data in the WKR1 record, but to do so it was necessary to increase the scale factor of the coWKR data by a factor of 2.8 since this instrument incompletely spanned the fault zone. The necessity for this scaling is illustrated in Bilham (2005, his figure 2) which shows that the coWKR meter captures about 50 percent of the total slip relative to the combination of coWKR and its western extension, coWKRW, that was added about 2 weeks following the Parkfield mainshock. In turn, the combination of the coWKR east and west, captures 70 percent of that observed at WKR1.

The effect of using data covariance that incorporates temporal covariance is significant. For the time series using 3-day sampling and incorporating the long-term creep, the covariance makes allowance for "drift" characterized by power-law noise, in these data without necessarily penalizing the overall fit (Langbein, 2004). On the other hand, the short-term, 10-minute data are not severely affected by "drift" but are more affected by the white noise component or least-count noise of 0.01 mm. Although the long-period data have the same least-count noise, the apparent higher precision of the short-term, high-rate data, will tend to over-weight these data relative to the longer-term data. Consequently, an *ad hoc* weighting scheme is used where the amplitudes of the noise components of the 1-hour data are multiplied by 5 and, for the 10-minute data, the amplitudes are multiplied by 20.

Except for XTA1, which visually and numerically shows good agreement, none of the four models fully capture the postseismic deformation since 2005. Quantifying the fit in terms of reduction of variance due to the postseismic function in table 3, there is a 77 percent variance reduction for XTA1 when all its data are considered; the next closest in terms of variance reduction is 56 percent and 34 percent for XMM1 and XGH1, respectively. For XTA1, the double Omori function has a 77.7 percent reduction in variance, followed by *After* at 77.6 percent, with the stretched exponential and modified Omori with 77.5 percent and 77.0 percent. Table 3 shows two entries for WKR, one that uses only WKR1 data, and a second entry that substitutes coWKR data for the 12-day period spanning the mainshock. The addition of coWKR improves the fit as measured by the reduction of variance, from 18.6 percent using only WKR1 to 50.1 percent when coWKR is added. The improved fit results from the availability of early afterslip data.

Table 3. Percent reduction of variance from four functions representing postseismic slip associated with the September 28, 2004, *M*6.0 Parkfield earthquake, Parkfield, California (Langbein and others, 2005). Bold script indicates "best fit" function. An empirical function developed to characterize alignment array measurements of fault slip following earthquakes (Boatwright and others, 1989) termed "After" describes slip at time, *t*, after the mainshock. The stretched exponential is discussed by Mignan (2015) and references within. A prototype rupture meter (Bilham, 2005), was operated adjacent to WKR1, called coWKR. XMM, Middle Mountain; XMD, Middle Ridge; XVA, Varian; XPK, Parkfield; XTA, Taylor Ranch; WKR, Work Ranch, CRR; Carr Ranch; XGH, Gold Hill. See appendix 1 for locations and summaries of creepmeter sites.

Creepmeter Site	Modified Omori	Double Omori	After function	Stretched exponential
XMM	56.8	**56.9**	56.1	56.3
XMD	**3.4**	**3.4**	3.3	3.3
XVA	3.5	**3.6**	**3.6**	**3.6**
XPK	10.1	10.1	10.1	10.1
XTA	77.0	**77.7**	77.6	77.5
WKR	**18.6**	**18.6**	18.5	18.4
WKR + coWKR	49.0	**50.0**	**50.1**	49.9
CRR	**8.5**	**8.5**	7.8	7.9
XGH	**34.1**	**34.1**	33.3	33.4

However, at Middle Ridge (XMD) and XVA all the postseismic functions show a minimal, 3 percent, variance reduction. These two sites show significant "drift" (appendix 1) that are not modeled by any of the simple functions used here. A better model would incorporate a change in rate as the residual trend suggests that the current slip rate is less than the pre-earthquake rate.

In conclusion, although all these functions provide a basic characterization of the postseismic period, there is no single function that is clearly the best choice. The absence of data in the first 2 days following the earthquake impairs the accuracy with which the delay term, τ, in the Omori function can be constrained. The recognition of this shortcoming was one of the reasons for introducing large-range rotary sensors along the Hayward Fault since these are designed to capture both coseismic slip and afterslip exceeding 1 m. In addition, the variability of secular creep rates makes it difficult to define a function that fits these data except for XTA1 which seems to have fewer and (or) smaller decadal to annual transients.

Yet, at four sites, XMM1, XTA1, WKR1, and XGH1, by adding the lower resolution creepmeter data to fill in the missing observations, the Omori delay times are 2 hours, 10 minutes, 10 minutes, and 2 hours, respectively, for these four sites. It is possible that the longer delay time observed at XMM1 is due to friction in the low-resolution sensor such that the measured slip lags the actual slip. At XGH1, there was no detectable coseismic slip and there was a delay of 2 hours before the deeper, postseismic slip propagated to the surface at this site.

Finally, we recognize that aftershocks from the Parkfield mainshock must be expected to initiate local afterslip decay processes, either by enhancing the original mainshock stress adjustment, or by initiating new minor afterslip decay curves in contiguous parts of the fault zone. Subsurface afterslip and aftershocks were observed to evolve in concert following the 2004 mainshock (Jiang and others, 2021). These subsequent afterslip initiation events are effectively superimposed on the primary afterslip curve that we have assumed here to represent a simple stress release process and may be responsible for some of the misfits we have identified.

Discussion

The results presented here update the information provided more than 30 years ago by Schulz (1989). The U.S. Geological Survey (USGS) creepmeter network has grown in the San Francisco Bay Area to measure slip on the Hayward Fault but has shrunk in the area south of the San Francisco Bay Area.

In 2004 the Parkfield earthquake occurred and fault-afterslip was measured on the 11 creepmeters of the network of instruments located along the San Andreas Fault. Both coseismic and postseismic slip were measured, but unfortunately, resolving the complete history of slip immediately after the Parkfield mainshock was impaired since most of the creepmeters went off scale shortly after the mainshock (Langbein and others, 2006). The recent development of rupture meters, discussed above, with sufficient range to capture coseismic slip and afterslip to high precision provides methods to capture the afterslip process in its entirety.

Table 1 within this report provides an updated list of creep rates that also account for the variability of slip rates over shorter time scales. In addition, creep variations occur over several timescales. For many of the sites, a significant portion of the slip occurs as short bursts over short periods, on the order of one day. For the Hayward creepmeters, this episodic creep is only a minor contribution to the total slip. For sites south of the San Francisco Bay Area, primarily

along the San Andreas Fault, episodic creep is a significant portion of the total slip for roughly one-half of those sites.

Even though almost one-half century of creep data exist, there are still questions that are unresolved. A short list follows:

- How deep does episodic creep extend? Hundreds of meters, or kilometers? Probably the best place to resolve that question is from the Parkfield network where there are borehole strainmeters located nearby. Gittins and Hawthorne (2022) have compiled a comprehensive catalog of creep events that are common to neighboring sites which could provide the signal needed to be measured by the strainmeters.
- Does the fault zone dilate during creep, and, if so, what are the timescales of these dilatational trends? Recently, at a few sites additional sensors have been installed to measure the dilation or fault perpendicular displacements. Convergence of the fault zone is manifest as an apparent reversal in slip direction in oblique sensors in the network. Minor opening or closing of the fault zone resulting from moisture changes in clay gouge is recorded as noise in the creep signal.
- Some sites record apparent left-lateral slip, especially during the winter rainy season. Is the fault, which over the long-term slips in a right-lateral sense, truly reversing in slip direction? One possibility (apart from fault zone convergence mentioned above), for example, is that dextral slip on a subparallel fault is briefly activated, which relaxes or reverses the shear strain applied to the fault strain monitored by the creepmeter. It is also possible that the monuments used with creepmeters where reversals are common are tilting when the ground is wet.
- How fast do creep events propagate laterally or vertically along the fault? An analysis of creep events south of Hollister reveals that they propagate in both directions at rates of approximately (~) 2 kilometers per hour (km/hour).
- The locations of creepmeters were guided by detailed alignment array measurements using the methods of Burford and Harsh (1980) and (or) damage to infrastructures such as echelon pavement cracks. However, detailed mapping of the nearby geologic structures that might also accommodate fault slip has not been done. This could be accomplished using a combination of light detection and ranging (lidar) imagery (available via https://opentopography.org) and on-site, mobile laser scanning surveys (Brooks and others, 2013). In addition, near surface geophysical measurements including seismic reflection methods and resistivity surveys could quantify the properties of the ground adjacent to the creepmeter.

Note that creepmeters are best suited for answering the temporal nature of creep. Spatial data, which comes from interferometric synthetic aperture radar (InSAR) (for example, Scott and others, 2020), GPS (for example, Lindsey and others, 2014), and (or) alignment arrays (for example, Burford and Harsh, 1980), provide the constraints to the overall slip budget and the locations of high versus low slip regions both along strike and at depth. In turn, there are obvious questions about the material properties of the fault and its surroundings that facilitate aseismic slip or not.

References Cited

Agnew, D.C., 1992, The time-domain behavior of power-law noises: Geophysical Research Letters, v. 19, no. 4, p. 333–336, accessed June 07, 2011, at https://doi.org/10.1029/91GL02832.

Bakun, W. H., and McEvilly T.V., 1984, Recurrence models and Parkfield, California, earthquakes, Journal of Geophysical Research, v. 89, no. B5, p. 3051–3058, accessed June 1, 1988 at doi:10.1029/JB089iB05p03051.

Bilham, R., and Whitehead, S., 1997, Subsurface creep on the Hayward Fault, Fremont, California: Geophysical Research Letters, v. 24, no. 11, p. 1307–1310, accessed September 10, 2021, at https://doi.org/10.1029/97GL01244.

Bilham, R., 2005, Coseismic strain and the transition to surface afterslip recorded by creepmeters near the 2004 Parkfield epicenter: Seismological Research Letters, v. 76, no. 1, p. 49–57, accessed June 3, 2022, at https://doi.org/10.1785/gssrl.76.1.49.

Boatwright, J., Budding, K., and Sharp, R.V., 1989, Inverting measurements of surface slip on the Superstition Hills Fault: Bulletin of the Seismological Society of America, v. 79, no. 2, p. 411–423, accessed October 10, 2021, at https://doi.org/10.1785/BSSA0790020411.

Burford, R.O., 1988, Retardations in fault creep rates before local moderate earthquakes along the San Andreas fault system, Central California: Pure and Applied Geophysics, v. 126, no. 2, p. 499–529, accessed April 8, 2022, at https://doi.org/10.1007/BF00879008.

Burford, R.O., and Harsh, P.W., 1980, Slip on the San Andreas Fault in central California from alinement array surveys: Bulletin of the Seismological Society of America, v. 70. no. 4, p. 1233–1261, https://doi.org/10.1785/BSSA0700041233.

California Data Exchange Center, 2021, California Data Exchange Center—Precipitation: California Department of Water Resources, California Data Exchange Center website, accessed January 2, 2021, at https://cdec.water.ca.gov.

Field, E.H., 2015, UCERF3—A new earthquake forecast for California's complex fault system: U.S. Geological Survey Fact Sheet 2015–3009, accessed February 7, 2024, at https://doi.org/10.3133/fs20153009.

Gittins, D.B., and Hawthorne, J.C., 2022, Are creep events big? Estimations of along-strike rupture lengths: Journal of Geophysical Research Solid Earth, v. 127, no. 1, accessed September 13, 2021, at https://doi.org/10.1029/2021JB023001.

Guo, G., 2021, Fibonacci sequence found in Parkfield earthquake: International Journal of Geosciences, v. 12, no. 1, 5 p., accessed July 29, 2022, at https://doi.org/10.4236/ijg.2021.121001.

Jiang, J., Bock, Y., and Klein, E., 2021, Coevolving early afterslip and aftershock signatures of a San Andreas Fault rupture: Science Advances, v. 7, no. 15, 15 p., accessed July 29, 2022, at https://doi.org/10.1126/sciadv.abc1606.

Langbein J., 2004, Noise in two-color electronic distance meter measurements revisited: Journal of Geophysical Research Solid Earth, v. 109, no. B4, 16 p., accessed November 14, 2007, at https://doi.org/10.1029/2003JB002819.

Langbein, J., Borcherdt, R., Dreger, D., Fletcher, J., Hardebeck, J.L., Hellweg, M., Ji, G., Johnston, M., Murray, J.R., Nadeau, R., Rymer, M.J., Treiman, J.A., 2005, Preliminary Report on the 28 September 2004, M 6.0 Parkfield, California Earthquake: Seismological Research Letters, v. 76, no. 1, p. 10–26, accessed June 1, 2006 at https://doi.org/10.1785/gssrl.76.1.10.

Langbein, J., 2010, Computer algorithm for analyzing and processing borehole strainmeter data: Computers and Geosciences, v. 36, no. 5, p. 611–610, accessed April 13, 2013, at https://doi.org/10.1016/j.cageo.2009.08.011.

Langbein, J., 2017, Improved efficiency of maximum likelihood analysis of time series with temporally correlated errors: Journal of Geodesy, v. 91, no. 8, p. 985–994, accessed September 1, 2017, at https://doi.org/10.1007/s00190-017-1002-5.

Langbein, J., Burford, R.O., and Slater, L.E., 1990, Variations in fault slip and strain accumulation at Parkfield, California—Initial results using two-color geodimeter measurements, 1984–1988: Journal of Geophysical Research Solid Earth, v. 95, no. B3, p. 2533–2552, accessed December 20, 2020 at https://doi.org/10.1029/JB095iB03p02533.

Langbein, J., Murray, J.R., and Snyder, H.A., 2006, Coseismic and initial postseismic deformation from the 2004 Parkfield, California, Earthquake, observed by global positioning system, electronic distance meter, creepmeters, and borehole strainmeters: Bulletin of the Seismological Society of America, v. 96, no. 4B, S304–S320, accessed November 9, 2007, at https://doi.org/10.1785/0120050823.

Langbein, J., Wyatt, F., Johnson, H., Hamann, D., and Zimmer, P., 1995, Improved stability of a deeply anchored geodetic monument for deformation monitoring: Geophysical Research Letters, v. 22, no. 24, p. 3533–3536, accessed May 10, 2010, at https://doi.org/10.1029/95GL03325.

Lienkaemper, J.J., Baker, B., and McFarland, F.S., 2006, Surface slip associated with the 2004 Parkfield, California, earthquake measured on alinement arrays: Bulletin of the Seismological Society of America, v. 96, no. 4B, p. S239–S249, accessed August 23, 2005, at https://doi.org/10.1785/0120050806.

Lienkaemper, J.J, Galehouse, J.S., and Simpson, R.W., 1997, Creep response of the Hayward Fault to stress changes caused by the Loma Prieta earthquake: Science, v. 276, no. 5321, p. 2014–2016, accessed October 1, 2023, at https://doi.org/10.1126/science.276.5321.2014.

Linde, A.T., Gladwin, M.T., Johnston, M.J.S, Gwyther, R.L., and Bilham, R.G, 1996, A slow earthquake sequence on the San Andreas fault: Nature, v. 383, no. 6595, p. 65–68, accessed October 1, 2023, at https://doi.org/10.1038/383065a0.

Marone, C.J., Scholtz, C.H., and Bilham, R., 1991, On the mechanics of earthquake afterslip: Journal of Geophysical Research Solid Earth, v. 96, no. B5, p. 8441–8452, accessed July 29, 2022, at https://doi.org/10.1029/91JB00275.

McFarland, F.S., Lienkaemper, J.J., and Caskey, S.J., 2016, Data from theodolite measurements of creep rates on San Francisco Bay Region faults, California (ver. 1.8, March 2016): U.S. Geological Survey Open-File Report 2009–1119, 21 p., and data files, accessed May 26, 2020, at http://pubs.usgs.gov/of/2009/1119/.

Mignan, A., 2015, Modeling aftershocks as a stretched exponential relaxation: Geophysical Research Letters, v. 42, no. 22, p. 9726–9732, accessed February 8, 2016, at https://doi.org/10.1002/2015GL066232.

Montési, L.G.J., 2004, Controls of shear zone rheology and tectonic loading on postseismic creep: Journal of Geophysical Research Solid Earth, v. 109, no. B10, 18 p., accessed January 13, 2006, at https://doi.org/10.1029/2003JB002925.

Schulz, S.S., 1989, Catalog of creepmeter measurements in California from1966 through 1988: U.S Geological Survey Open File Report 89–650, 139-p. pamphlet, 4 pl., accessed April 5, 2019, at https://doi.org/10.3133/ofr89650.

Schulz, S., and Burford, R.O., 1978, Installation of an Invar wire creepmeter, Elkhorn Valley, California, August 1977: U.S Geological Survey Open-File Report 78–203, 42 p., accessed October 3, 2023, at https:/doi.org/10.3133/ofr78203.

Schultz, S.S., Mavko, G.M. Burford, R.O., and Stuart, W.D. 1982, Long-term fault creep observations in Central California; Journal of Geophysical Research Solid Earth. v. 87, no. B8, p. 6977–6982, accessed March 21, 2017, at https://doi.org/10.1029/JB087iB08p06977.

Scott, C., Bunds, M., Shirzaei, M., and Toke, N., 2020, Creep along the central San Andreas Fault from surface fractures, topographic differencing, and InSAR: Journal of Geophysical Research Solid Earth, v. 125, no. 10, 16 p., article e2020JB019762, accessed January 21, 2021, at https://doi.org/10.1029/2020JB019762.

Steinbrugge, K.V., and Zacher, E.G., 1960, Creep on the San Andreas fault—Fault creep and property damage: Bulletin of the Seismological Society of America, v. 50, no. 3, p. 389–396, accessed October 3, 2023, at https://doi.org/10.1785/BSSA0500030389.

Tocher, D., 1960, Creep rate and related measurement at Vineyard, California: Bulletin of the Seismological Society of America, v. 50, no. 3, p. 396–404, accessed October 3, 2023, at https://doi.org/10.1785/BSSA0500030389.

USGS Creepmeter data, 2022, Earthquake Hazards Program, Download data for creepmeters, accessed February 7, 2022, at https://earthquake.usgs.gov/monitoring/deformation/data/download.php.

U.S. Geological Survey Earthquake Hazards Program, 2017, Advanced National Seismic System (ANSS) Comprehensive Catalog of Earthquake Events and Products: various, accessed February 1, 2024, at https://doi.org/10.5066/F7MS3QZH.

Utsu, T., Ogata, Y., and Matsu'ura, R.S., 1995, The centenary of the Omori formula for a decay law of aftershock activity, Journal of Physics of the Earth, v. 43, p. 1–33, accessed February 9, 2024, at https://doi.org/10.4294/jpe1952.43.1.

Appendix 1. Site Summaries for Creepmeter Sites for the Hayward, Calaveras, and San Andreas Faults in Northern and Central California

The following provides an update to the site catalog from Schulz (1989). The U.S. Geological Survey's (USGS's) creepmeter network monitors aseismic, surface slip at various locations on the Hayward, Calaveras, and San Andreas Faults in northern and central California. For sites that are listed in Schulz (1989), this summary will provide a plot of the data and updates on changes that could affect the analysis of these observations. For sites that were installed after Schulz (1989), more detail on the site conditions is provided along with plots of the data and other observations that could affect the analysis of these observations. The listing is from north to south starting with Pinole Point—Hayward Fault (CPP) and ending with Panorama Hills—San Andreas Fault (XPH) (fig. 1 in the main text). In most cases, the estimated creep rate is provided (table 1 in the main text), as well as the percentage of total slip that can be considered a creep events. That value is the average of the two listed in table 1.

Note that the active creepmeters on the Hayward Fault also have a rupture meter described as Bilham #2 sensor. These sensors were installed in 2014 primarily to record large creep transients (multiple centimeters [cm] to meters [m]) and with the second sensor, smaller displacements. In addition to the telemetered data at 1 sample per minute, a local recorder at each site records data at a 1 hertz (Hz) sampling rate, with enough memory for 11 days of recording. Due to the experimental nature of these sensors, the data from the rupture meters are not discussed other than being noted in the site summaries.

The data from these creepmeters, along with a few discontinued instruments are presented in this appendix can be downloaded from (USGS Creepmeter data, 2022). Data entries include a short summary of changes that might affect the data, periodic manual measurements, and in most cases, two sets of time series, one that provides 10-minute sampled data, and the second that provides 1-day sampled data. In many cases, the daily sampled data extend further back in time than the 10-minute data. In a few cases, there are only daily data available. The files are formatted in ASCII with each record containing the time of the observation and the cumulative value of creep in millimeters (mm). Time consists of year and day of year. The creep data use the obliquity listed in the site descriptions provided below. In addition, the data have been adjusted for changes in the sensitivity of the electro-mechanical sensor (typically a linear voltage displacement transformers/transducer [LVDT]) as discussed in the main text and detailed in appendix 3. Site locations for creepmeters that have not been active since about 2000 are approximate and are taken from plotting their locations on digital topographic maps using the maps provided by Schulz (1989). Otherwise, the site locations are from a handheld global positioning system (GPS), which should be accurate to about 10 m.

CPP Pinole Point—Hayward Fault
Location: 37.9895° N., 122.3559° W.
Orientation: 30°, 2-m depth; initially Invar, After January 12, 2020, 5 mm diameter carbon fiber; 30-m length. LVDT sensor
LVDT sensitivity: 10.167 mm/volt
Sample interval: 10 minutes but changed to 1 minute in late 2019;
Creep rate: 5.12±0.04 mm/yr
Percentage of creep that occurs in discrete events: 5%

The site was installed in 1995 in Point Pinole Regional Park, California. The monuments at each end consist of two inclined helical piles driven to 8-m depth and a vertical 6.5-m tube whose deformation can be measured by lowering an inclinometer. From the last inclinometer measurement in 2005, there was no detectable tilt or flexure of the vertical tubes. In 2014, a second sensor, initially called a rupture meter, was installed to better capture slip from the anticipated coseismic deformation of a Hayward Fault earthquake. Those sensors, described above as Bilham #2, have been upgraded from using potentiometers to Hall-effect sensors. In addition, rather than attaching the sensors to the sides of the vault, the sensors are now attached, along with the LVDT, to the helical-pile monument. With the recent installation, there are two sensors that measure displacement with having one low-resolution used to capture large displacements, and the second having a high-sensitivity sensor to measure small displacements along with the LVDT.

Creep at this site is relatively steady, averaging 5.12±0.04 mm/yr. Deviations from the long-term trend are within roughly 3 mm. The creepmeter acts as a strainmeter and records the tidal load strain from San Francisco Bay (appendix 6). Operationally, the site has experienced excessive electronic noise related to the long cable between the sensors and its telemetry. Various mitigation measures, both through processing and onsite modifications, have reduced the noise. When possible, the telemetry logger may be moved closer to the sensor.

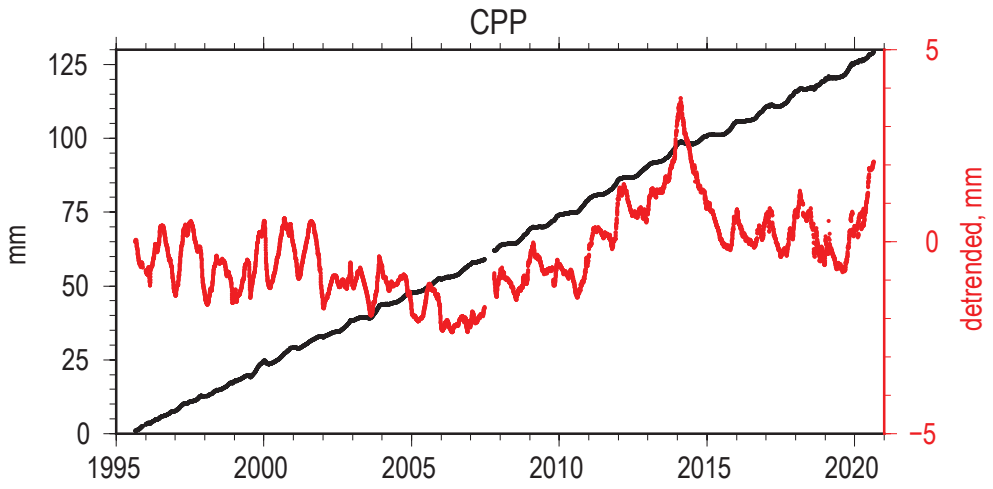

Figure 1.1. Plot showing the observed values of right-lateral slip at the Pinole Point (CPP) creepmeter, located on the Hayward Fault near Pinole Point, California. The black is the long-term trend, while the red is the residual after removing a constant rate and seasonal sinusoids (365.25- and 182.625-day periods). mm, millimeter.

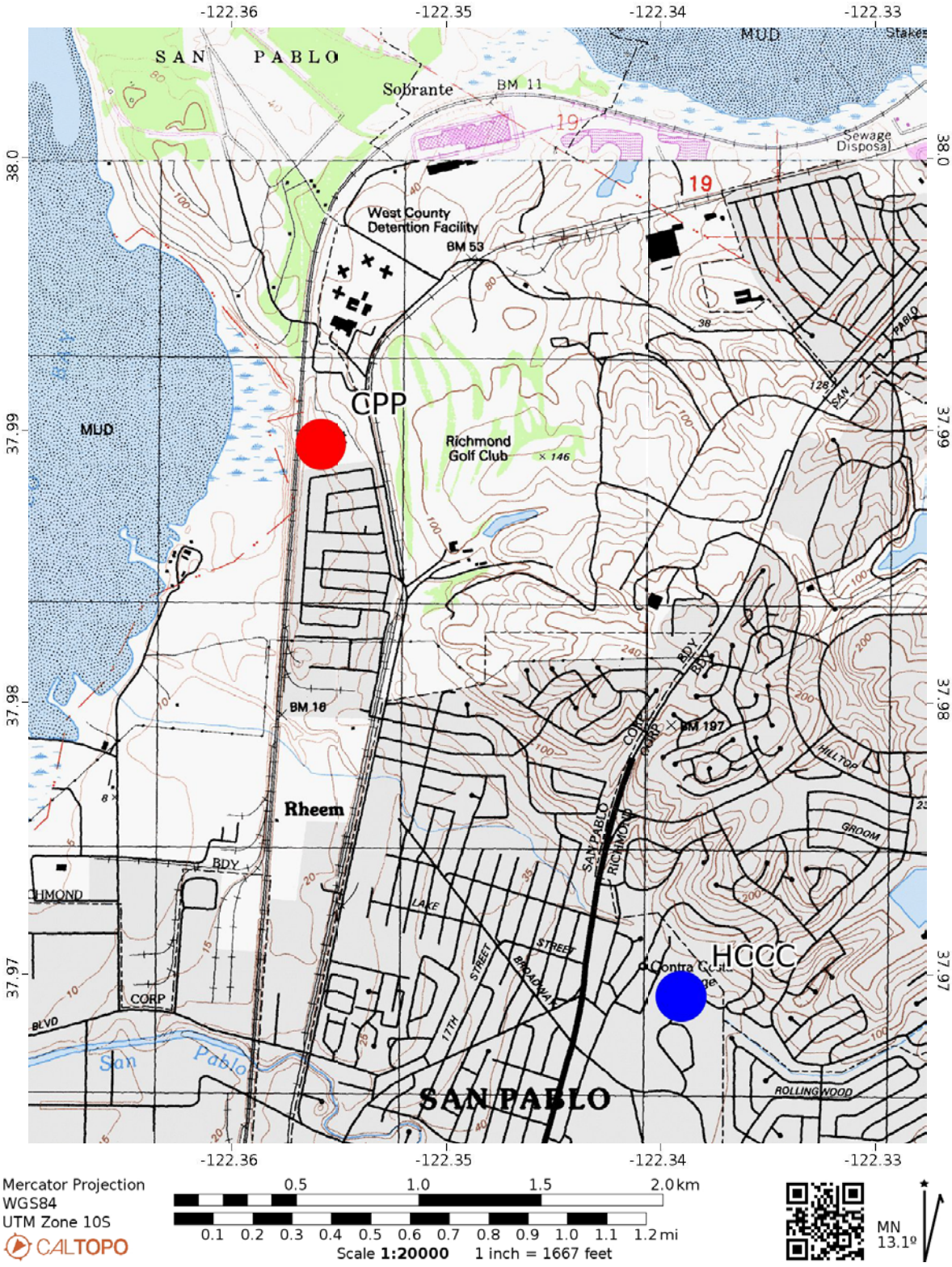

Figure 1.2. Location map of the Pinole Point (CPP) creepmeter on the Hayward Fault near Pinole Point near the shoreline of the San Pablo Bay, northern California. The creepmeter is plotted as a red dot in the center of the map. The property is part of the Point Pinole Regional Park run by East Bay Parks. The nearest alignment array, HCCC, is shown with a blue dot.

CTM Temescal—Hayward Fault
Location: 37.8439° N., 122.2273° W.
Orientation: 30°, 1-m depth; initially Invar, now carbon fiber; 30-m length. Three 3/16" rods are clamped and epoxied together at 60 cm intervals. A single rod extends the last 30 cm to each mount. LVDT sensor
LVDT sensitivity: 10.22 mm/volt through January 6, 2020, now 20.32-mm/volt
Sample interval: 10 minutes, but changed to 1 minute in late 2019
Creep rate: 4.07±0.12 mm/yr
Percentage of creep that occurs in discrete events: 2%

The Temescal creepmeter (CTM) was installed in 1997 next to the headquarters building for Temescal Regional Recreation Area managed by East Bay Parks in the city of Oakland, California. The monuments each consist of three helical piles (fig. 2). At the passive west end, the piles extend to 10-m depth while the sensor at the east end extend to only 3–5 m as bedrock was encountered because the Oakland Hills rise immediately to the east. The creepmeter passes above a 60-cm diameter gas pipe which is vulnerable to rupture in the next earthquake. About one half of the creepmeter lies below an asphalt surface and the other half lies beneath grass. The current fault-crossing rod is a triple 5-mm pultruded carbon fiber bundle (effective cross section 59 mm^2) which was installed in January 2020 along with a new 100-mm LVDT. Both ends, especially the west end, are prone to flooding and for a substantial period, the LVDT operates under water. Excursions of ±5 mm are present at this site from its background rate 4.07±0.12 mm/yr.

A rupture meter was installed 2012 in a separate trench located approximately (~) 20 m north of the creepmeter. The passive end uses a shallow, 1-m-depth monument while the sensor, consisting of a pair of potentiometers, was bolted to the building. In May 2020, to ensure operation during flooded conditions, a vertical bell-type sensor was installed on a new stainless steel tripod mount driven to 1.5 m depth and isolated from the building. At the same time, the sensors were replaced with Hall-effect sensors.

The nearby 154-m-wide HTEM alignment array records a creep rate of 4.3±0.3 mm/yr (McFarland and others, 2016) which is close to the 4.1 mm/yr rate recorded by the creepmeter.

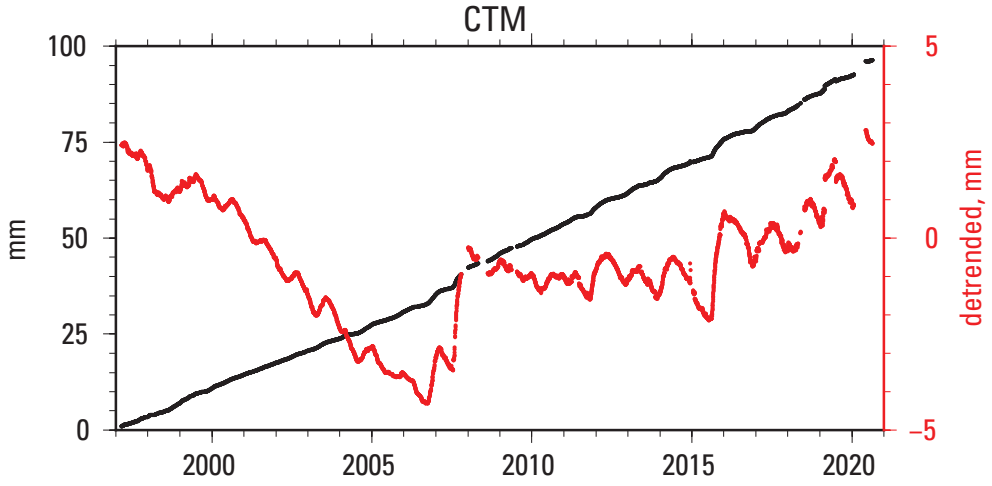

Figure 1.3. Plot showing the observed values of right-lateral slip at the Temescal (CTM) creepmeter on the Hayward Fault in Lake Temescal Regional Recreation Area, Oakland, California. The black is the long-term trend, while the red is the residual after removing a constant rate and seasonal sinusoids (365.25- and 182.625-day periods). mm, millimeter.

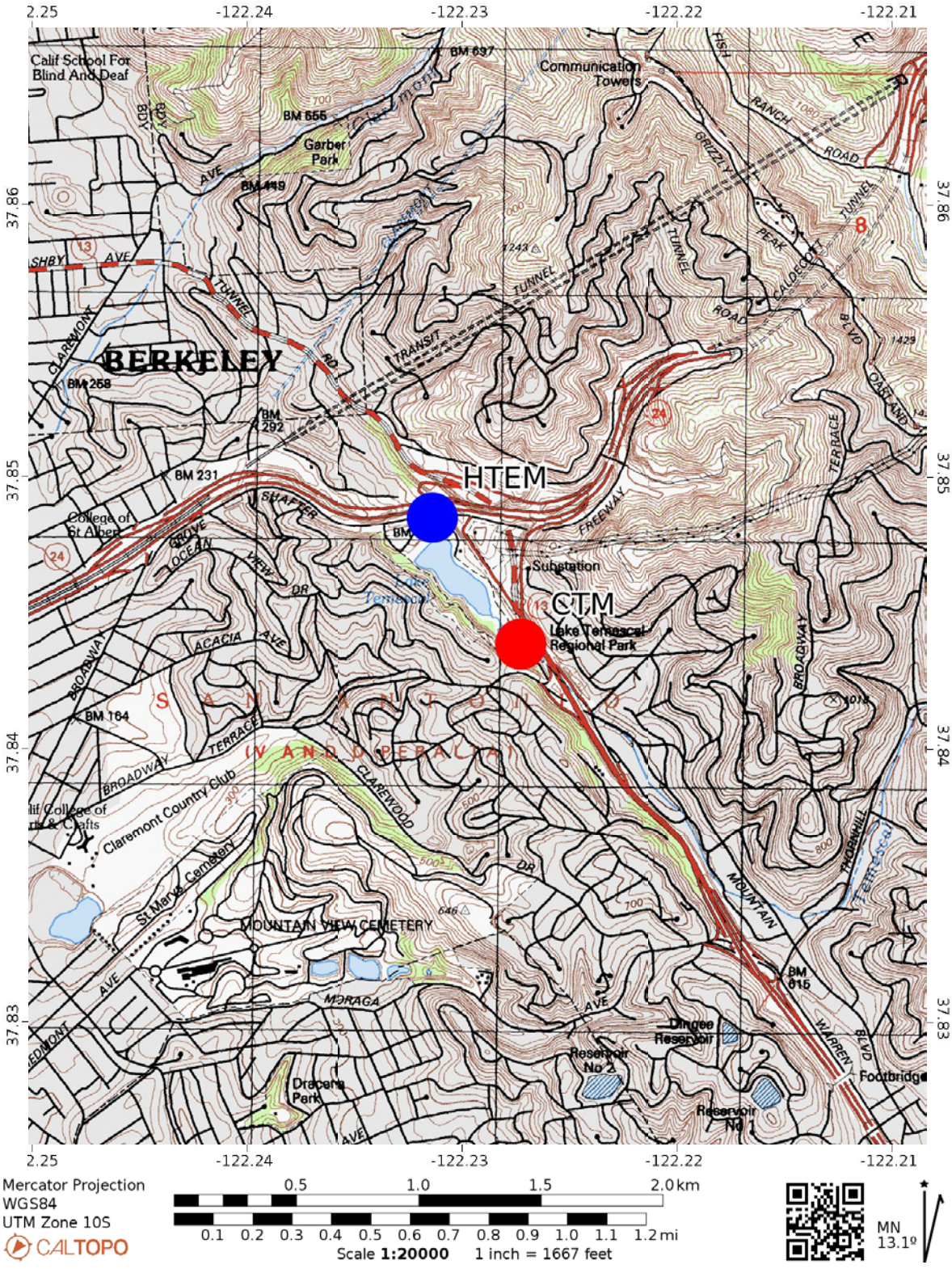

Figure 1.4. Location map of the Temescal (CTM) creepmeter on the Hayward Fault at Lake Temescal Regional Recreation Area in Oakland, California. It was installed in 1997 next to the headquarters building for the Temescal Regional Recreation Area. The creepmeter location is plotted as a red dot in the center of the map. The nearest alignment array, HTEM, is plotted as a blue dot.

COZ Oakland Zoo—Hayward Fault
Location: 37.7535° N., 122.1505° W.
Orientation: 30°, 1.5-m depth; both glass and carbon fiber rods; 30-m length. LVDT sensor.
LVDT sensitivity: 10.13 mm/volt through January 7, 2020, now 20.52-mm/volt
Sample interval: 10 minutes, but changed to 1 minute in late 2019.
Creep rate: 3.53±0.19 mm/yr
Percentage of creep that occurs in discrete events: 15%

The creepmeter was installed in late 1996 adjacent to the north entrance of the Oakland Zoo. Both monuments consist of three helical piles driven to 10-m depth. The trench of the creepmeter is buried to about 1.5-m depth and is beneath a grassy field. Water is drained through the sensor's east-end vault through a drain to the nearby creek. The instrument access vault was initially accessible via a surface manhole but is now completely buried and part of the Oakland Zoo's spill-over parking lot, that is, during major holidays cars are parked above the creepmeter.

Originally set-up with a 50-mm range LVDT, it failed in late 2019 and was replaced by a 100-mm range LVDT. The LVDT is connected to the glass fiber rod. Excursions of ±7.5 mm are present at this site from its background rate of 3.5±0.2 mm/yr. Periodic surges in slip were seen in late 2004, early 2010, late 2013, early 2015, and late 2019. The possible implications as they relate to local earthquake activity are discussed in appendix 5.

The observed rate of 3.5±0.2 mm/year is consistent with that recorded by nearby alignment array (McFarland and others, 2016) with a four-decade data span, and a >100 m fault-normal aperture near the creepmeter. That alignment array, HENC, has a rate of 3.2±0.3 mm/yr and is located 150 m to the north of the creepmeter. It is thus probable that the 15 m fault-normal aperture COZ creepmeters, despite their low rate compared to other Hayward creepmeters, capture most of the fault creep at this location.

A rupture meter consisting of low range and high range sensors was installed in 2014 initially with potentiometers as sensors but changed to Hall-effect sensors in late 2019. The rupture meter uses the carbon fiber rod and a local recorder sample at a 1 Hz rate.

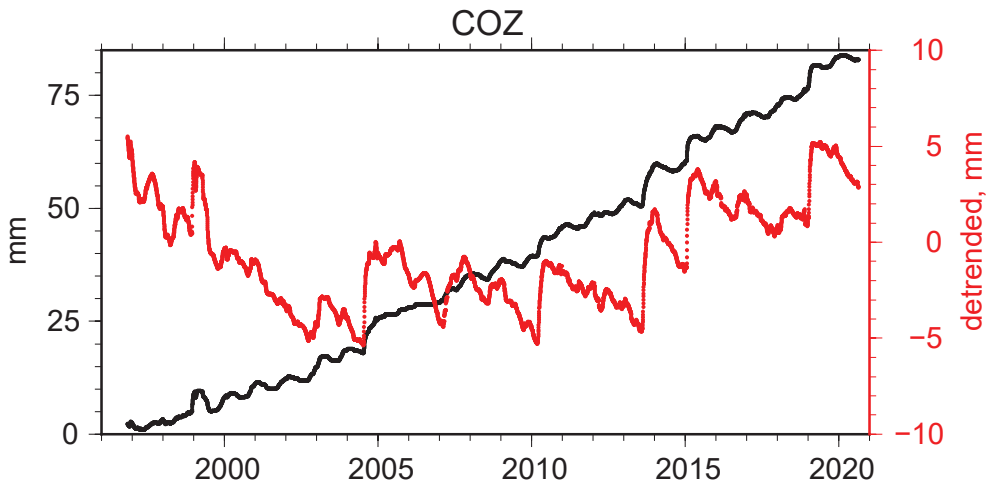

Figure 1.5. Plot showing the observed values of right-lateral slip at the Oakland Zoo (COZ) creepmeter on the Hayward Fault, Oakland, California. The black is the long-term trend, while the red is the residual after removing a constant rate and seasonal sinusoids (365.25- and 182.625-day periods). mm, millimeter.

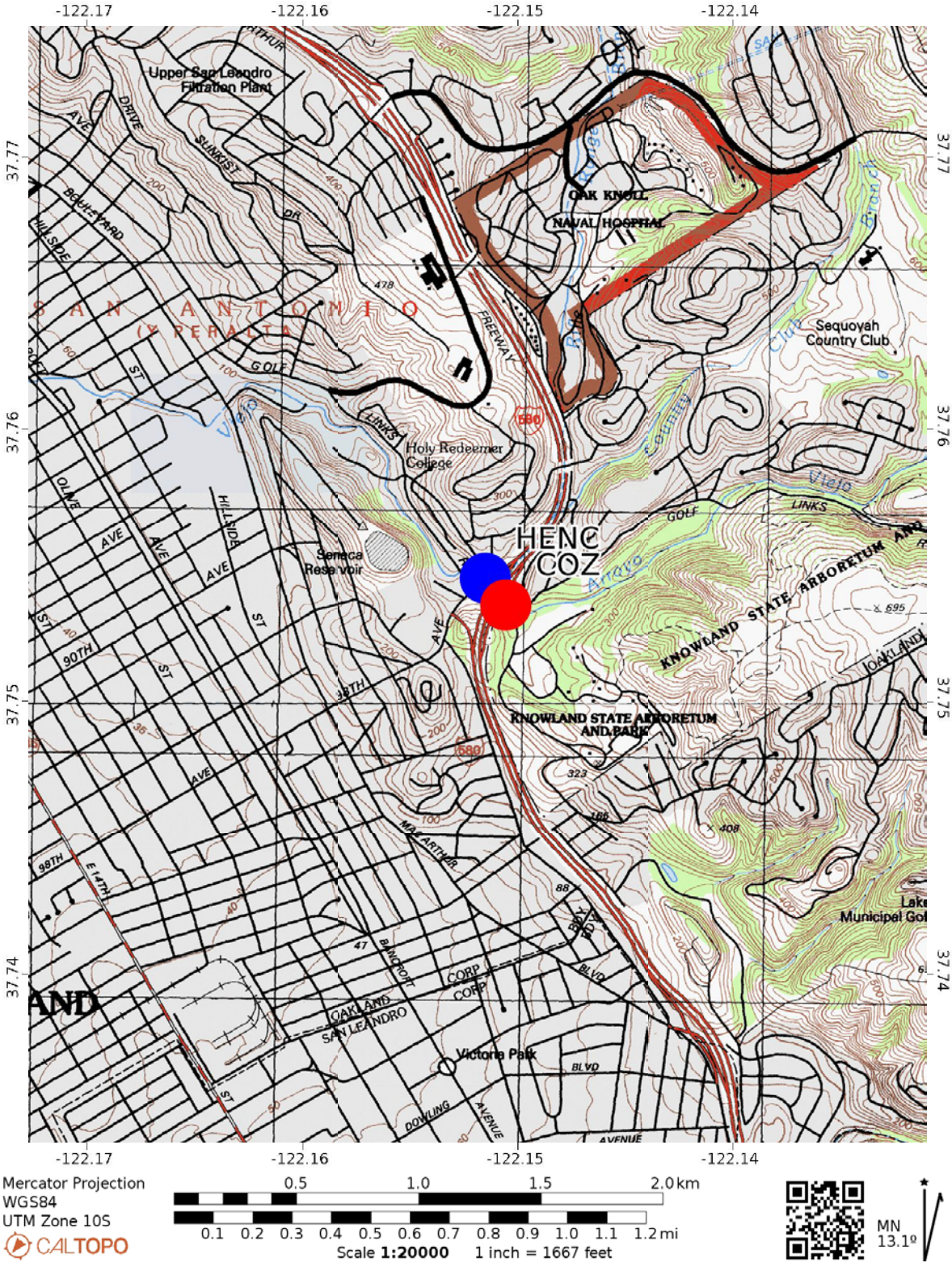

Figure 1.6. Location map of the Oakland Zoo (COZ) creepmeter on the Hayward Fault at Oakland Zoo in Oakland, California. The creepmeter was installed in late 1996 adjacent to the north entrance of the Oakland Zoo. The creepmeter location is plotted as a red dot in the center of the map. The nearest alignment array, HENC, is plotted as a blue dot.

HWR/HWE/HWW—City of Hayward, Rose Street, and D Street—Hayward Fault

These creepmeters, located in the downtown section of the city of Hayward, California, are discussed in Schulz (1989). The USGS ceased collecting manual measurements from these sites in 1995. Plots of these data are provided. Note that the configuration of the two D Street creepmeters, HWE1 and HWW1, probably spans two traces of the Hayward Fault; the creep rate for HWE1 is 0.91±0.45 mm/yr and the rate for HWW1 is 3.27±0.46 mm/yr. In contrast, the two Rose Street creepmeters, HWR1 and HWR2, have essentially the same rates, 3.98±0.64 and 4.10±0.45 mm/yr, respectively. The sum of the rates for the D Street meters is the same as that for Rose Street and is within 0.2 to 0.3 mm/yr rate of the Palisade Street creepmeter, HWP/CHP, which is located 1 km SE of the D Street site. The locations of these sites are shown in the next section that describes CHP to the southwest (fig. 1.9).

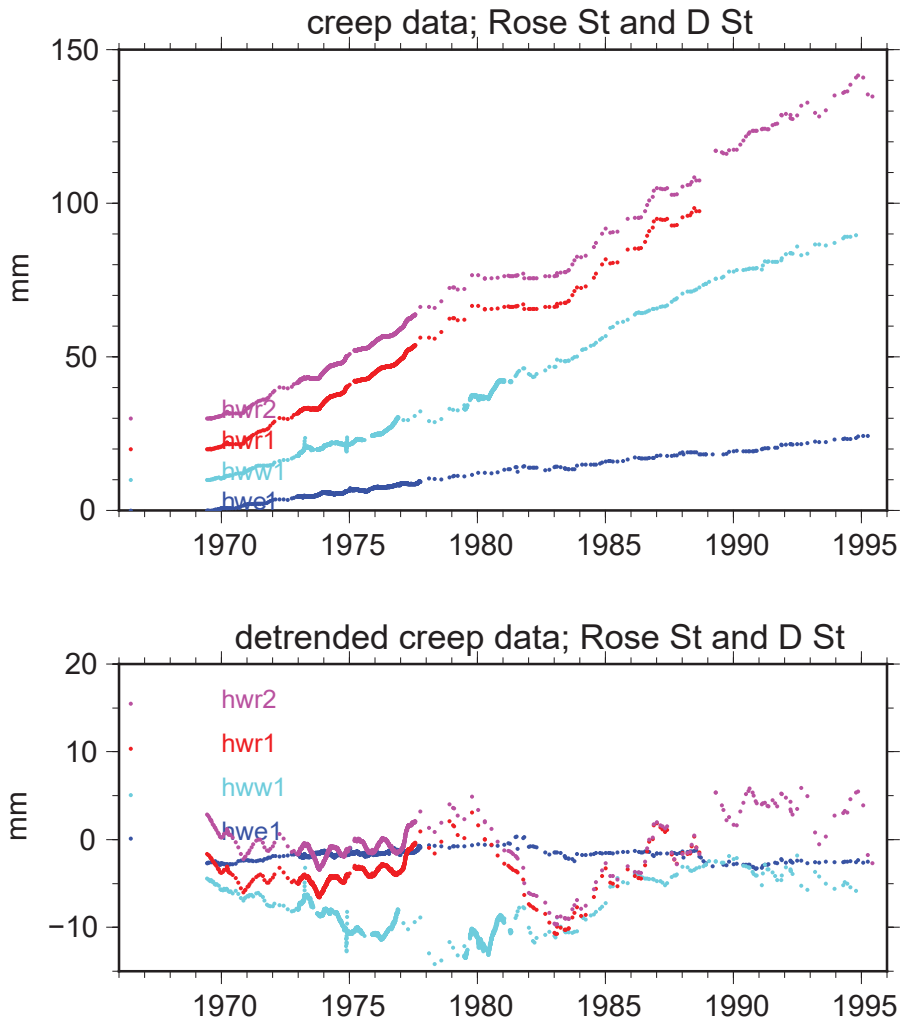

Figure 1.7. Plots showing slip at two locations near downtown in the City of Hayward, California. HWR1 and HWR2 are located on Rose Street, and HWE1 and HWW2 cover two strands of the Hayward Fault as it crosses D Street. The USGS ceased collecting manual measurements from these sites in 1995. The upper plots show the data, and the bottom plots show the residuals after a trend was removed. mm, millimeter.

CHP/HWP—City of Hayward, Palisade Street—Hayward Fault
Location: 37.66274° N., 122.07400° W.
Orientation: 30°, 1-m depth; initially Invar, now glass fiber; 20-m length. LVDT sensor
LVDT sensitivity: 10.19 mm/volt
Sample interval: 10 minutes, but changed to 1 minute in late 2019
Creep rate CHP only: 4.22±0.07 mm/yr
Percentage of creep that occurs in discrete events: 7%
Creep rate HWP and CHP: 4.84±0.04 mm/yr

The Palisades creepmeter (CHP) is in the city of Hayward, California, and was installed in 1993. It occupies the same location as its predecessor, HWP, which was installed in 1970. HWP is described in Schulz (1989). CHP uses helical piles driven to a depth of 10 m. The trench containing the glass fiber rod is 60 cm beneath the black asphalt street which tends to amplify the diurnal temperature swings. The curbs are offset, and cracks are apparent in the pavement. It is noted that the guide tube for the rod has a severe bend preventing smooth movement of the rod. The average creep rate is 4.2±0.1 mm/yr with an apparent decrease in rate starting coincident with the 1989 Loma Prieta earthquake, followed by an 8-year increase in rate starting in 1997. Superimposed on these longer-term excursions are variations of less than 5 mm. With the relatively shallow burial of the rod beneath black asphalt, thermoelastic diurnal variations are significant due to localized heating.

In 2014, a rupture meter was installed but changed in late 2019 to a vertical oriented sensor using a bell housing to prevent flooding of the sensor. These sensors are also connected to the same rod as the LVDT.

This instrument is the only one of the five Hayward creepmeters installed beneath a road in the Bay Area. The passive end of the creepmeter on the east side of the road can be accessed via a circular steel cover flush with the road surface (labeled “Christy Concrete”). The road is quite busy, and trucks and cars are often parked on the instrument. Their presence has no measurable effect on its observed data.

The HPAL alignment array with an aperture of 132 m spans the location of the creepmeter. The long-term rate from the HPAL alignment array, spanning 39 years, is 4.7±0.5 mm/yr, which exceeds the combined rate from CHP and its predecessor, HWP1 of 3.84±0.04 mm/yr. This missing slip occurs on a secondary fault segment ~30 m west of the creepmeter.

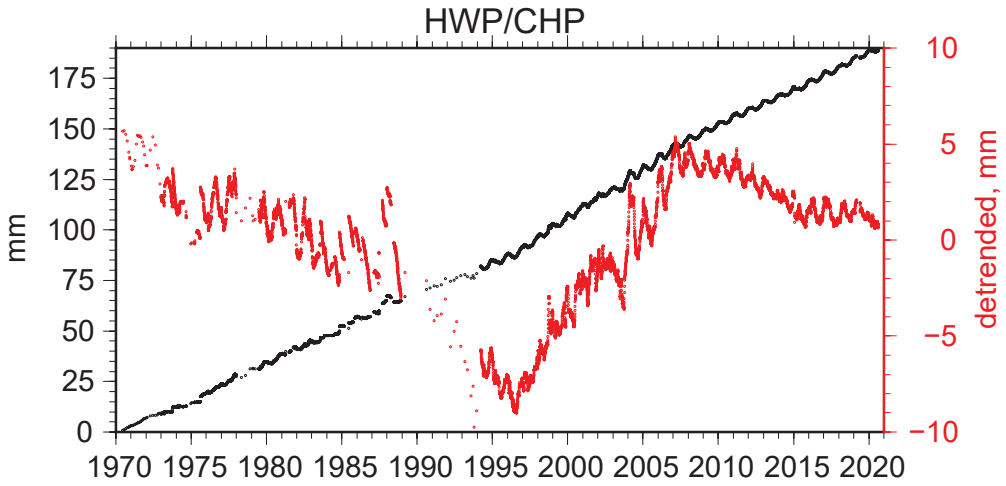

Figure 1.8. Plot showing the observed values of right-lateral slip using a combination of HWP and CHP data. The city of Hayward, California, Palisade Street (CHP) creepmeter was installed in 1993. It occupies the same location as its predecessor, HWP, which was installed in 1970. The black is the long-term trend, while the red is the residual after removing a constant rate and seasonal sinusoids (365.25- and 182.625-day periods). The two time-series were connected across their break in 1994. mm, millimeter.

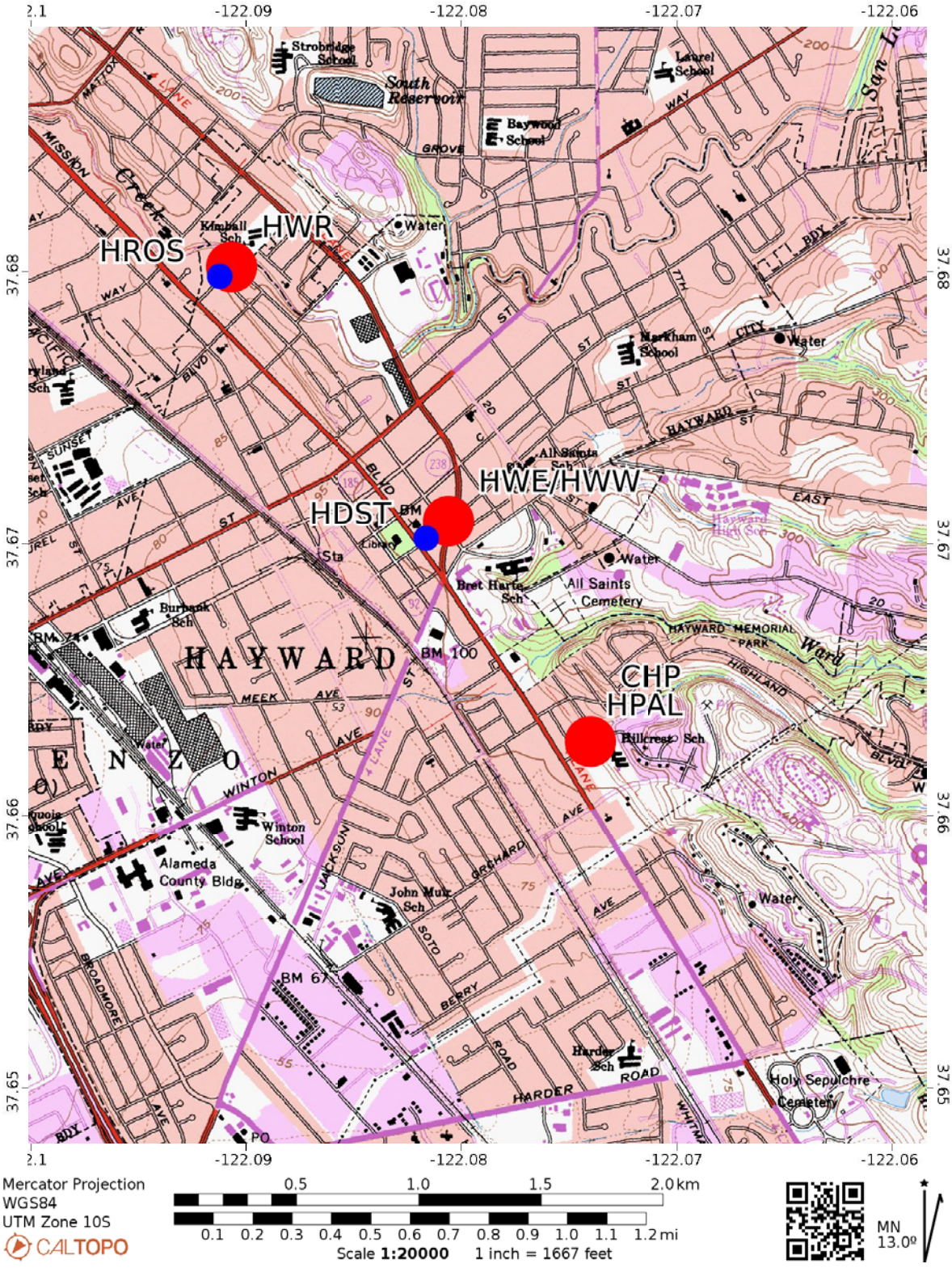

Figure 1.9. Location map of the creepmeters and alignment arrays in the city of Hayward, California. The creepmeter locations, Palisade Street (CHP), D Street (HWW/HWE), and Rose Street (HRW), are plotted as red dots. Note that the configuration of the two D Street creepmeters, HWE and HWW probably spans two traces of the Hayward Fault. The locations of the alignment arrays (HROS, HDST, HPAL) are plotted with blue dots.

CFW—Fremont—Hayward Fault
Location: 37.53237° N., 121.95230° W.
Orientation: 30°, 1-m depth; silica-glass fiber and invar (two separate instruments); 25-m length. LVDT sensor.
LVDT sensitivity: 10.13 mm/volt
Sample interval: 10 minutes, but changed to 1 minute in late 2019
Creep rate: 6.64±0.04 mm/yr
Percentage of creep that occurs in discrete events: 38%

Installation of the creepmeter was completed in late 1993. The creepmeter is installed among the ruins of Gallegos Winery in Fremont, California, which was destroyed in the 1906 San Francisco Earthquake. Evidence for a century of creep is evident in the ruined foundation of the winery which has now been offset by >90 cm. The creepmeter installation consists of two sets of monument pairs. The most distant pair of monuments consists of three helical piles driven to 10-m depths and uses a silica-glass fiber rod as the length standard between the two monuments. Each of the second pair consists of 30-m-deep vertical boreholes filled with reinforced concrete surrounding a grooved inclinometer tube within which an inclinometer can be inserted to measure the offset of the tube as a function of depth. The inclinometer measurements indicate that the western borehole intersects the fault at 21 m depth consistent with the fault dipping 70° to the SW (Bilham and Whitehead, 1997). To measure creep, this pair uses a 25-m-long invar rod.

Initially both mounting systems used LVDTs as sensors, but the borehole mount measurement system was briefly terminated in 2018 and restarted in 2022 along with an orthogonal sensor. The LVDT and the rupture meter both measure between the helical pile monument pairs (30 m Invar rod). The first rupture meter used potentiometers as the sensors. These were replaced in 2020 with Hall-effect sensors and a vertical bell housing to permit operation during occasional flooding of the vault.

The background creep rate for this site from the creepmeter data is 6.64±0.04 mm/yr. The closest alignment array, HUNI, located 0.5 km to the NW, has recorded a rate of 6.6±0.1 mm/yr over the past 23 years, and its rate is equivalent to that estimated from the creepmeter data. The rate is modulated by many short intervals of accelerated slip. Of the five Hayward Fault creepmeters, this site has the highest ratio of creep events at 38%. The next closest in terms of episodic creep of the Hayward network has 15% at COZ.

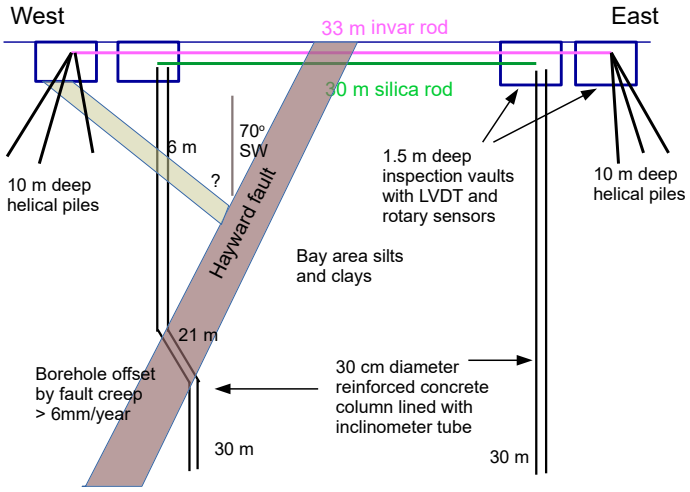

Figure 1.10. Cross-section showing the layout of the monument pairs for the Fremont, California, Creepmeter (CFW) on the Hayward Fault. The creepmeter was installed in 1993 among the ruins of the Gallegos Winery that was destroyed in the 1906 San Francisco Earthquake. The profile of the fault at this site is from the interpretation by Bilham and Whitehead (1997). LVDT, linear voltage displacement transformers/transducers; SW, southwest; m, meter, cm, centimeter; mm, millimeter.

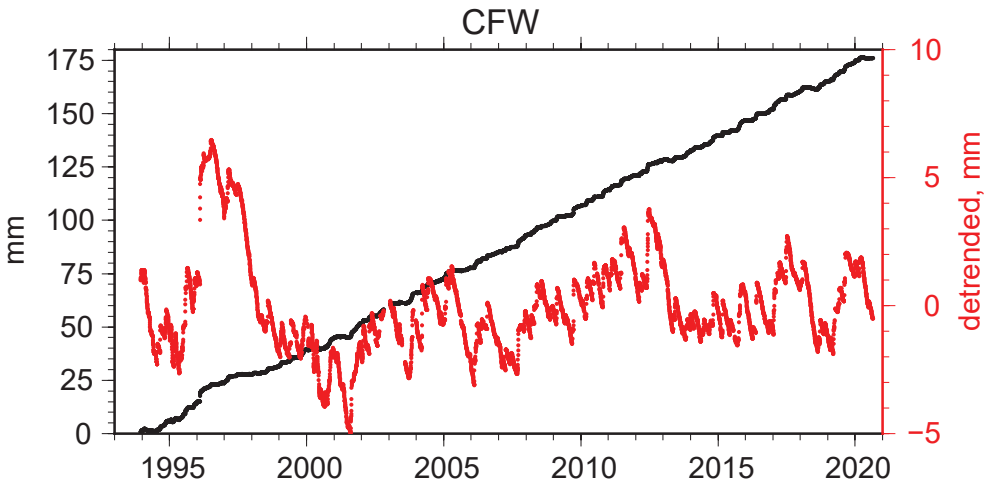

Figure 1.11. Plot showing the observed values of right-lateral slip at the Fremont, California (CFW) creepmeter on the Hayward Fault. The black is the long-term trend, while the red is the residual after removing a constant rate and seasonal sinusoids (365.25- and 182.625-day periods). mm, millimeter.

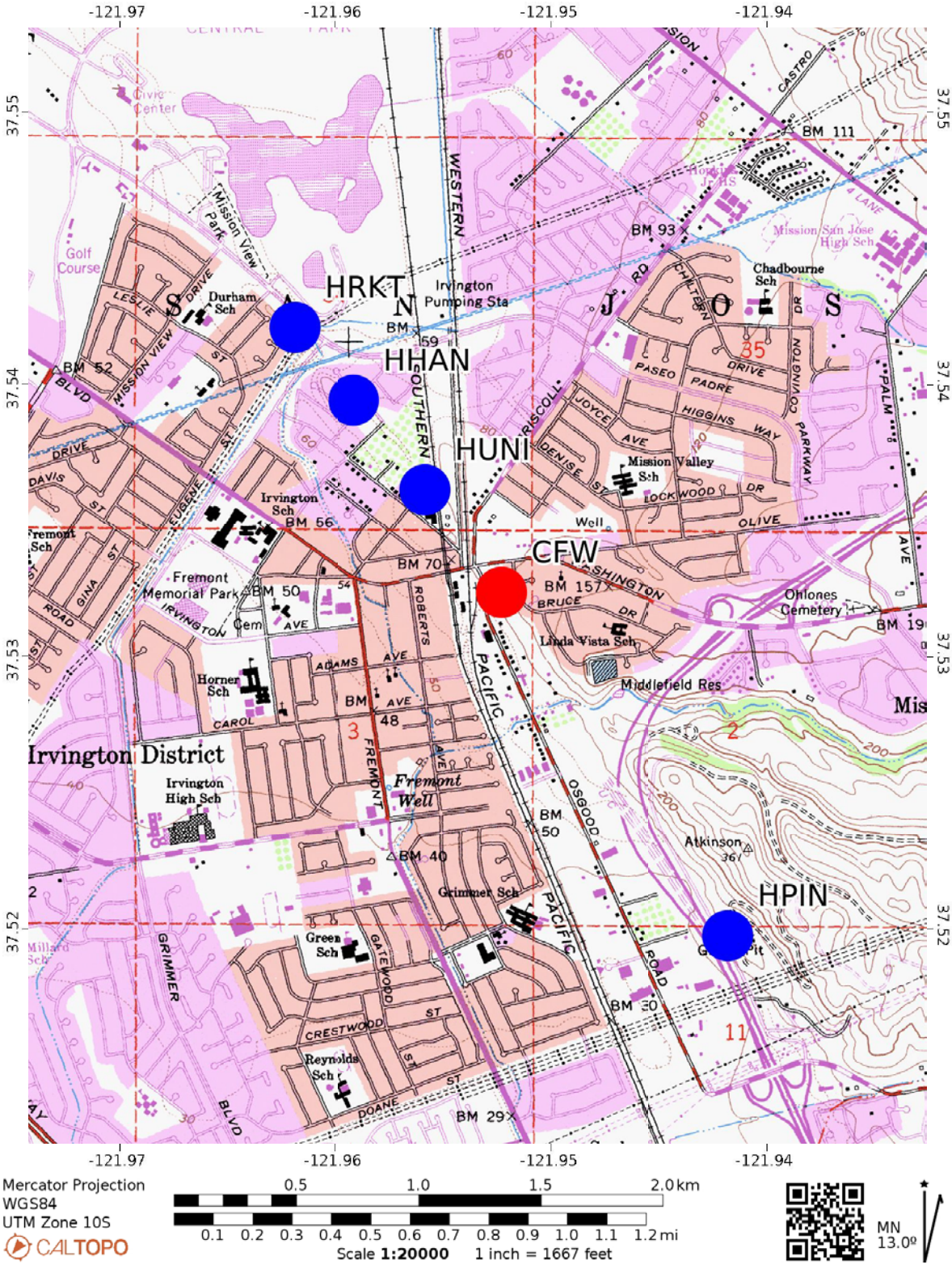

Figure 1.12. Location map of the Fremont (CFW) creepmeter in Fremont, California, on the Hayward Fault. The creepmeter was installed in 1993 among the ruins of the Gallegos Winery that was destroyed in the 1906 San Francisco Earthquake. The creepmeter location is plotted as a red dot in the center of the map. The locations of four nearby alignment arrays (HRKT, HHAN, HUNI, HPIN) are plotted as blue dots.

XSH/SHR—Shore Rd—Calaveras Fault
Location: 36.9426° N., 121.4447° W.
Orientation: 41.5°, USGS standard, 14-m wire through 2017.
Creep rate: 9.46±0.41 mm/yr
Percentage of creep that occurs in discrete events: ~100%

The Shore Road (XSH) creepmeter is located north-northwest of Hollister, California. The merged data from the original, SHR1 creepmeter, installed in 1971, along with data from the replacement instrument, XSH1, installed in 1986, are shown in the plot of the data. The telemetry stream ceased in 1997 due to vandalism, yet occasional manual measurements have been made through 2017. A typo in Schulz (1989) incorrectly describes the site as operating in contraction (should have stated extension). In 2017 a truck destroyed the western vault, and its instrumentation was again subsequently vandalized. The instrument was rebuilt in October 2020 using a carbon rod connected passively within the repaired western vault near the road and with a vertical bell sensor with 10 mm and 117 mm ranges in the eastern vault, furthest from the road.

Results show multiple creep events modulating a relatively steady creep rate of 9.5 mm/yr. It is difficult to accurately estimate the contribution of episodic creep to the total slip at this site as there are periods when this site appears to slip in a left lateral sense. If one discounts any left lateral motion, then creep events contribute to 60% of the total slip. The likely cause of the sinistral displacement may be related to the water level in the small creek that is less than 10 m north of the western vault. The creepmeter is embedded in thick clays that extend hundreds of meters below the site. Expansion of the surface clays away from the stream would tend to shorten the creepmeter measurement path, which would be interpreted as sinistral displacement.

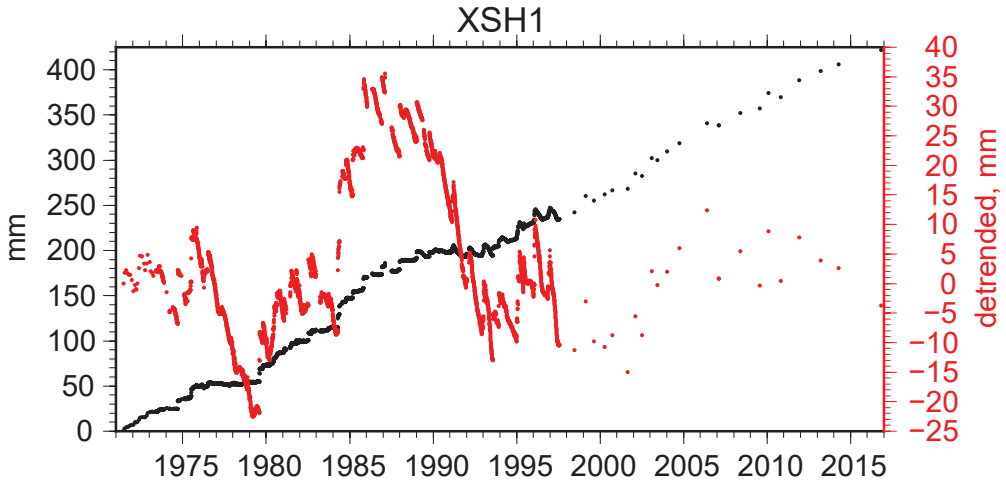

Figure 1.13. Plot showing the observed values of right-lateral slip at the Shore Road (XSH) creepmeter on the Calaveras Fault north-northwest of Hollister, California. The merged data is from the original SHR1 creepmeter installed in 1971, along with data from the replacement instrument, XSH1, are shown. The telemetry stream ceased in 1997, yet occasional manual measurements have been made through 2017. The black is the long-term trend, while the red is the residual after removing a constant rate and seasonal sinusoids (365.25- and 182.625-day periods). Infrequent dots following 1997 are manual measurements of the creepmeter. mm, millimeter.

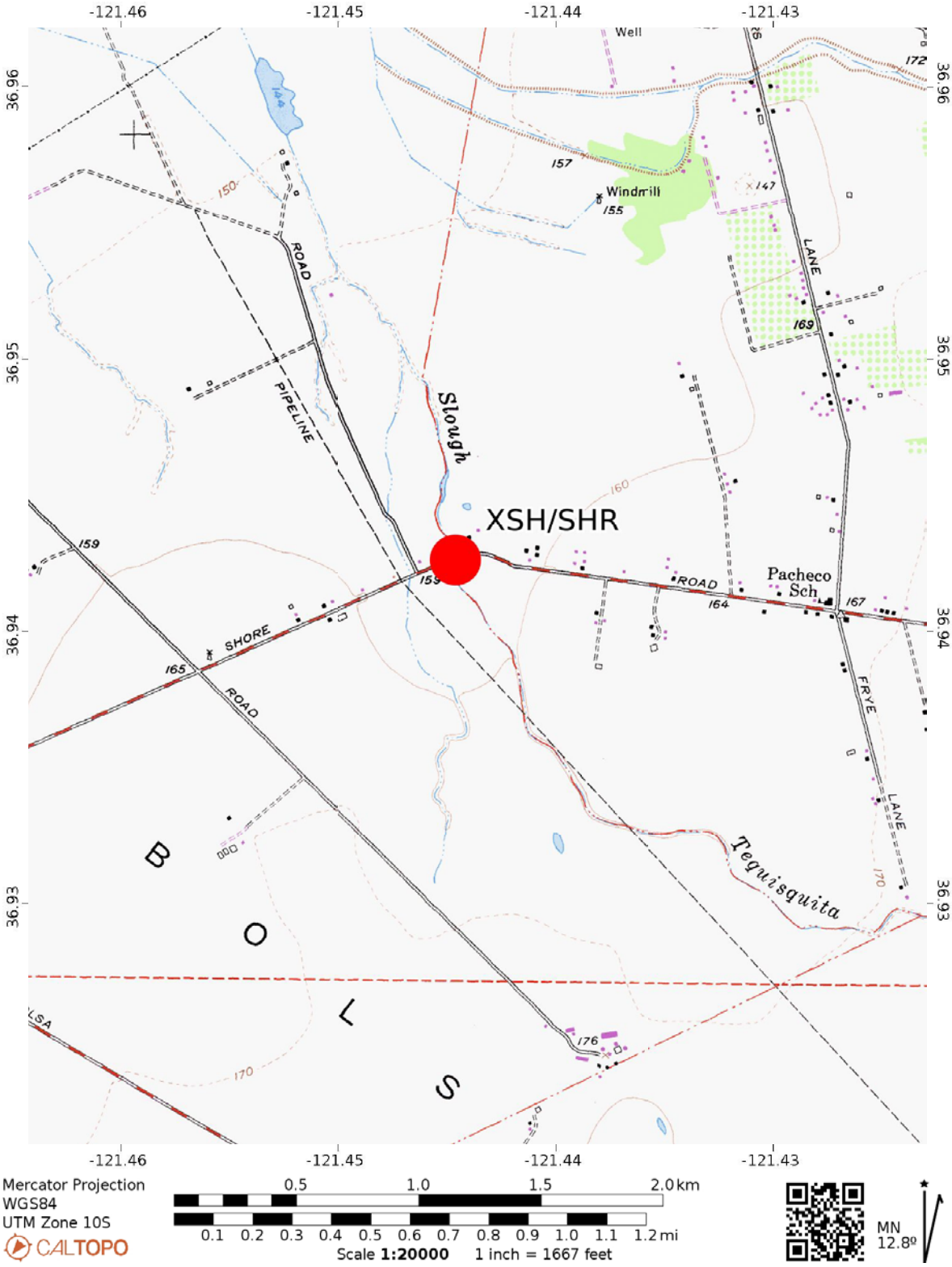

Figure 1.14. Location map of the Shore Road (XSH) creepmeter on the Calaveras Fault located north-northwest of Hollister, California. The original SHR1 creepmeter was installed in 1971, and the replacement instrument is XSH. The creepmeter location is plotted as a red dot in the center of the map.

HLC/HLD—Hollister—Central and D St—Calaveras Fault

HLC
HLD
Location: 36.85399° N., 121.40759° W.
Location: 36.84079° N., 121.40644° W.
Orientation: 45°
Orientation: 45°
14-m "Rod" creepmeter (Schulz, 1989)
14-m "Rod" creepmeter (Schulz, 1989)
Creep rate: 5.21±0.28 mm/yr
1.53±0.29 mm/yr

These two creepmeters are buried beneath the sidewalk and pavement on two roads in Hollister, California. Long term creep rates are 5.0 mm/yr for the more northerly Hollister Central (HLC) and 1.5 mm/yr for Hollister D Street (HLD). Schulz (1989) suggests that HLD may only span a portion of the creeping Calaveras Fault. At HLC, the creep rate prior to late 1989 was 8.7 mm/yr, a value noted in Schulz (1989). However, post 1990 and through 2009, the rate is 2.0 mm/yr. Neither of these sites have been maintained since about 1998. The mechanics of the "rod" creepmeter are discussed in Schulz (1989) and references therein. All measurements at these two sites are manual readings of the micrometer. With infrequent measurements, there is insufficient temporal resolution to detect creep events.

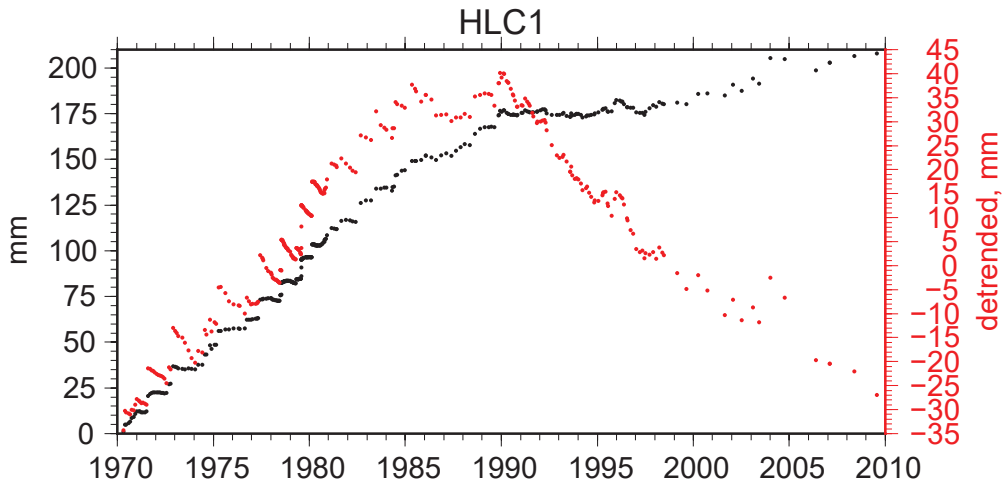

Figure 1.15. Plots showing the observed values of right-lateral slip at the Hollister Central (HLC) creepmeter on the Calaveras Fault, Hollister California. The site has not been maintained since 1998. The black is the long-term trend, while the red is the residual after removing a constant rate and seasonal sinusoids (365.25- and 182.625-day periods). mm, millimeter.

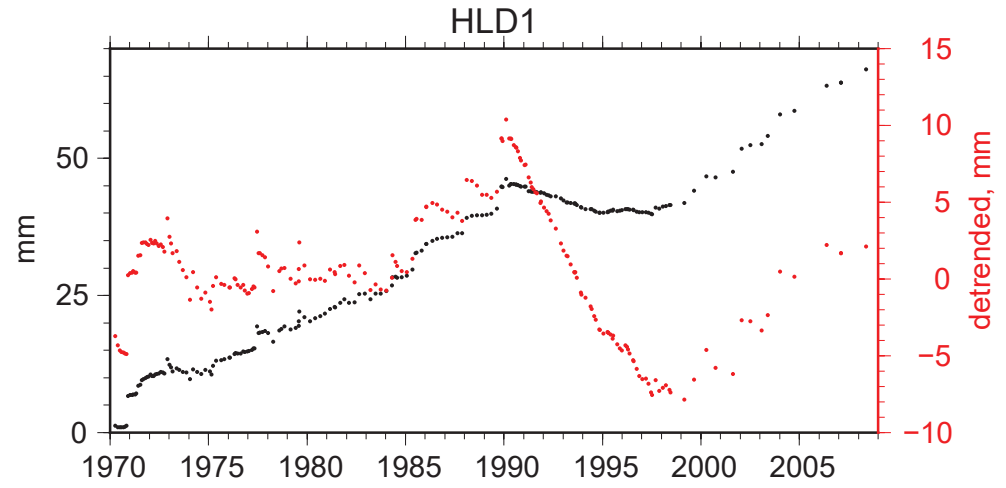

Figure 1.16. Plots showing the observed values of right-lateral slip at the Hollister D Street (HLD) creepmeter on the Calaveras Fault, Hollister California. The site has not been maintained since 1998. The black is the long-term trend, while the red is the residual after removing a constant rate and seasonal sinusoids (365.25- and 182.625-day periods). mm, millimeter.

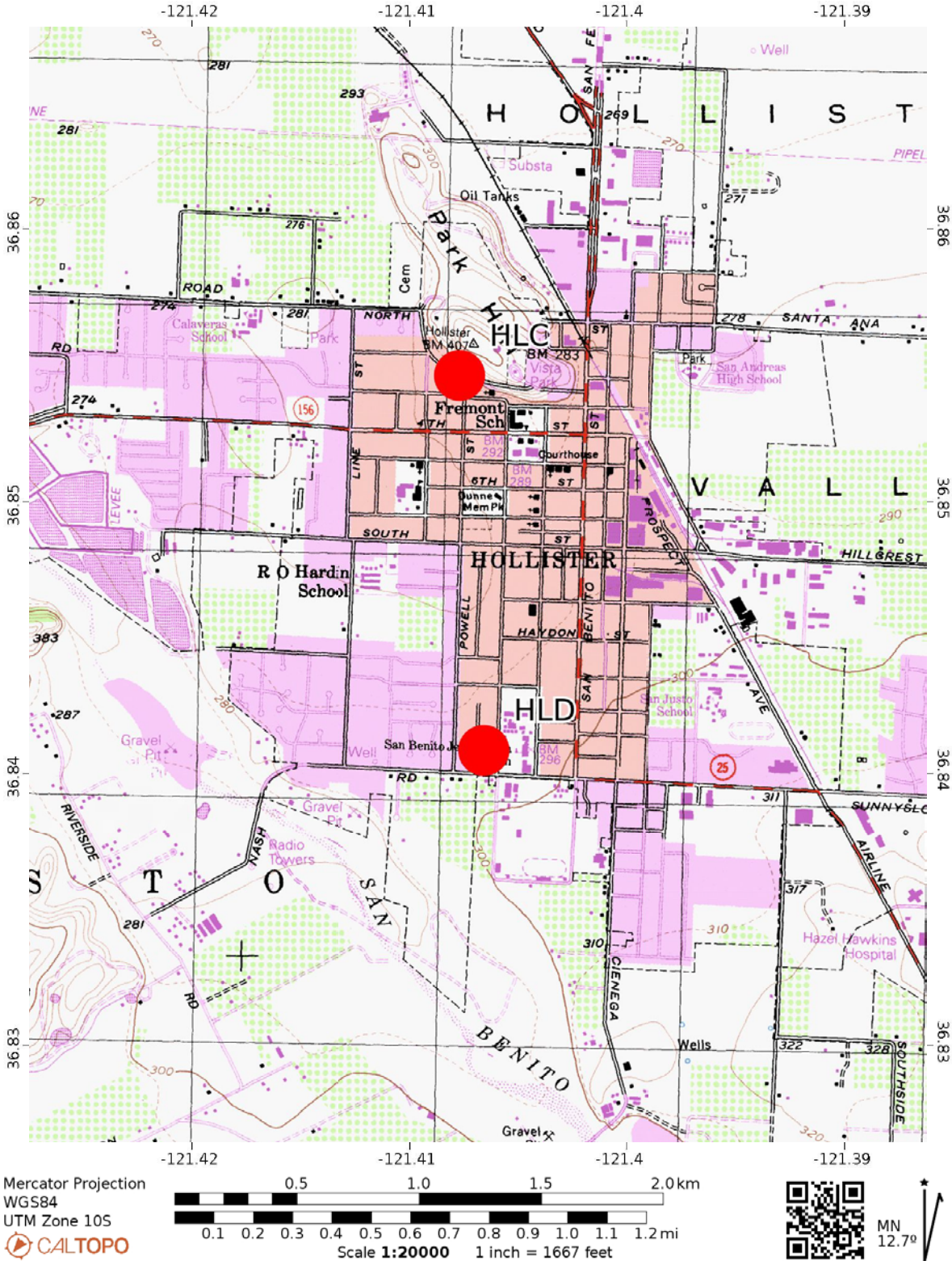

Figure 1.17. Location map of two creepmeters, Hollister Central (HLC) and Hollister D Street (HLD), on the Calaveras Fault located in Hollister, California. These two creepmeters are buried beneath the sidewalk and pavement on two roads, respectively. Neither of these sites have been maintained since 1998. The creepmeter locations are plotted as red dots in the map.

SJN/NYL—Nyland Ranch—San Andreas Fault
Location: 36.85456° N., 121.54673° W.
Orientation 45°, Originally installed using an Invar rod with LVDT sensor. Upgraded 2020 to 30° and carbon rod. 15-m length.
Creep rate: 8.87±0.17 mm/yr
Percentage of creep that occurs in discrete events: 11%

The creepmeter and alignment array are located within the transition between the southernmost end of the 1906 earthquake rupture, and the central creeping zone to the southeast, about 1.5 km northwest of the city of San Juan Bautista, California. The creepmeter is a reoccupation of the Nyland Ranch (SJN1) site initially installed by Robert Nason in 1967 and described in Schulz (1989). That creepmeter was abandoned in 1985 following several problems at the site. Here, the data are presented for a 10-year interval starting in 2004. Again, NYL was abandoned in 2013 due to frequent flooding. The rate for this 10-year interval is 8.9 mm/yr, consistent with the value of 8 mm/yr noted by Schulz for the 1969–1985 interval.

In late 2020 a new instrument was installed at 30° to the fault with anchors driven to 3 m depth. This instrument uses a Bilham #2 sensor to render it immune to flooding. Initial measurements indicated that the creepmeter does not fully span the fault, and in 2022 the creepmeter was lengthened eastward. The current observed rate is like the long-term rate noted above. Those data are not included here as this study only extends to 2020.

The location map is provided in the next section for XSJ (fig. 1.20).

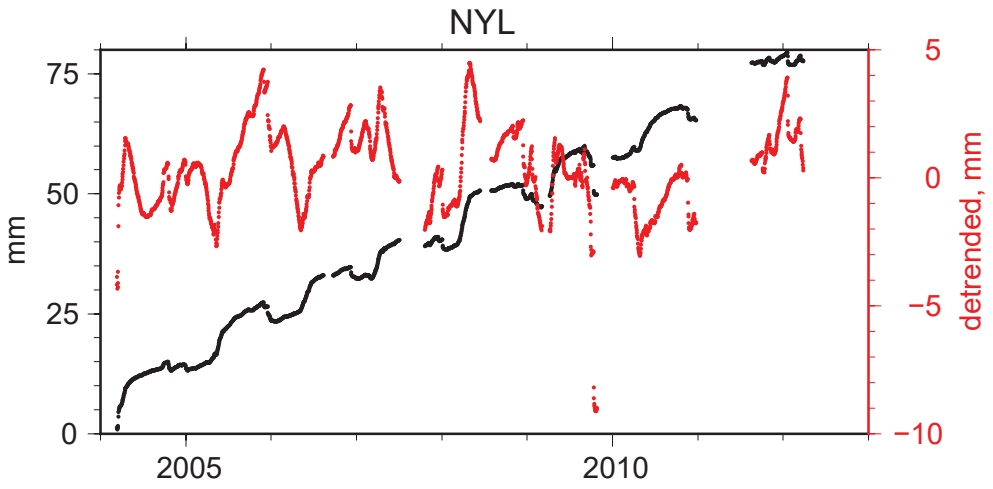

Figure 1.18. Plot showing the observed values of right-lateral slip at the Nyland Ranch (NYL) creepmeter on the San Andreas Fault, northwest of the town of San Juan Bautista, California. The NYL creepmeter is a reoccupation of the SJN1 site that was abandoned in 1985. The data are presented for a 10-year interval starting in 2004. NYL was abandoned again in 2013 due to frequent flooding. In late 2020 a new instrument was installed. Initial measurements indicated that the creepmeter does not fully span the fault, and in 2022 the creepmeter was lengthened eastward. The black is the long-term trend, while the red is the residual after removing a constant rate and seasonal sinusoids (365.25- and 182.625-day periods). For the location of this site see figure 1.20. mm, millimeter.

XSJ—San Juan Bautista—San Andreas Fault
Location: 36.83599° N., 121.52136° W.
Orientation: 30°, USGS standard, 20-m wire
Creep rate: 9.02±0.41 mm/yr
Percentage of creep that occurs in discrete events: 55%

The data shown are from three different installations at the same site, San Juan Bautista (XSJ), about 1.6 km southeast of the town of San Juan Bautista, California. Schulz (1989) describes the first two sets, and the third set starts in early 2007 after the wire broke in mid-2006. The site was abandoned in 2017 when the main vault containing the sensing electronics was destroyed by field reconfiguration. Note that the comparison between the electronic and manual measurements indicated that the LVDT had a 4% change in scale after April 2011.

Like the two other creepmeters located to the southeast, XHR (fig. 1.22) and CWN (fig. 1.25), this site has a transient that coincides with the time of the 1989, *M*6.9 Loma Prieta earthquake. A smaller transient is associated with the 1972 moment magnitude (M_w) 4.8 earthquake (Wesson, 1987).

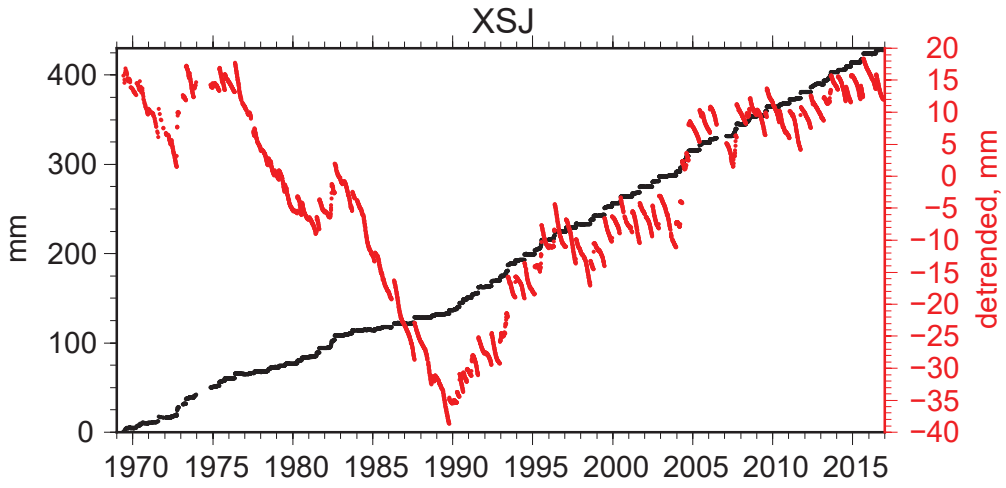

Figure 1.19. Plot showing the observed values of right-lateral slip at the San Juan Bautista (XSJ) creepmeter on the San Andreas Fault, San Juan Bautista, California. The data shown are from three different installations at the same site. The third set starts in early 2007 after the wire broke in mid-2006. The site was abandoned in 2017 when the main vault containing the sensing electronics was destroyed. The black is the long-term trend, while the red is the residual after removing a constant rate and seasonal sinusoids (365.25- and 182.625-day periods). mm, millimeter.

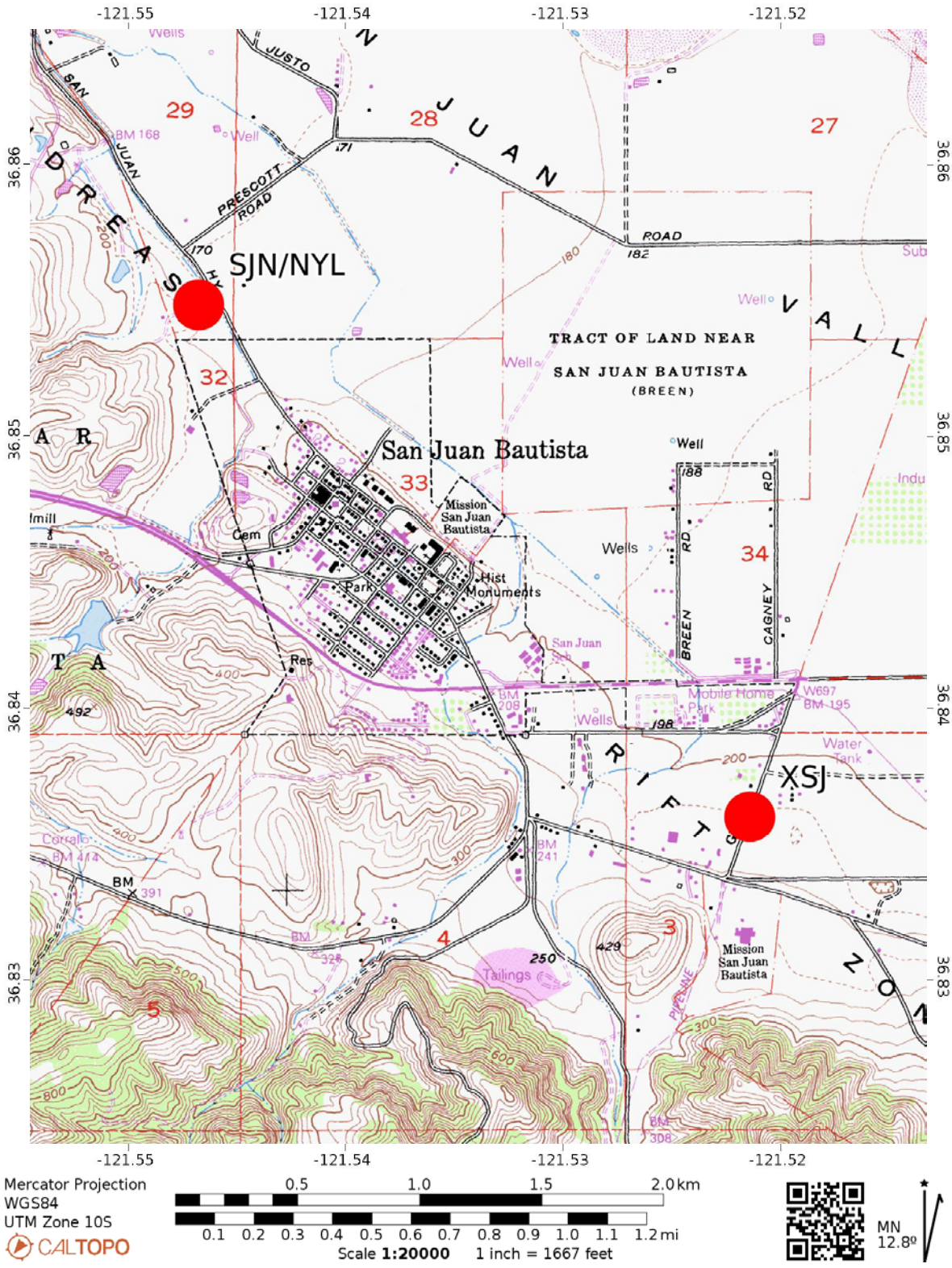

Figure 1.20. Location map of the San Juan Bautista (XSJ) and Nyland Ranch (SJN/NYL) creepmeters on the San Andreas Fault located near San Juan Bautista, California. The creepmeter locations are plotted as red dots. NYL is a reoccupation of the SJN1 creepmeter initially installed by Robert Nason in 1967 and described in Schulz (1989). The XSJ data are from three different installations at the same site. The site was abandoned in 2017 when the landowner reconfigured the field and destroyed the main vault containing the sensing electronics.

XHR—Harris Ranch—San Andreas Fault
Location: 36.77184° N., 121.42253° W.
Orientation: 22°, USGS standard, 30-m wire
Creep rate: 11.36±0.49 mm/yr
Percentage of creep that occurs in discrete events: 68%

The Harris Ranch site (XHR) is located southeast of the town of San Juan Baptista, California. The plot of XHR is the result of merging the data from three intervals: the data prior to 1985 which is described by Schulz (1989); the interval from 1985 to 2005; and the interval that starts in 2009. In 2005, the conduit caved in and the wire broke. The conduit was retrenched and the wire was replaced in 2009 causing a break in the time series. To present the data as a plot, the gap is bridged using least squares and the data were weighted assuming temporal correlation. Many of the creep events seen at XHR are also seen at CWN (fig. 1.25), located 4 km to the southeast. Although the rate over the 50 years of observation is ~11.4 mm/yr, the plot reveals that the rate is highly variable with the initial 15 years of observation suggesting a 5 mm/yr deficit.

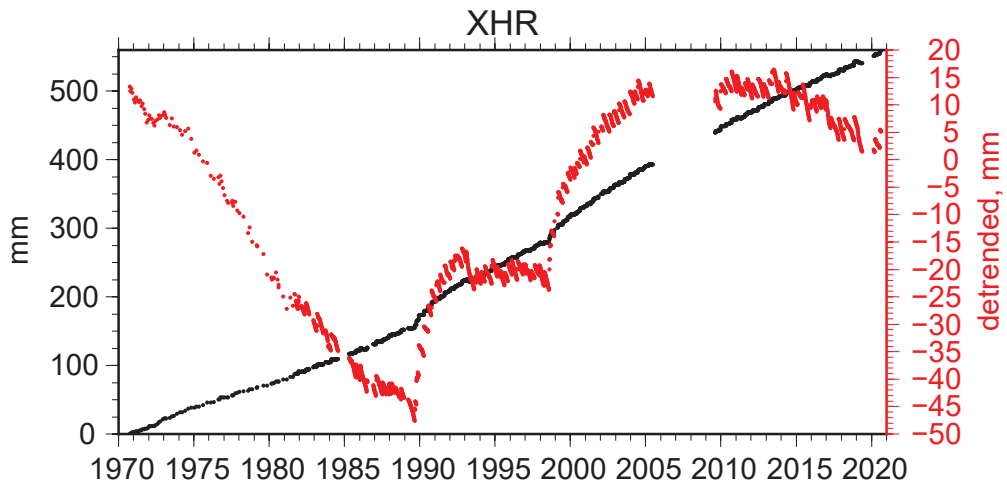

Figure 1.21. Plot showing the observed values of right-lateral slip at the Harris Ranch (XHR) creepmeter located on the San Andreas Fault southeast of San Juan Bautista, California. The plot is the result of merging the data from three intervals: the data prior to 1985, the interval from 1985 to 2005, and the interval that starts in 2009. The wire was replaced in 2009 causing a break in the time series. The gap is bridged using least squares and the data were weighted assuming temporal correlation. The black is the long-term trend, while the red is the residual after removing a constant rate and seasonal sinusoids (365.25- and 182.625-day periods). mm, millimeter.

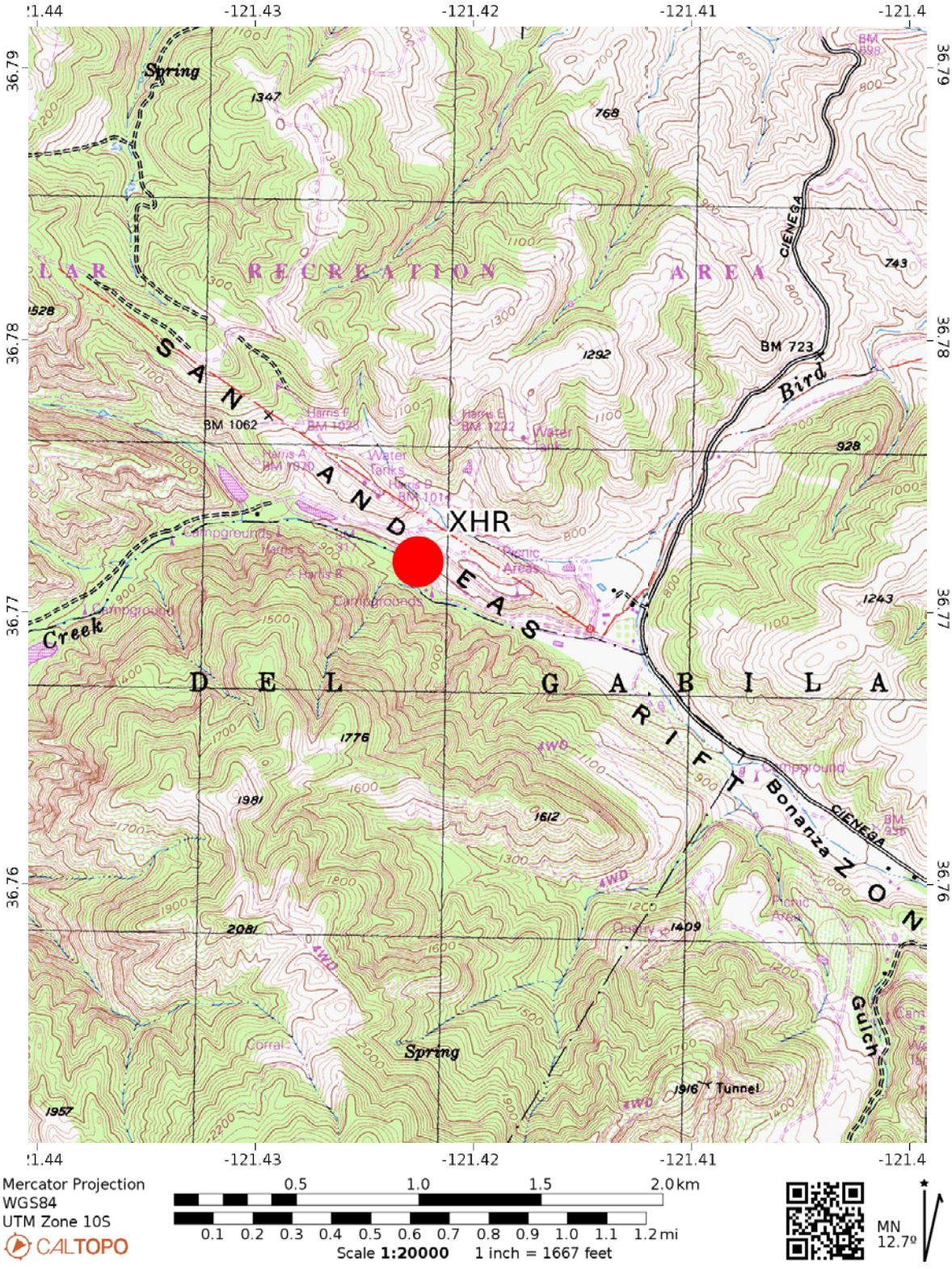

Figure 1.22. Location map of the Harris Ranch (XHR) creepmeter located on the San Andreas Fault southeast of San Juan Bautista, California.

CWN/CWC—Cienega Winery North and Central—San Andreas Fault
Location: 36.74968° N., 121.38498° W.
Orientation: 0°, 15-cm beam; see below
Creep rate for CWN: 13.25±0.39 mm/yr
Creep rate for CWC: 10.99±0.33 mm/yr
Percentage of creep that occurs in discrete events: CWN, 61%
CWC, 68%

Two or more instruments have operated at this location in a building containing a winery on Cienega Road south of Hollister, California, for much of the past five decades. Telemetered data for most of this period have come from instruments of similar design installed across the northern and central parts of a construction joint on the floor of an active winery. The geometry of each of the sensors is unusual in that, unlike all the other creepmeters in the USGS network, the creepmeter geometries are compact (<30 cm), the obliquity to the fault strike is less than 3 degrees, and as a result the sensors effectively require no obliquity correction. In each, a passive anchor is bolted to the edge of the western slab and a linear, variable resistor attached to the edge of the eastern slab.

Although the record of creep extends back to 1948 (Burford, 1988), continuous measurement started in 1968. The record at CWC stops in 1998 because the bolts holding the creepmeter corroded and broke. A similar problem occurred in 2003 for CWN, and those bolts were replaced in 2005. The bolts failed again in 2021 and were replaced with a stainless-steel assembly. In addition, the variable resistor sensor was replaced with an LVDT. Least squares regression that factors the temporal correlations in these data was used to bridge gaps in the data.

Note that the comparison between the electronic and manual measurements for CWN indicated that the potentiometer had a 7% change in scale after July 2013.

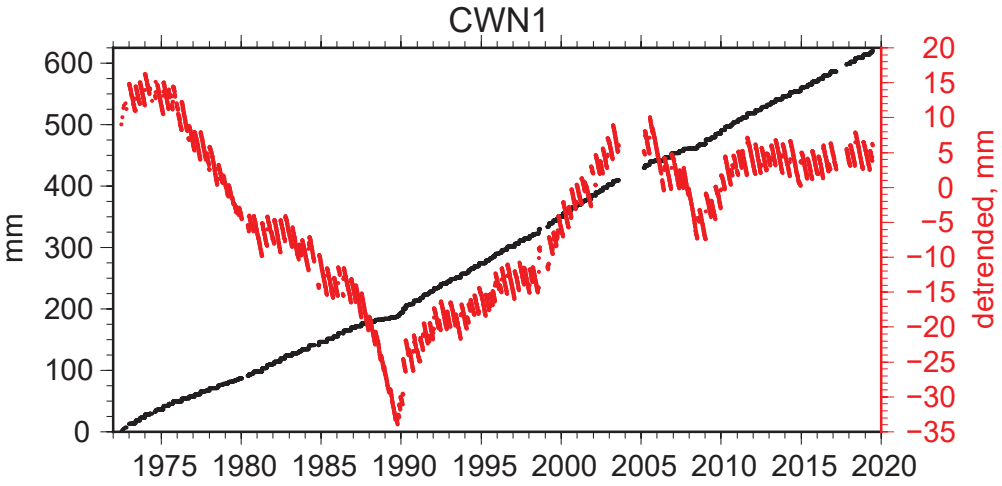

Figure 1.23. Plot showing the observed values of right-lateral slip at the Cienega Winery North (CWN) creepmeter on the San Andreas Fault south of Hollister, California. The bolts holding the creepmeter broke in 2003 but were replaced in 2005. Those bolts failed again in 2021 and were replaced with a stainless-steel assembly. Least squares regression that factors the temporal correlations in these data was used to bridge gaps in the data. The black is the long-term trend, while the red is the residual after removing a constant rate and seasonal sinusoids (365.25- and 182.625-day periods). mm, millimeter.

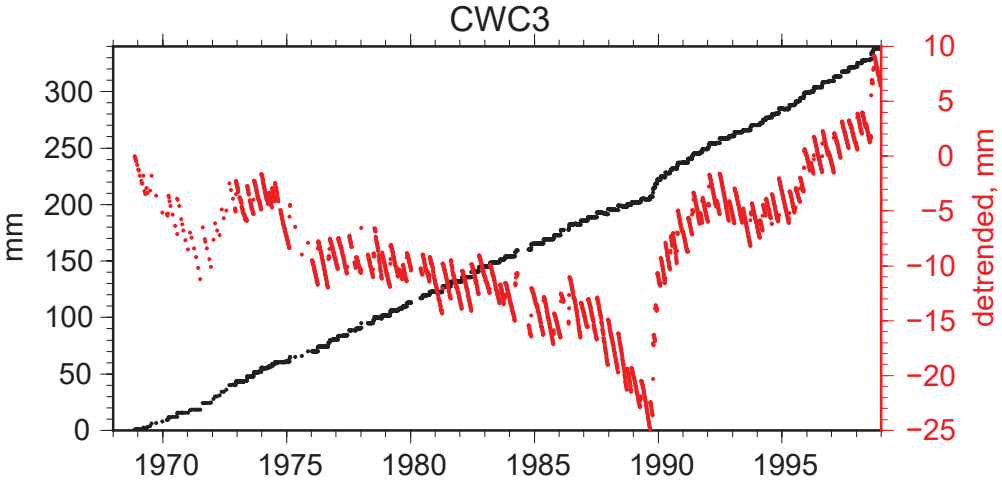

Figure 1.24. Plots showing the observed values of right-lateral slip at the Cienega Winery Central (CWC) creepmeter on the San Andreas Fault south of Hollister, California. The record at CWC stops in 1998 because the bolts holding the creepmeter corroded and broke. The black is the long-term trend, while the red is the residual after removing a constant rate and seasonal sinusoids (365.25- and 182.625-day periods). The 1972 Mw 4.8 San Juan Bautista and Loma Prieta 1989 (see figure 10 in main text) earthquakes are each followed by accelerated slip.

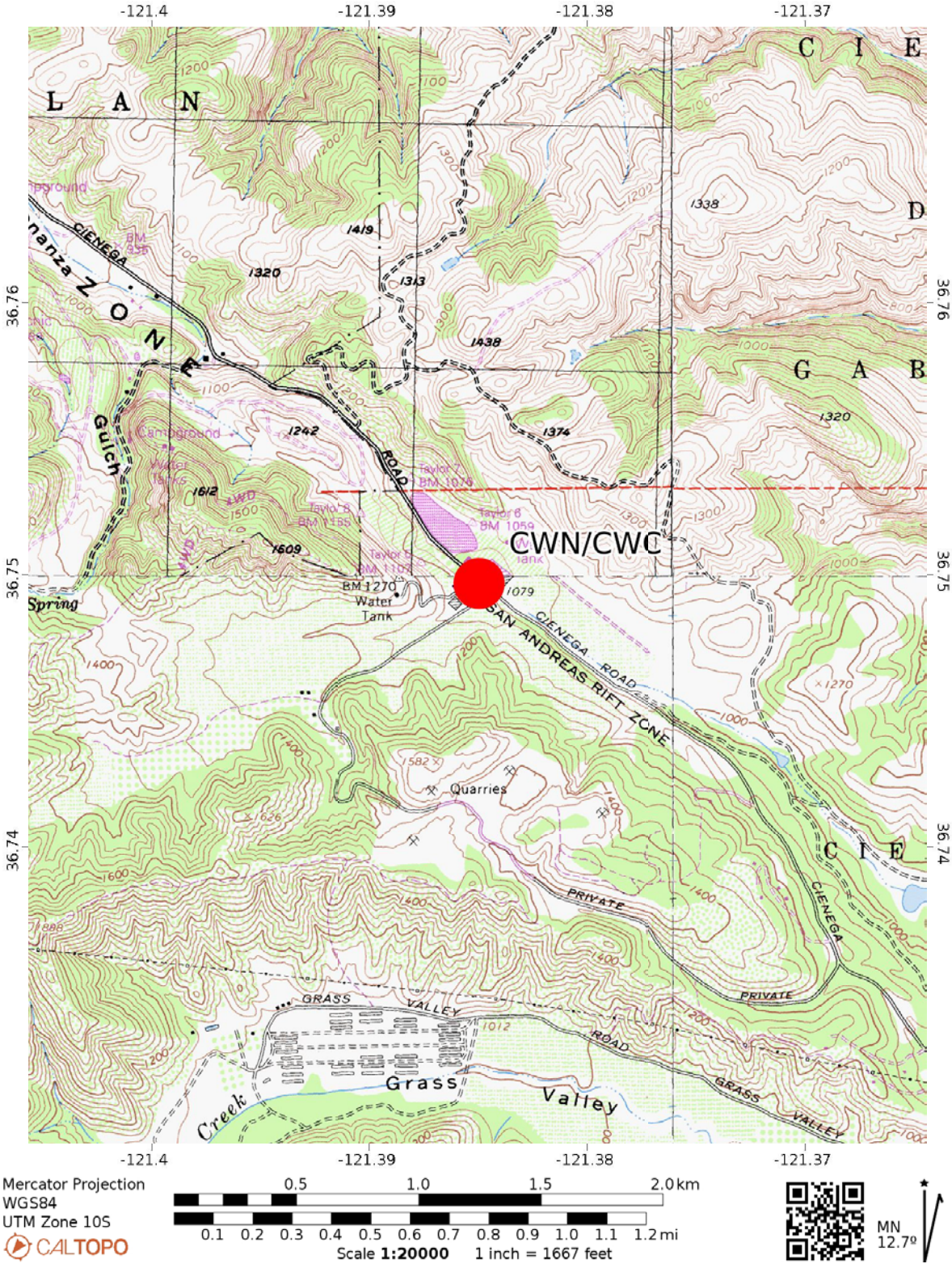

Figure 1.25. Location map of the Cienega Winery North (CWN) and Cienega Winery Central (CWC) creepmeters in the San Andreas Fault located south of Hollister, California. Telemetered data come from instruments of similar design installed across the northern and central parts of a construction joint on the floor of an active winery. The record at CWC stops in 1998 because the bolts holding the creepmeter corroded and broke. The creepmeter location is plotted as a red dot in the center of the map.

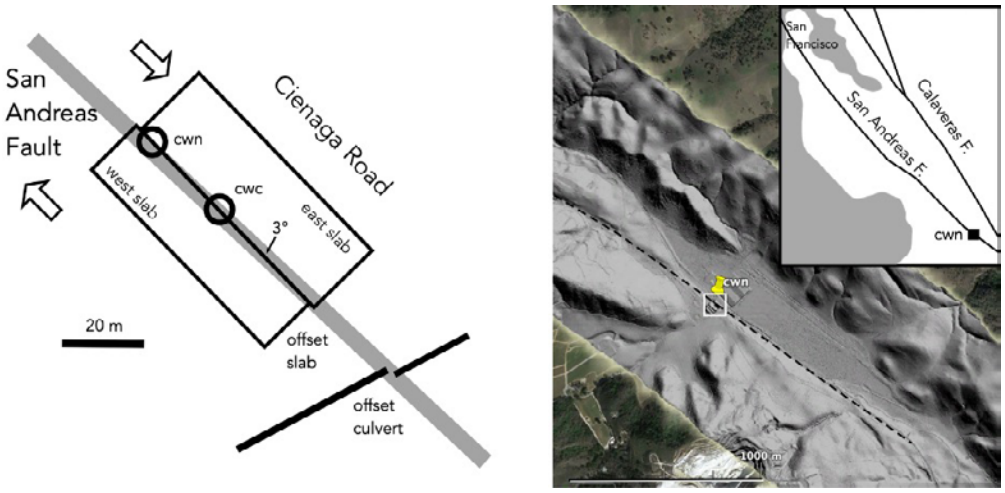

Figure 1.26. Plan and light detection and ranging (lidar) view of the Cienega Winery showing creepmeter locations in the winery on the San Andreas Fault located south of Hollister, California. CWN, Cienega Winery North; CWC, Cienega Winery Central.

Historical note: Creep was first quantified in 1955 on the San Andreas Fault at Cienega winery building (then known as the W.A. Taylor Winery, and now known as the DeRose Winery) on Cienega Road, 10 km south of Hollister by Steinbrugge and Zacher (1960). The fault passes close to the construction joint between two contiguous ~20-m-wide horizontal concrete slabs poured in late 1948 at 3° to the strike of the fault. By 1956, when creep was first reported, the slabs had been offset in a dextral sense by ~15 cm (Tocher, 1960). The first continuous record of creep was obtained using a modified clockwork barometer with its ink-pen linked to the far side of the fault, writing on a paper chart that was replaced weekly. Various instruments have recorded their incremental offset since then at 11–15.5 mm/year (Schulz, 1989).

The other unique property of the CWN creep location is that since the date of the construction is known (1948), the absolute offset since then provides a measure of cumulative slip. Certain difficulties existed in February 2022 in accessing the original corners of the two foundation slabs, but the following measurements are on record. The slabs had been cumulatively offset in a dextral sense by 99.7±4 cm and had separated orthogonally by 5.8±0.3 cm in the north and by 7.3±0.3 mm in the south. Hence, mean dextral slip since 1948 has been 13.47 mm/year accompanied by an opening rate 0.89 mm/yr. At the north end near the presently operating creepmeters, the slabs had separated obliquely at an angle of 3.3° and at the southern end at 4.2°, corresponding to counterclockwise rotation of the eastern foundation slab of 3.6 microradians/year (μrad/year) relative to the western slab.

The observed separation vector at CWN (3.3°) is almost identical to the mapped obliquity of the fault relative to the foundation construction joint (3°) and hence the fault can be assumed to undergo pure dextral slip with no significant dilation. During this same time interval (1948–2022) the east slab had subsided approximately equal to (≈) 5 mm relative to the west slab, corresponding to a mean subsidence rate of ≈14 micrometers/year (μm/yr).

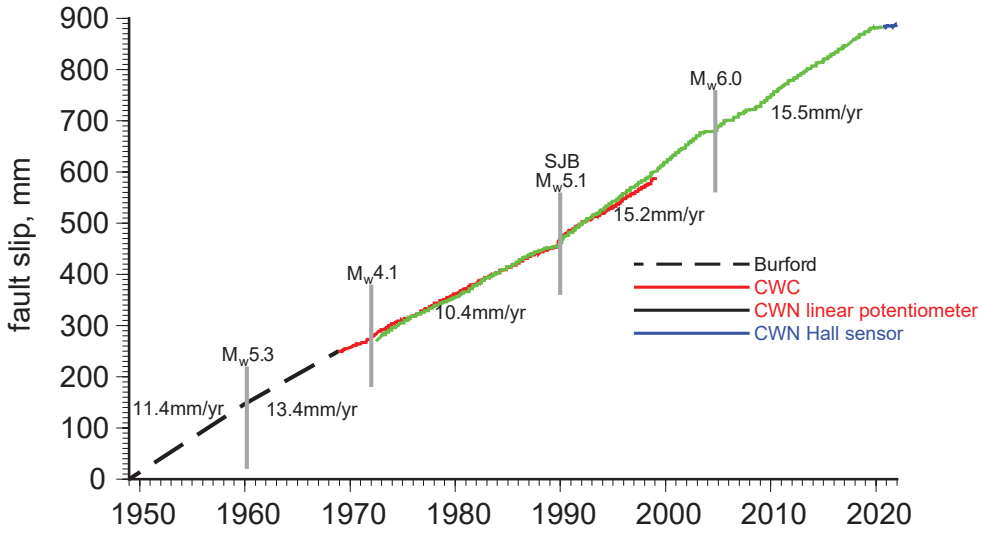

Figure 1.27. Summary of rate changes for Cienega Winery Central (CWC) and Cienega Winery North (CWN) located on the San Andreas Fault south of Hollister, California. The record of creep extends back to when the slab was poured in 1948 (Burford, 1988) and continuous measurement started in 1968. Flat portions of the record correspond to corrosion of the instrument attachment bolts. The record at CWC stops in 1998 because the bolts holding the creepmeter corroded and broke. A similar problem occurred in 2003 for CWN, and those bolts were replaced in 2005. Those bolts failed again in 2021 and were replaced with a stainless-steel assembly. Least squares regression that factors the temporal correlations in these data was used to bridge gaps in the data. mm, millimeter.

XFL—Frank Lewis Long—San Andreas Fault
Location: 36.66560° N., 121.27267° W.
Orientation: 30°, USGS standard, 27-m wire
Creep rate: 7.21±0.10 mm/yr
Percentage of creep that occurs in discrete events: 30%

The Frank Lewis Long (XFL) creepmeter was installed in 1973 south of Hollister, California, and operated until 1995. The creep rate was 7.2 mm/yr, substantially lower than its neighboring instrument to the north, CWN (fig. 1.25), and to the south, XMR (fig. 1.31). It is possible that additional slip occurs on a nearby mapped trace of the fault.

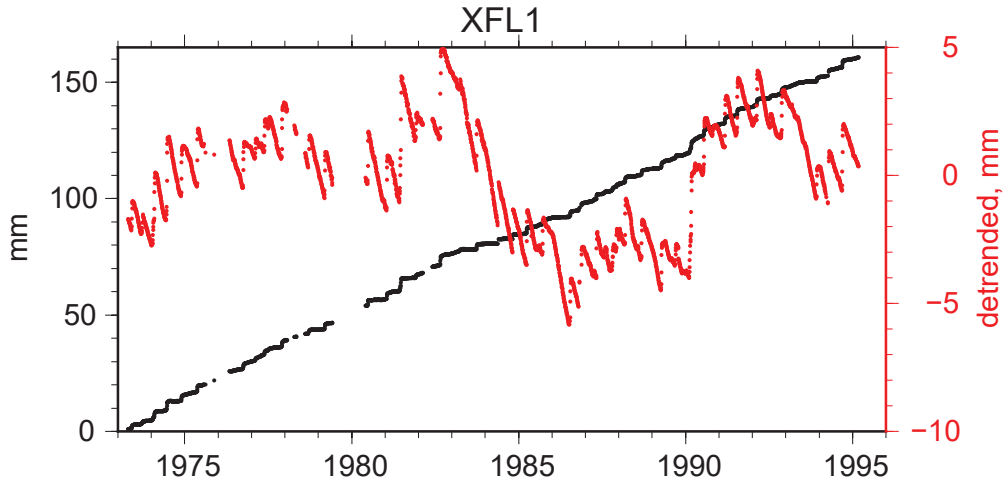

Figure 1.28. Plot showing the observed values of right-lateral slip at the Frank Lewis Long (XFL) creepmeter on the San Andreas Fault south of Hollister, California. The creepmeter was installed in 1973 and operated until 1995. The black is the long-term trend, while the red is the residual after removing a constant rate and seasonal sinusoids (365.25- and 182.625-day periods). mm, millimeter.

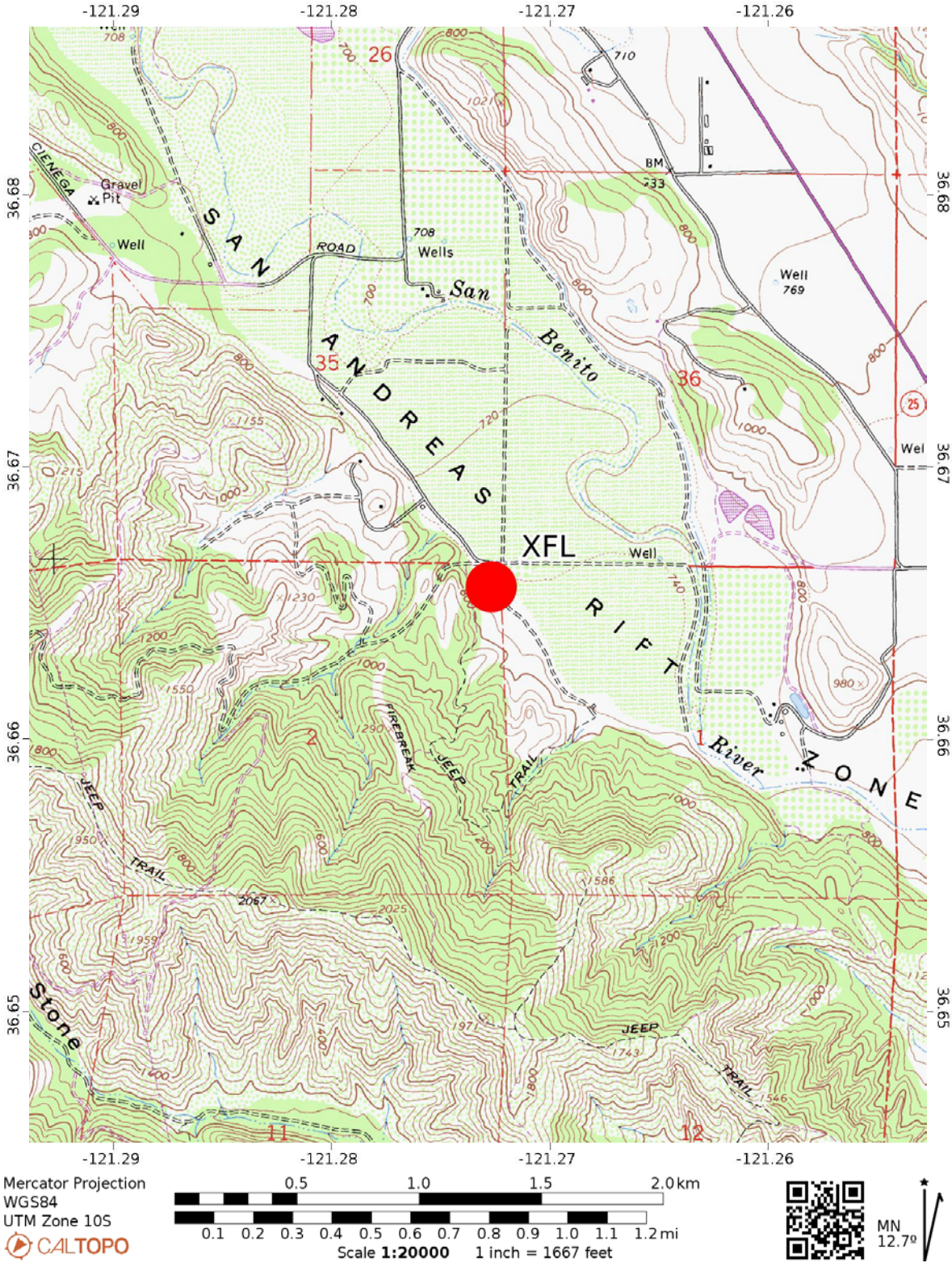

Figure 1.29. Location map of the Frank Lewis Long (XFL) creepmeter on the San Andreas Fault located south of Hollister, California. The creepmeter was installed in 1973 and operated until 1995. The creepmeter location is plotted as a red dot in the center of the map.

XMR—Melendy Ranch—San Andreas Fault
Location: 36.59334 ° N., 121.18705 ° W.
Orientation: 30°, USGS standard, 10-m Invar wire; Replaced in 2018 with Bilham #2 mechanism with a carbon fiber rod.
Creep rate: 16.85±0.33 mm/yr
Percentage of creep that occurs in discrete events: 46%

This instrument was installed in 1969 south of Hollister, California, and operated continuously through mid-2014, when the wire broke due to a cave-in of the conduit. In 2018, the site was rebuilt using a Bilham #2 style set-up with a Hall-effect sensor and a carbon fiber rod. The same monuments have been retained. Note that the post-2018 data have been appended to the pre-2014 data by extrapolating the long-term trend. Formal least squares using the assumption of temporally correlated data was employed to bridge the absence of observations.

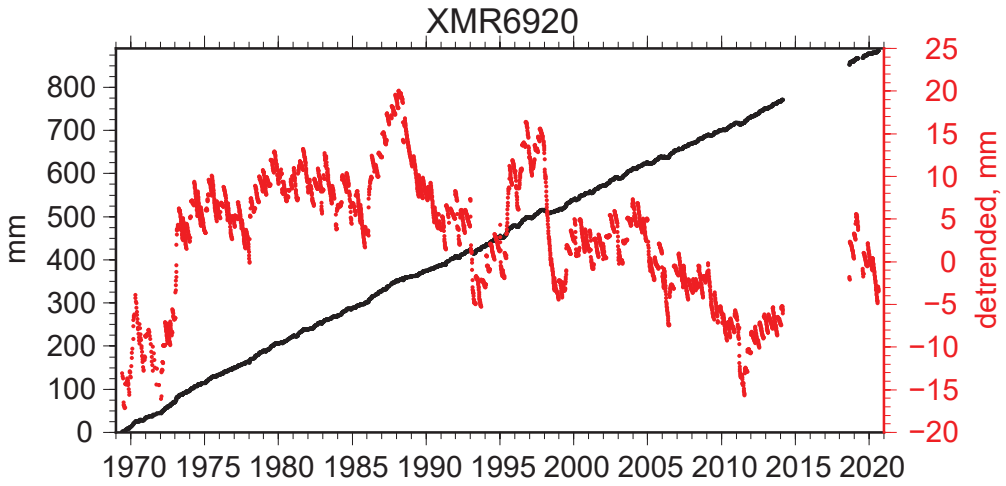

Figure 1.30. Plot showing the observed values of right-lateral slip at the Melendy Ranch (XMR) creepmeter on the San Andreas Fault south of Hollister, California. XMR was installed in 1969 and operated continuously through mid-2014, when the wire broke. In 2018, the site was rebuilt. Note that the post-2018 data have been appended to the pre-2014 data by extrapolating the long-term trend. Formal least squares using the assumption of temporally correlated data was employed to bridge the absence of observations. The black is the long-term trend, while the red is the residual after removing a constant rate and seasonal sinusoids (365.25- and 182.625-day periods). mm, millimeter.

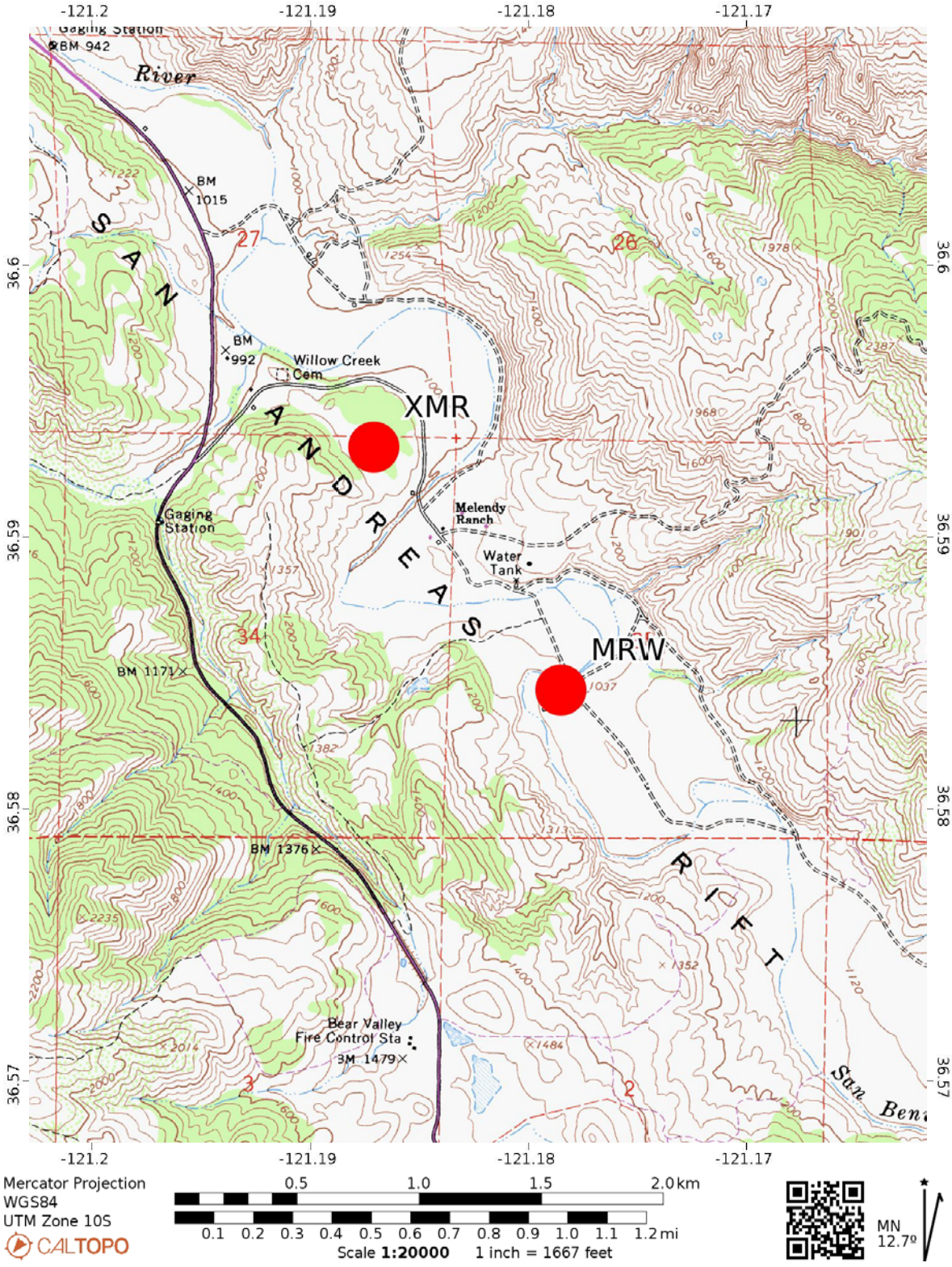

Figure 1.31. Location map of the Melendy Ranch (XMR) and Melendy Windmill (MRW) creepmeters on the San Andreas Fault south of Hollister, California. The creepmeter locations are plotted as red dots.

MRW—Melendy Windmill—San Andreas Fault
Location: 36.58438° N., 121.17851° W.
Orientation: 45°, USGS standard, 23-m rod
Creep rate: 17.19±0.36 mm/yr

This instrument was initially installed in 1972 and rebuilt in 1981, and the last set of manual measurements were made in late 2004. The long-term rate is 17.2 mm/yr. The MRW site was the southernmost creepmeter of five creepmeters located on the Melendy Ranch south of Hollister, California. These meters covered about a 1.3 km stretch of the San Andreas Fault and Schulz (1989) reported between 16 and 20 mm/yr creep rates for these sites during the 1970s and 1980s when the full array was actively recording data. For the location of this site, see map in the preceding description for XMR (fig. 1.31).

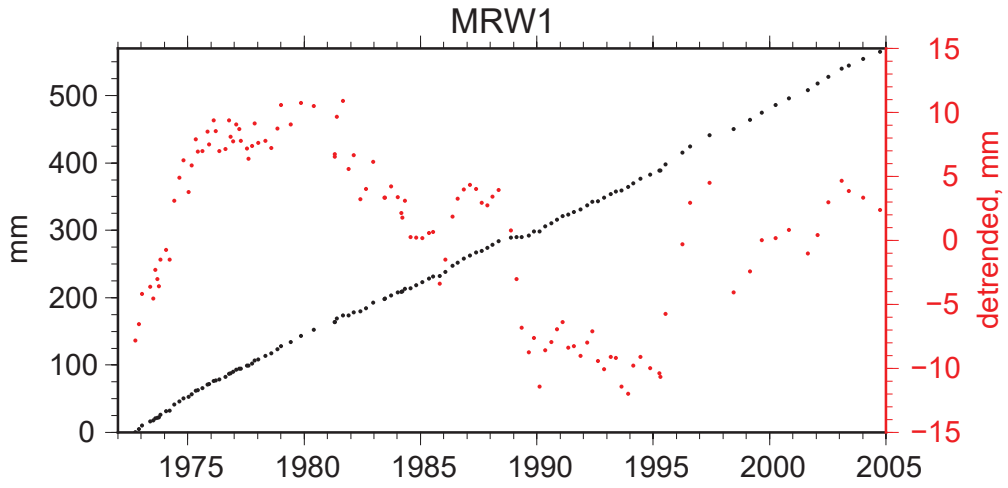

Figure 1.32. Plot showing the observed values of right-lateral slip at the Melendy Windmill (MRW) creepmeter on the San Andreas Fault south of Hollister, California. This instrument was initially installed in 1972 and rebuilt in 1981, and the last set of manual measurements were made in late 2004. The black is the long-term trend, while the red is the residual after removing a constant rate and seasonal sinusoids (365.25- and 182.625-day periods). mm, millimeter.

XDL2—Dry Lake Long—San Andreas Fault
Location: 36.49066° N., 121.07805° W.
Orientation 30°, USGS standard, 12-m wire
Creep rate: 0.73±0.51 mm/yr

This creepmeter was installed in 1973 northwest of Parkfield, California, and the last measurement was in 2002 before it was abandoned. The rate was 0.7 mm/yr. Unfortunately, this instrument did not span the fault as intended.

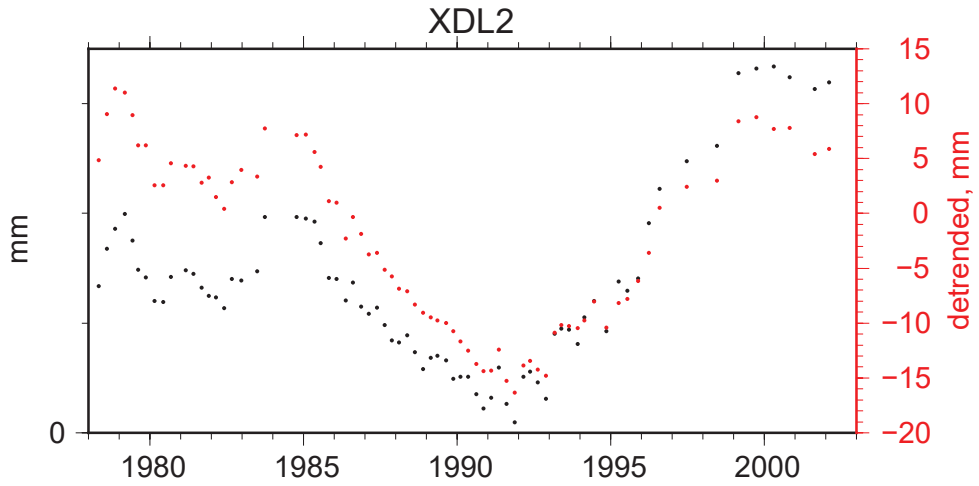

Figure 1.33. Plot showing the observed values of right-lateral slip at the Dry Lake Long (XDL) creepmeter on the San Andreas Fault northwest of Parkfield, California. XDL was installed in 1973 and the last measurement was in 2002 before it was abandoned. Unfortunately, this instrument did not span the fault as intended. The black is the long-term trend, while the red is the residual after removing a constant rate and seasonal sinusoids (365.25- and 182.625-day periods). mm, millimeter.

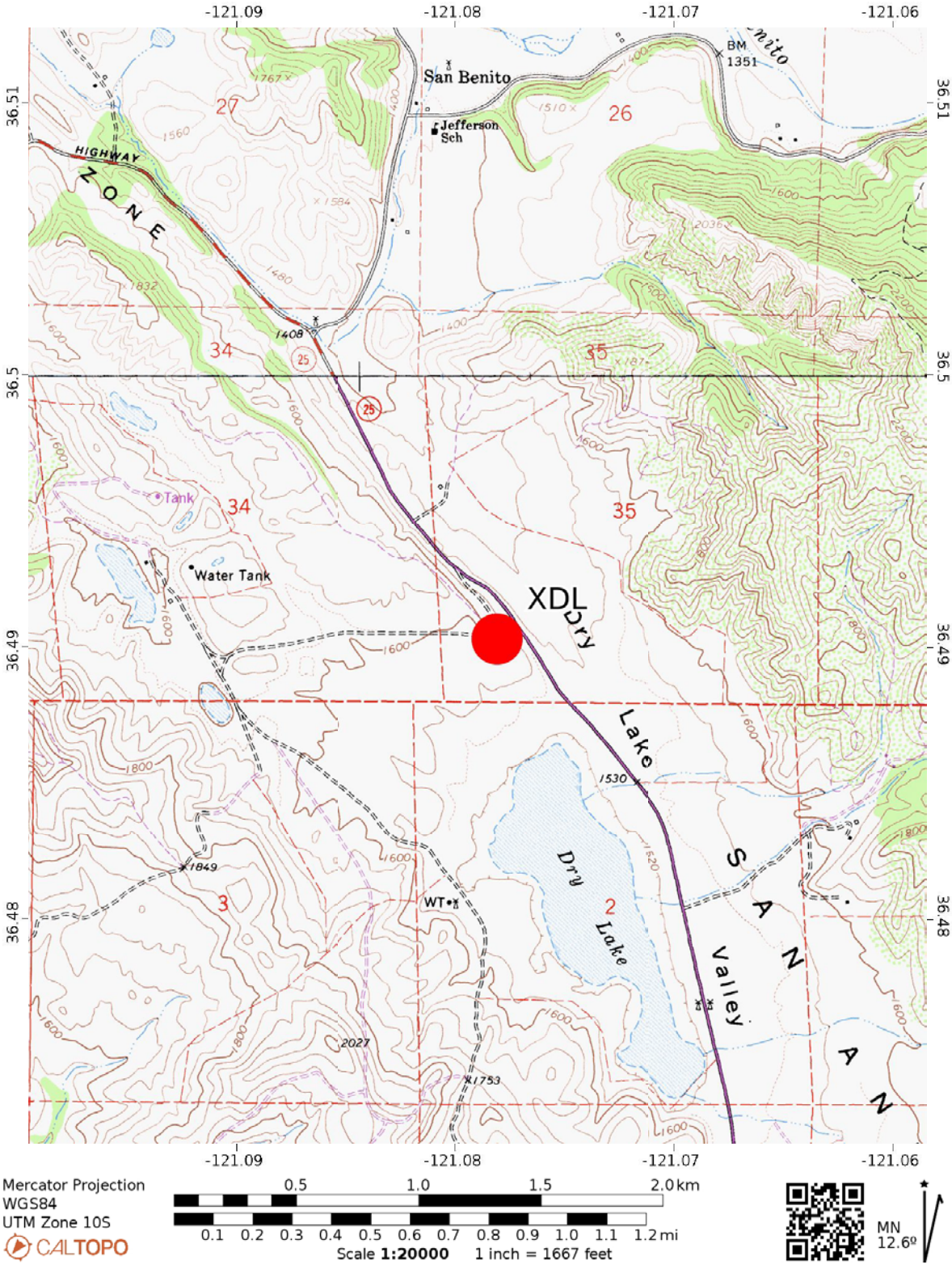

Figure 1.34. Location map of the Dry Lake Long (XDL) creepmeter on the San Andreas Fault located northwest of Parkfield, California. XDL was abandoned in 2002. Unfortunately, this instrument did not span the fault as intended. The creepmeter location is plotted as a red dot.

BIT—Bitterwater—San Andreas Fault
Location: 36.39745° N., 120. 98325° W.
Orientation: 45°, USGS standard, 18-m rod
Creep rate: 16.48±0.44 mm/yr

This site was installed in 1969 and abandoned in 1995.

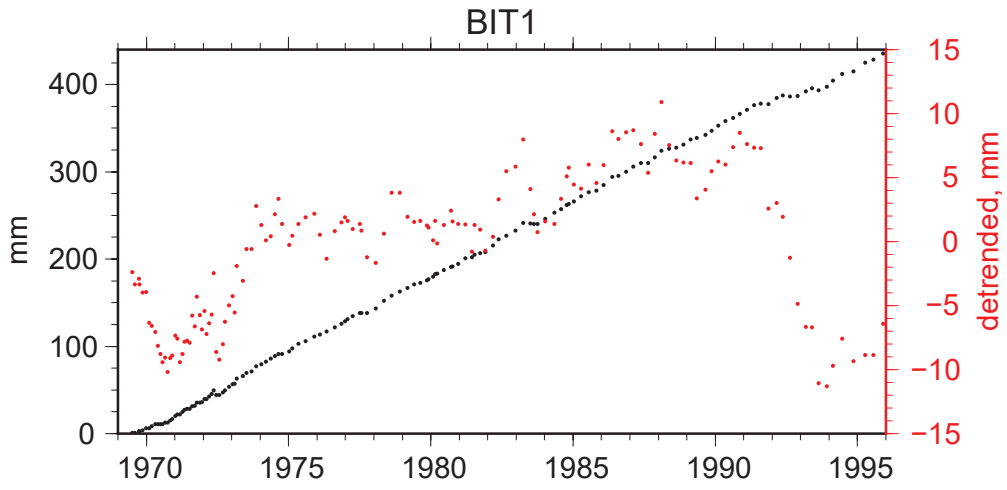

Figure 1.35. Plots showing the observed values of right-lateral slip at the Bitterwater (BIT) creepmeter on the San Andreas Fault northwest of Parkfield, California. BIT was installed in 1969 and abandoned in 1995. The black is the long-term trend, while the red is the residual after removing a constant rate and seasonal sinusoids (365.25- and 182.625-day periods). mm, millimeter.

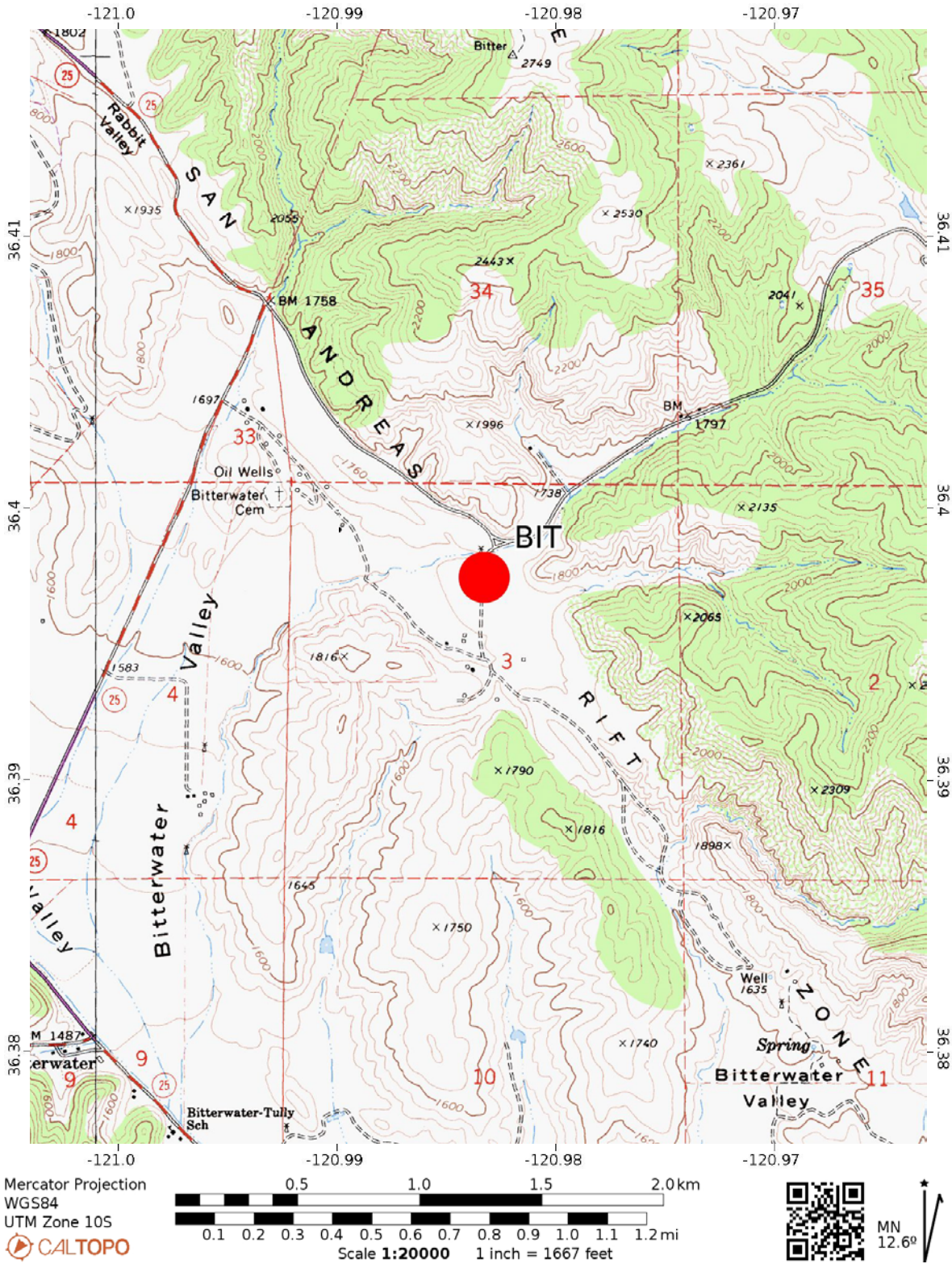

Figure 1.36. Location map of the Bitterwater (BIT) creepmeter on the San Andreas Fault located northwest of Parkfield, California. This site was installed in 1969 and abandoned in 1995. The creepmeter location is plotted as a red dot.

XMP Monarch Peak—San Andreas Fault
Location: 36.21699° N., 120.79760° W.
Orientation: 30°, USGS standard, 10-m wire
Creep rate: 14.66±0.42 mm/yr

This site was installed northwest of Parkfield, California, in 1969 and abandoned in 1997. Schulz (1989) cautions that this instrument spans the northeastern trace and consequently misses some of the slip. The wire broke in 1988, and the site was repaired but the reference length of the creepmeter was lost. The data were bridged together using measurements from the adjacent alignment array (Burford and Harsh, 1980).

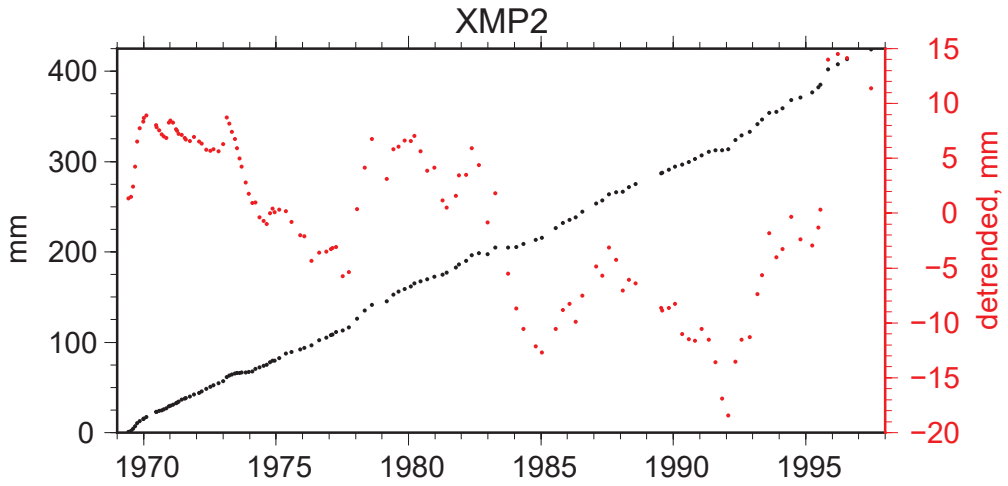

Figure 1.37. Plots showing the observed values of right-lateral slip at the Monarch Peak (XMP) creepmeter on the San Andreas Fault northwest of Parkfield, California. XMP was installed in 1969 and abandoned in 1997. Schulz (1989) cautions that this instrument spans the northeastern trace and consequently misses some of the slip. The wire broke in 1988, and the site was repaired but the reference length of the creepmeter was lost. The data were bridged together using measurements from the adjacent alignment array. The black is the long-term trend, while the red is the residual after removing a constant rate and seasonal sinusoids (365.25- and 182.625-day periods). mm. millimeters.

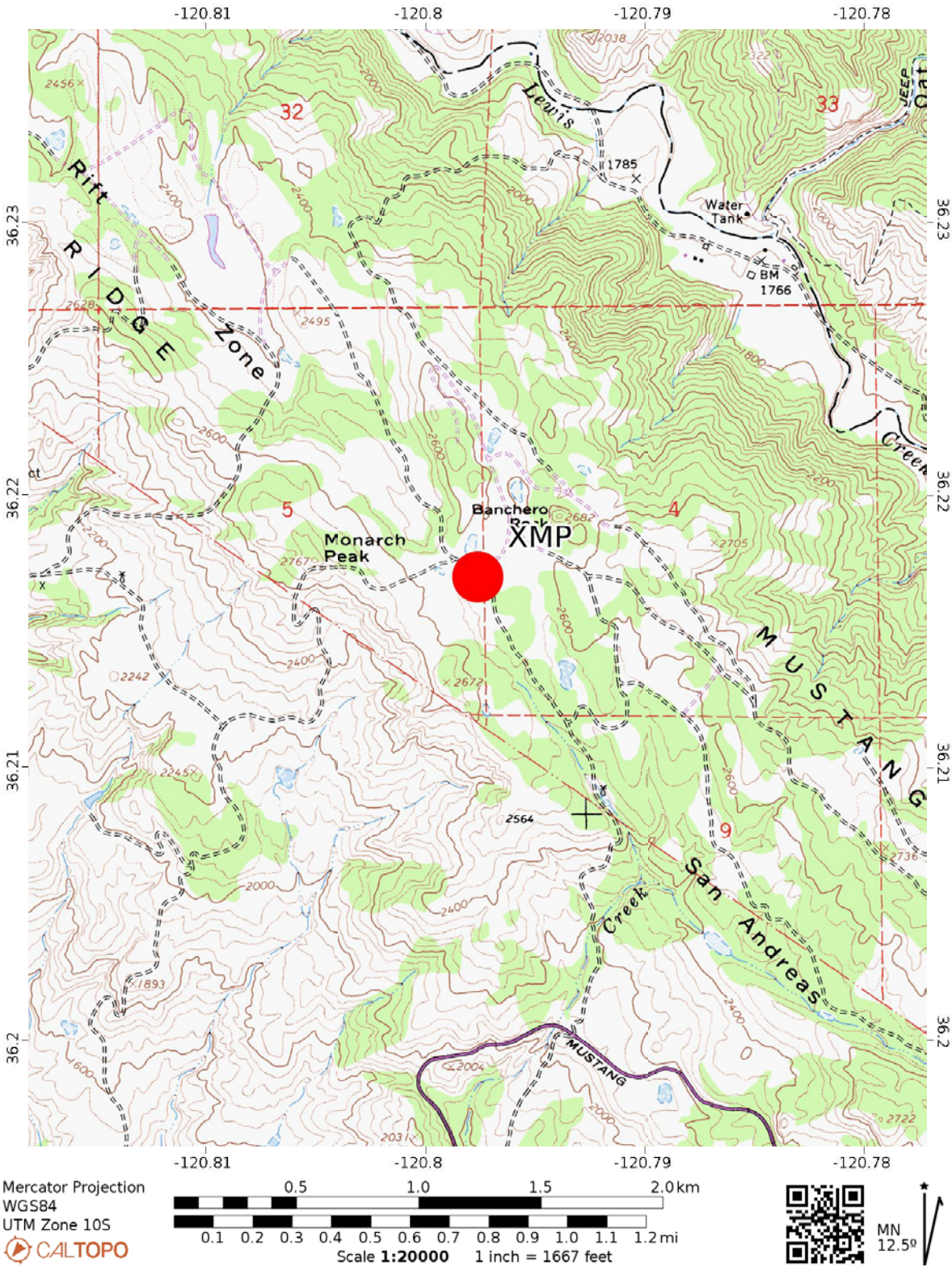

Figure 1.38. Location map of the Monarch Peak (XMP) creepmeter on the San Andreas Fault located northwest of Parkfield, California. This site was installed in 1969 and abandoned in 1997. The creepmeter location is plotted as a red dot.

XSC—Slacks Canyon—San Andreas Fault
Location: 36.06440° N., 120.62937° W.
Orientation: 27°, USGS standard, 10-m wire
Creep rate: 21.30±0.34 mm/yr
Percentage of creep that occurs in discrete events: 3%

This instrument was installed in 1969 northwest of Parkfield, California. Although the orientation of this meter is listed as 27°, its orientation has probably been reduced due to steady, high rate of slip; 21.3 mm/yr since then. There has been a small correction due to the orientation becoming more parallel to the surface trace of the fault. Although this instrument is considered part of the Parkfield network, only insignificant coseismic offset was measured in 2004. The postseismic transient of about a 1-year period essentially recovered the decrease in slip rate between 2000 and the time of the 2004 Parkfield earthquake. Note that the comparison between the electronic and manual measurements indicated that the LVDT had a 3.5% change in scale after July 2011.

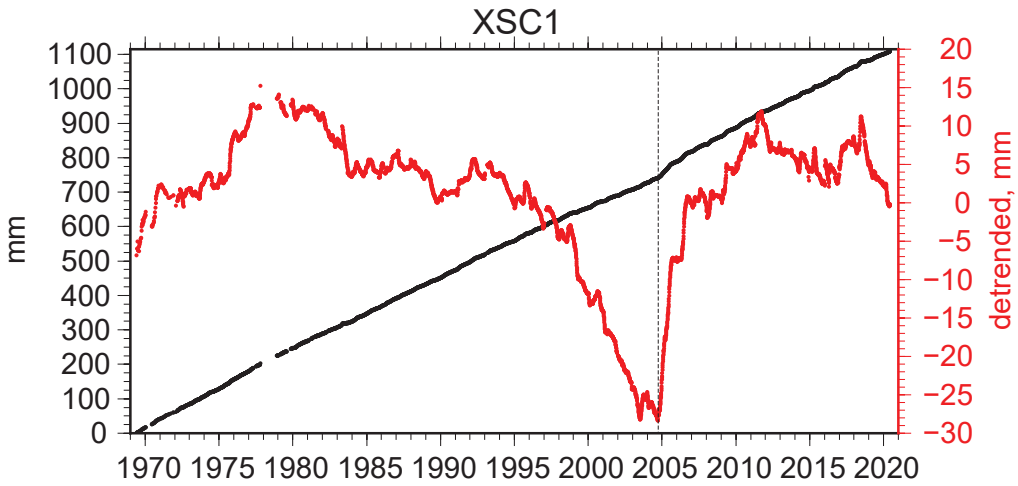

Figure 1.39. Plot showing the observed values of right-lateral slip at the Slacks Canyon (XSC) creepmeter on the San Andreas Fault northwest of Parkfield, California. This instrument was installed in 1969. The black is the long-term trend, while the red is the residual after removing a constant rate and seasonal sinusoids (365.25- and 182.625-day periods). A dashed vertical line shows the time of the 2004 Parkfield earthquake. mm, millimeter.

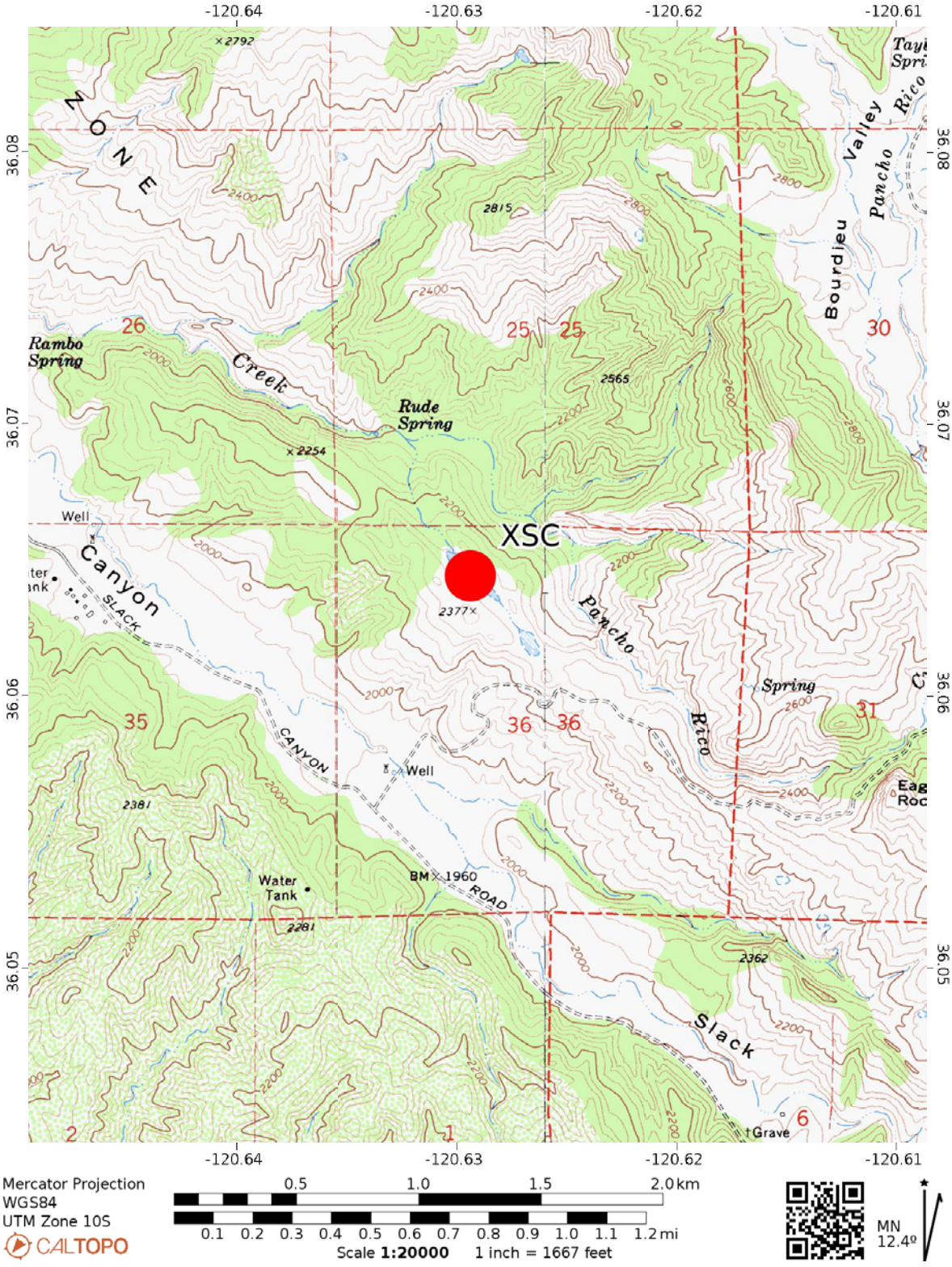

Figure 1.40. Location map of the Slacks Canyon (XSC) creepmeter on the San Andreas Fault located northwest of Parkfield, California. The creepmeter location is plotted as a red dot.

XMM—Middle Mountain—San Andreas Fault
Location: 35.95777° N., 120.50325° W.
Orientation: 30°, USGS standard, 26-m wire
Creep rate: 1980.0–2004.7, 14.98±0.56 mm/yr
Creep rate: 2009.0–2019.4, 17.90±0.95 mm/yr
Percentage of creep that occurs in discrete events: 51%

The creepmeter was installed in 1979 northwest of Parkfield, California. As noted by Schulz (1989), the 1983, *M*6.2 Coalinga Earthquake caused a transient. Immediately following the 2004 Parkfield earthquake, the combination of coseismic offset and early postseismic deformation caused this meter to extend beyond the range of the LVDT sensor. This occurred about 2.5 hours after the time of the mainshock of the Parkfield earthquake. Two days later, the site was serviced, and apparent stretch was measured such that the total displacement was recovered. However, at this site, a low-resolution sensor, using a wire wrapped around the shaft of a linear potentiometer was able to measure the coseismic and immediate postseismic transient. These data are included in the plots of the 10 days spanning the earthquake.

In September 2005, it was noted that there was significant friction on the Invar wire due to the conduit housing the wire being pulled apart from 35 years of slip. In October 2005, the wire was replaced, and the conduit patched.

The long-term plot of the data for XMM1 shows that the Omori functions, both the modified and double, fit the postseismic interval through 2011, when the slip-rate decreased (Langbein and others, 2006). The index, ρ, for the double Omori function is estimated to be 0.9 and its corresponding delay, τ, for the onset of postseismic slip is estimated to be 7 hours. Examination of the raw data from the low-resolution sensor suggests a delay time closer to 2 hours. It is possible that the internal friction with this rupture meter biased the measurement of the delay time and that afterslip could have started immediately after the coseismic displacement.

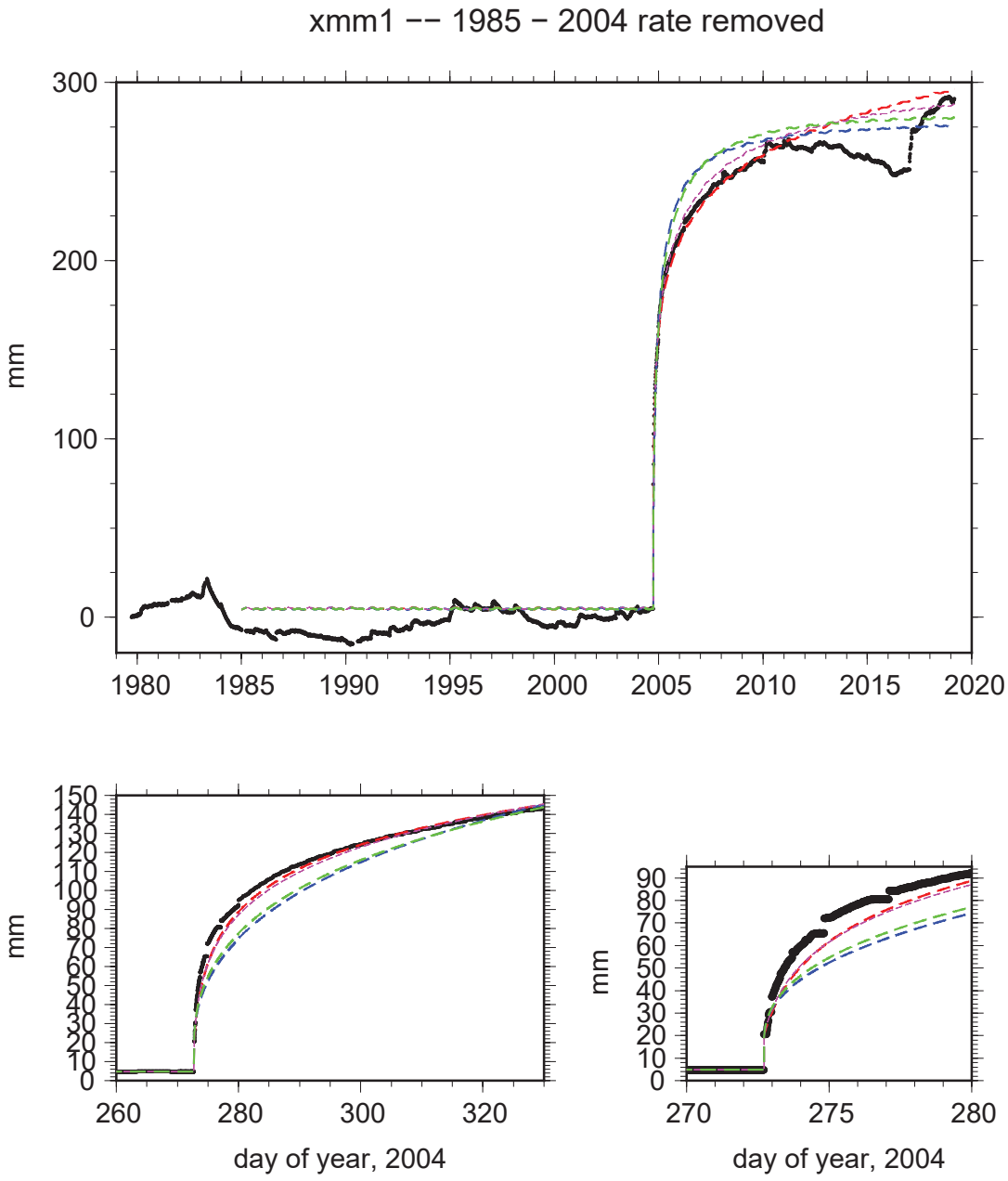

Figure 1.41. Plots of data from the Middle Mountain (XMM) creepmeter on the San Andreas Fault northwest of Parkfield, California, from 1979 to 2020 and spanning the 2004 Parkfield Earthquake (black line). The data prior to the earthquake have had the rate removed using observations between 1985.0 and the time of the Parkfield earthquake, 2004.74. The two lower plots show more detailed data that span the Parkfield earthquake and the initial postseismic slip. The results of fitting four different functions representing postseismic slip are shown. The red curve is result of fitting the modified Omori function to the 1985 to 2020 interval, the blue curve is a fit of the After function, the green curve is a fit to a stretched exponential, and the thin magenta curve is a fit to a double Omori function. See main text, under the heading "Parkfield Postseismic Creep," for discussion about the four functions and the method to fit these models to the data.

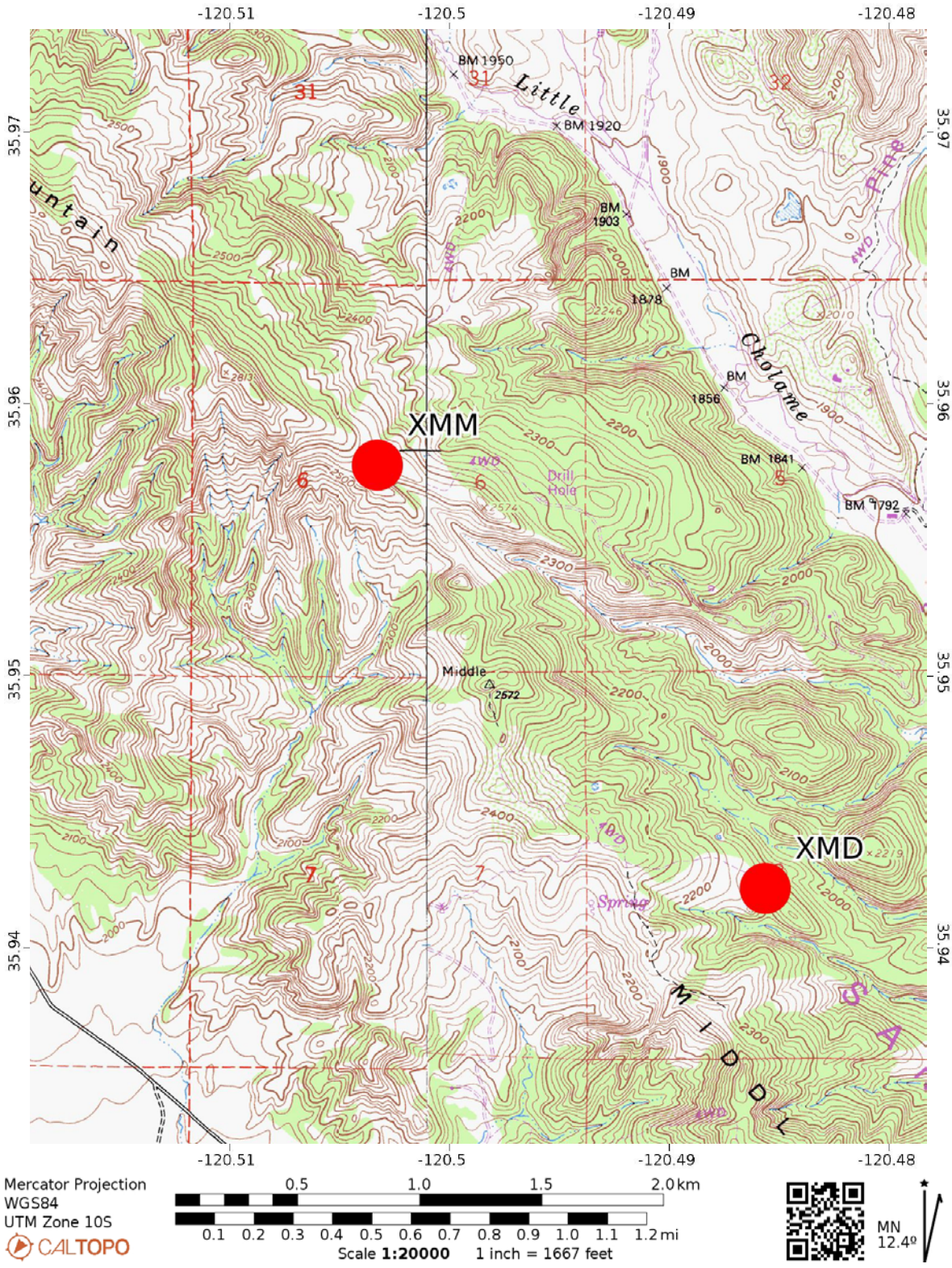

Figure 1.42. Location map of the Middle Mountain (XMM) creepmeter on the San Andreas Fault northwest of Parkfield, California. The creepmeter location is plotted as a red dot. The location of XMM creepmeter's neighbor, Middle Ridge (XMD) is shown on the southeast corner of the map.

XMD—Middle Ridge—San Andreas Fault
Location: 35.94216° N., 120.48560° W.
Orientation: 27°, USGS standard, 36-m wire
Creep rate: 1986.7–2004.7, 11.87±1.42 mm/yr
Creep rate: 2009.0–2020.7, 9.60±2.22 mm/yr
Percentage of creep that occurs in discrete events: 56%

This meter was installed in 1986 northwest of Parkfield, California. From Schulz (1989), the meter spans the most active of the parallel traces of the fault confined to a narrow zone that had been inferred from alignment array measurements dating from 1979. Consequently, Schulz (1989) suggested that seasonal reversal of slip seen on this meter is due to slip occurring on neighbor strands not spanned by the creepmeter.

Immediately following the 2004 Parkfield earthquake, the coseismic offset caused this meter to extend beyond the range of the LVDT sensor. Three days later the site was serviced and apparent stretch was measured such that the total displacement was recovered.

In May 2015, it was noted that the Invar wire was binding because the conduit housing the wire may have stretched beyond its limits allowing the soil to fill the void. To date, this has not been addressed.

Fits of all four postseismic functions are nearly indistinguishable from each other. The fits revealed only a 3% reduction in the variance during the postseismic interval. All four functions overpredict the rate of slip in the postseismic interval. For the Omori law functions either the index, or the delay time, are not resolved due to lack of 10-minute sampled data during the initial days of postseismic deformation (Langbein and others, 2006).

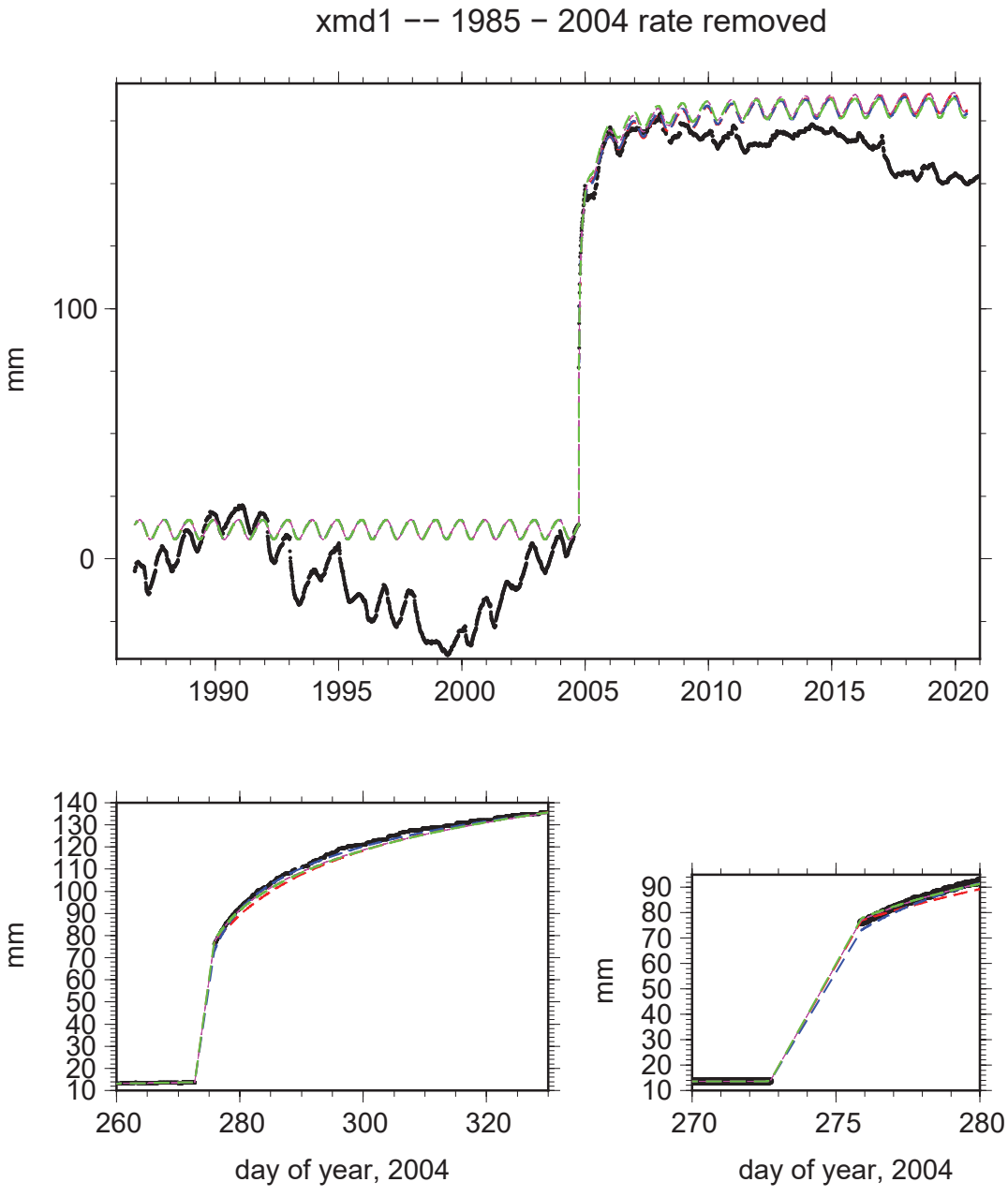

Figure 1.43. Plots of data from Middle Ridge (XMD) creepmeter on the San Andreas Fault northwest of Parkfield, California, from 1986 to 2020 and spanning the 2004 Parkfield earthquake (black line). The data prior to the earthquake have had the rate removed using observations between 1986.0 and the time of the Parkfield earthquake, 2004.74. The two lower plots show more detailed data that span the Parkfield earthquake and the initial postseismic slip. The results of fitting four different functions representing postseismic slip are shown. The red curve is result of fitting the modified Omori function to the 1985 to 2020 interval, the blue curve is a fit of the After function; the green curve is a fit to a stretched exponential, and the thin magenta curve is a fit to a double Omori function. See main text, under the heading "Parkfield Postseismic Creep," for discussion about the four functions and the method to fit these models to the data. Mm, millimeter.

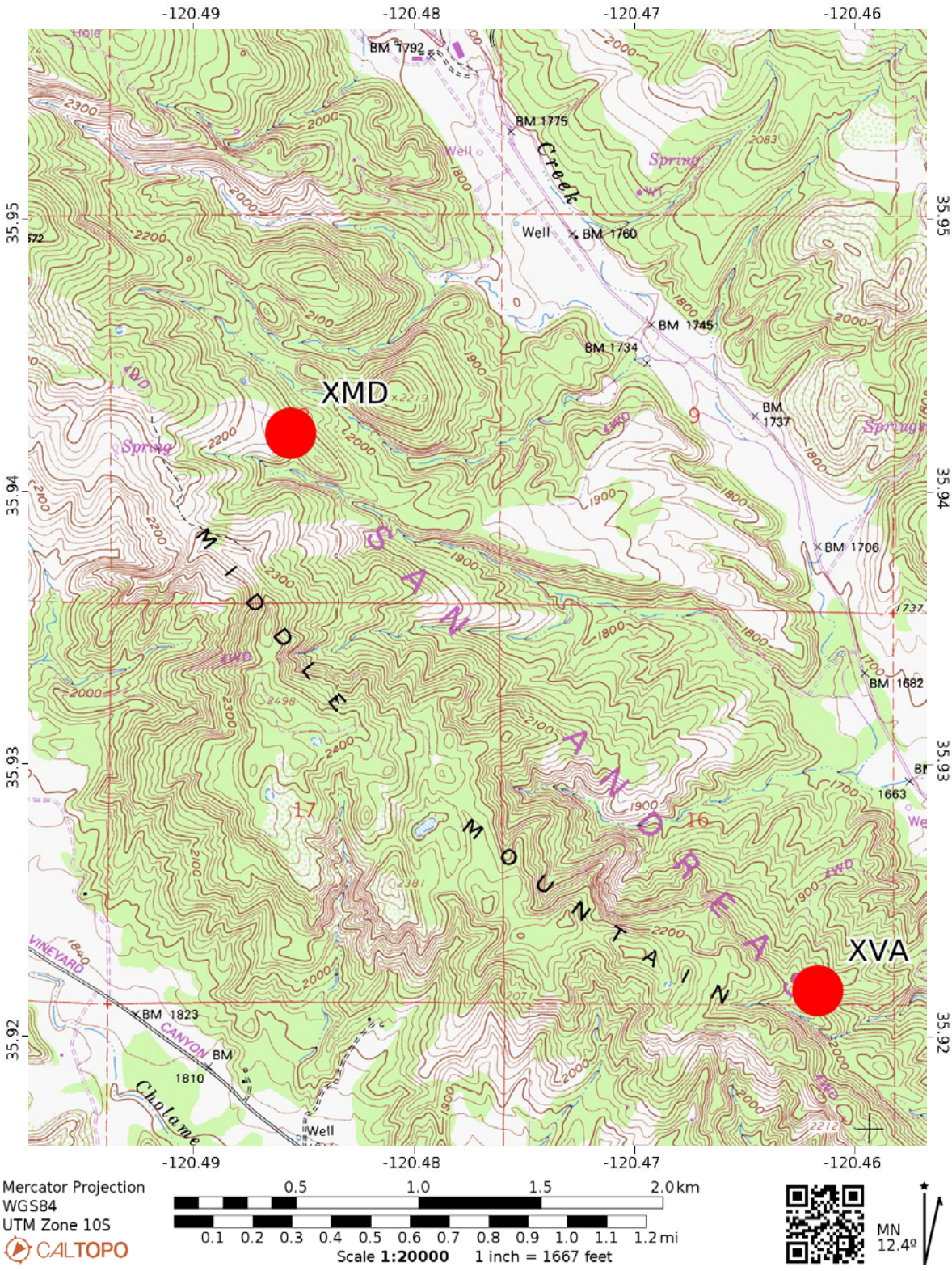

Figure 1.44. Location map of the Middle Ridge (XMD) creepmeter on the San Andreas Fault located northwest of Parkfield, California. The creepmeter location is plotted as a red dot. The location of the XVA creepmeter is shown at the southeast corner of the map.

XVA—Varian—San Andreas Fault
Location: 35.92167° N, 120.46166° W
Orientation 30°, USGS standard, 30-m wire
Creep rate: 1987.4–2004.7, 9.18±1.20 mm/yr
Creep rate: 2009.0–2017.8, 6.45±1.66 mm/yr
Percentage of creep that occurs in discrete events: 66%

This site was installed in 1987 northwest of Parkfield, California. It was removed in November 2017 when the wire broke because the conduit caved in.

Note that the comparison between the electronic and manual measurements indicated that the LVDT had a 2% change in scale after December 2006.

Immediately following the 2004 Parkfield earthquake, the coseismic offset caused this meter to extend beyond the range of the LVDT sensor. Two days later the site was serviced and apparent stretch was measured such that the total displacement was recovered.

Like XMD, the fits of all four postseismic functions are nearly indistinguishable from each other. All four functions overpredict the rate of slip in the postseismic interval. For the Omori law functions either the index, ρ, or the delay time, τ, are not resolved due to lack of 10-minute sampled data during the initial days of postseismic deformation. The fits revealed only a 7% reduction in the variance during the postseismic interval (Langbein and others, 2006).

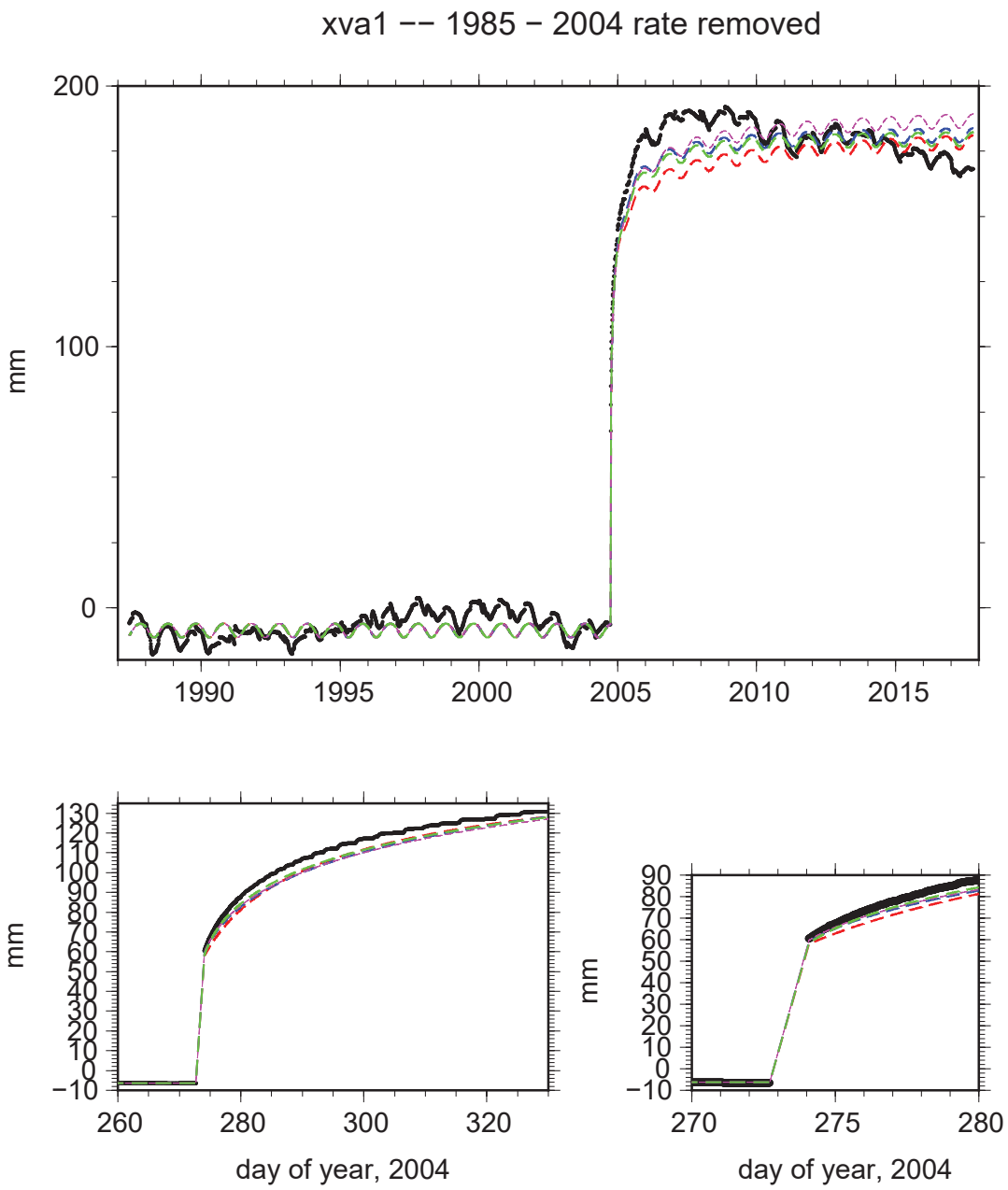

Figure 1.45. Plots of data from the Varian (XVA) creepmeter on the San Andreas Fault northwest of Parkfield, California, from 1986 to 2017 and spanning the 2004 Parkfield earthquake (black line). This site was installed in 1987 and was removed in November 2017 when the wire broke because the conduit caved in. The data prior to the earthquake have had the rate removed using observations between 1986.0 and the time of the Parkfield earthquake, 2004.74. The two lower plots show more detailed data that span the Parkfield earthquake and the initial postseismic slip. The results of fitting four different functions representing postseismic slip are shown. The red curve is result of fitting the modified Omori function to the 1985 to 2020 interval, the blue curve is a fit of the After function, the green curve is a fit to a stretched exponential, and the thin magenta curve is a fit to a double Omori function. See main text, under the heading "Parkfield Postseismic Creep," for discussion about the four functions and the method to fit these models to the data. mm, millimeter.

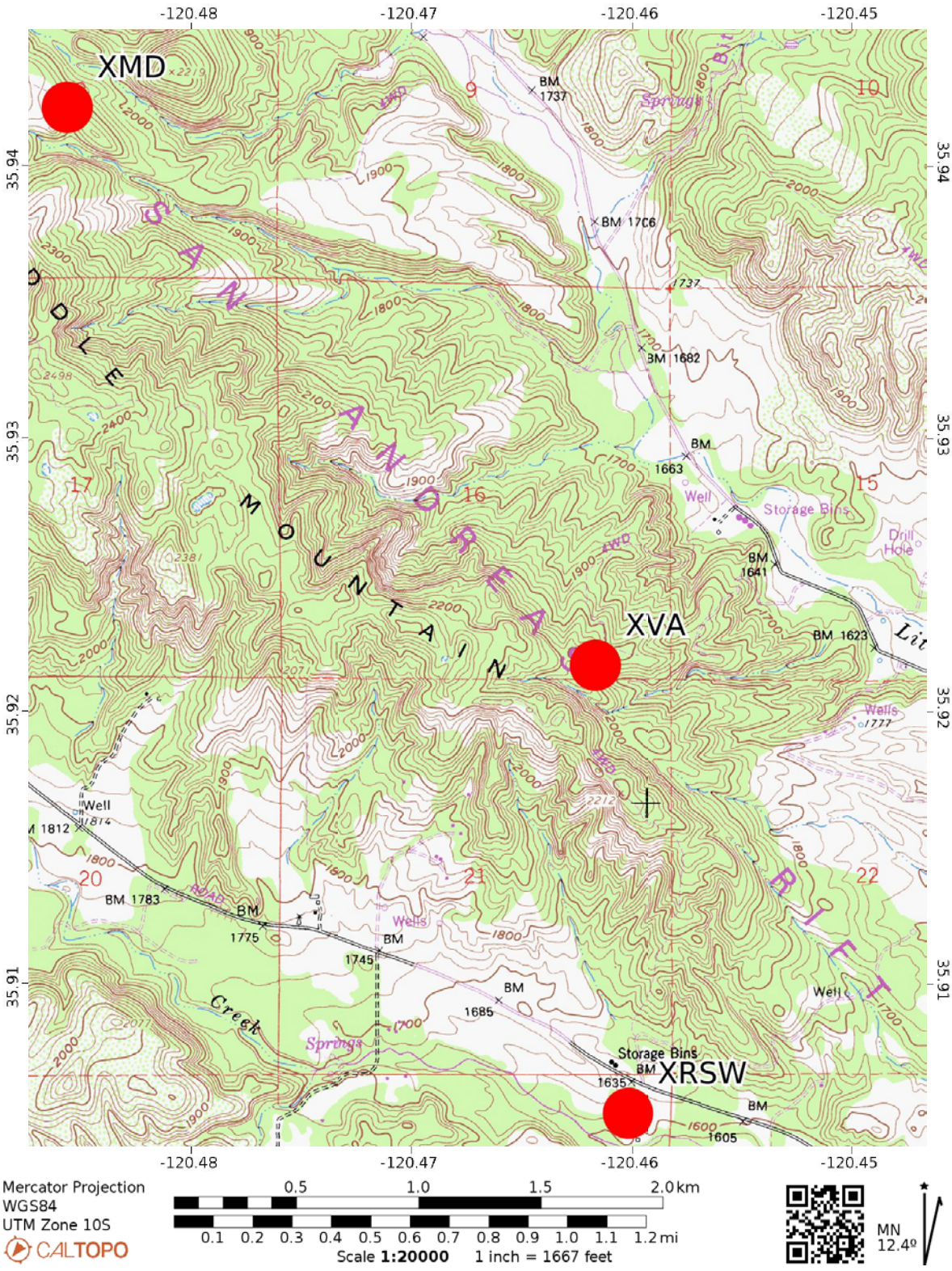

Figure 1.46. Map of the Varian (XVA) creepmeter along with its neighboring instruments Middle Ridge (XMD), both on the San Andreas fault, and Roberson SW Trace (XRSW), that is on the southwest trace of the San Andreas Fault located northwest of Parkfield, California. The creepmeter locations are plotted as red dots.

XRSW—Roberson—San Andreas Fault, SW trace
Location: 35.90522° N, 120.46015° W
Orientation: 30°, USGS standard, 30-m wire
Creep rate: 0.04±0.05 mm/yr

This instrument was installed northwest of Parkfield, California, in 1987 and abandoned in 2005 after the wire broke when the conduit caved in. The instrument is located on a projection of the southwest trace of the San Andreas Fault that was detected by observing echelon cracks in a nearby road. There was 10-mm of slip from the 2004 Parkfield earthquake. The observed, postseismic slip differs from that of the other Parkfield sites as the afterslip ceased within 10 hours. Although none of the four functions modeling afterslip, or an exponential curve, best fits these data.

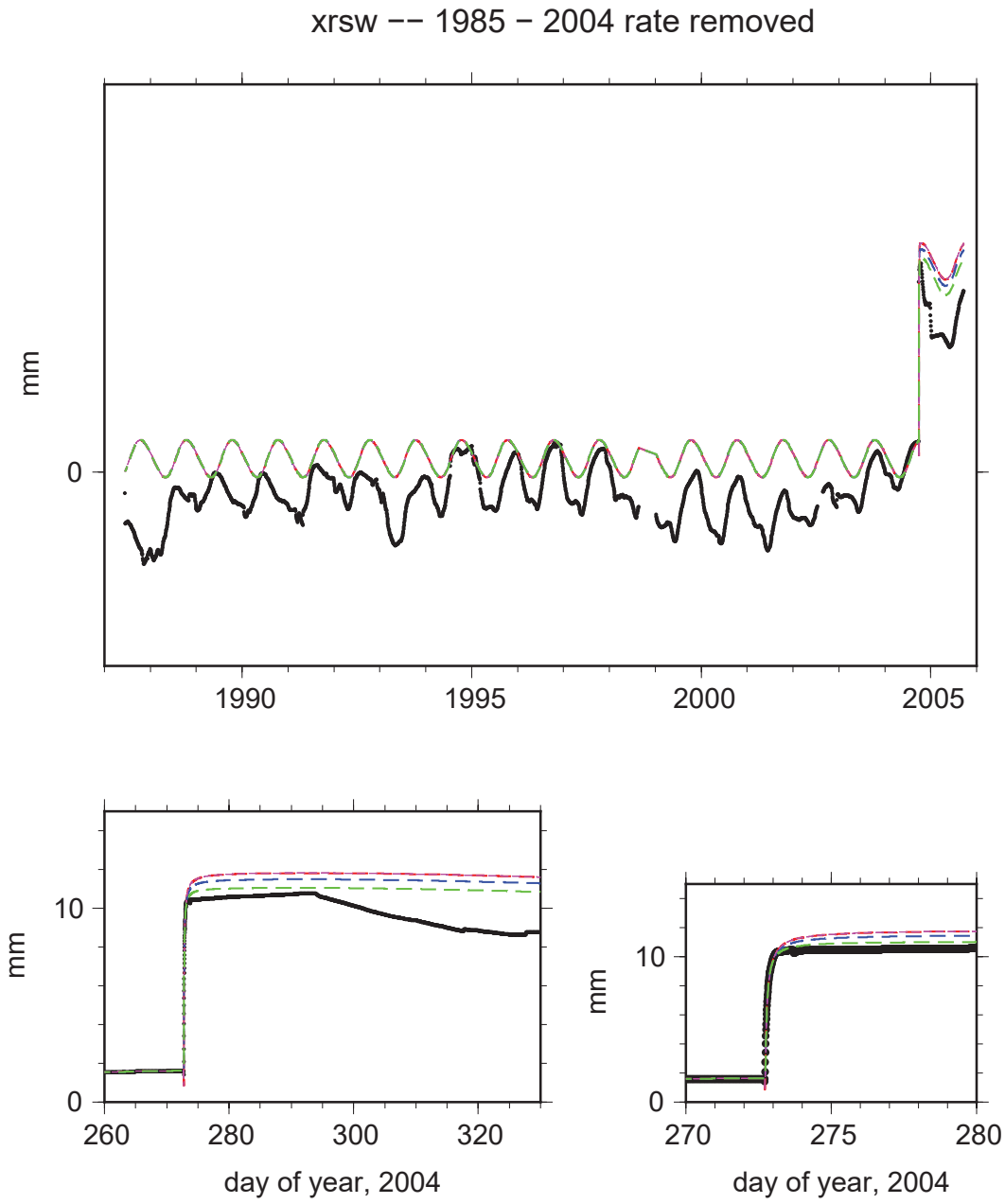

Figure 1.47. Plots of data from Roberson SW trace (XRSW) creepmeter from 1980 to 2005 and spanning the 2004 Parkfield earthquake along the southwest trace of the San Andreas Fault northwest of Parkfield, California (black line). This instrument was installed in 1987 and abandoned in 2005 after the wire broke when the conduit caved in. The data prior to the earthquake have had the rate removed using observations between 1985.0 and the time of the Parkfield earthquake, 2004.74. The two lower plots show more detailed data that span the Parkfield earthquake and the initial postseismic slip. The results of fitting four different functions representing postseismic slip are shown. The red curve is result of fitting the modified Omori function to the 1985 to 2020 interval, the blue curve is a fit of the After function, the green curve is a fit to a stretched exponential, and the thin magenta curve is a fit to a double Omori function. Note that the Invar wire of this creepmeter broke at the time of the earthquake and consequently, the data prior and post-earthquake have been joined using an arbitrary offset at the time of the earthquake. See main text, under the heading "Parkfield Postseismic Creep," for discussion about the four functions and the method to fit these models to the data. mm, millimeter.

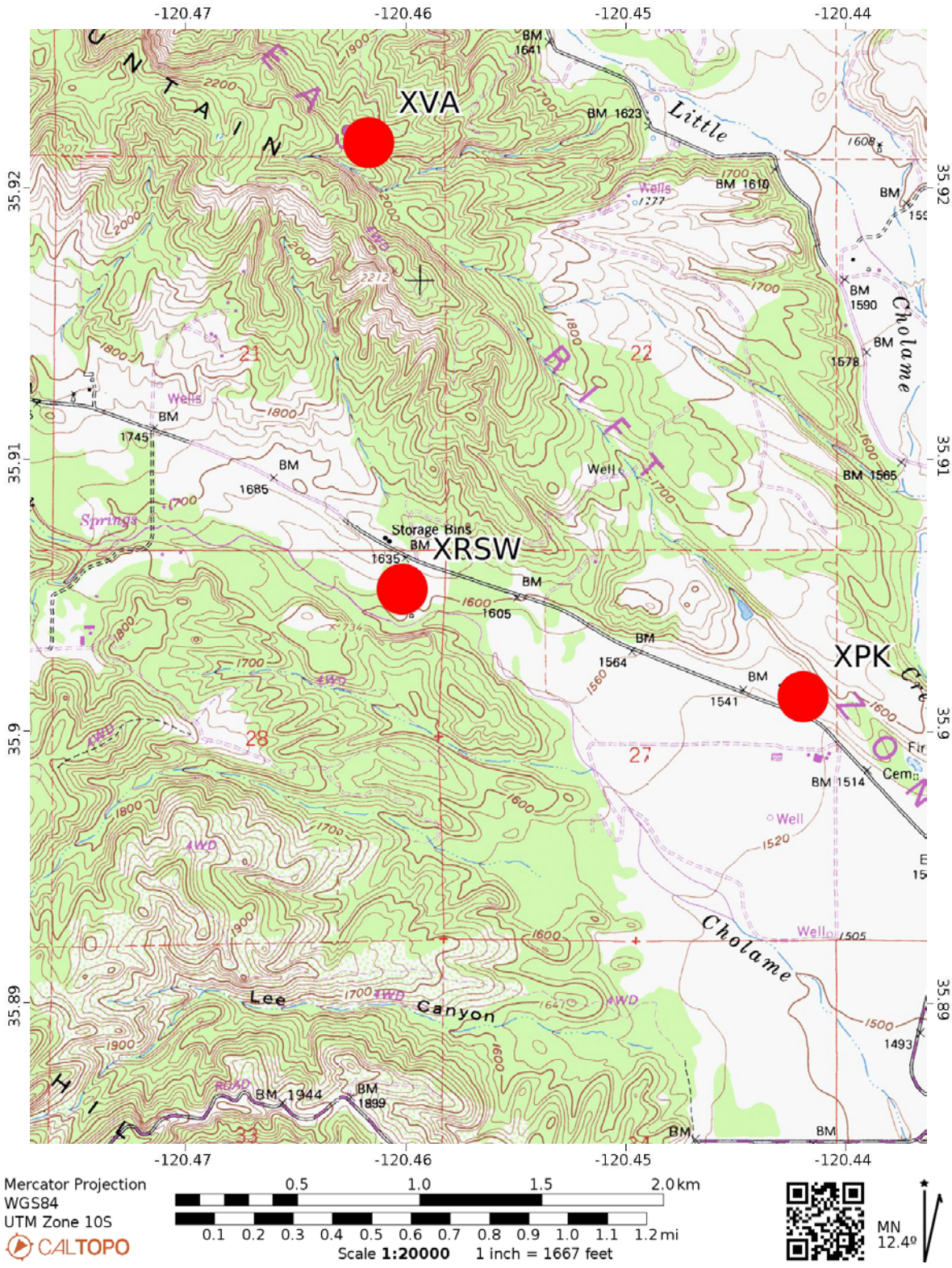

Figure 1.48. Map showing the location of the Roberson SW Trace (XRSW) creepmeter northwest of Parkfield, California. The XRSW creepmeter spans the southwest trace of the San Andreas Fault. Two neighboring creepmeters, Varian (XVA) and Parkfield (XPK), are shown; they are located on the main San Andreas Fault. The creepmeter locations are plotted as red dots.

XPK—Parkfield—San Andreas Fault
Location: 35.90129° N., 120.44191° W.
Orientation: 30°, USGS standard, 23-m wire
Creep rate: 1980.0–2004.7, 8.60±0.60 mm/yr
Creep rate: 2009.0–2020.0, 9.49±1.46 mm/yr
Percentage of creep that occurs in discrete events: 49%

The Parkfield (XPK) creepmeter was installed in 1979 northwest of Parkfield, California. The meter records episodic creep events, but some of these are triggered (or at least coincident) with heavy rainfall. Most notably, a heavy rainstorm triggered a 5-mm event in 1991.

Note that the comparison between the electronic and manual measurements indicated that the LVDT had a 4.3% change in scale after December 2006.

During the 2004 Parkfield earthquake, the Invar wire connecting the two monuments broke. A new wire was installed two days later. However, total slip during this interval is not known. For the analysis of postseismic slip, an arbitrary, but small, offset is introduced to tie pre- and postseismic intervals together. The time-series plots reflect this operation where there is no visual slip seen in the plots of the high-rate data.

Visually, the double Omori, *After*, and stretched exponential tend to fit the longer-term record better than the modified Omori function. The difference is best depicted in the plot spanning the 10-day interval where the dashed, red curve for the Omori function under predicts the observations. However, from evaluating the reduction of variance, none of these models could be termed "best." All had a modest variance reduction to the postseismic interval of 10%. For the Omori law functions either the index, ρ, or the delay time, τ, are not resolved due to lack of 10-minute sampled data during the initial days of postseismic deformation (Langbein and others, 2006). Highly variable creep following the Parkfield earthquake limits the ability of any of the four functions to optimally fit these data.

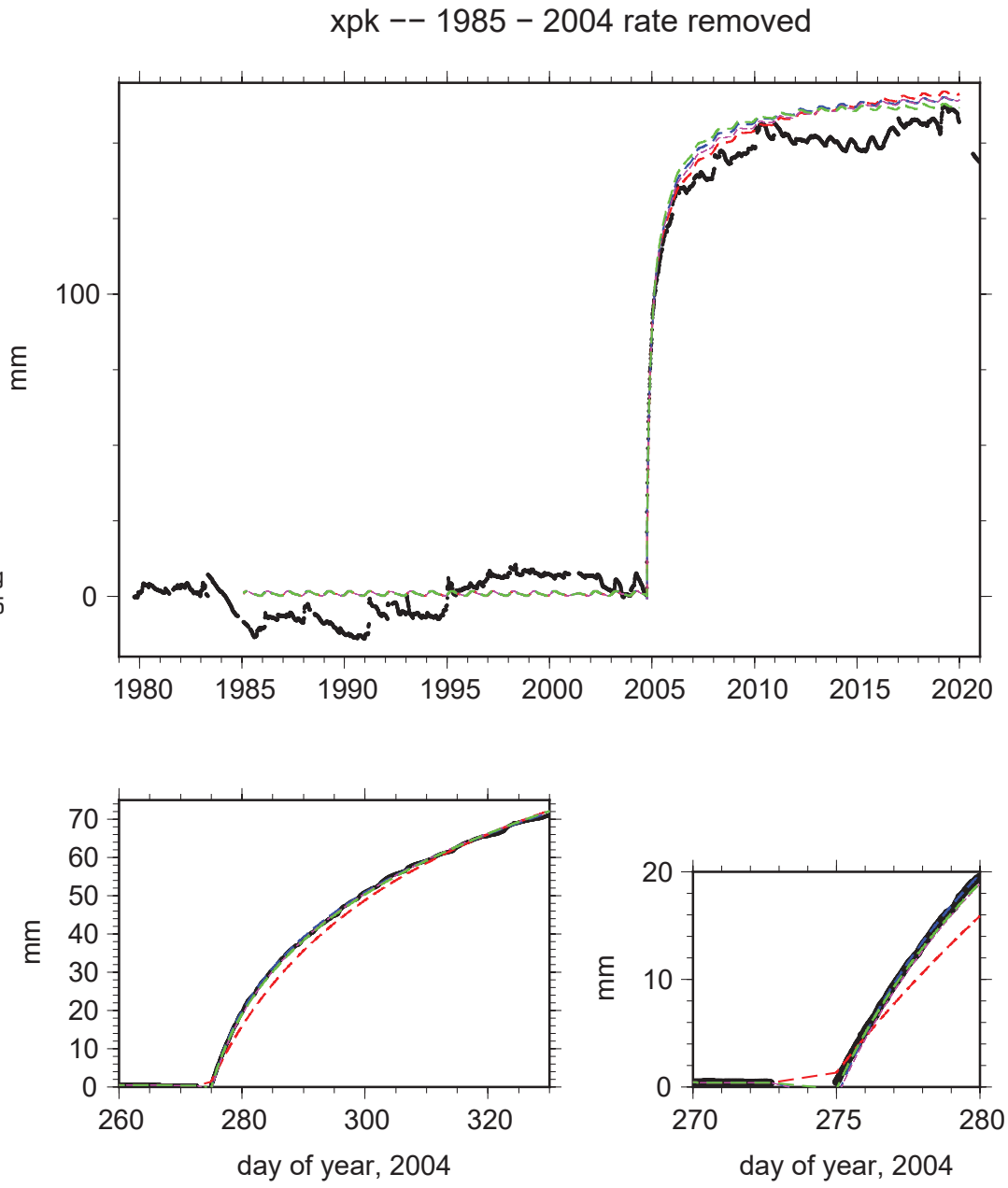

Figure 1.49. Plots of data from the Parkfield (XPK) creepmeter on the San Andreas Fault northwest of Parkfield, California, from 1980 to 2020 and spanning the 2004 Parkfield earthquake (black line). The data prior to the earthquake have had the rate removed using observations between 1985.0 and the time of the Parkfield earthquake, 2004.74. The two lower plots show more detailed data that span the Parkfield earthquake and the initial postseismic slip. The results of fitting four different functions representing postseismic slip are shown. The red curve is result of fitting the modified Omori function to the 1985 to 2020 interval, the blue curve is a fit of the After function, the green curve is a fit to a stretched exponential, and the thin magenta curve is a fit to a double Omori function. Note that the Invar wire of this creepmeter broke at the time of the earthquake and consequently, the data prior and post-earthquake have been joined using an arbitrary offset at the time of the earthquake. See main text, under the heading "Parkfield Postseismic Creep," for discussion about the four functions and the method to fit these models to the data. mm, millimeter.

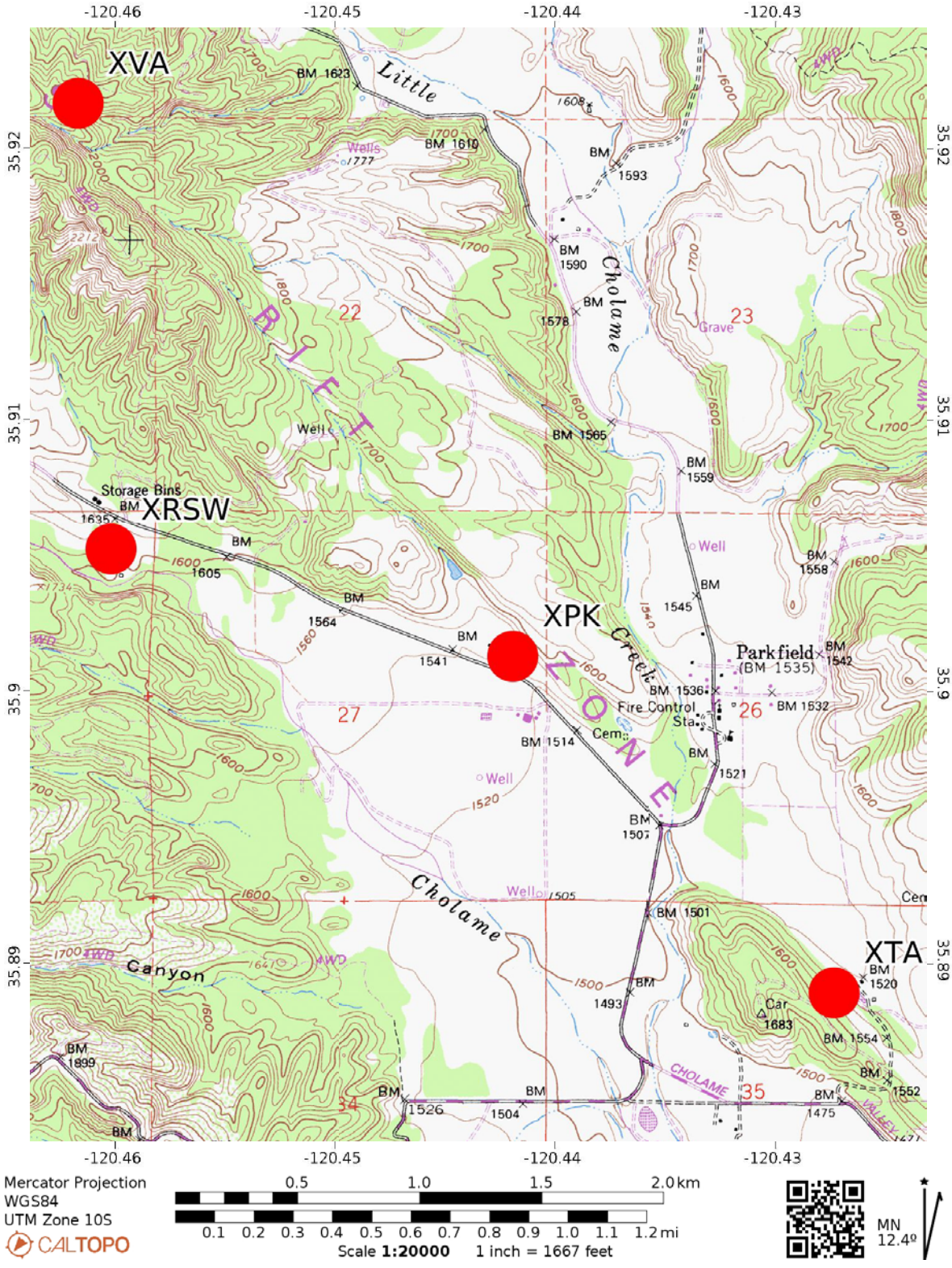

Figure 1.50. Map showing the location of the Parkfield (XPK) creepmeter on the San Andreas Fault northwest of Parkfield, California. Two neighboring creepmeters, Varian (XVA) and Taylor Ranch (XTA), also on the San Andreas Fault are shown along with Roberson SW Trace (XRSW) which is located on the southwest trace of the San Andreas Fault. The creepmeter locations are plotted as red dots.

XTA—Taylor Ranch—San Andreas Fault
Location: 35.88889° N., 120.42728° W.
Orientation: 30°, USGS standard, 30-m wire
Creep rate: 1986.0–2004.7, 9.26±0.49 mm/yr
Creep rate: 2009.0–2020.7, 10.19±0.90 mm/yr
Percentage of creep that occurs in discrete events: 3%

This instrument was installed in 1985. Unlike many of the neighboring Parkfield creepmeters, this site exhibits steady slip that is modulated by a seasonal signal.

Note that the comparison between the electronic and manual measurements indicated that the LVDT had a 3.2% change in scale after December 2006.

During the 2004 Parkfield earthquake, the limit of the LVDT was exceeded. In the 1.5 hours following the mainshock, the meter stayed within its measurement range and those data have been retained. Three days later the site was serviced and apparent stretch was measured such that the total displacement was recovered. However, at this site a low-resolution sensor using a wire wrapped around the shaft of a linear potentiometer was able to measure the coseismic and immediate postseismic transient. These data are included in the plots of the 10 days spanning the earthquake.

Fitting any of the four postseismic functions had better than a 77% reduction in variance with the double Omori function providing the best reduction of 77.7% (followed by the *After* function with 77.6%). This site is unique amongst the Parkfield network of creepmeters in the fitting of these models; the next highest variance reduction is 57% at XMM (fig. 1.41). The index, ρ, for the modified Omori law is estimated to be 0.8 and its corresponding delay, τ, for the onset of postseismic slip is estimated to be 10 minutes suggesting no delay on the onset of postseismic slip (Langbein and others, 2006).

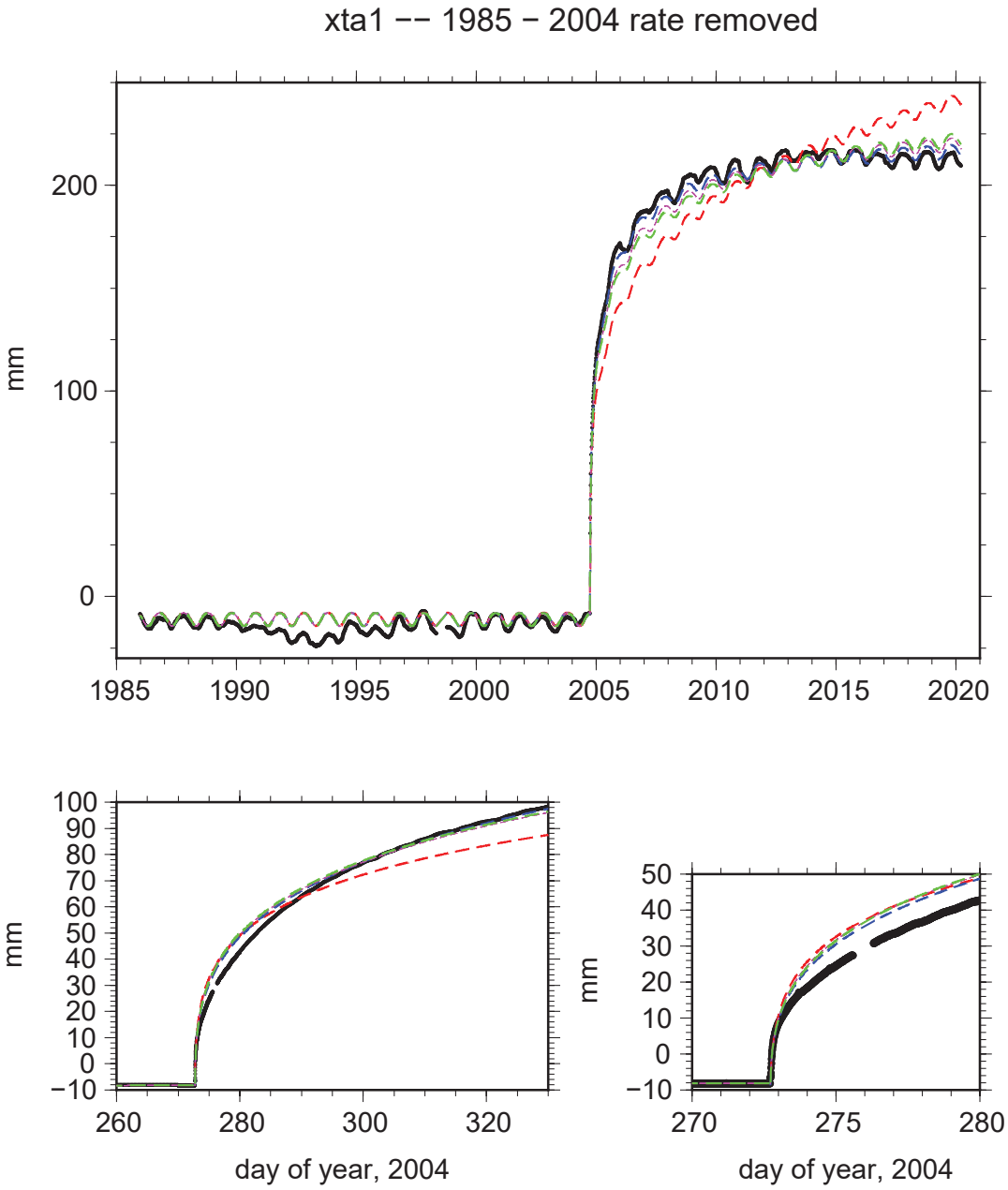

Figure 1.51. Plots of data from the Taylor Ranch (XTA) creepmeter on the San Andreas Fault southeast of Parkfield, California, from 1986 to 2020 and spanning the 2004 Parkfield Earthquake (black line). The data prior to the earthquake have had the rate removed using observations between 1986.0 and the time of the Parkfield earthquake, 2004.74. The two lower plots show more detailed data that span the Parkfield earthquake and the initial postseismic slip. The results of fitting four different functions representing postseismic slip are shown. The red curve is result of fitting the modified Omori function to the 1985 to 2020 interval, the blue curve is a fit of the After function, the green curve is a fit to a stretched exponential, and the thin magenta curve is a fit to a double Omori function. See main text, under the heading "Parkfield Postseismic Creep," for discussion about the four functions and the method to fit these models to the data. mm, millimeter.

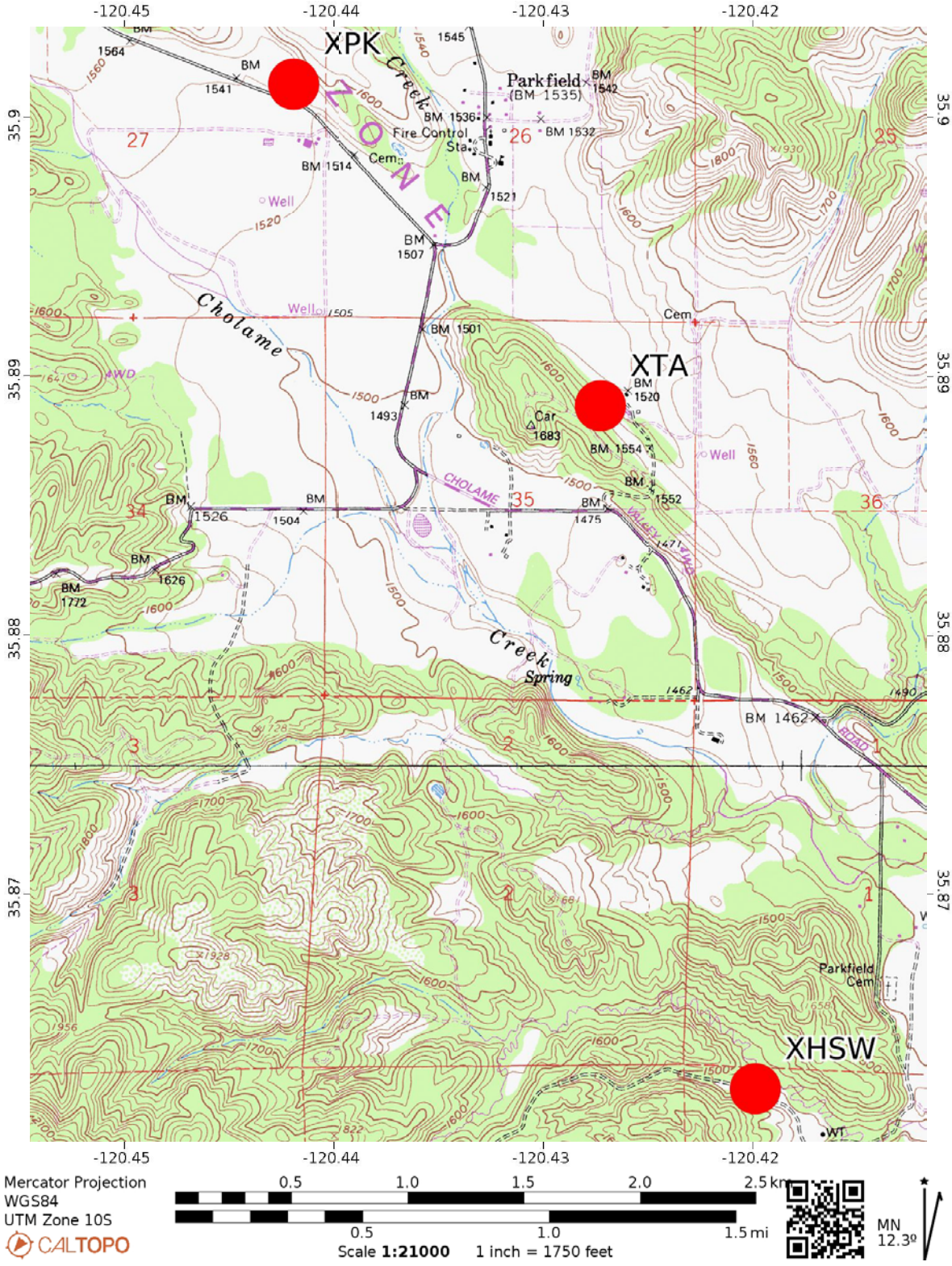

Figure 1.52. Map showing the location of the Taylor Ranch (XTA) creepmeter on the San Andreas Fault southeast of Parkfield, California. Two neighboring creepmeters, Parkfield (XPK) on the San Andreas, and Hearst SW Trace (XHSW) located on the southwest trace of the San Andreas Fault are shown. The creepmeter locations are plotted as red dots.

XHSW—Hearst—San Andreas Fault, SW Trace
Location 35.86248N, 120.41986W
Orientation 45°, USGS standard, 30-meter wire
Creep rate: -0.46±0.12 mm/yr

This instrument was installed south of Parkfield, California, in 1987 and operated until 2010 when the conduit housing the Invar wire caved in. The instrument spans the southwest trace of the San Andreas Fault on which fractures were observed following the 1966 Parkfield earthquake. Coseismic slip was only 1 mm from the 2004 Parkfield earthquake.

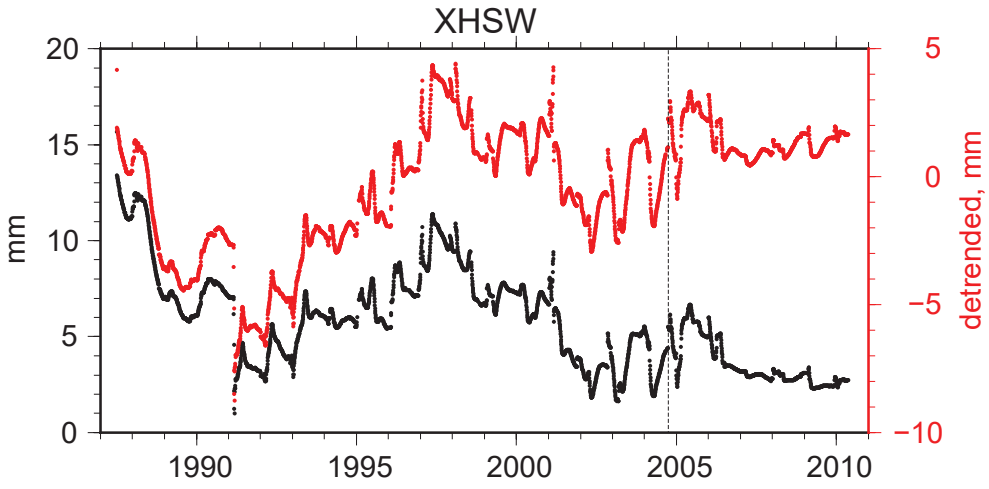

Figure 1.53. Plot showing the observed values of right-lateral slip at the Hearst SW Trace (XHSW) creepmeter on the southwest trace of the San Andreas Fault south of Parkfield, California. The black is the long-term trend, while the red is the residual after removing a constant rate and seasonal sinusoids (365.25- and 182.625-day periods). A dashed vertical line shows the time of the 2004 Parkfield earthquake.

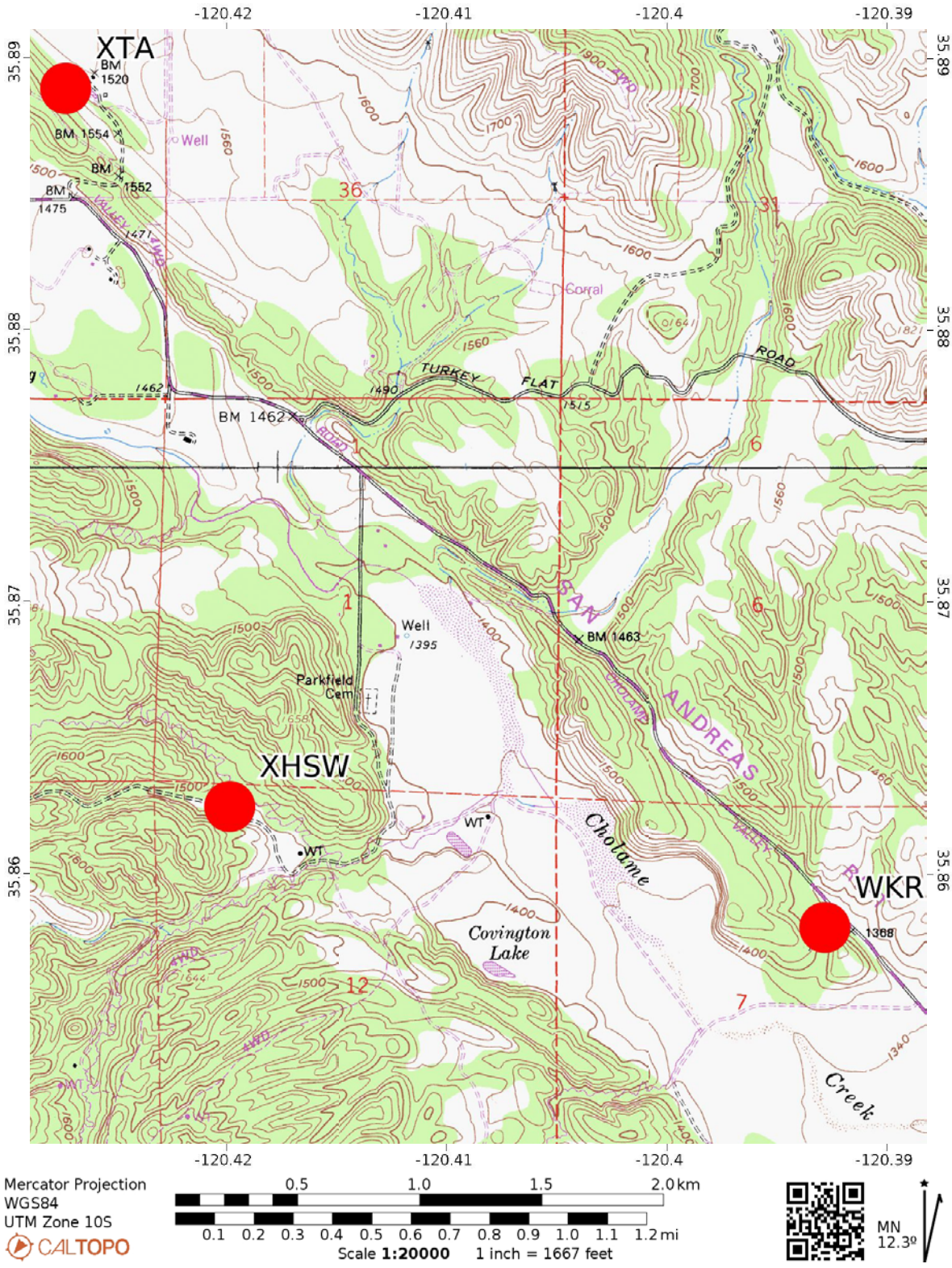

Figure 1.54. Location map of the Hearst SW trace (XHSW) creepmeter on the southwest trace of the San Andreas Fault south of Parkfield, California. Two neighboring creepmeters, Taylor Ranch (XTA) and Work Ranch (WKR) are also shown, with WKR located on the southeast edge of the map. The creepmeter locations are plotted as red dots.

WKR—Work Ranch—San Andreas Fault
Location: 35.85800° N., 120.39280° W.
Orientation: 45°, Caltech design, 9.4-m wire
Creep rate: 1980.0–2004.7, 8.05±1.18 mm/yr
Creep rate: 2009.0–2020.7, 7.00±1.71 mm/yr
Percentage of creep that occurs in discrete events: 11%

This instrument was installed by California Institute of Technology personnel in 1976 and was incorporated into the USGS network in 1979. The instrument and sensing element, shared with CRR, differ from the standard USGS instruments and the differences have been described above in the "Caltech Design" section of this report.

At the time of the 2004 Parkfield earthquake, the instrument had been offline for a few days. The site became operational two days after the mainshock. The earthquake and the initial postseismic slip exceeded the range of the sensing element. When the site was serviced the apparent stretch was measured such that the total displacement was recovered.

Fits to the models of postseismic slip show nearly equal performance of three of the four models with the modified Omori being least suitable. Note that the data from coWKR (Bilham, 2005) have been substituted for WKR1 data for day of year 268 to 280 since WKR1 was both offline and off scale during the critical moment of the mainshock and its immediate, postseismic interval. For the long-term data, there is difficulty in fitting these data due to the apparent decrease of creep rate starting around 2014. However, with the insertion of the coWKR data into the analysis, the delay time, τ, is estimated to be less than 10-minutes using the double Omori function.

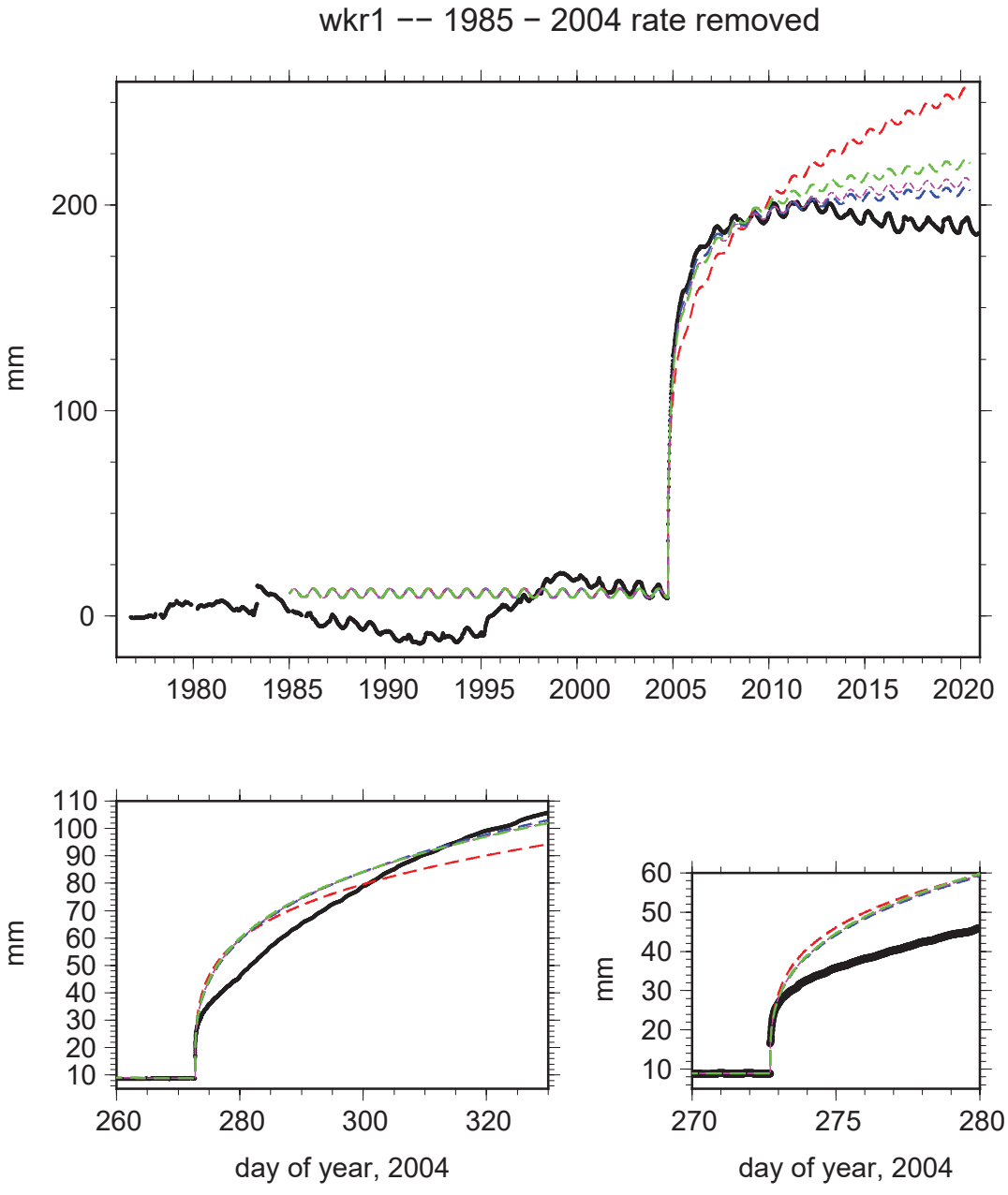

Figure 1.55. Plots of data from the Work Ranch (WKR) creepmeter (black line) on the San Andreas Fault southeast of Parkfield, California, from 1976 to 2020 and spanning the 2004 Parkfield earthquake. The data prior to the earthquake have had the rate removed using observations between 1985.0 and the time of the Parkfield earthquake, 2004.74. The two lower plots show more detailed data that span the Parkfield earthquake and the initial postseismic slip. Note that coWKR data (Bilham, 2005) have been used for the day of year 268 to 280 interval, and those displacements have been multiplied by 2.8 to bring those data to match the WKR1 displacements. The results of fitting four different functions representing postseismic slip are shown. The red curve is result of fitting the modified Omori function to the 1985 to 2020 interval, the blue curve is a fit of the After function, the green curve is a fit to a stretched exponential, and the thin magenta curve is a fit to a double Omori function. See main text, under the heading "Parkfield Postseismic Creep," for discussion about the four functions and the method to fit these models to the data. mm., millimeter.

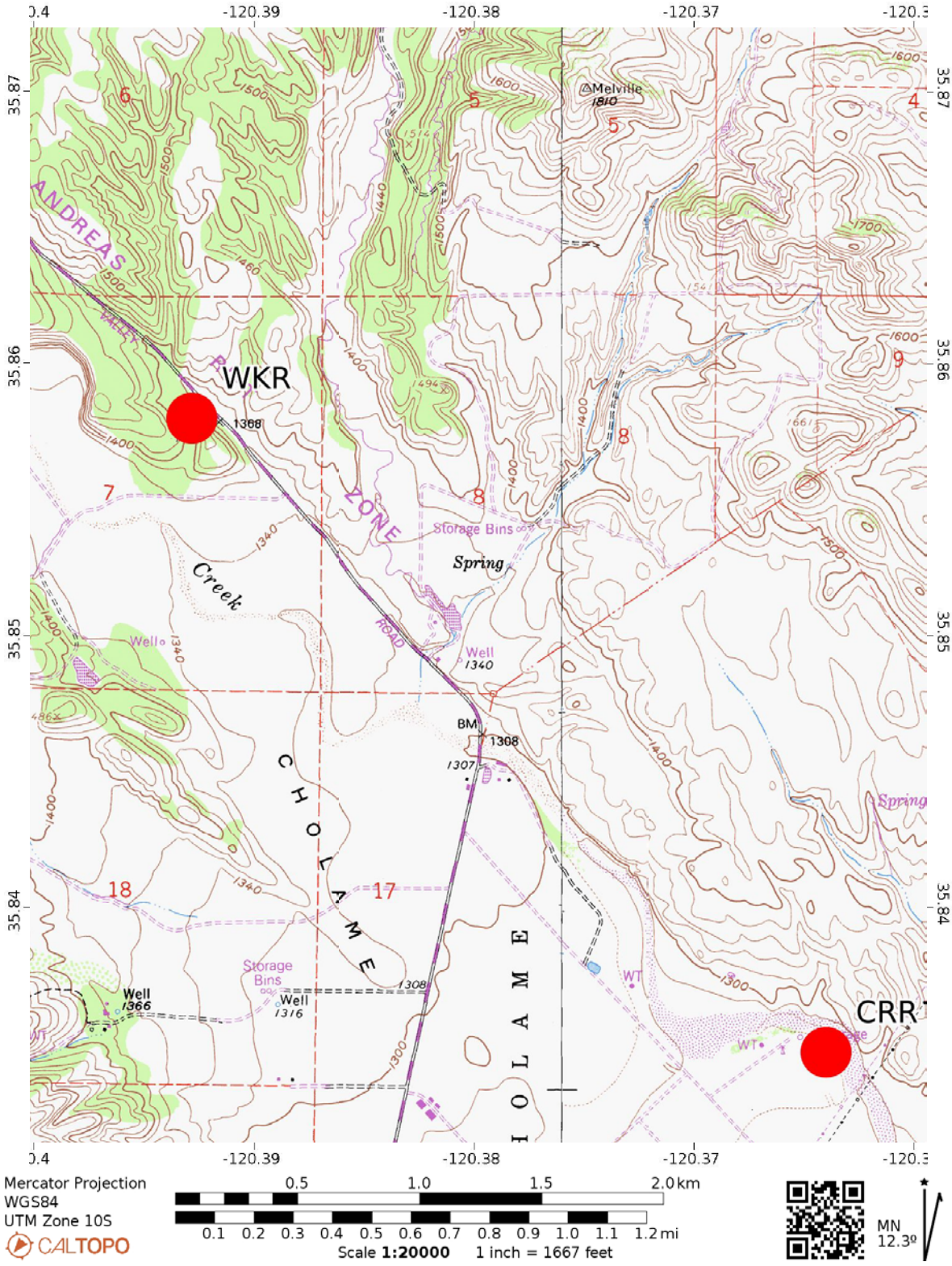

Figure 1.56. Map showing Work Ranch (WKR) and Carr Ranch (CRR) creepmeters on the San Andreas Fault, southeast of Parkfield, California. The creepmeter locations are plotted as red dots.

CRR—Carr Ranch—San Andreas Fault
Location: 35.83465° N., 120.36398° W.
Orientation: 45°, Caltech design, 9.4-m wire
Creep rate: 1980.0–2004.7, 4.83±0.81 mm/yr
Creep rate: 2009.0–2017.2, 2.15±1.93 mm/yr
Percentage of creep that occurs in discrete events: 66%

This instrument was installed southeast of Parkfield, California, by California Institute of Technology personnel in 1966 immediately following the 1966 Parkfield earthquake and was incorporated into the USGS network in 1979. Schulz (1989) discusses the measurements prior to 1979 and how they are merged with the data from telemetry in 1979. The instrument and sensing element, shared with WKR, differ from the standard USGS instruments and the differences have been described above in the "Caltech Design" section of the report.

Note that the lack of creep events and a reduction in rate after mid-2013 suggests that the wire between the ends of the creepmeter is broken. The site was abandoned in 2017.

Following the 2004 Parkfield earthquake, the instrument stayed on scale for 1.5 hours before transient slip exceeded the range of the instrument. The site was serviced two days later, and the offset was recovered by manually measuring the stretch of the wire needed to bring the instrument back on scale.

Fits of the four functions representing postseismic slip reduce the variance by 8% for the data following the 2004 Parkfield earthquake. None of the models fit significantly better than the others; visually, the two Omori functions seem to provide a better fit than the other two functions, but none of the functions can fit the apparent low creep rate following 2009 (Langbein and others, 2006).

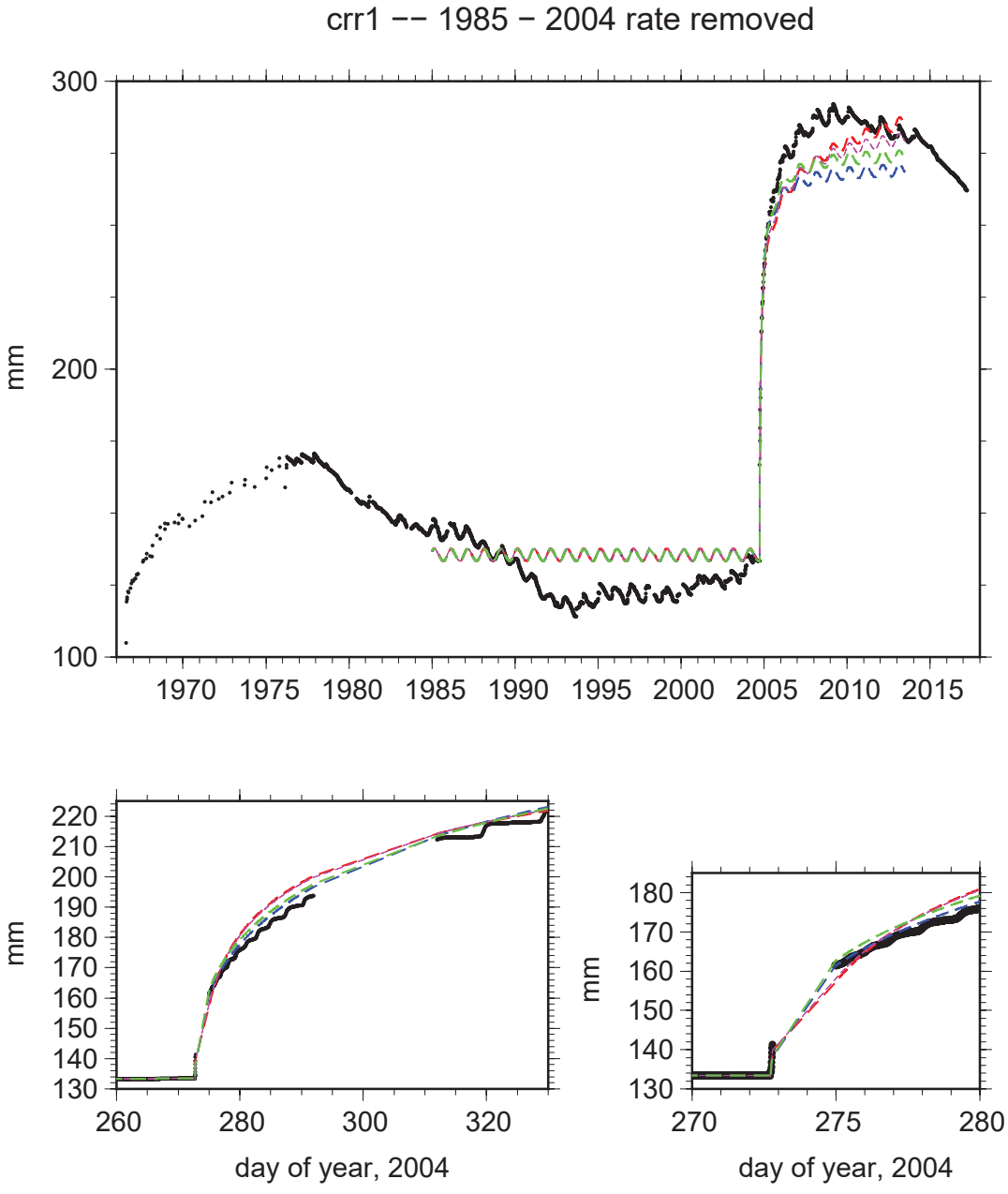

Figure 1.57. Plots of data from Carr Ranch (CRR) creepmeter (black line) on the San Andreas Fault southeast of Parkfield, California, from 1966 to 2017 and spanning the 2004 Parkfield earthquake. The data prior to the earthquake have had the rate removed using observations between 1985.0 and the time of the Parkfield earthquake, 2004.74. Note that the lack of creep events and a reduction in rate after mid-2013 suggests that the wire between the ends of the creepmeter is broken. The site was abandoned in 2017. The two lower plots show more detailed data that span the Parkfield earthquake and the initial postseismic slip. The results of fitting four different functions representing postseismic slip are shown. The red curve is result of fitting the modified Omori function to the 1985 to 2013 interval, the blue curve is a fit of the After function, the green curve is a fit to a stretched exponential, and the thin magenta curve is a fit to a double Omori function. See main text, under the heading "Parkfield Postseismic Creep," for discussion about the four functions and the method to fit these models to the data. mm, millimeter.

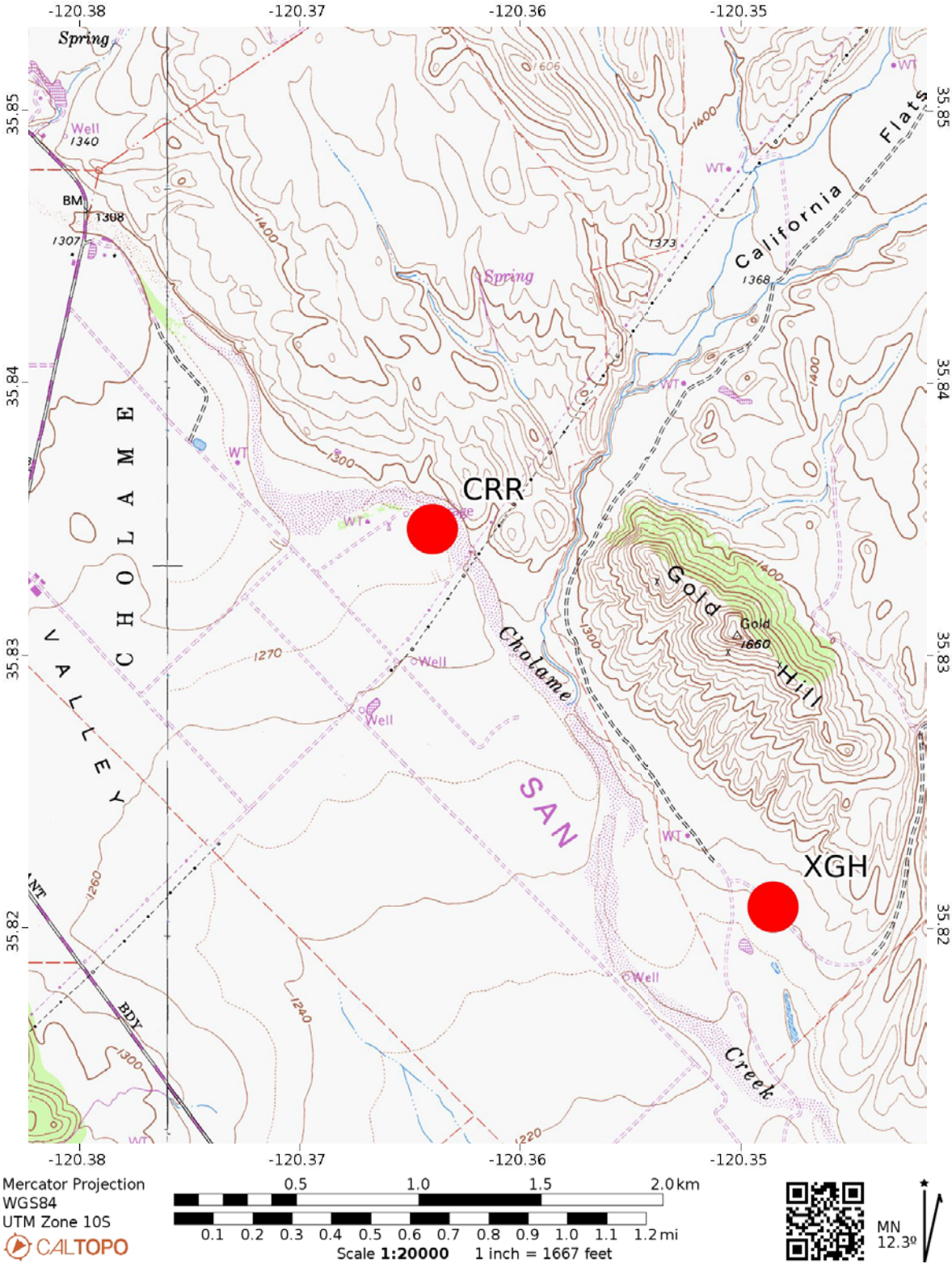

Figure 1.58. Location map showing Carr Ranch (CRR) and Gold Hill (XGH) creepmeters on the San Andreas Fault southeast of Parkfield, California. CRR was abandoned in 2017. The creepmeter locations are plotted as red dots.

XGH—Gold Hill—San Andreas Fault
Location: 35.82075° N., 120.34853° W.
Orientation: 30°, USGS standard, 10-m wire
Creep rate: 1980.0–2004.7, 2.11±0.47 mm/yr
Creep rate: 2009.0–2020.7, 4.96±0.69 mm/yr
Percentage of creep that occurs in discrete events: 75%

This site was installed in 1969 southeast of Parkfield, California. Note that this site exhibited a large change in electronic scaling between the manually read, micrometer measurements and those measured with the LVDT. As described in the above text and appendix 3, these have been reconciled, but leaves open that the LVDT has been failing to operate correctly after early 2014. During the site visit in 2018, it was noted that the conduit had started to cave-in in response to cattle grazing next to the instrument.

Even though this instrument was the closest creepmeter to the epicenter of the 2004 Parkfield earthquake, it stayed on scale throughout the event and the initial postseismic slip. Fits of the four functions to the postseismic interval indicate a 34% reduction of variance. Visually, no one model seems to fit as none of them can follow the continued, high rate of slip after 2008. The values of the index, ρ, and the delay time, τ, for the Omori function are 1.1 and 5 hours. Inspection of the raw data indicates a 2-hour delay time. Note, for this site there is no detectable coseismic displacement (Langbein and others, 2006).

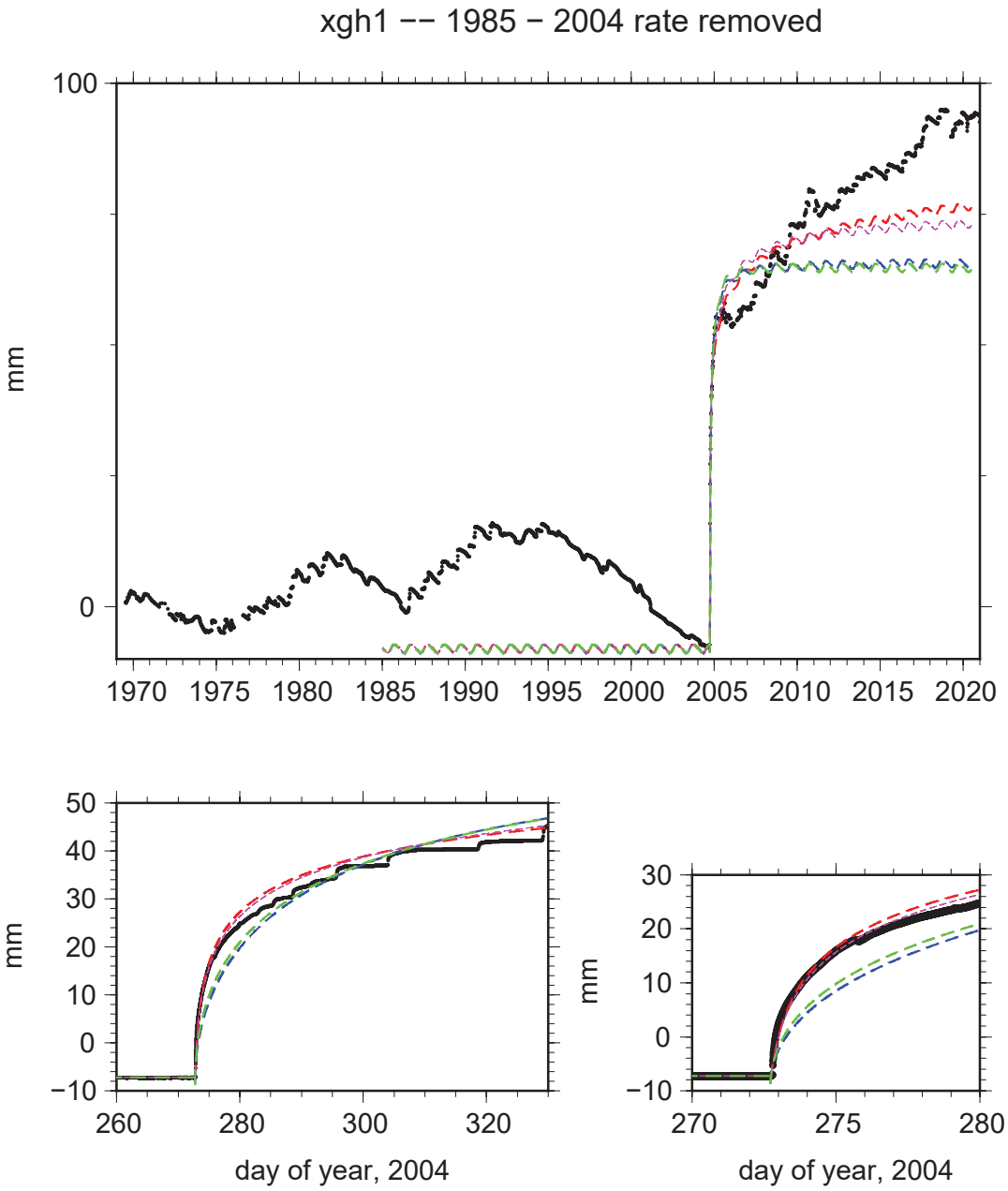

Figure 1.59. Plots of data from the Gold Hill (XGH) creepmeter (black line) on the San Andreas Fault southeast of Parkfield, California, from 1969 to 2020 and spanning the 2004 Parkfield earthquake. The data prior to the earthquake have had the rate removed using observations between 1985.0 and the time of the Parkfield earthquake, 2004.74. The LVDT may have been failing to operate correctly after early 2014. The two lower plots show more detailed data that span the Parkfield earthquake and the initial postseismic slip. The results of fitting four different functions representing postseismic slip are shown. The red curve is result of fitting the modified Omori function to the 1985 to 2020 interval, the blue curve is a fit of the After function, the green curve is a fit to a stretched exponential, and the thin magenta curve is a fit to a double Omori function. See main text, under the heading "Parkfield Postseismic Creep," for discussion about the four functions and the method to fit these models to the data. mm, millimeter.

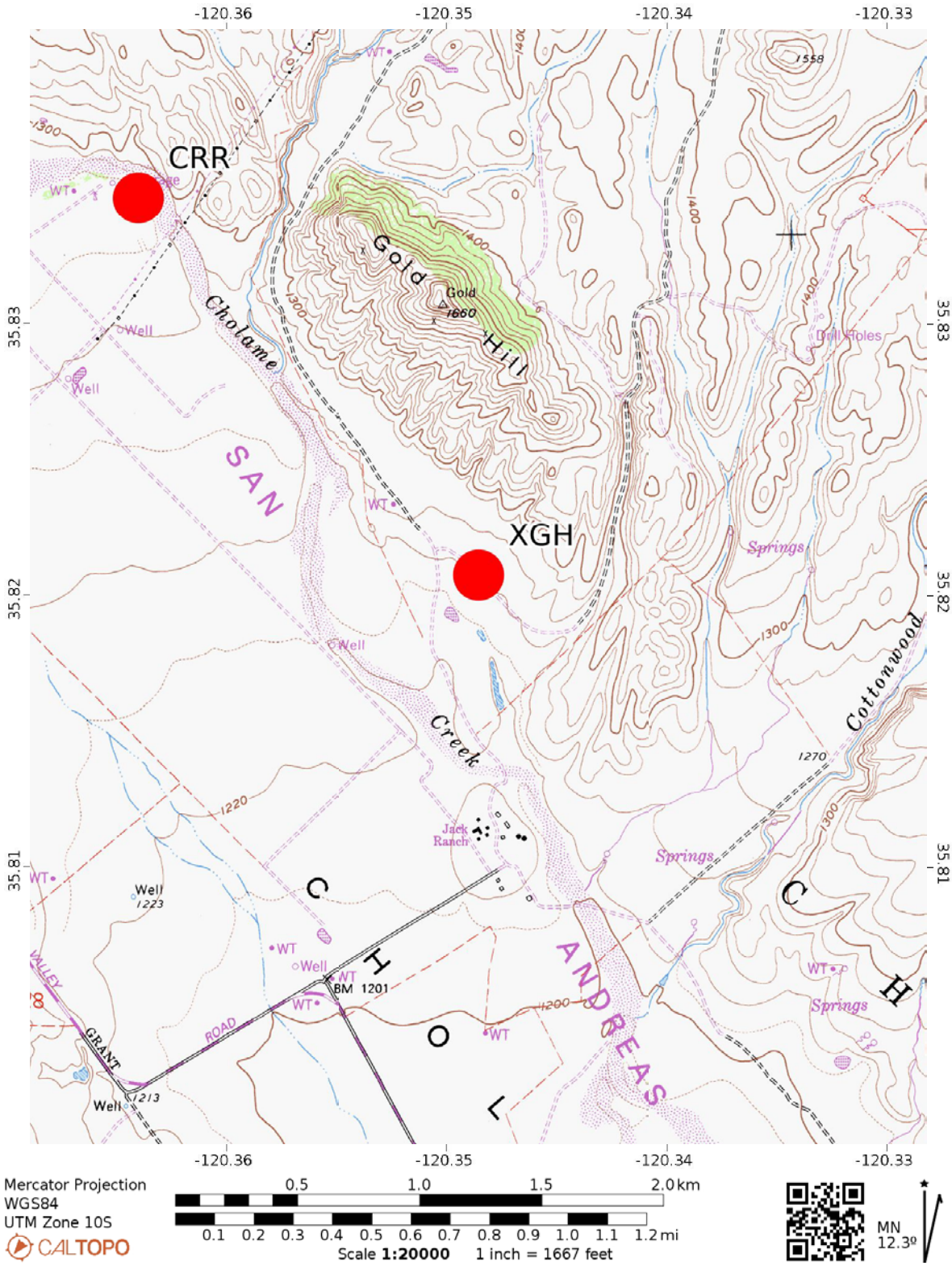

Figure 1.60. Location map showing Gold Hill (XGH) and Carr Ranch (CRR) creepmeters on the San Andreas Fault located southeast of Parkfield, California. CRR was abandoned in 2017. The creepmeter locations are plotted as red dots.

C46—Highway 46—San Andreas Fault
Location: 35.72432° N., 120.28188° W.
Orientation: 30°. Instrument type, Bilham #1
Creep rate: 3.84±0.10 mm/yr
Percentage of creep that occurs in discrete events: 44%

Following the 2004 Parkfield earthquake this site was installed southeast of Parkfield and ~1 km south of State Route 46 by one of the co-authors (R. Bilham, USGS), consisting of two hand-driven monuments to 1-m depth using an Invar rod and LVDT to measure the displacement between the monuments. In late 2010, the creepmeter was rebuilt with an attempt to improve the stability of the monuments. A backhoe was employed to press in, using its bucket, three 3-m-long, 6-cm-wide, galvanized-steel H-channels to make each end of the creepmeter; one channel aluminum was pressed vertically, the second approximately 45° from vertical but oriented in line with the creepmeter's length, and a third driven approximately 45° from vertical but perpendicular to the creepmeter's baseline. The objective was to suppress the apparently left lateral motions recorded by the earlier instrument. The massive mounts have not eliminated this tendency to record left-lateral data during the wet season.

An LVDT is used to measure the displacement between the two monuments with a carbon-fiber rod. A rupture meter with 1.7-m range is also provided. The instrument is known to be located near a stream that was offset by approximately this amount in the 1857 rupture. After the 2004 earthquake only minor afterslip was observed.

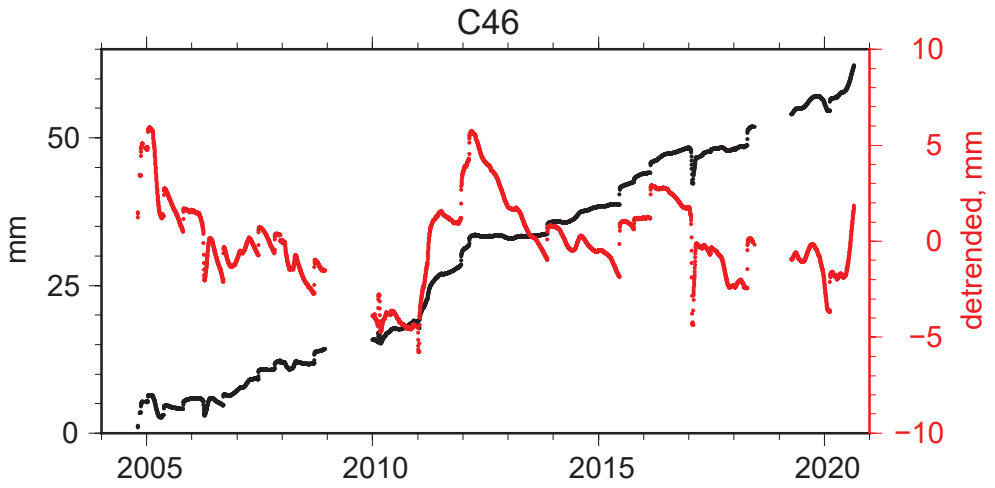

Figure 1.61. Plot showing the observed values of right-lateral slip at the Highway 46 (C46) creepmeter on the San Andreas Fault southeast of Parkfield, California, and ~1 kilometer south of State Route 46. This meter was installed in 2004 and in late 2010 the creepmeter was rebuilt. The black is the long-term trend, while the red is the residual after removing a constant rate and seasonal sinusoids (365.25- and 182.625-day periods). mm, millimeter.

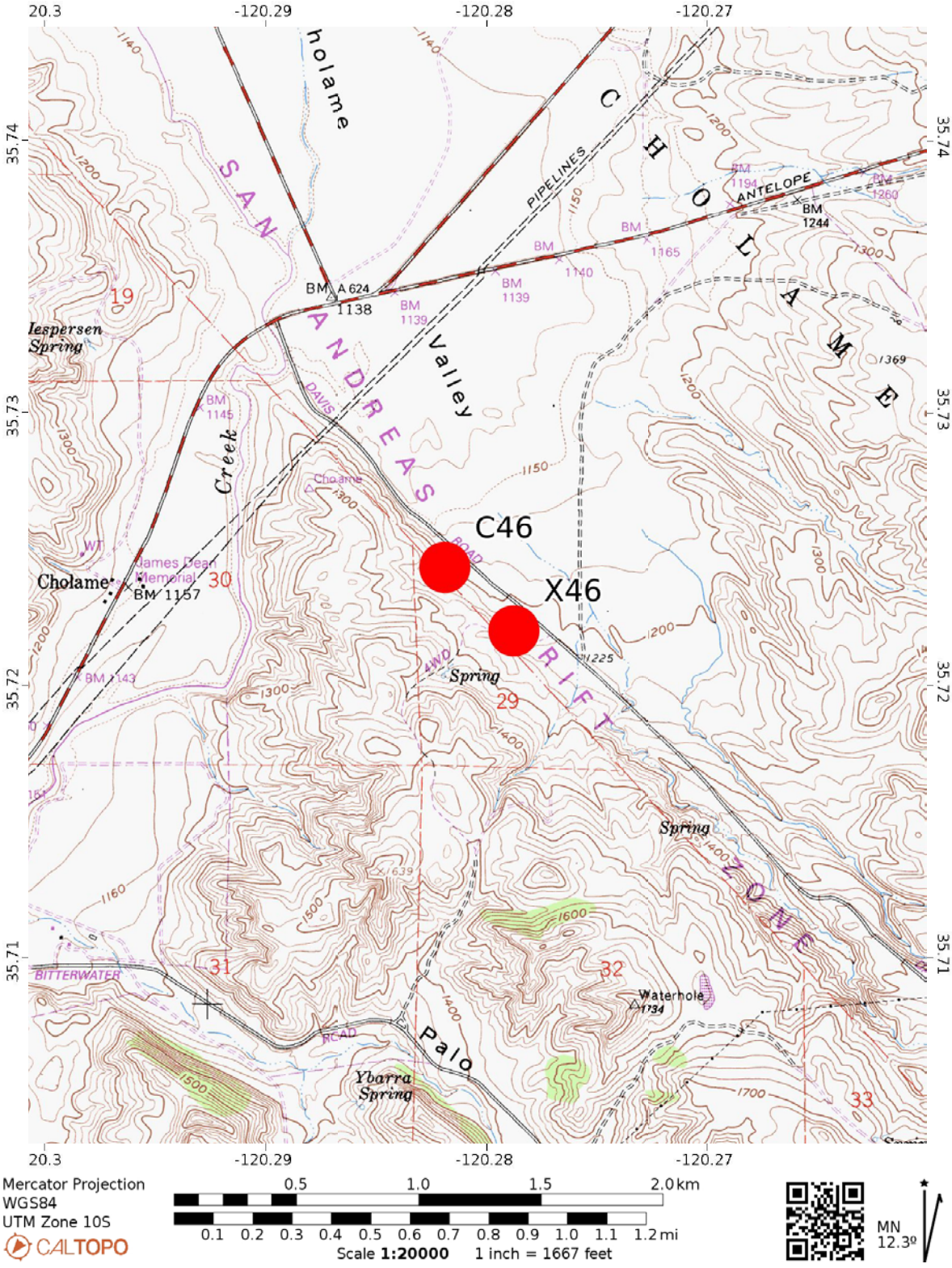

Figure 1.62. Location map showing both Highway 46 (C46) and Highway 46 (X46) creepmeters on the San Andreas Fault southeast of Parkfield and ~1 kilometer south of State Route 46. X46 was installed in 1986 and operated until late 2016 when the conduit and wire broke. Since C46 is located nearby, no attempt was made to repair this instrument. The creepmeter locations are plotted as red dots.

X46—Highway 46—San Andreas Fault
Location: 35.72199° N., 120.27875° W.
Orientation: -44°, USGS standard, 27-m wire; contraction is equivalent to dextral slip
Creep rate: 1986.8–2004.7, -0.03±0.65 mm/yr
Creep rate: 2009.0–2017.0, +0.02±1.60 mm/yr

This instrument was installed in 1986 and operated until late 2016 when the conduit and wire broke. Since C46 is located nearby, no attempt was made to repair this instrument. The location map for X46 is shown in the previous section for C46 (fig. 1.62).

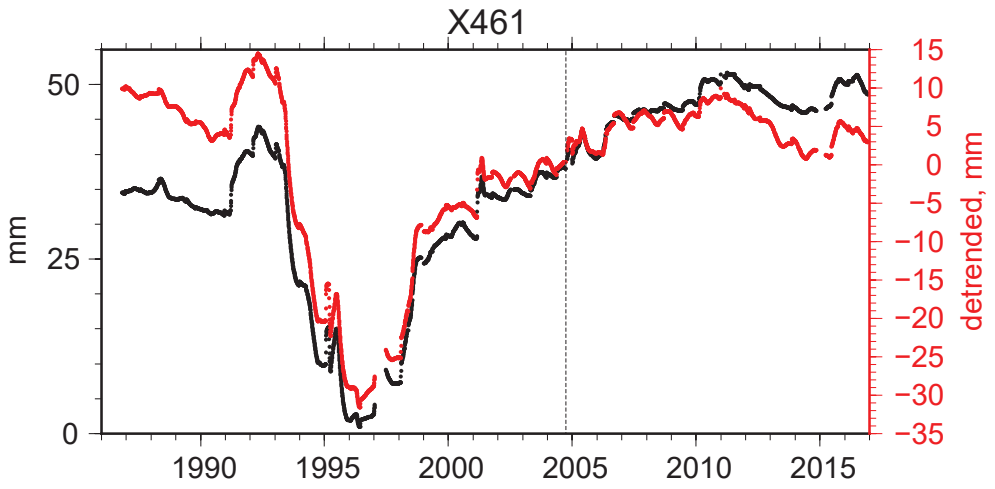

Figure 1.63. Plot showing the observed values of right-lateral slip at the Highway 46 (X46) creepmeter on the San Andreas Fault southeast of Parkfield and ~1 kilometer south of State Route 46. This instrument was installed in 1986 and operated until late 2016 when the conduit and wire broke. Since C46 is located nearby, no attempt was made to repair this instrument. The black is the long-term trend, while the red is the residual after removing a constant rate and seasonal sinusoids (365.25- and 182.625-day periods). A dashed vertical line shows the time of the 2004 Parkfield earthquake. mm, millimeter.

TWR—Twisselman Ranch—San Andreas Fault
Location: 35.59569° N., 120.14777° W.
Orientation: 45°, Caltech design, 10-m wire
Creep rate: -0.69±0.08 mm/yr

Although Schulz (1989) states that this instrument was installed by California Institute of Technology in 1976, only data after 1979 exist. The site was on telemetry from late 1979 through 1992. After 1992, only occasional, manual measures were taken. The long-term trend suggests a low level of sinistral slip.

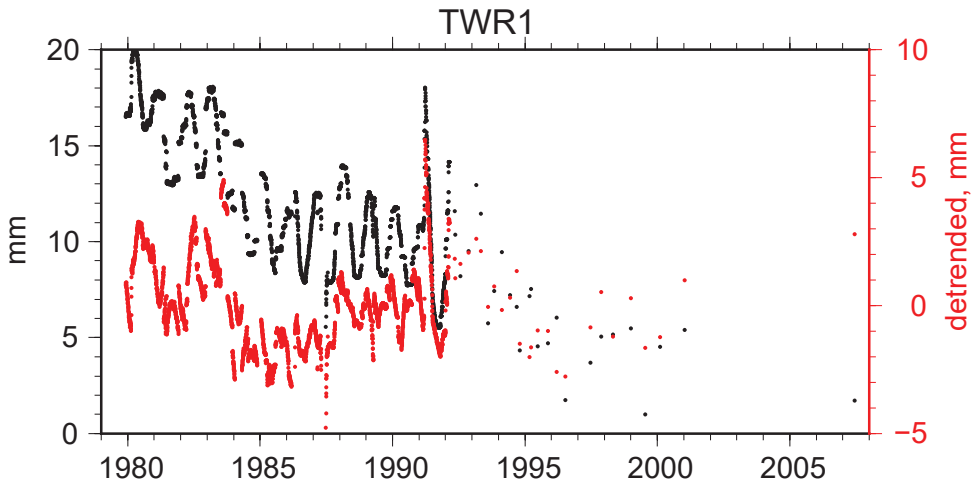

Figure 1.64. Plots showing the observed values of right-lateral slip at the Twisselman Ranch (TWR) creepmeter on the San Andreas Fault located 45 kilometers southeast of Parkfield, California. This instrument was installed in 1976; only data after 1979 exist. The site was on telemetry from late 1979 through 1992. After 1992, only occasional, manual measures were taken. The black is the long-term trend, while the red is the residual after removing a constant rate and seasonal sinusoids (365.25- and 182.625-day periods). mm, millimeter.

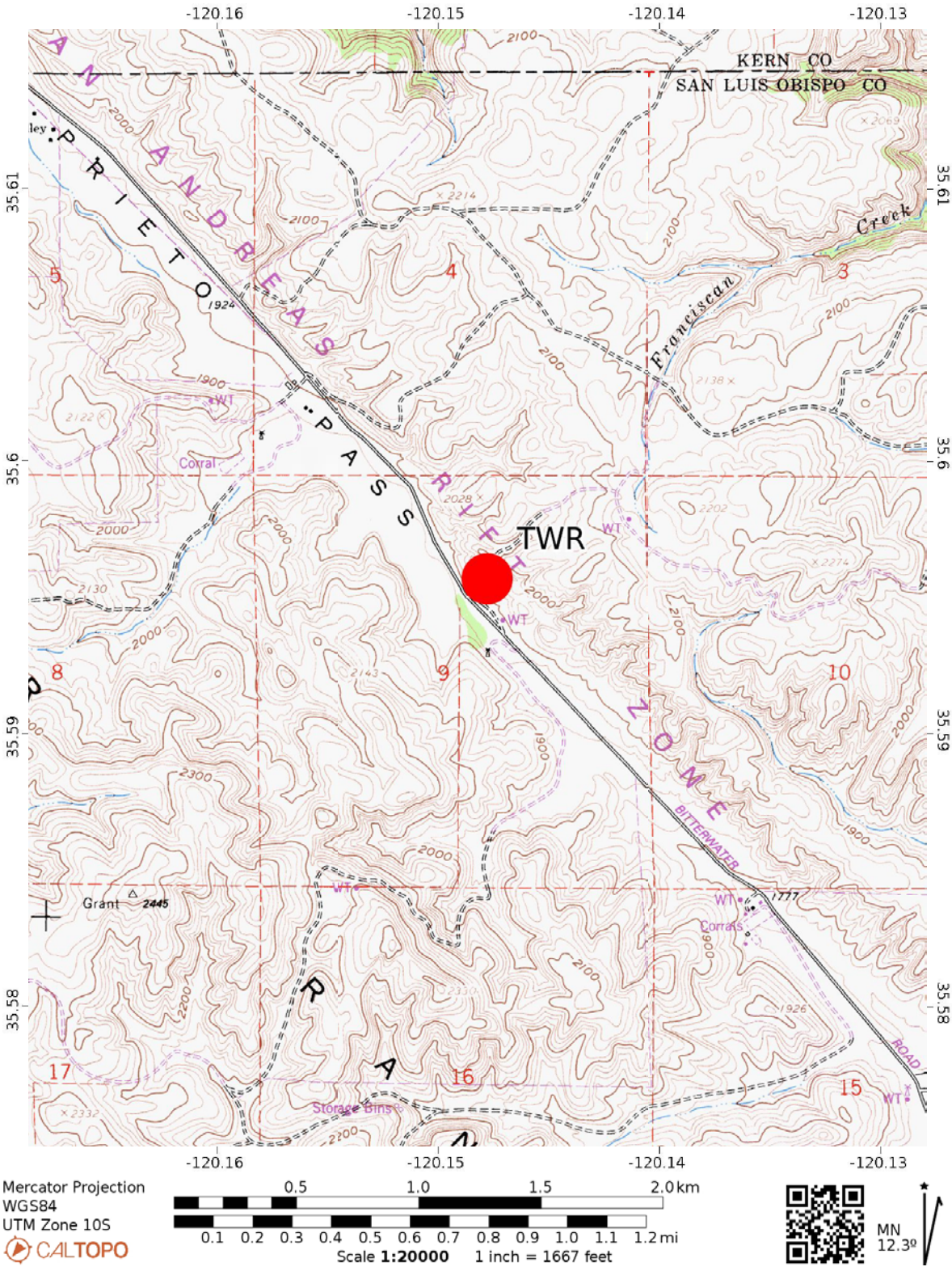

Figure 1.65. Location map of the Twisselman Ranch (TWR) creepmeter on the San Andreas Fault located 45 kilometers southeast of Parkfield, California. The creepmeter location is plotted as a red dot.

XPH—Panorama Hills—San Andreas Fault
Location: 35.14904° N., 119.69115° W.
Orientation: 30°, USGS standard, 20-m wire
Creep rate: -0.11±0.01 mm/yr

This site was installed in 1977 (Schulz and Burford, 1978) and operated with telemetry though 1991. From 1991 until 2007, occasional manual measurements were taken. Long term creep rate is -0.4 mm/yr. Schulz (1989) implies that the creepmeter may not have spanned the entire trace of the fault. Unlike the other creepmeters in this report, this site shows no transient deformation other than a seasonal sinusoid.

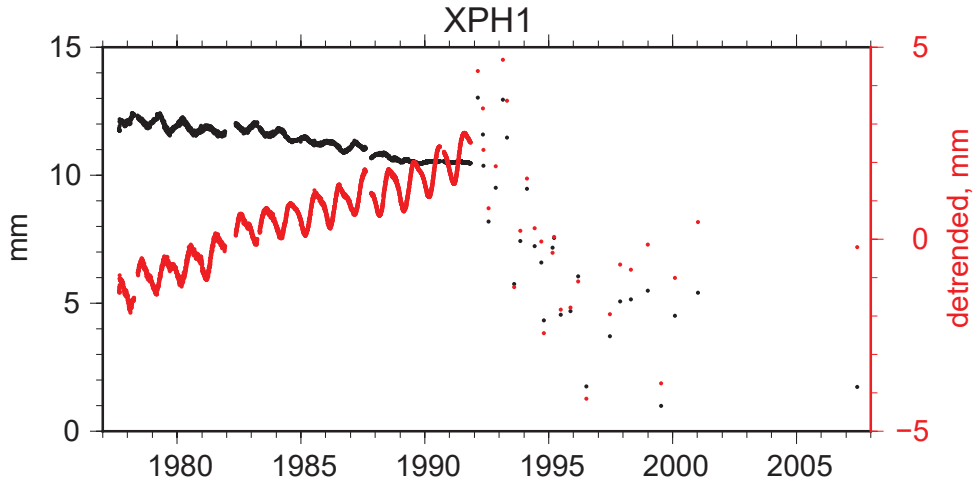

Figure 1.66. Plot showing the observed values of right-lateral slip at the Panorama Hills (XPH) creepmeter on the San Andreas Fault 110 kilometers southeast of Parkfield, California. This site was installed in 1977 and operated with telemetry though 1991. From 1991 until 2007, occasional manual measurements were taken. The black is the long-term trend, while the red is the residual after removing a constant rate and seasonal sinusoids (365.25- and 182.625-day periods). mm, millimeter.

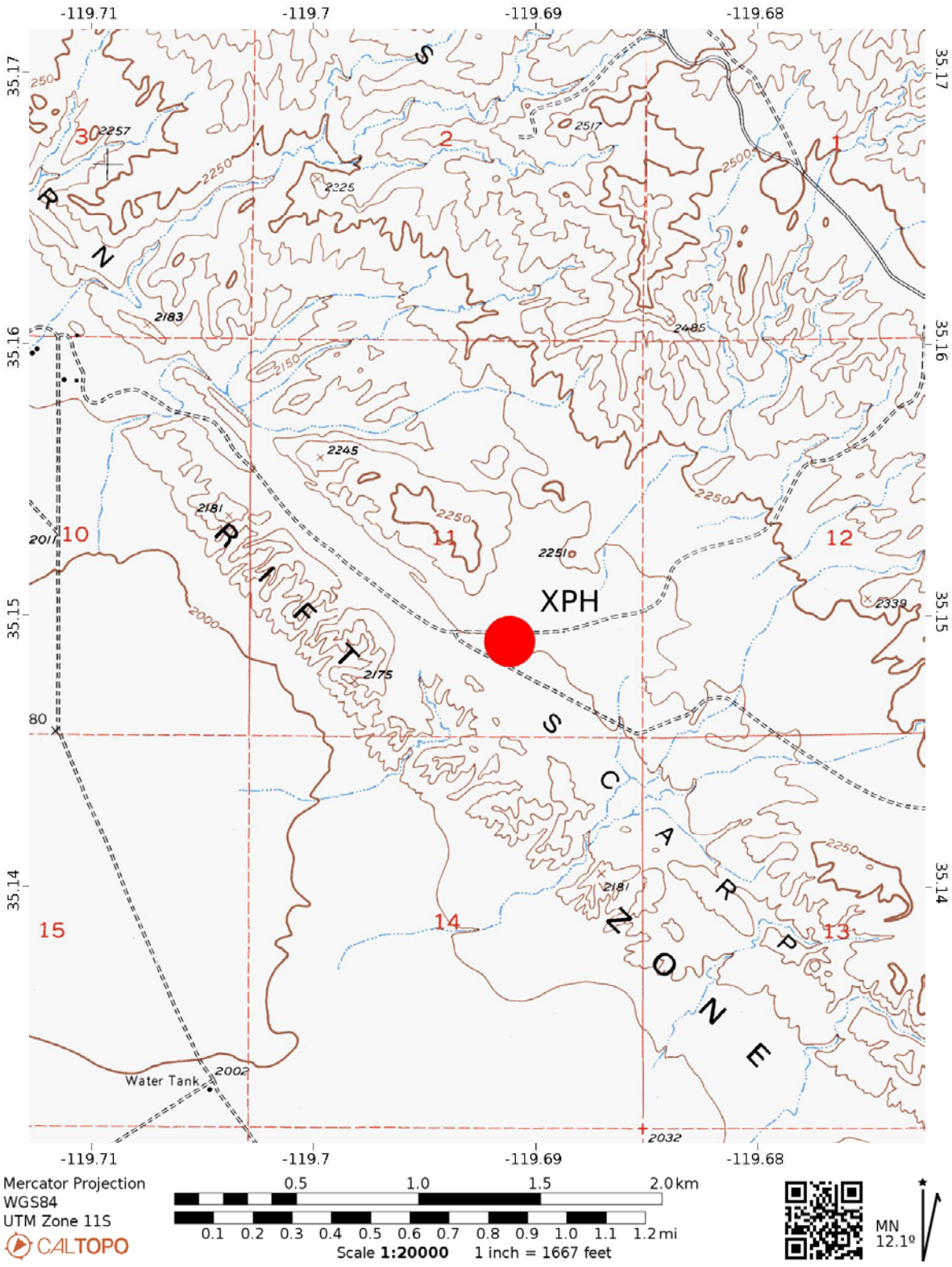

Figure 1.67. Location map of the Panorama Hills (XPH) creepmeter on the San Andreas Fault located 110 kilometers southeast of Parkfield, California. The creepmeter location is plotted as a red dot.

References Cited

Bilham, R., 2005, Coseismic strain and the transition to surface afterslip recorded by creepmeters near the 2004 Parkfield epicenter: Seismological Research Letters, v. 76, no. 1, p. 49–57, accessed June 3, 2022, at https://doi.org/10.1785/gssrl.76.1.49.

Bilham, R. and Whitehead, S., 1997, Subsurface creep on the Hayward Fault, Fremont, California: Geophysical Research Letters, v. 24, no. 11, p. 1307–1310, accessed June 3, 2022, at https://doi.org/10.1029/97GL01244.

Brooks, B.A., Glennie, C., Hudnut, K.W., Ericksen, T., and Hauser, D., 2013, Mobile laser scanning applied to the Earth sciences: EOS, v. 94, no. 36, p. 313–315, accessed June 3, 2022, at https://doi.org/10.1002/2013EO360002.

Burford, R.O., 1988, Retardations in fault creep rates before local moderate earthquakes along the San Andreas fault system, Central California: Pure and Applied Geophysics, v. 126, no. 2, p. 499–529, accessed April 8, 2022, at https://doi.org/10.1007/BF00879008.

Burford, R.O., and Harsh, P.W., 1980, Slip on the San Andreas Fault in central California from alinement array surveys: Bulletin of the Seismological Society of America, v. 70. no. 4, p. 1233–1261, accessed February 3, 2020, at https://doi.org/10.1785/BSSA0700041233.

Gittins, D.B., and Hawthorne, J.C., 2022, Are creep events big? Estimations of along-strike rupture lengths: Journal of Geophysical Research Solid Earth, v. 127, no. 1, accessed January 23, 2022, at https://doi.org/10.1029/2021JB023001.

Langbein, J., Murray, J.R., and Snyder, H.A., 2006, Coseismic and initial postseismic deformation from the 2004 Parkfield, California, Earthquake, observed by global positioning system, electronic distance meter, creepmeters, and borehole strainmeters: Bulletin of the Seismological Society of America, v. 96, no. 4B, p. S304–S320, accessed November 9, 2007, at https://doi.org/10.1785/0120050823.

Lindsey, E.O., Fialko, Y., Bock, Y., Sandwell, D.T., and Bilham, R., 2014, Localized and distributed creep along the southern San Andreas Fault: Journal of Geophysical Research Solid Earth, v. 119, no. 10, p. 7909–7922, accessed June 3, 2022, at https://doi.org/10.1002/2014JB011275.

McFarland, F.S., Lienkaemper, J.J., and Caskey, S.J., 2016, Data from theodolite measurements of creep rates on San Francisco Bay Region faults, California (ver. 1.8, March 2016): U.S. Geological Survey Open-File Report 2009–1119, 21 p. and data files, accessed June 8, 2020, at https://doi.org/10.3133/ofr20091119.

Schulz, S.S., 1989, Catalog of creepmeter measurements in California from 1966 through 1988: U.S Geological Survey Open File Report 89–650, 139-p. pamphlet, 4 pl., accessed April 5, 2019, at https://doi.org/10.3133/ofr89650.

Schulz, S., and Burford, R.O., 1978, Installation of an Invar wire creepmeter, Elkhorn Valley, California, August 1977: U.S Geological Survey Open File Report 78–203, 42 p., accessed November 1, 2010, at https:/doi.org/10.3133/ofr78203.

Steinbrugge, K.V., and Zacher, E.G., 1960, Creep on the San Andreas fault—Fault creep and property damage: Bulletin of the Seismological Society of America, v. 50, no. 3, p. 389–396, accessed June 3, 2022, at https://doi.org/10.1785/BSSA0500030389.

Tocher, D., 1960, Creep rate and related measurement at Vineyard, California: Bulletin of the Seismological Society of America, v. 50, no. 3, p. 396–404, accessed June 3, 2022, at https://doi.org/10.1785/BSSA0500030389.

USGS Creepmeter data, 2022, Earthquake Hazards Program, Download data for creepmeters, accessed February 7, 2022, at https://earthquake.usgs.gov/monitoring/deformation/data/download.php.

Wesson, R.L., 1987, Modelling aftershock migration and afterslip of the San Juan Bautista, California, earthquake of October 3, 1972: Tectonophysics, v. 144, nos. 1–3, p. 215–229, accessed May 11, 2011, at https://doi.org/10.1016/0040-1951(87)90019-9.

Appendix 2. Calculation of Fault Slip from Creepmeter Data—Effect of Obliquity and Fault-Normal Displacements

The U.S. Geological Survey's (USGS's) creepmeter network monitors aseismic surface slip at various locations on the Hayward, Calaveras, and San Andreas Faults in northern and central California. The creepmeter is composed of two monuments, located on either side of the identified fault-trace, plus a means to measure the change in distance between the two monuments. The angle formed by a line representing the distance between the two monuments and the fault-trace is termed obliquity, θ. In this report, the measured fault-slip, s, is calculated as

$$s = d/\cos(\theta) \tag{2.1}$$

where

d is the change in distance between the two end monuments, and

θ is the angle of the creepmeter relative to the fault,

This calculation ignores that the fault crossing-angle changes as slip accumulates over time. In addition, fault normal displacements also affect d. Figure 2.1 shows the geometry of the creepmeter and how it responds to fault-parallel displacements.

When the creepmeter is installed, it crosses the fault at an angle, θ, and has an initial length of L_0. Over time, as one end monument displaces by s, due to fault parallel motion, the length changes by d, to become length L_1. Therefore

$$L_1 = [(L_0\cos(\theta) + s)^2 + (L_o\sin(\theta))^2]^{0.5} = L_0 + d \tag{2.2}$$

After some algebra, the above is rearranged to be

$$s^2 + 2sL_0\cos(\theta) - (d^2 + 2dL_0) = 0 \tag{2.3}$$

Taking advantage of the contrast between large numbers, L_0, and smaller quantities, s and d, the above is simplified to be:

$$e2sL_0\cos(\theta) = 2dL_0 \tag{2.4}$$

Dividing by L_0, yields the simplified calculation of slip, (eq. 2.1)

This relation is illustrated by the dashed-dotted red line in figure 2.1, where s, the slip, is projected onto L, the baseline, to become d, its measured change in length.

However, the more complete value of fault parallel motion, s, is calculated by the quadratic formula, or

$$s = -L_0\cos(\theta) + [L_0\cos(\theta)^2 + d^2 + 2L_0d]^{0.5} \tag{2.5}$$

The effect of not taking the change in obliquity depends upon the total amount of slip, the length of the creepmeter, and the initial obliquity. For instance, with a 10-meter (m) long creepmeter with a 30º obliquity and a rate of 20 millimeters per year (mm/yr), then, after 60 years (or 1,200 mm of accumulated slip), the error using the simplified formula is approximately (~1.5) percent which would decrease the calculated slip rate from 20 to 19.7 mm/yr. Equivalently, this represents a change in obliquity from 30º to 27º. For the longer creepmeters, (and lower rates), the effect of changing obliquity becomes less of a problem in determining the accuracy of the creep rate.

Complications arise when the length change is not only a product of fault parallel motion s, but also fault-normal motion, o. This change in geometry is shown in figure 2.2.

Therefore, the new length becomes

$$L_1 = [(L_0\cos(\theta) + s)^2 + (L_o\sin(\theta) + o)^2]^{0.5} = L_o + d \tag{2.6}$$

However, using the approximate method of projecting the fault parallel and normal displacements on to the baseline, L, yields the change in length, d, measured by the creepmeter is

$$d = s\cos(\theta) + o\sin(\theta) \tag{2.7}$$

For instance, if the obliquity is 30º, then a 1 mm fault-normal displacement would result in an increase in length of 0.5 mm of the extensometer, and if fault-normal displacement is assumed to be zero, then the implied creep would be 0.58 mm from that 1 mm of unrecognized, fault-normal displacement.

To estimate both s and o requires installing a second extensometer. Optimally, the new extensometer would cross the fault at 90º so that the fault normal displacement is measured directly. However, as slip accumulates, the end monument of the fault-normal extensometer also moves in a fault parallel direction. Therefore, the equation governing the length change of the fault-normal extensometer is

$$N_1 = [(N_0\cos(\phi) + s)^2 + (N_o\sin(\phi) + o)^2]^{0.5} = N_o + \Delta \tag{2.8}$$

where

N_0 and N_1 are the values of the initial and final lengths of the extensometer,

Δ is the measured length change, and

ϕ is the obliquity of this extensometer relative to the fault and is close to 90º.

Then, with two sets of extensometer measurements equations 2.6 and 2.8 can be solved iteratively to calculate fault parallel and normal slip.

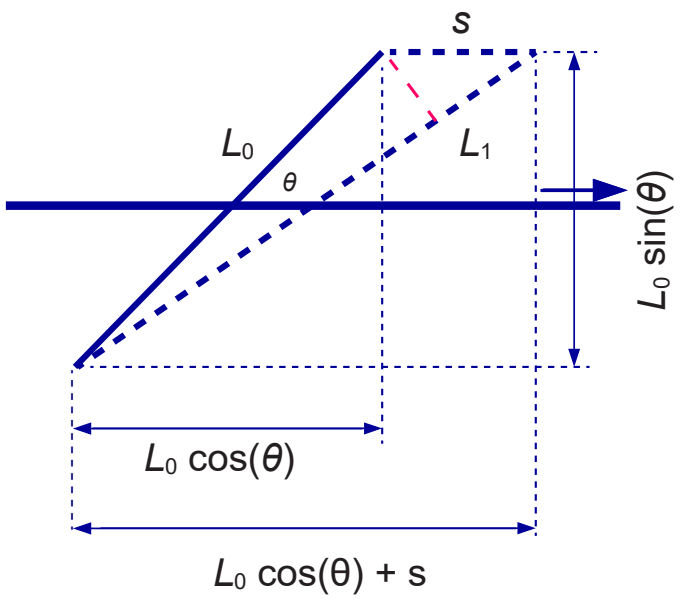

Figure 2.1. Diagram of the geometry of a creepmeter relative to a strike-slip fault and how it responds to fault-parallel displacement. When the creepmeter is installed, it crosses the fault at an angle θ, and has an initial length of L_0. Over time, as one end monument displaces by s, the component for slip due to fault parallel motion, the length changes by d, to become length L_1. Note that the thin dashed-dotted red line indicates the projection of slip, s, onto the baseline, L, which becomes the change in length due to slip.

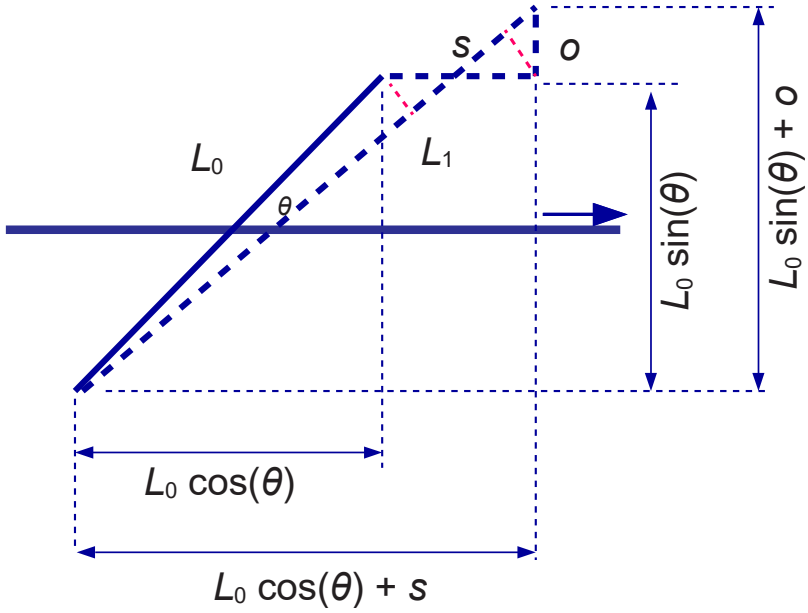

Figure 2.2. Diagram of the geometry of a creepmeter relative to a strike-slip fault and how it responds to fault-parallel and fault-normal displacement. When the creepmeter is installed, it crosses the fault at an angle θ, and has an initial length of L_0 Over time, as one end monument displaces by s, the component for slip due to fault-parallel motion, the length changes by d to become length L_1. Note that the thin dashed red lines indicate the projection of slip, s, and o, fault-normal displacement onto the baseline, L, which becomes the change in length. Large arrow indicates the direction of fault-parallel slip.

Appendix 3. Creepmeter Calibration Issues Addressing the Potential Scaling Problem for the Gold Hill (XGH1) Creepmeter Located on the San Andreas Fault Southeast of Parkfield, California.

This report is an update to the presentation by Schulz (1989) introducing potential users to the creepmeter data collected between the publication of Schulz's report and mid-2020. The U.S. Geological Survey's (USGS's) creepmeter network monitors aseismic surface slip at various locations on the Hayward, Calaveras, and San Andreas Faults in northern and central California. This appendix shows the calculations undertaken to address the potential scaling problem for the Gold Hill (XGH1) creepmeter by comparing the manually observed micrometer measurements with the voltages measured by the electronics from the output of the linear voltage displacement transformers/transducers (LVDT). Site XGH1 is located on the San Andreas Fault southeast of Parkfield, California, and is part of the Parkfield network of the larger USGS creepmeter network in central and northern California (fig.1). Detailed information on site XGH is given in appendix 1 section "XGH—Gold Hill—San Andreas Fault."

Table 3.1 shows a listing of the micrometer data along with two sets of voltage measurements; V2 is from the LVDT and V5 is from the output of the amplifier (which is input to the telemetry data logger). Note that these measurements spanning the 2006 to 2018 interval are more numerous than the points shown in figure 4 in the main text as this tabulation shows data when the creepmeter was reset (for example, 151015 or October 15, 2015), and other times when the LVDT was calibrated on site, which occurred three times, 180426, 070312, and 061128.

The information in table 3.1 is broken into shorter intervals and the combinations of columns are regressed. For instance, V2 and V5 are fit to a function, $V5 = mV2 + b$ and the coefficients m and b are estimated. For this, both L2-norm, standard least squares, and L1-norm (minimizes the median difference between predicted and observed) are employed. The L1 solution is relatively immune to outliers for these experiments using only a few observations. For the V2/V5 regression, the above consistently provides coefficients of $m = -1.0$. On the other hand, there are variations in both m and b when the micrometer data are fit to V5 voltages. These are shown in table 3.2.

By grouping the estimates of scale factors, m, for the LVDT, it becomes apparent that in-situ calibrations prior to 2014 (that is, 140101), differ from those after 2014. Averaging the estimates of scale factors prior to 2014 yields 6.109 millimeters per volt (mm/V), while after 2014 yields 3.789 mm/V, which represents a large change. That estimate relies primarily on the on-site calibration measurements made 180426. In addition, prior to 2006, the calibration of this LVDT provided a sensitivity of 5.932 mm/V.

References Cited

Schulz, S.S., 1989, Catalog of creepmeter measurements in California from1966 through 1988: U.S Geological Survey Open File Report 89–650, 13-p. pamphlet, 4 pl., accessed April 5, 2019, at https://doi.org/10.3133/ofr89650.

Table 3.1. Micrometer and voltage measurement for the creepmeter at Gold Hill (XGH1) from 2006 to 2018, on the San Andreas Fault southeast of Parkfield, California. V2 is from the linear voltage displacement transformers/transducers (LVDT) and V5 is from the output of the amplifier (which is input to the telemetry data logger). Note that these measurements spanning the 2006 to 2018 interval are more numerous than the points shown in figure 4 in the main text as this tabulation shows data when the creepmeter was reset (for example, 151015, or October 15, 2015), and other times when the LVDT was calibrated on site, which occurred three times: 180426, 070312, and 061128. yr, last two digits of the year; mo, month; da, day; mm, millimeter; with weight defined as measure of reliability of observation provided in the Notes column.

Date (yrmoda)	Micrometer (mm)	V2 (volt)	V5 (volt)	Weight	Notes
180426	6.66	1.991	0.498	100	Outlier calibration experiment
180426	3.35	2.746	0.581	1	V2 doesn't look right
180426	4.96	1.473	1.023	1	
180426	10.4	0.054	2.462	1	
180426	15.935	−1.368	3.904	1	
180426	20.615	−2.605	5.158	1	
180426	19.055	−2.181	4.729	1	
180426	2.76	2.3	0.185	100	Outlier
151015	13.377	0.484	2.022	1	
151015	8.26	1.645	0.852	1	
171221	11.52	0.68	1.826	1	
171221	3.6	2.699	−0.246	1	
171221	6.65	1.967	0.523	1	
170508	15.425	−0.165	2.679	1	
170508	5.74	2.138	0.352	1	
140514	8.6	1.44	1.038	1	
140910	10.807	0.913	1.589	1	
140910	9.707	1.282	1.217	1	
140506	8.6	1.44	1.058	1	
140225	12.75	0.973	1.529	100	Outlier
120905	11.41	0.542	1.963	1	
121115	11.778	0.495	2.009	1	
121115	2.323	1.948	0.547	1	
110414	5.073	1.51	0.977	1	
110201	4.057	1.609	0.887	1	
110127	4.922	1.499	0.977	1	
091006	9.72	0.993	1.503	1	
090310	9.75	1.172	1.298	1	
090310	4.418	2.042	0.451	1	
080723	8.26	1.176	1.325	1	
071008	9.987	1.038	1.463	1	
071008	2.163	2.228	0.268	1	
070604	5.553	1.482	1.017	1	
070312	25.5	−1.677	4.184	1	Calibration experiment
070312	20.2	−0.814	3.32	1	
070312	14.5	0.102	2.401	1	
070312	8.42	1.051	1.451	1	
070312	3.19	1.92	0.579	1	
070301	1.75	2.16	0.337	1	
061128	3.47	1.7	0.8	100	Outlier; calibration experiment
061128	−0.45	2.247	0.253	100	Outlier
061128	3.18	1.533	0.966	1	
061128	8.2	0.646	1.853	1	
061128	13.46	−0.213	2.712	1	
061128	17.54	−0.8	3.382	1	
061128	21.86	−1.598	4.093	1	
061128	25.19	−2.197	4.688	1	
061128	1.42	1.746	0.754	100	Outlier

Table 3.2. Fit V5 voltage to micrometer measurements from table 3.1 for creepmeter site Gold Hill (XGH1) on the San Andreas Fault southeast of Parkfield, California. V5 is from the output of the amplifier. V5 and the micrometer measurements are fit to a function, $mic = mV5 + b$ and the coefficients m and b are estimated. For this, both L2-norm, standard least squares, and L1-norm (minimizes the median difference between predicted and observed) are employed. There are variations in both and when the micrometer data are fit to V5 voltages.; column listing are time interval (yr, last two digits of the year; mo, month; da, day) number of observation misfit to the L1 norm, values of m (mm/V) from both the L1 and L2 methods, and the value of b (mm).

Time span (yrmoda)		Number	L1-misfit (mm/mm)	LVDT scale factor		*b* from L1 (mm)
Start date	End date			*m* from L1 (mm/V)	*m* from L2 (mm/V)	
061128	061129	9	7.93	5.913	5.965±0.032	−2.532
070301	070313	6	7.58	6.174	6.195±0.027	−0.331
070311	070313	5	8.21	6.206	6.213±0.032	−0.403
070601	071101	3	1.51	6.547	6.547±0.018	0.408
070601	080801	4	41.93	6.547	6.252±0.470	0.408
070601	090401	6	105.94	6.547	6.035±0.946	0.408
100101	110501	3	15.1	9.611	10.450±1.453	−4.468
100101	130101	6	16.86	6.427	6.553±0.141	−1.206
140101	180101	12	24.32	4.07	4.100±0.112	4.521
180401	180501	8	4	3.803	3.787±0.009	1.069

Appendix 4. Seasonal Variations in Creep for the Hayward, Calaveras, and San Andreas Faults in Northern and Central California

This report is an update to the presentation by Schulz (1989) introducing potential users to the creepmeter data collected between the publication of Schulz's report and mid-2020. The U.S. Geological Survey's (USGS's) creepmeter network monitors aseismic surface slip at various locations on the Hayward, Calaveras, and San Andreas Faults in northern and central California. As noted in the main text, the observed creep has seasonal variations that have been modeled using two sinusoids, one at the annual period and a second at the semi-annual period. The amplitude of these variations can be as large as 3.7 millimeters (mm) (fig. 4.1). For many of the sites, the minimum of the function describing the seasonality is during late winter, at a time when there is the greatest amount of rainfall. However, as will be shown below, this wintertime minimum is not a universal characteristic that can be applied to all creepmeters.

There are two methods that are available to characterize the seasonality. One method is to fit two sinusoids, 365.25- and 182.625-day periods, along with the rate to a time series of creep data. Examples from four creepmeters are shown in figure 4.1 with the sinusoidal function drawn as a black line. An alternative method of deriving a seasonal "correction" is shown in red. The seasonal adjustment is determined by splitting the time series into yearly intervals, removing the mean and trend for each interval. Then, for each day of the year, calculate the average value. In general, the fitting of two sinusoids seems to adequately reproduce the seasonal adjustments derived from stacking the annual data. Apparent from the four examples is that the phases of the seasonals are variable. For example, site Melendy Ranch (XMR) on the San Andreas Fault has a minimum value of creep on day-of year (DOY) 120, or early May. However, site Shore Road (XSH) on the Calaveras Fault has a minimum value of creep on DOY 180, or July.

The results of estimating the amplitude and the time of minimum value of seasonal creep are shown in figure 4.2. The left-hand plot shows the values and their uncertainties of amplitude and time, and the right-hand plot replots the amplitude and time but identifies each pair as a creepmeter. The value of the uncertainty for the amplitude is the value calculated from least squares regression when the seasonal terms and the rate are estimated. The uncertainty for time is derived from identifying the time of minimum creep from the addition of the two sinusoids, then adding an arbitrary value of 0.2 mm to that minimum. The uncertainty then is one-half the time interval between the two values of the dithered creep. Using the sinusoidal function in preference to the stacking method provides a simple method of calculating the amplitude uncertainty. The example results in figure 4.1 indicate that both methods provide nearly equivalent descriptions of the seasonal variations. Not captured, however, is the yearly modulation of seasonal variations that one sees when looking at a multi-year time-series of creepmeter data. Instead, that modulation is modeled as a stochastic process (Langbein, 2004) when fitting the annual and semi-annual periods to the data.

The strongest seasonal variations are at four sites on the San Andreas Fault: Varian (XVA), Taylor Ranch (XTA), Middle Ridge (XMD), and Nyland Ranch (NYL). All four of those sites do indeed have their minimum creep in late winter or early spring (day of year [DOY] 60 to 120) when the ground is most moist from the wintertime rainy season, which typically extends from November through April of each year. In addition, four other sites: Gold Hill (XGH), Roberson SW Trace (XRSW), Melendy Ranch (XMR), and Slacks Canyon (XSC) also on the San Andreas Fault, have the same interval of slow creep but with lower amplitude. On the other hand, 13 sites have their minimum creep occurring sometime after late July.

There are several mechanisms that might explain the seasonal variations. These include thermal expansion and contraction of the Invar or carbon-fiber length standard, temperature sensitivity of the electronics, fault-zone expansion or compaction in response to seasonal rainfall and/ (or) displacements of the end monuments due to soil expansion and contraction due to the seasonal rainfall. For instance, both Invar and carbon-fiber have a temperature coefficient of approximately (~) 1 part per million per °Celsius (ppm/°C) (which is a factor of 10 less than many materials). With a 20 °C change in temperature seen over a one-year period at XMR (less than [<]1-meter [m] depth), the 10-m long wire could change length by 0.2 mm due to annual temperature swings. Instead, the annual variation observed at XMR is 2.5 mm, much larger than predicted from stretching of the Invar wire. In addition, if thermal expansion of the length standard is the cause of the observed periodicity, then for all the creepmeters the periodicities should be in-phase with each other; figure 4.2 indicates that this is not the case. Although the temperature sensitivity of the electronics is currently unknown, all the USGS style instruments use the same electronics and, again, since the annual periodicities are out of phase, one can rule-out the electronics as the cause.

This leaves two possible explanations: (1) fault-zone contraction, or (2) expansion due to soil moisture, or random displacements of the end monuments due to changes in soil moisture. Currently, (early 2023), a few of the creepmeter sites now have extensometers that cross the fault at 90° which should provide some data related to the fault-zone contraction hypothesis. However, the random changes in soil-moisture inducing tilting and displacement of the two end monuments remains untested other than to note, as mentioned in the main text, that many of the monuments used for the creepmeters are similar to that employed by a geodetic network at Parkfield and discussed by Langbein and others (1990). Many of those monuments exhibited tilt, and that affected the measured line-length changes observed in that network. However, those monuments extended above the grounds surface, where in contrast, the creepmeter monuments are installed below grade and should be less affected by seasonal changes in soil moisture.

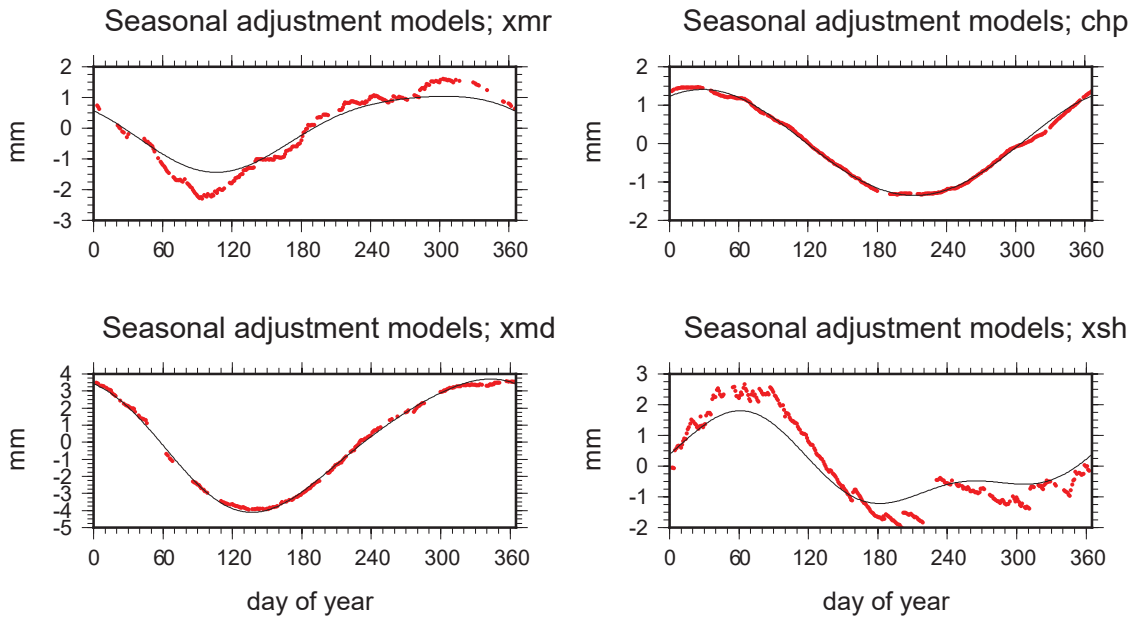

Figure 4.1. Graphs of four examples of U.S. Geological Survey creepmeters for the central and northern California network showing the results of two methods for calculating the repeating seasonal variations. The black line is the result of fitting two sinusoids, 365.25- and 182.625-day periodicities, to the entire record of creep. The red line is the result of stacking one-year long intervals and extracting the average creep for each day of the year. XMR, Melendy Ranch; CHP, City of Hayward; XMD, Middle Ridge; XSH, Shore Road; mm, millimeters.

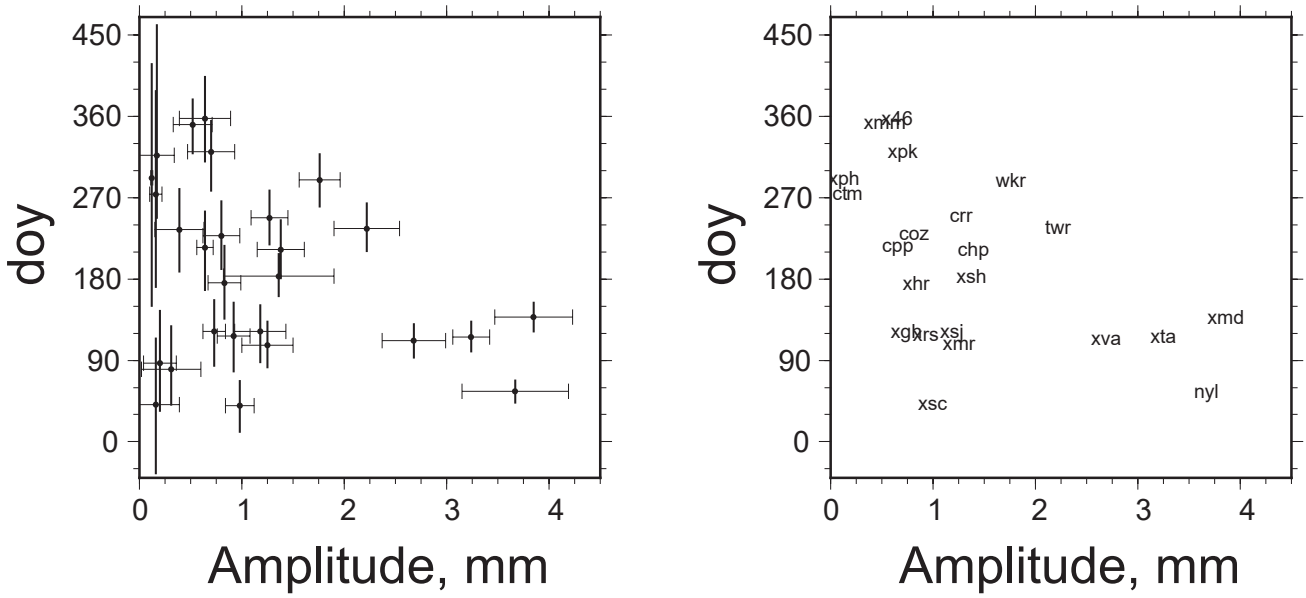

Figure 4.2. Plot of the relationship between the amplitude of seasonal variations in creep and the time when the seasonal variations are a minimum for some U.S. Geological Survey creepmeters for the central and northern California network. Day of year (DOY) 1 is January 1. The left-hand panel shows, for each site, the estimates of the amplitude and minimum time along with their uncertainties. The right-hand panel shows the name of each site plotted at their locus of amplitude and minimum time. Sites where the amplitude is not significant (<2σ) are not shown in the right-hand panel. mm, millimeters.

References Cited

Langbein J., 2004, Noise in two-color electronic distance meter measurements revisited: Journal of Geophysical Research Solid Earth, v. 109, no. B4, 16 p., accessed August 17, 2021, at https://doi.org/10.1029/2003JB002819.

Langbein, J., Burford, R.O., and Slater, L.E., 1990, Variations in fault slip and strain accumulation at Parkfield, California—Initial results using two-color geodimeter measurements, 1984–1988: Journal of Geophysical Research Solid Earth, v. 95, no. B3, p. 2533–2552, accessed May 11, 2021, at https://doi.org/10.1029/JB095iB03p02533.

Schulz, S.S., 1989, Catalog of creepmeter measurements in California from1966 through 1988: U.S Geological Survey Open File Report 89–650, 139-p. pamphlet, 4 pl., accessed October 9, 2021, at https://doi.org/10.3133/ofr89650.

Appendix 5. Creep, Earthquakes, and Strain for the Hayward, Calaveras, and San Andreas Faults in Northern and Central California

This report is an update to the presentation by Schulz (1989) introducing potential users to the creepmeter data collected between the publication of Schulz's report and mid-2020. The U.S. Geological Survey's (USGS's) creepmeter network monitors aseismic surface slip at various locations on the Hayward, Calaveras, and San Andreas Faults in northern and central California. We describe here several associations of shallow seismicity with observations of anomalous surface creep and strain. While it has been clearly established that accelerated surface creep occurs in the form of afterslip following moderate earthquakes at seismogenic depth (for example, moment magnitude [M_w] 6 earthquakes in Parkfield, California, in 1966 and 2004; 1987 M_w 6.5 Superstition Hills, and so forth), the association of accelerated creep with microseismicity (M_w less than [<] 4), though anticipated, is less well established. Accelerated surface creep also follows slow earthquakes (Linde and others, 1996), that is, fault slip at depth that occurs over intervals of minutes to hours. In that case, a slow-slip event with moment release equivalent to M_w approximately equal to (≈) 5 occurred on the San Andreas Fault near San Juan Bautista which was recorded by two creepmeters and two borehole strainmeters. The slow-slip event was accompanied by a few small, M<3.7, earthquakes located nearby.

Every few years the Oakland Zoo (COZ) creepmeter, located on the Hayward Fault in the Oakland Zoo, exhibits accelerated creep with durations of several weeks. The signature of these events is an emergent onset attaining maximum dextral slip velocities exceeding 300 micrometers per day (µm/day) (a thirty-fold increase in slip velocity above the mean creep rate at this location) that persist for 3–7 days, then decaying over the next few weeks to background levels of ≈8 µm/day. The onset and duration of these events are an order of magnitude slower than creep events seen elsewhere in the San Andreas Fault system. Six of these slow creep events are identified in figure 5.1*C* with thick, red lines.

The relationship of these creep events with nearby earthquakes and rainfall is explored in figures 5.1 and 5.2. The locations of nearby earthquakes with magnitudes greater than (>) M1 have been downloaded from the U.S. Geological Survey, Earthquake Hazards Program, (2017). The earthquakes can be characterized as occurring in two clusters, one close to the COZ creepmeter, identified as the San Leandro cluster, and a second cluster located to the northwest, identified as the Piedmont cluster. The catalog locations have not been refined using more sophisticated algorithms to improve their estimated locations. The temporal relation of the creep transients and local earthquakes from the San Leandro cluster, figure 5.1*D*, indicates a causal relationship, especially in February 2022. Figure 5.1*B* shows the temporal relation between two M3 events that occurred 10 days and 3 days prior to the onset of creep on day of year (DOY) 46. The first event (M_w 3.1 at 01:01 Universal Time [UT] on 7 Feb 2022) was registered as a 41 µm of apparent dextral displacement by the glass-fiber/LVDT creepmeter, and 3 µm on the carbon-fiber/rotary Hall sensor (fig. 5.2). The second event (M_w 3.2 at 03:13:42 on 12 Feb 2022) was recorded by three sensors: (1) the carbon rod creepmeter operating with a local 1 hertz (Hz) recording rate registered it as a 0.44 millimeter (mm) offset over a time interval of 2–3 seconds (s), (2) the offset recorded by the low-resolution rupture meter was 0.33 mm, but (3) the offset recorded by the LVDT on the glass fiber rod was only 0.16 mm. Thus, although the offset triggered by the two events may in part be a measure of co-seismic strain from slip in the subsurface, the factor of two discrepancy in amplitudes recorded during shaking in each event indicates that mechanical imperfections in the instruments are responsible for differences in the coseismic offset.

The earthquakes occurred at hypocentral distances of 2.5–4.5 kilometers (km) from the creepmeter, and surface slip was delayed by 6.9 days after the first earthquake and 1.9 days after the second earthquake (fig. 5.2). If we assume that a subsurface dislocation propagated northwards towards the creepmeter from either of these earthquakes the required propagation velocities are ≈18 and 35 meters per hour (m/h) respectively to the initial onset of afterslip on 14 February, or 14 and 17 m/h to the time of rapid slip-on 16 February.

The total surface slip that developed in the following month amounted to 4.5 mm. The rupture dimensions for a M_w 3.2 earthquake with this amount of slip is calculated to be 750×750 square meters (m^2), somewhat larger than expected from a M_w 3.2 earthquake, suggesting that the earthquake may have been associated with a component of slow slip incompletely characterized by the radiated seismic energy.

A nearby borehole (installed at 125 m depth) tensor strainmeter, CHT, also responded to strain associated with an earlier event (data are available from 1993 to late 2016, when the instrument failed). The location of this instrument is 6 km east-southeast of the COZ creepmeter (fig. 5.1) and is 3.4 km from the Hayward Fault. Creep and strain data from four of the six creep events are plotted in figure 5.2. The response of the strainmeter to Earth tides has been removed. Earth tides are used for in-situ calibration of these types of strainmeters as the presence of the borehole modifies the observed strain in the borehole from the strain that is in the surrounding rock (Hart and others, 1996).

In figure 5.3, the tensor strain quantities are shown as different colors with dilatation being green; the first shear component, Eee–Enn, plotted as red, and the second shear component, 2Een; plotted as blue for a north-south, east-west coordinate system. For three of the four transients, the first shear component, Eee–Enn, has a significant signal, like that of creep. For a fault that is oriented northwest-southeast, as is the Hayward Fault, right-lateral slip on that fault should cause the Eee–Enn to be negative. On the other hand, the dilatational response to creep shows insignificant changes, and for the 2013 transient, the second shear component also responded, but over the one-month interval

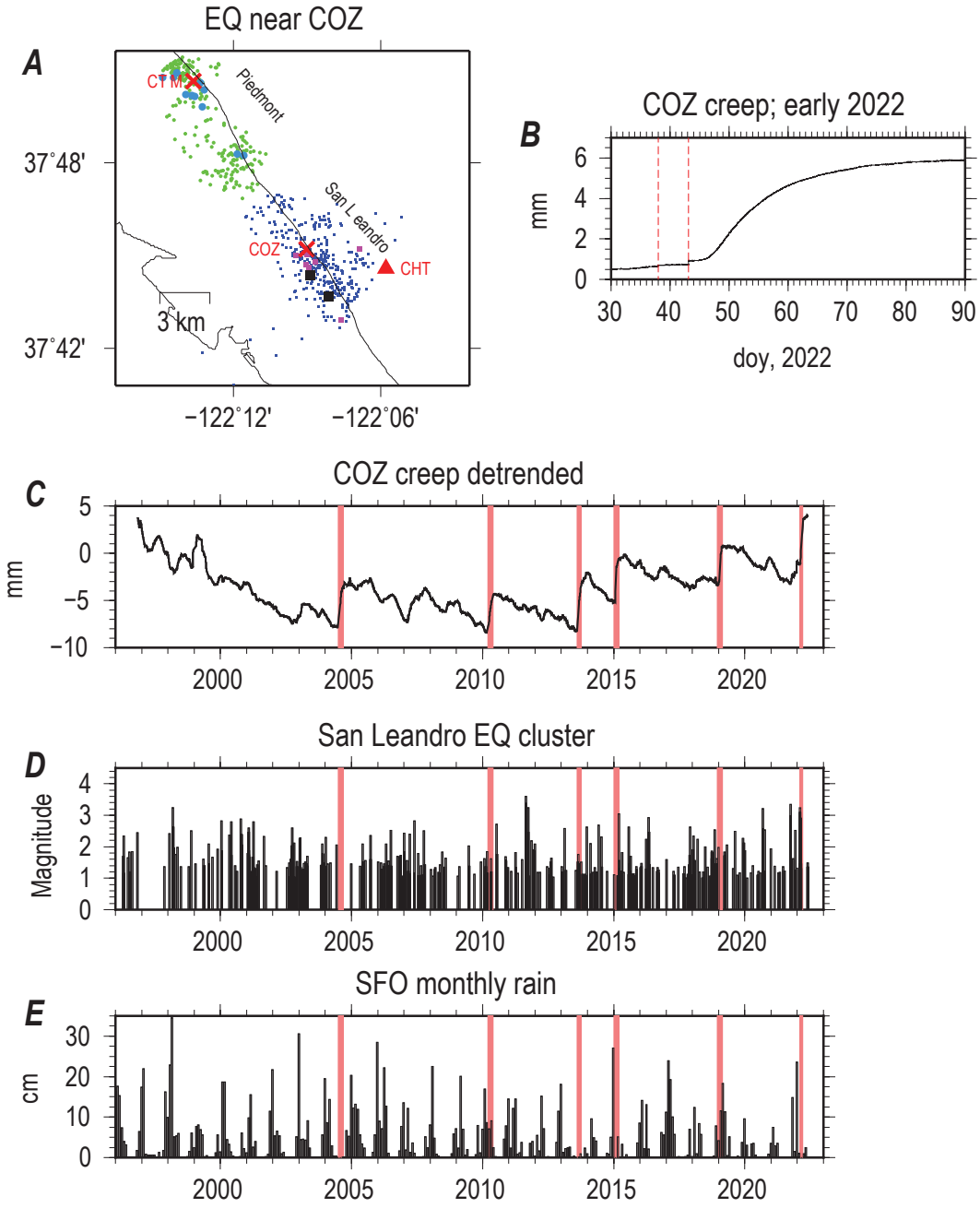

Figure 5.1. Map and graphs of the relationships between transient creep at the Oakland Zoo (COZ) site, on the Hayward Fault, local earthquake activity, and rainfall for the period between 1996 and 2022. *A*, The map shows the locations of earthquakes, creepmeters, and a strainmeter near Oakland, California. The green dots are earthquakes (EQ) from the Piedmont cluster, the blue from the San Leandro cluster. The larger colored dots are earthquakes with magnitude *M* greater than (>) 3.0. The black squares are the locations of two earthquakes, *M*3.09 and *M*3.24, that occurred in early 2022. The location of the CHT tensor strainmeter is shown as a red triangle. The locations of earthquakes with magnitudes greater than (>) *M*1 have been downloaded from the U.S. Geological Survey Earthquake Hazards Program, (2017). *B*, The time series is the creep at COZ between days of year (DOY) 30 and 90 for 2022. The two vertical lines represent the times of the two earthquakes plotted as large black squares in *A*. *C*, The residual creep from COZ is plotted after removing a linear trend and two sinusoids with 365.25- and 182.625-day periods. The thick red lines representing approximately one month are periods of accelerated transient creep detected visually and carried through onto *D* and *E*. *D*, The time and magnitude of earthquakes in the San Leandro cluster are plotted. *E*, The time series of monthly rainfall totals from the San Francisco Airport (SFO) is plotted (California Data Exchange Center, 2021. mm, millimeter; cm, centimeter.

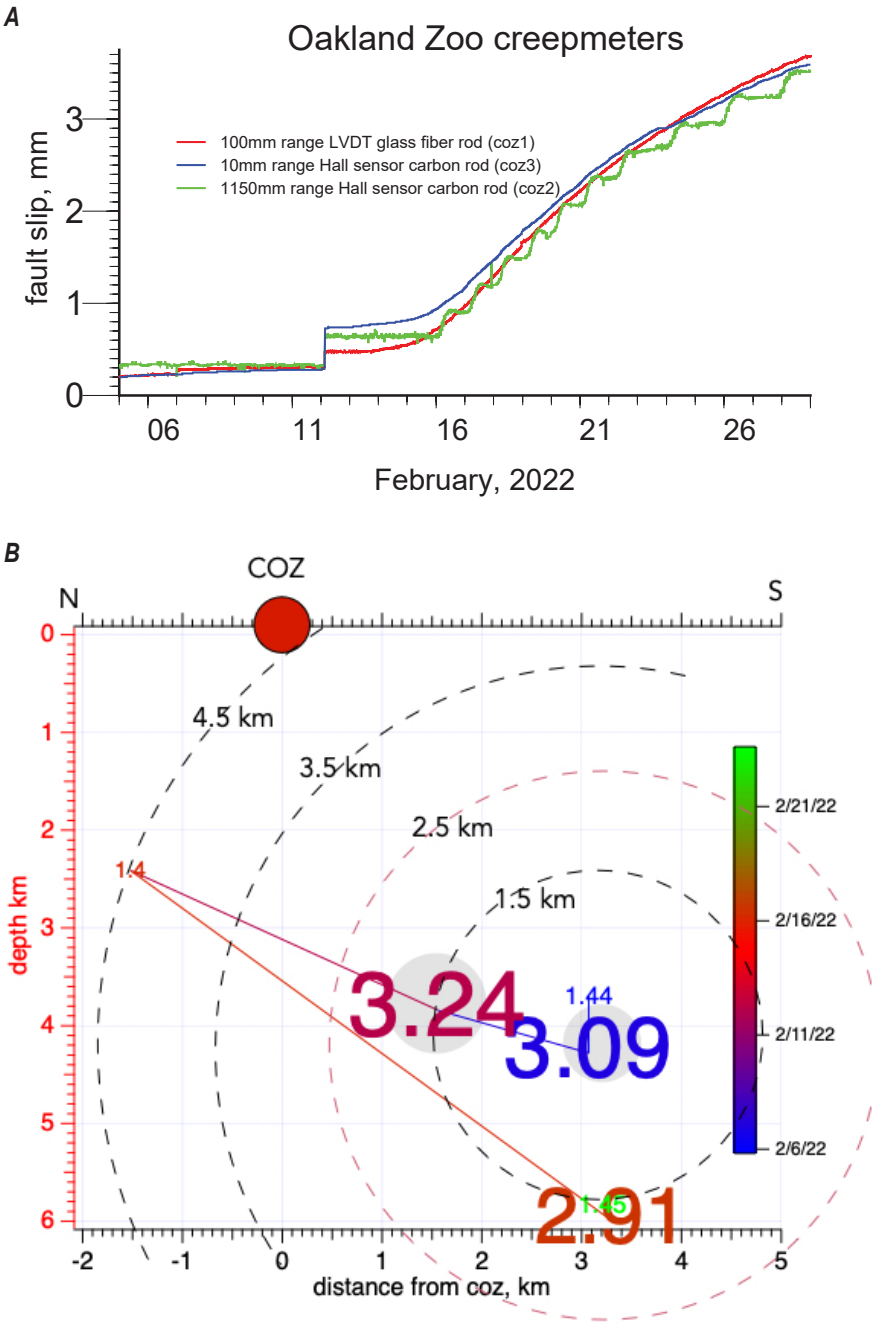

Figure 5.2. *A*, Coseismic offsets on 7 and 12 February 2022 at the Oakland Zoo (COZ) creepmeter and the onset of the slow surface-creep event. A two-day delay in the onset of surface creep occurs, followed by an additional 2-to-3-day delay before all three sensors at Oakland Zoo, California, responded with maximum velocities. The steps in the rupture meter trace (green) correspond to the 12-bit resolution (~0.2 millimeter [mm]) of the 1.15-meter (m) range rupture meter. *B*, Depth section showing earthquakes on February 2022 scaled to magnitude and colored according to time with dashed circles with increasing radius centered on the first earthquake. Onset of creep at the COZ creepmeter (red dot) occurred between 14–16 February implying creep propagation velocities 14–35 meters per hour (m/h). LVDT, linear voltage displacement transformers/transducers; km, kilometer.

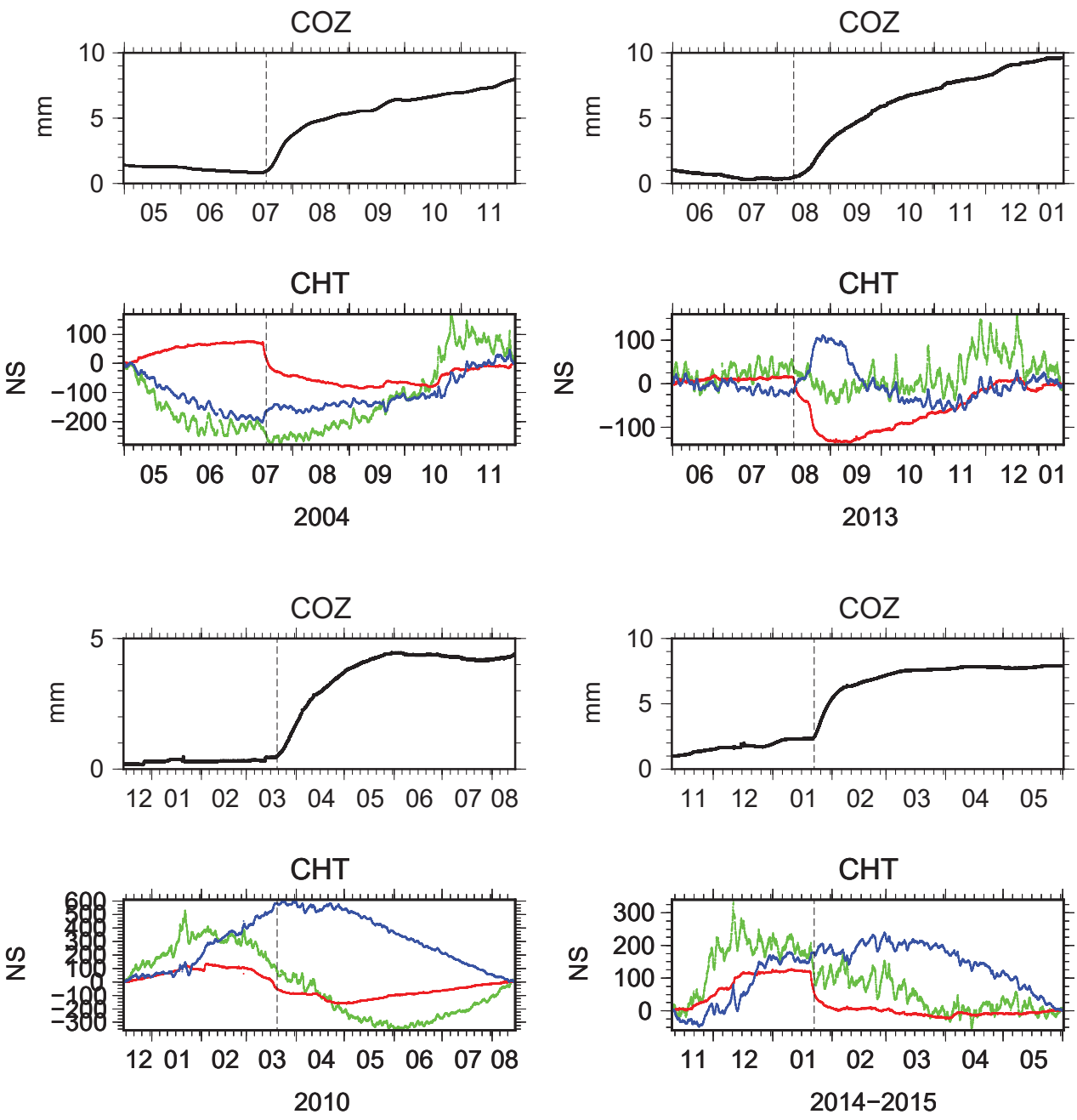

Figure 5.3. Plots of creep from the Oakland Zoo (COZ) creepmeter and strain from the CHT strainmeter on the Hayward Fault near Oakland, California, for four of the six transients in creep identified in figure 5.1. For each of the transients, two plots are provided, one for the creep and a second one for strain. In general, the intervals cover ½ to ¾ of a year centered on the transient. Thin, vertical dashed lines help with relative timing of the onset of transient creep and strain. The strain data are presented in three colors: green being dilatation; red being the first shear component, Eee-Enn; and blue being the second shear component, 2Een. mm, millimeter; with the components of strain being expressed in a N-S/E-W coordinate system.

of the transient, there is no net change in that component of strain. In addition, the signal from the strainmeter preceded the surface creep by a few hours to one day. This would suggest that slip propagated upwards to the surface.

Although the combination of creep and strain can be modeled, as has been done for other slow-slip events detected by both creepmeters and strainmeters (Linde and others, 1996), we believe this analysis is beyond the scope of this report, which concentrates on providing data. Nonetheless, we note that slip measured at COZ extending to ~0.5 km depth is consistent with the observed shear strain measured at CHT. However, more detailed modeling could provide a better estimate of the extent of slip, both horizontally and vertically.

Another example of coincident creep and strain is from the Parkfield network for an event in August 2008. That creep event, which occurred at Varian (XVA1), is centered within a network of four borehole strainmeters and an additional four continuously recording GPS (global positioning system) receivers shown in figure 5.4.

The creep event at XVA evolved over ~5 days, see figure 5.5, but the signals at the strainmeters differed from XVA and from each other. Although the creep event at Parkfield evolved over a shorter period than the one described for the Hayward Fault events, the amplitude of the Parkfield event is only 1 mm, in contrast to the 5 mm for the Hayward events. The sequence of strain and creep suggests a complicated evolution of slow slip. Initially, there was a "creep" like signal at the DL dilatometer that preceded the slow initiation of creep at XVA. The co-located tensor strain at DL shows no significant changes. Then, in early DOY 230 of 2008, the creep accelerated and both the FR dilatometer and B073 tensor strainmeter saw the event quickly transpire. Although there are GPS stations nearby, the displacements from this 1-mm creep event are below the precision of the GPS.

Initial modeling suggests a limited horizontal extent since creep is not observed at adjacent sites to the northwest (Middle Ridge, XMD) or to the southeast (Parkfield, XPK). Depth extent is poorly constrained but suggests that the event extended to 0.5 km.

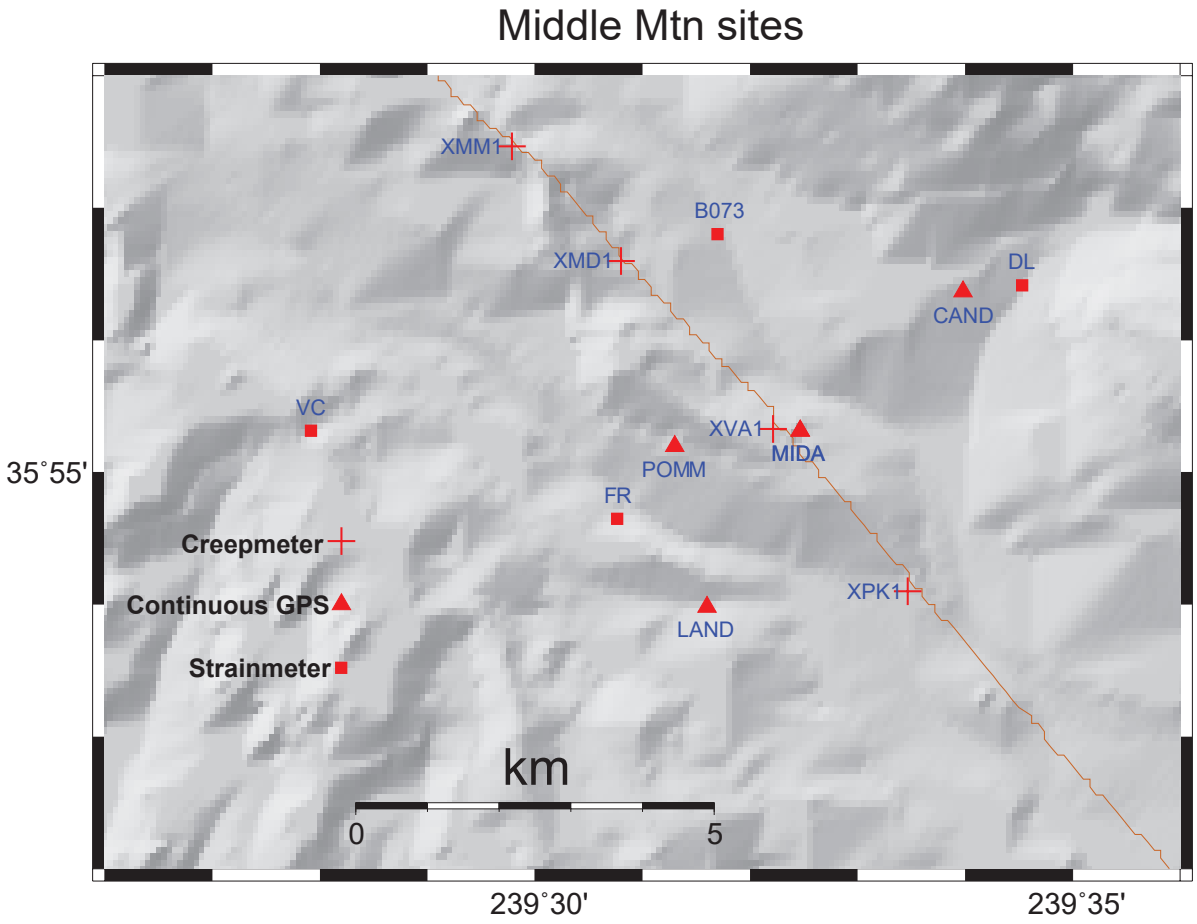

Figure 5.4. Map showing a portion of the San Andreas Fault and its relation to creepmeter, borehole strainmeters, and global positioning system (GPS) on Middle Mountain, northwest of Parkfield, California. Creepmeters: XMM, Middle Mountain; XMD, Middle Ridge; XVA, Varian; XPK, Parkfield.

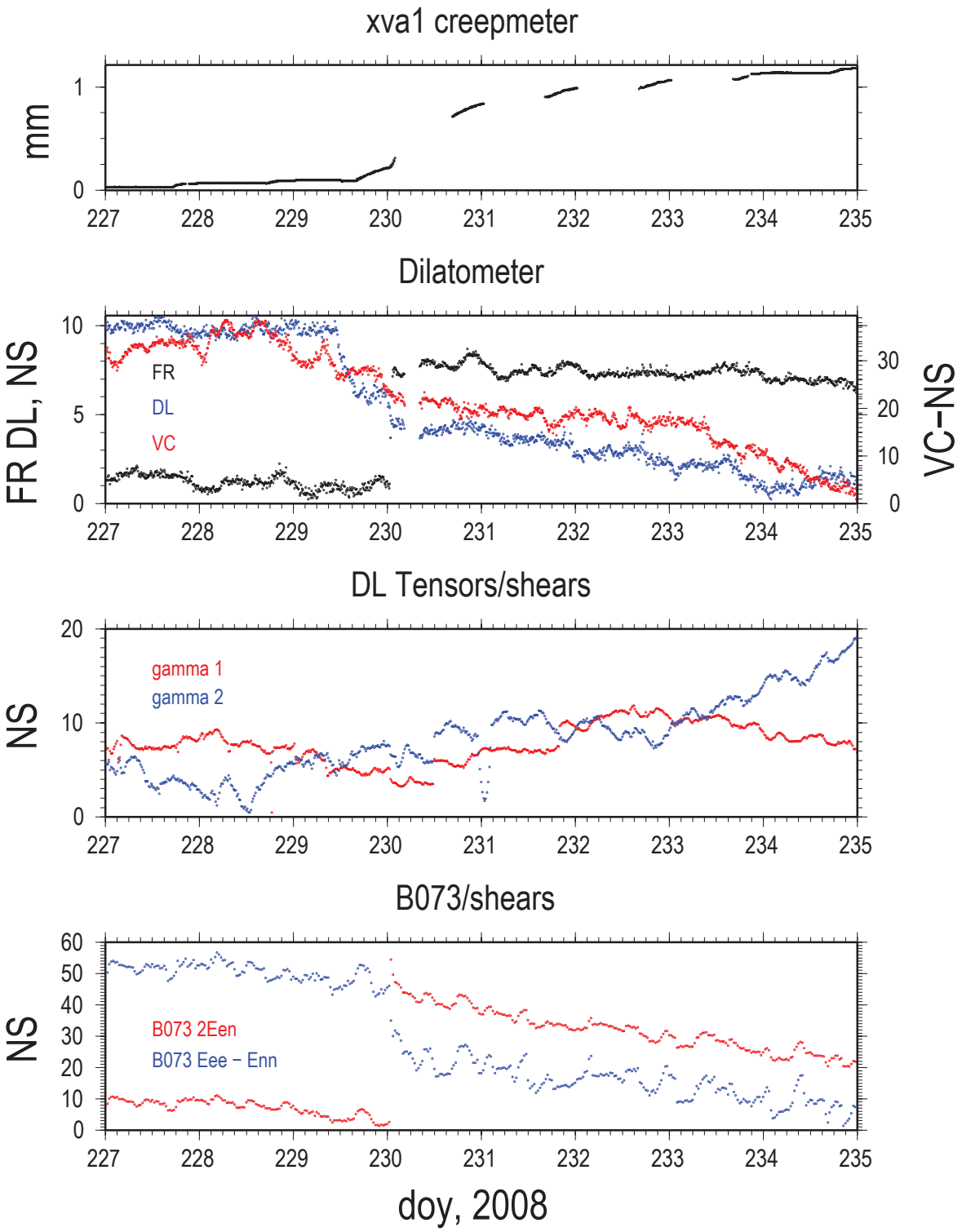

Figure 5.5. Graphs of data from the Varian (XVA1) creepmeter on the San Andreas Fault northwest of Parkfield, California, and the borehole strainmeters from the August 2008 creep event. Gamma 1 or Eee-Enn, first shear component; gamma 2 or 2Een, the second shear component. Amplitude of strain NS represents 0.001 parts-per-million, Strain is represented in N-W/E-W; coordinate system; mm, millimeter; doy, day of year. The locations of the creepmeter and borehole strainmeters (FR, DL, VC, B073) can be found on figure 5.4.

References Cited

California Data Exchange Center, 2021, California Data Exchange Center—Precipitation: California Department of Water Resources, California Data Exchange Center website, accessed June 6, 2021, at https://cdec.water.ca.gov.

Hart, R.H.G, Gladwin, M.T., Gywther, R.L., Agnew, D.C., and Wyatt, F.K. 1996, Tidal calibration of borehole strain meters—Removing the effects of small-scale inhomogeneity: Journal of Geophysical Research Solid Earth, v. 101, no. B11, p. 25553–25571, accessed January 18, 2008, at https://doi.org/10.1029/96JB02273.

Linde, A.T., Gladwin, M.T., Johnston, M.J.S, Gwyther, R.L., and Bilham, R.G, 1996, A slow earthquake sequence on the San Andreas fault: Nature, v. 383, no. 6595, p. 65–68, accessed October 4, 2023, at https://doi.org/10.1038/383065a0.

Schulz, S.S., 1989, Catalog of creepmeter measurements in California from1966 through 1988: U.S Geological Survey Open File Report 89–650, 139-p. pamphlet, 4 pl., accessed April 5, 2019, at https://doi.org/10.3133/ofr89650.

U.S. Geological Survey Earthquake Hazards Program, 2017, Advanced National Seismic System (ANSS) Comprehensive Catalog of Earthquake Events and Products: Various, https://doi.org/10.5066/F7MS3QZH.

Appendix 6. Earth Tide Effects on Selected Creepmeters in Northern and Central California

This report is an update to the presentation by Schulz (1989) introducing potential users to the creepmeter data collected between the publication of Schulz's report and mid-2020. The U.S. Geological Survey's (USGS's) creepmeter network monitors aseismic surface slip at various locations on the Hayward, Calaveras, and San Andreas Faults in northern and central California. A 30-meter (m)-long creepmeter with a displacement sensitivity of 3 micrometers (μm) acts as a strainmeter with a resolution of 10^{-7}. Hence, the creepmeters in California should not be expected to record the Earth tides, with amplitudes of typically a few parts in 10^{-8} strain. However, the Hayward fault creepmeters which adjoin the San Francisco and San Pablo Bays are exposed to the somewhat larger load tides induced by tidal motions of these bodies of water.

An examination of the spectral content of the past 25 years of data from all five sites (CPP, Pinole Point; CFW, Fremont; CTM, Temescal; COZ, Oakland Zoo; CHP, City of Hayward, Palisade St.) on the Hayward Fault in the San Francisco Bay Area reveals that for only the northernmost creepmeter on the Hayward Fault, CPP, are the two load tide peaks, M_2 (semi-diurnal lunar constituent) and O_1 (lunar diurnal constituent), significantly above the thermoelastic response of the ground. Their periods are 0.518 days for M_2 and 1.076 days for O_1. Of all the creepmeters operated by the USGS, CPP is the closest to a body of water that has substantial tidal changes. In contrast, the remaining Hayward Fault creepmeters are several kilometers from the San Francisco Bay. The power spectra of all five Hayward creepmeters are shown in figure 6.1. The plots of the spectrum for each site are broken into two plots to show both the 12-hour and 24-hour components. In all the spectra, both the diurnal, lunar constituent/solar diurnal constituent (K_1/S_1) period, and the semi-diurnal period, S_2, are present. Only in CPP are the M_2 and O_1 tides seen, with O_1 being much weaker than M_2. From the spectra the amplitudes of the M_2 and O_1 tides are 1.8 and 1.0 micrometer (μm).

To better estimate the tidal components of CPP data, a 5.4-year interval was chosen (2005.0 to 2010.4) and decimated to 4-hour samples and analyzed using the est_noise program (Langbein, 2017, 2019), where 27 tidal constituents, along with rate and annual and semi-annual periods, are simultaneously estimated under the assumption that the data are temporally correlated. For M_2 and O_1, the results, table 6.1, suggest that these are nearly equivalent in amplitude and phase.

The SPOTL software package, v3.3.0.2 (Agnew, 1997, 2012), predicts tidal strains using a combination of the body tide and the contribution from ocean loading. Importantly, the load tides include the presence of the San Francisco Bay. Taking the CPP creepmeter as a 30-meter (m) long strainmeter oriented N. 75° W., the output of SPOTL is converted to displacement and those predictions for M_2 and O_1 are provided in table 6.1. For M_2, the observed amplitude is 2.4 times that of the predicted amplitude; for O_1, that ratio is 7.8. Both Beaumont and Berger (1975) and Langbein (2010) caution that the tidal predictions are from a model that could be incomplete in characterizing the geologic structure near the observation site. In addition, the local configuration and bathymetry of the Bay near CPP can alter the measured tides from the predicted. The observed tides are within an order of magnitude from the predicted tides. On the other hand, the observed tides, especially O_1, exceed the predicted, suggesting that a locally compliant fault zone amplifies the tides at CPP. However, with none of the other Hayward Fault sites detecting tidal signals above their background noise, fault-zone compliance seems not to be a factor at the other sites. More likely, with CPP being within a few hundred meters of the shoreline of the Bay, an incomplete tidal model should be considered the cause of the discrepancy between the observed and predicted load tides at this site.

Table 6.1. Comparison of observed load tides with predicted solid Earth tides for San Francisco and San Pablo Bays, California.

[SPOTL software package, v3.3.0.2 (Agnew, 1997, 2012); M_2, smaller lunar elliptical diurnal constituent; O_1, lunar diurnal constituent tides; μm, micrometer.]

Tide	Amplitude from power spectrum (μm)	Estimated tide from least squares fit to data		Predicted tide from SPOTL software	
		(μm)	degrees	(μm)	degrees
M_2	1.8	1.1±0.1	−128±5	0.46	−32
O_1	1.0	1.1±0.1	−124±5	0.14	−86

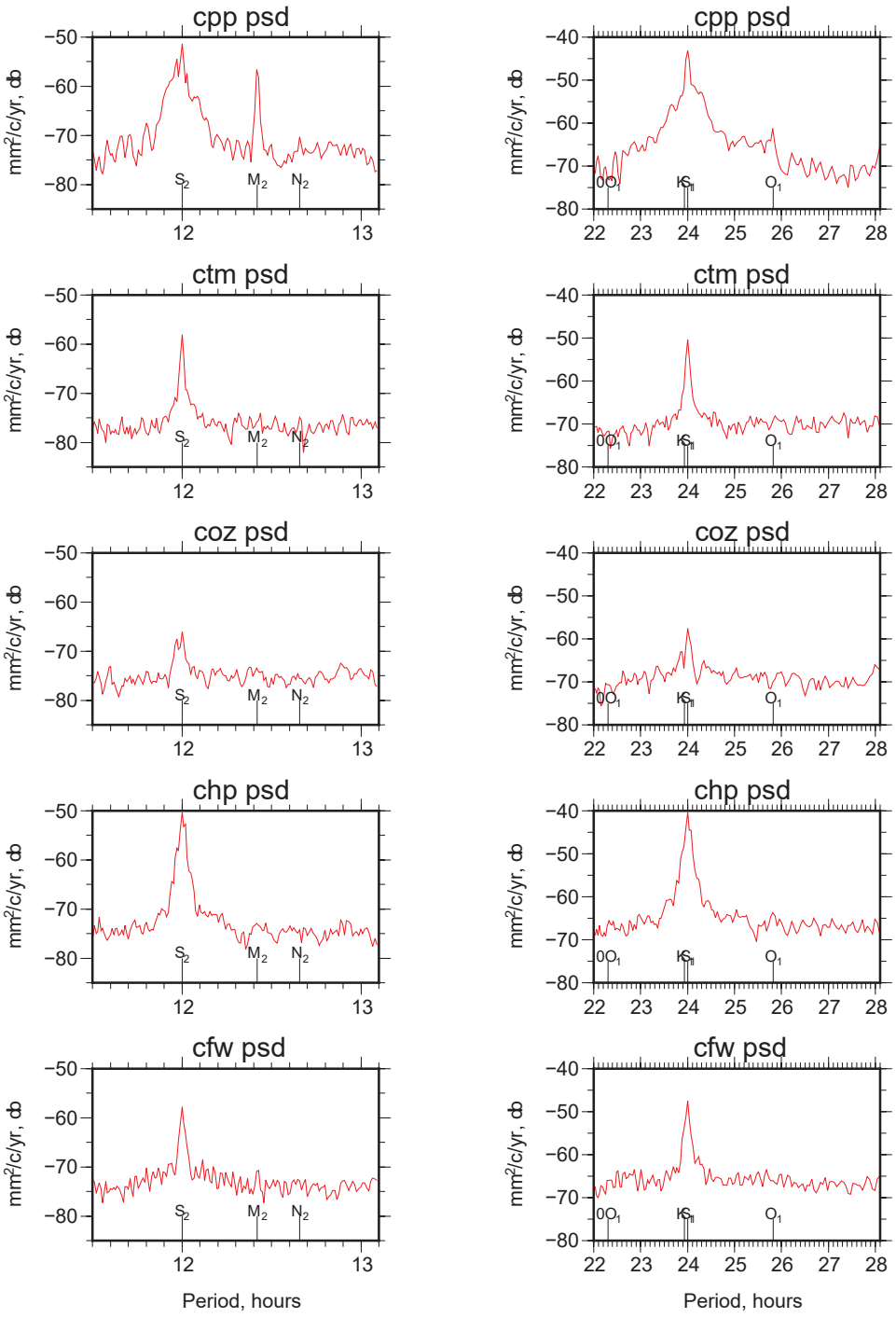

Figure 6.1. Power spectra for the five Hayward Fault creepmeters, California. For each spectrum, the plotted spectrum only spans the tidal periods of M_2 (simi-diurnal constituent) and O_1 (lunar diurnal constituent). The spectrum for each site used all the data, decimated to 10-minute intervals, with a 2-year window. CPP, Pinole Point; CTM, Temescal; COZ, Oakland Zoo; CHP, City of Hayward, Palisade St.; CFW, Fremont. PSD, power spectral density; mm²/c/yr, millimeter; squared, with db being 10x of the logarithm of the PSD.]

References Cited

Agnew, D.C., 1997, NLOADF—A program for computing ocean-tide loading: Journal of Geophysical Research, v. 102, no. B3, p. 5109–5110, accessed December 24, 2022, at https://doi.org/10.1029/96JB03458.

Agnew, D.C., 2012, SPOTL—Some programs for ocean-tide loading (version 3.3.0): University of California San Diego, Scripps Institute of Oceanography Technical Report, accessed December 24, 2022, at https://escholarship.org/uc/item/954322pg.

Beaumont, C., and Berger, J., 1975, An analysis of tidal strain observations from the United States of America—1. The laterally homogeneous tide: Bulletin of the Seismological Society of America, v. 65, no. 6, p. 1613–1629, accessed October 4, 2023, at https://doi.org/10.1785/BSSA0650061613.

Langbein, J., 2010, Effect of error in theoretical Earth tide on calibration of borehole strainmeters: Geophysical Research Letters, v. 37, no. 21, accessed November 8, 2010, at https://doi.org/10.1029/2010GL044454.

Langbein, J., 2017, Improved efficiency of maximum likelihood analysis of time series with temporally correlated errors: Journal of Geodesy, v. 91, no. 8, p. 985–994, accessed October 4, 2023, at https://doi.org/10.1007/s00190-017-1002-5.

Langbein, J., 2019, Est_noise: U.S. Geological Survey software release, accessed December 1, 2022, at https://www.usgs.gov/node/279390.

Schulz, S.S., 1989, Catalog of creepmeter measurements in California from1966 through 1988: U.S Geological Survey Open File Report 89–650, 139-p. pamphlet, 4 pl., accessed April 5, 2019, at https://doi.org/10.3133/ofr89650.

Appendix 7. Propagating Creep Events for Selected Creepmeters in Northern and Central California

This report is an update to the presentation by Schulz (1989) introducing potential users to the creepmeter data collected between the publication of Schulz's report and mid-2020. The U.S. Geological Survey's (USGS's) creepmeter network monitors aseismic surface slip at various locations on the Hayward, Calaveras, and San Andreas Faults in northern and central California. Numerous creep events have occurred on the San Andreas Fault near and south of San Juan Bautista. We present here a brief analysis of propagation directions and velocities between creepmeters Melendy Ranch (XMR), Cienega Winery North (CWN), Harris Ranch (XHR), and San Juan Bautista (XSJ) between 1996 and 2006. Events were detected using an algorithm that searched for changes in long-term/short-term averages, initial and subsequent slip velocity, with empirically determined threshold levels and window-lengths. The data were then plotted as event time-series stacked according to distance from south to north and inspected for potential creep event propagation directions assuming linear velocities along the fault.

The difficulties in drafting figure 7.1 were that not all creep events appeared to have a corresponding event at the next closest site. We chose not to impose a propagation velocity on our selection of the most likely direction of slip. With this somewhat subjective criterion, we deduce that most creep events (30) propagated from north to south, but that a subset (5) nucleated near XHR and propagated to the north. A handful of creep events have no obvious correlation with contiguous creepmeters.

Our assumption that creep event propagation velocities are uniform along the fault is evidently an approximation. If uniform velocities prevailed, we would anticipate that all the "connecting" lines were straight lines. Only a few are straight, some are curved, and some have a small jog near the XHR/CWN instruments.

That 30 coherent southward propagating events occur in ten years, implies that the events are triggered in the north where surface creep velocities slow, and where presumably slip deficits leading to a stick-slip instability are small, but that they sequentially trigger slip southward (domino-like) where surface creep rates are faster.

This raises the interesting question as to whether the creep events grow in amplitude southward, or whether they are the same amplitude and surface creep between slip events increases southward. Resolving this issue would provide considerable insight into the mechanism and possible depth of creep events.

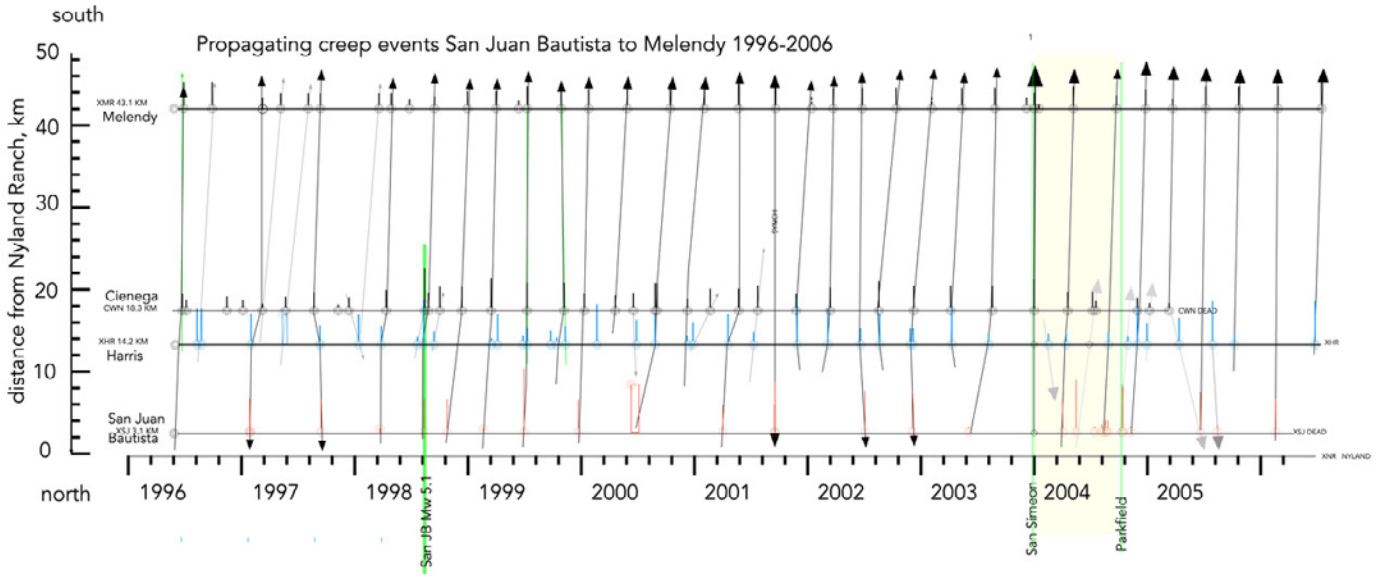

Figure 7.1. Creep events at four locations spanning 42 kilometers (km) of the San Andreas Fault, in central and northern California, from south to north. Creep event amplitudes are plotted as a small vertical line at each site, with a connecting line ending with an arrow indicating propagation direction. There is no propagation velocity on our selection of the most likely direction of slip. With this somewhat subjective criterion, we deduce that most creep events (30) propagated from north to south, but that a subset (5) nucleated near XHR and propagated to the north. XMR, Melendy Ranch; CWN, Cienega Winery North; XHR, Harris Ranch; XSJ, San Juan Bautista. km, kilometer.

Reference Cited

Schulz, S.S., 1989, Catalog of creepmeter measurements in California from1966 through 1988: U.S Geological Survey Open File Report 89–650, 139 p. pamphlet, 4 pl., accessed April 5, 2019, at https://doi.org/10.3133/ofr89650.

Publishing support by the Moffett Field Publishing Service Center
Manuscript approved February 2, 2024
Edited by Lisa Binder
Layout and design by Cory Hurd

ISSN 2331-1258 (online)
https://doi.org/10.3133/ofr20241011